SLIDING FRICTION AND FRACTURE OF ROCKS

A Dissertation
Presented to the Faculty
of the New Mexico Institute of
Mining and Technology

In Partial Fulfillment
of the Requirements for the Degree of
Doctor of Philosophy
in Geoscience

by
Jerrald S. Durtsche
December 1973

ABSTRACT

The mechanical and frictional properties of two rocks, the Mesa Verde Sandstone and Kelly Limestone, were determined by using a conventional triaxial apparatus at maximum normal stresses of 2.5 kb (or crustal depths to 10 km). By defining "resistance to fracture" μ_f as the ratio of shear stress $\tau(\sigma)$ to normal stress σ at fracture and the coefficient of friction μ as the ratio of $\tau(\sigma)$ to σ for pure frictional sliding, a direct comparison of the two processes is facilitated.

The mechanical behavior of both the Kelly Limestone and Mesa Verde Sandstone are related to small-scale structural inhomogeneities in the rocks. Calcite glide planes appear to control deformation leading to ductility and fracture in the limestone, while weak cementation of the sandstone is a controlling factor during its deformation.

For frictional sliding experiments using the conventional triaxial apparatus more accurate values of μ, obtained when partial contact between sliding surfaces is taken into account, are nearly an order of magnitude greater than those obtained when entire fault-surface areas are used (~0.78 vs. ~0.1, respectively). Results of friction experiments indicate that surface roughness does not affect resistance to sliding in the limestone but is a factor in the sandstone,

which is explained as being due to the relative degrees of cementation and porosities of the rocks. Experiments involving synthetic limestone and sandstone gouge indicate that gouge type, grain size, and thickness do not influence resistance to sliding, especially at relatively high stresses, because of the cataclastic buildup of a secondary gouge matrix that produces a steady-state condition of sliding equilibrium. Fault angle affects resistance to sliding in a similar manner observed in stick-slip experiments, for which μ at $\alpha=45^{\circ}$ is greater than μ at $\alpha=30^{\circ}$. Pore pressure affects resistance to sliding by enlarging the difference between the static and kinetic coefficients of friction, a discovery which may be used to explain observed increases in magnitude of stress drops related to stick-slip events at high pore pressures.

The similarity of mechanical processes associated with the fracture of rocks and the pure frictional sliding of rocks containing planes of weakness implies that frictional processes play an important part in the fracture process. One observed difference between the two processes is the relative degree of freedom for grains to rotate along incipient or pre-existing fault surfaces. Based on Orowan's theory of the brittle-ductile transition, it is predicted that the limestone would become fully ductile at crustal depths of 3 km and the sandstone at 5.3 km. The fact that a fractured rock mass is capable of supporting as much stress as unfractured rocks is suggestive that such processes as dilatancy and ductility may occur in fractured rock masses.

ACKNOWLEDGMENTS

I wish to thank Dr. A. J. Budding, Chairman of the Advisory Committee, for his many thoughtful suggestions and constructive criticism of the research and original manuscript. Dr. Budding always offered ideas on solutions to problems that developed during the research and was always eager to assist in any way possible. His lasting inspiration, guidance, and patience, not only during the research, but long before its initiation, are deeply appreciated.

I wish also to thank the other members of the Advisory Committee, Dr. J. Klett, Dr. M. Reiter, and Dr. A. Sanford, who each offered invaluable advice and guidance throughout the research. Dr. Klett was always eager to discuss physical concepts and offered possible explanations to experimental observations. Dr. Reiter suggested several methods that reduced the complexity of sample preparation and was very kind in allowing use of his porosity-determination apparatus. Dr. Sanford was always interested in progress of the research; his many thoughtful criticisms and advice are very much appreciated.

Special appreciation is due Dr. G. Billings, Chairman of the Geoscience Department, and Dr. M. Wilkening, Dean of Graduate Studies, who offered financial assistance throughout the author's education at the New Mexico Institute of Mining and Technology.

I Wish to Dedicate this Dissertation

to

My Mother, Mrs. Nina Durtsche,

and

in Memory of My Father, Mr. Lloyd Durtsche

TABLE OF CONTENTS

Page

LIST OF FIGURES

LIST OF TABLES

INTRODUCTION

One of the most direct methods of understanding the dynamics of processes in the earth's crust and upper mantle is through a laboratory study of the mechanical properties of rocks. Because most rock masses on the earth's surface contain weakness planes such as joints and faults, an important connection between the behavior of rock specimens in the laboratory and rock masses in the field is afforded by the study of the conditions affecting relative movement and friction along pre-existing surfaces of discontinuity.

It has long been recognized that earthquakes may occur along pre-existing fault zones in rock which has already been fractured due to excessive geotectonic stresses (e.g. McKenzie, 1969). This general observation and the fact that only shallow-focus earthquakes are potentially hazardous to man have initiated research into the deformation of rocks which contain macroscopic defects. The objective has been to gain a better understanding of fault mechanics through theoretical, experimental, and field studies of the mechanical properties of rocks and rock masses.

The basic question concerns just what can be said quantitatively about faults, especially active faults, in the field. It is possible to describe the nature or makeup of the gouge or pulverized material in the fault zone, such as its composition, grain size, porosity, thickness, moisture content, and structure or fabric, but what effect do these properties have on the history of the fault or on the stresses which have been or can be supported by the fault? In order to draw any conclusions about the function and behavior of fault systems it is important to know what effect each condition has upon the nature of the faulting process. The obvious approach is to perform a set of experiments in the laboratory and to investigate independently the effect of gouge composition, thickness, porosity, moisture content, etc. on rock fracture and friction.

The entire fault system also includes the adjacent rock masses in which the fault has formed. Thus the mechanical behavior of the original parent rock material from which the gouge was generated is necessarily a contributing factor to fault behavior and therefore must also be considered in laboratory studies. Indeed, it is very possible that the frictional properties of fault gouge is directly related to the original mechanical properties of the rock from which the gouge was derived.

Basic Concepts and Definitions

There are several terms frequently associated with the deformation of rocks, and rocks containing planes of weakness. A few important concepts related to the nature of whole-rock deformation include Young's modulus, elasticity, ultimate or fracture strength, yield strength, and ductility. Initially, most rocks deform under uniaxial compression in an elastic manner such that the applied differential stress is proportional to strain; the constant of proportionality is Young's modulus and the rock is considered elastic. The ultimate strength of a rock is defined as the maximum differential stress required to cause shear failure or fracture of the rock. Before fracture, at a certain differential stress, known as the yield strength, a rock may begin to "yield" in a nonelastic manner resulting in permanent axial strain. The nonelastic permanent deformation is called ductility.

The concept of internal friction is quite similar to that of sliding friction in that a whole rock usually displays a resistance to deformation and failure, whereas a rock containing planes of weakness generally exhibits a resistance to sliding. Specifically, the ratio of effective shearing stress to normal stress needed to cause fracture is defined as the coefficient of internal friction μ_i, or, as proposed by the author, the direct ratio of shear stress to normal stress may be used to define a "coefficient of fracture" μ_f. The coefficient of sliding friction μ is defined as the ratio of the shear stress to normal stress needed to cause relative movement between surfaces in contact, or that ratio during movement (Rabinowicz, 1965).[1] The static coefficient of sliding friction μ_s is determined at the point immediately prior to the onset of movement and the kinetic coefficient μ_k is determined when relative movement has just occurred.

The general notion of friction is associated with conditions of stability that can be established for a given rock mass which may or may not contain a pre-existing fault. For example, for a given μ_f or μ_s it is possible to have only a certain combination (ratio) of applied stresses which determine if sudden failure or perhaps relative sliding movement will occur in a rock mass. By convention a fracture-stability curve or fracture-strength curve, known as the

---

[1] By defining μ_f and μ in this analogous manner, a more direct comparison of the two concepts may be obtained for a particular rock. For later discussions of μ_f it is intended that the "coefficient of fracture" is equivalent to a revised definition of the "coefficient of internal friction." Some authors prefer to define μ as the slope of the shear stress-normal stress curve, but problems develope if the curve is nonlinear. This is discussed more thoroughly in a subsequent section.

Mohr envelope, has been established as a means of defining relative stability of whole rocks based upon the plot of applied shear stress versus normal stress at fracture.

Other more qualitative observations of sliding friction include the kind of sliding which takes place during relative movement along an interface. There are two basic types of sliding, stable sliding and stick-slip. Stable sliding is slow, frictional sliding unaccompanied by measurable stress drops, while stick-slip is sliding characterized by rapid jerks with significant displacements and stress drops. Stable sliding has been proposed as a mechanism of fault creep (Byerlee and Brace, 1968; Scholz, 1969), and stick-slip may very well be the mechanism responsible for most earthquakes (Brace and Byerlee, 1966; Johnson et al., 1973). Figure 1 shows the typical behavior of stick-slip in the laboratory.

Previous Investigations

Mechanical properties of whole rocks. There have been many attempts at explaining the physical processes associated with the formation of observed structural features of rock masses in the field. The fact that rock masses contain joints and faults is reason to believe that mechanical processes

Fig. 1. (a) Force-displacement curve showing stick-slip behavior of a Westerly Granite core with sawcut under a confining pressure of 2.1 kb (Brace and Byerlee, 1966). (b) Stress-strain behavior of solid gabbro cores at three different confining pressures. Note stick-slip behavior after fracture (Byerlee and Brace, 1968). The exact shape of the curves during stress drops is not known and is shown by a broken line.

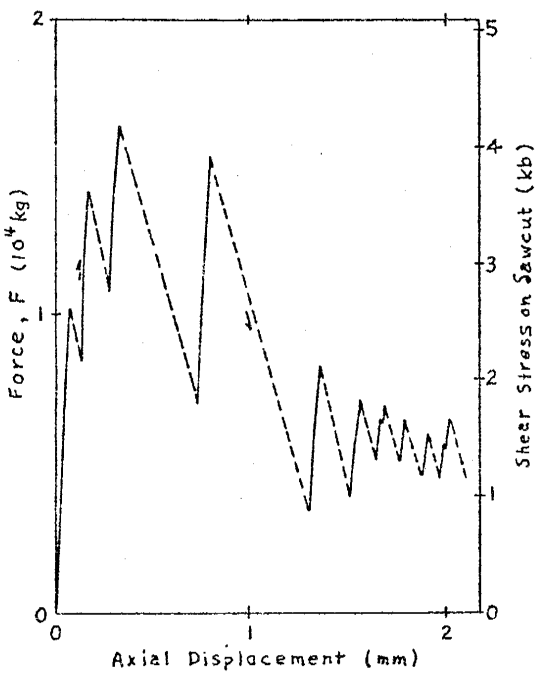

Force, F (10^4 kg)
Sheer Stress on Sawcut (kb)
Axial Displacement (mm)

(a)

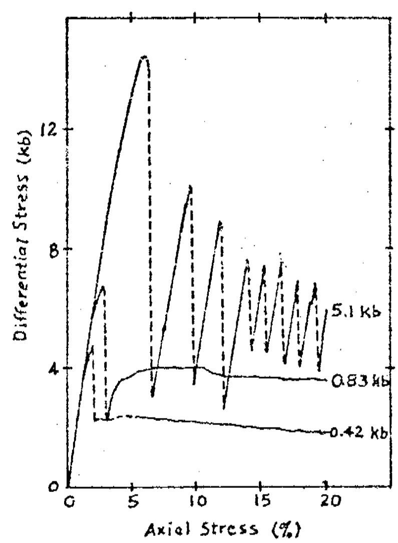

Differential Stress (kb)
Axial Stress (%)
5.1 Kb
0.83 kb
0.42 kb

(b)

producing planes of weakness must have been associated with the original deformation and even fracture of the rocks. This idea leads to small-scale laboratory studies on rocks in an effort to produce the same structural effects as are observed in the field.

Rock deformation has been studied by various laboratory methods, but usually involves the use of a "triaxial" testing apparatus. The "triaxial" apparatus does not actually involve a triaxial set of principal stresses; instead, experiments are made on jacketed cylindrical rock cores subjected to an axial load applied at a uniform strain rate (Donath and Fruth, 1971) and a hydrostatic confining pressure. The latter involves the special case where two of the principal stresses are equal.

The conventional triaxial experimentation of rocks has produced fracture-strength envelopes which may be linear, parabolic, or, in general, curved. A linear Mohr envelope (Coulomb criterion) usually intersects the shear-stress or τ-axis, which reflects a cohesive-strength term τ_o; the slope represents an internal friction term μ_i such that $\tau=\tau_o+\mu_i\sigma$, where σ is the normal stress on the incipient plane of fracture.[1] The general Mohr envelope may be represented by

[1] The following sign convention will be used: compressive normal stresses are considered positive; shear stresses are considered positive if acting in a clockwise direction.

$\tau=(A+B_f\sigma)^{1/n}$, where $\tau_0=A^{1/n}$, B_f is a constant, and n usually varies between 1 (linear case) and 2 (parabolic case). When n=2, the fracture criterion follows the Griffith theory, which assumes the existence of small elliptical cracks in the rock (Griffith, 1921; Jaeger and Cook, 1971a, pp. 310-334).

Studies of the effects of fluid pore pressure on the deformation and strength of rocks tend to confirm that pore pressure p generally reduces the applied normal stress according to the Hubbert-Rubey (1959) concept of "effective stress" σ_e, such that the form of the Mohr envelope $\tau(\sigma)$ is changed by $\sigma_e=\sigma-p$ to $\tau(\sigma-p)=[A+B_f(\sigma-p)]^{1/n}$ (e.g. Robinson, 1959; Handin et al., 1963; Murrell, 1963; Brace and Martin, 1968). Recently, Nur and Byerlee (1971) and Garg and Nur (1973) have proposed that most saturated rocks are likely to obey a law of the form $\sigma_e=\sigma-\alpha' p$ during deformation, where α' is a function of the grain compressibility or bulk modulus of the rock. However, they point out that failure is one aspect of rock material response for which the conventional stress law ($\alpha'=1$) is useful.

It has been observed that there is a general increase in fracture strength and ductility with increasing applied external stresses (e.g. Heard, 1960; Brace, 1964; Murrell, 1965; Mogi, 1967, 1971). The "strength-increasing" or "work-hardening" nature of rocks appears to be related to the mechanical behavior of very small cracks. Orowan (1960) and Maurer (1965) have proposed that rocks eventually become ductile because of the high frictional resistance, presumably between grains, that develops at certain confining pressures. This has been shown to hold experimentally for several rocks (e.g. Murrell, 1966; Byerlee, 1968; Edmond and Murrell, 1973). In this sense the theory of dislocations, as originally applied to the study of metals (e.g. Cottrell, 1953), appears to explain the macroscopic deformation of certain rocks. For example, based upon a theoretical migration of dislocations, McGarr (1971) presents a quantitative description of inelastic deformation that occurs near deep tabular excavations associated with mining, while Ryabinin et al. (1971) have attempted to explain strength-increasing and plasticity processes by means of a dislocation accumulation which changes the internal stresses and increases discontinuity strength (see also Weertman, 1973).

Morland (1971) has attempted to satisfy the need for a finite-deformation theory to explain processes of elastic response, yield, and plasticity. His theory is promising but is weak in one respect in that his model supposes a nonporous solid, a condition which may not be valid for rocks near the earth's surface. Nevertheless, porous rocks generally exhibit compaction at very low applied pressures due to closing of pre-existing cracks and pores (e.g. Walsh and

Brace, 1966) such that perhaps during the early part of their deformation history most rocks may be considered nonporous elastic solids.

On the other hand, at high stresses greater than about half the fracture strength, brittle rock is nonelastic and undergoes an <u>increase</u> in volumetric strain as opposed to the decrease expected for linear elasticity. Brace et al. (1966) and Schock et al. (1973) have explained this dilatancy as being due to the formation of small cracks within the rock. Schock et al. (1973) have postulated that after most of the pores in a rock are removed at high stresses, intergranular friction leads to strong work hardening and soon additional intergranular fractures develop, which thus leads to the dilatant behavior. Microscopic observations of Borg (1971) on fracturing of quartz grains in sandstone during the ductile stage have reinforced this interpretation. For materials that are primarily ductile, the existence of relatively large intervals of dilatancy has prompted Edmond and Paterson (1972) to propose competing processes of compaction and dilatancy.

Small cracking events, known as microfractures, were first observed during dilatancy by Obert and Duval (1942). Recently, Brown (1965), Brown and Singh (1967), Scholz (1967, 1968a-e, 1970), Chugh et al. (1968), and Hardy (1969) have studied in detail microfracturing during deformation and fracture of brittle rocks, for which it was shown that microfracturing increases rapidly as fracture stress (inherent strength) is approached. Scholz (1968b) observed that microfracturing obeys a frequency-magnitude relation identical to that of earthquakes, and that under fixed stresses the frequency of microfracturing decreases hyperbolically with time. This he explained by static fatigue of individual grains, and such a process was proposed as the mechanism of creep in brittle rock (Scholz, 1968c; Hardy et al., 1969) and ultimately as a mechanism of earthquake aftershock sequences (Scholz, 1968d).

The influence of fluid pressure on microfracturing or dilatancy has not been thoroughly investigated, although recently, Byerlee et al. (1972) injected water into stressed rock containing a pre-existing fault and measured the elastic shock activity as a function of pore pressure. They found the maximum number of microfractures (per unit time) decreased with additional injections. It is interesting to note that at about this same time, Nur and Booker (1972) suggested that earthquake aftershocks may be caused by a redistribution of pore pressure as a result of fluid flow within rocks.

Sliding friction. It has been suspected that sliding friction plays an important role in the various criteria of rock fracture (e.g. Orowan, 1960; Murrell, 1965; Hoek, 1968;

Lajtai, 1969; Byerlee, 1967a, 1968, 1969; Handin, 1969; Wawersik and Fairhurst, 1970). The fact that most seemingly homogeneous rocks contain flaws in the form of cracks and pores (Brace et al., 1972; Bombolakis, 1973) that may close under low applied compressive stresses or may grow and coalesce at stresses near the fracture strength of the rock implies a theoretical connection between processes of frictional sliding and processes associated with purely mechanical deformation of rocks. Indeed, Walsh (1965) has suggested that mechanical properties, such as Young's modulus, may be affected by the presence of microcracks.

Previous experimental studies have investigated sliding friction under varying conditions of normal stress, surface roughness, displacement, gouge generation, rock type, strain rate, pore pressure, and temperature. As indicated in Table 1, not all investigators agree as to what effect, if any, these factors have on coefficients of friction, stable sliding, stick-slip, and gouge generation. Brace (1972) has summarized the results of current laboratory studies concerning factors which determine conditions of stable sliding. He points out that (Brace, 1972, p. 189):

> "In general stable sliding is enhanced by high temperature [Brace and Byerlee, 1970], low dffective pressure [Byerlee and Brace, 1968, 1969, 1970], high porosity [Byerlee and Brace, 1969; Byerlee, 1970a], thick gouge [Byerlee, 1970a], and the presence of even small quantities of

TABLE 1. Factors Influencing Coefficients of Friction, Stable Sliding, Stick-Slip, and Gouge Formation*

Condition	Normal Stress	Surface Roughness**	Displacement	Rock Type	Fault Angle	Gouge	Strain Rate	Pore Press.	Temp.
μ_s	decr.[1] unaff.[2]	incr.[3] unaff. at high P.[14,20] incr. at low P.[8]	incr.[7]	unaff.[14,22]	unaff.[4]	decr.[16]	decr.[7]	conv. eff.-str. law holds[4,8] unaff.[24]	decr.[11]
μ_k	decr.[8]		incr. to const. then decr.[4] incr.[5,7]			decr.[16,8]		unaff.[24] incr. by chem.-activ.[24] dec. or unaff.[25] conv. eff.-str. law holds[8] decr.[8]	
Stable Sliding	inhib.[9,12,13]	enhan. at low P.[14]		serp.- & CO_3-rich rks.[2,9] weath. rks.[11]	enhan.[23] unaff.[1]	enhan.[14]			enhan.[11]
Stick-Slip	enhan.[9,13]	enhan. at low P.[14]		ss.'s & qtz.-rich rcks.[8]		enhan.[6] inhib.[7,8]	unaff.[9,10,21] inhib.[6,7]	enhan.[17]	inhib.[11]

TABLE 1. (Continued)

Condition	Normal Stress	Surface Roughness**	Displacement	Rock Type	Fault Angle	Gouge	Strain Rate	Pore Press.	Temp.
Gouge Formation	enhan.[15]	enhan.[6]	enhan.[4] enhan. then uniform[7]		enhan.[8]			enhan. by chem.-activ.[24]	

* Porosity inhibits stick-slip (Refs. 9 and 14) and enhances gouge formation (Ref. 14)
** Condition at initiation of sliding unless otherwise noted

References:

1. Handin, 1969
2. Logan et al., 1973
3. Pratt et al., 1972
4. Byerlee, 1967a
5. Coulson, 1970
6. Dieterich, 1972
7. Scholz et al., 1972
8. Handin and Engelder, 1973
9. Byerlee and Brace, 1968
10. Coulson, 1970
11. Brace and Byerlee, 1970
12. Byerlee and Brace, 1969
13. Byerlee and Brace, 1970
14. Byerlee, 1970a
15. Brace, 1972
16. Logan, 1972
17. Brace and Martin, 1968
18. Jaeger and Cook, 1971b
19. Logan et al., 1970
20. Byerlee, 1966
21. Wolters, 1970
22. Brace, 1971
23. Humston, 1972
24. Swolfs, 1971
25. Blackwell, 1973

> [weak] minerals like serpentine and calcite [Byerlee and Brace, 1968; Logan et al., 1970]."

Brace also notes that surface roughness is an important parameter for stable sliding, in that (Brace, 1972, p. 197):

> "... frictional resistance increases markedly with surface roughness (J. Handin, personal communication, 1971)."

An excellent review which also summarizes current studies of rock friction, but includes a more thorough explanation of principles and theory, is given by Jaeger (1971).

Drennon and Handy (1972) have observed the nature of stick-slip of lightly loaded limestone and the influence of buildup of rock debris (gouge) along the surfaces of contact. They note that coefficients of friction are apparently a function of cumulative slip, similar to Byerlee's (1967a) indication that friction depends upon displacement.

Conditions of stable sliding in the laboratory for different types of rocks with pre-existing faults or sawcuts containing various controlled gouge materials, dry or fluid-saturated, have not been investigated in detail. However, a laboratory study of a rock with gouge has been conducted by Logan (1972), and preliminary results in the form of an abstract have been published. Logan has found that fault-surface roughness influences frictional sliding when macroscopically interlocking asperities are sheared off during initial deformation, and then stress drops occur, producing stick-slip only when the surfaces are planar and smooth. He has proposed that the shearing of macroscopic asperities is a more reasonable mechanism of earthquake generation than stick-slip. In addition, Logan has introduced fault gouge, which tends to inhibit stick-slip. However, none of the investigations has involved a close analysis of rock friction and gouge character.

Although experiments with fluid injection into pre-fractured rocks containing synthetically regulated gouge have not been conducted, fluid injection has been observed to cause stress drops in cleanly pre-cut rocks (Byerlee, 1967b; Brace and Martin, 1968). Byerlee (1967a) concluded that the effective stress theory, whereby pore pressure reduces applied normal stress in an arithmetic manner, holds for the Westerly Granite such that slopes of the $\tau(\sigma)$ curve remain essentially constant for various pore pressures. Swolfs (1971) has shown that coefficients of friction for dry and water-saturated Coconino Sandstone are the same, but that the kinetic coefficient μ_k increases upon injection of a chemically-active fluid. He proposes that a weakening effect of the fluids has caused an increase in the amount of gouge along the sliding surface, thus causing an increase in μ_k. Blackwell (1973) has noted that pore fluids lower μ_k for the relatively low-porosity Tennessee Sandstone but have little effect on the more porous Coconino Sandstone.

In a recent semi-annual progress report to the U.S.

Geological Survey, John Handin and James Engelder (1973) have discussed in detail the development and deformation of quartz fault gouge through experimental, field, and microscopic observations of natural and artificial fault zones. They have concluded that μ_k decreases with increasing normal stress for both stick-slip and stable sliding and that during stable sliding it tends to be higher for dry specimens than for saturated ones. In addition they have observed that quartz gouge is sufficiently permeable to allow fluid-pressure equilibration through a compacted layer of gouge, thus suggesting that the principle of effective stress should hold for the fault-zone system. Based upon stick-slip experiments involving stress drops they conclude that the magnitude of stick-slip events increases in the presence of water. Values of kinetic coefficients of friction associated with stick-slip events along sawcuts in Tennessee and Coconino Sandstone containing quartz and calcite gouge range from 0.68 to 0.86, with apparently no effect of gouge type.

One can postulate that the kinds of sliding and the frictional coefficients must be related by the various influencing factors such as rock type, surface roughness, gouge properties, etc., as may be inferred from a study of Table 1. Indeed, it has even been established that the interplay of the static and kinetic coefficients of friction are what determine the magnitude of stress drops during stick-slip events (Rabinowicz, 1965, pp. 97-98; Byerlee, 1970b; Scholz et al., 1972). Some recent results were published by Scholz et al. (1972) pertaining to new facets of frictional sliding of rock, such as episodic stable sliding, pre-stick-slip stable sliding, transitions from stick-slip to stable sliding, time dependence of friction, and the influence of stress drop and gouge on the kinetic coefficient of friction. But, as they pointed out, much more work needs to be done, particularly with different rock types and different surface conditions, before an adequate understanding of these phenomena can be obtained.

Present Investigation

The present study has been an investigation of the mechanical (including frictional) properties of two rocks, the Mesa Verde Sandstone and the Kelly Limestone, with the use of a triaxial-cell apparatus at maximum applied stresses of 2.5 kb. The overall objective was to compare coefficients of sliding friction under certain conditions of surface roughness, porosity, gouge grain size, moisture content, thickness, pore pressure, and fault angle to the mechanical properties associated with whole-rock deformations, in an effort to gain a better understanding of fault mechanics.

The effect of sawcut surface preparation upon values of friction coefficients determined with the triaxial-cell apparatus has also been investigated by using several "controlled," perfectly matched contact areas along the sawcuts. Maximum coefficients of friction obtained in this manner were then used as a means of comparison with values obtained using unmatched surfaces produced by uneven polishing.

It should be emphasized that any attempt to explain the faulting process <u>must</u> account for the influence of gouge. The ultimate goals of the investigation were to gain an insight into the nature of faulting through a study of the mechanical properties of rock masses under the influence of gouge, and, whenever possible, to apply the results, at least qualitatively, to problems of fault stability and earthquake source mechanisms.

EXPERIMENTAL PROCEDURE

Triaxial Apparatus and Sample Preparation

For determining mechanical properties of rocks it is common practice to use a triaxial-cell apparatus similar to the one used in the present study, which is shown in Figure 2 (Handin and Stearns, 1964; Lane and Heck, 1964; Byerlee, 1966; Humston, 1972; Handin and Engelder, 1973; etc.). A dual-channel, Hewlett-Packard strip-chart recorder automatically records the axial load and displacement via a 250,000 lb (maximum) load cell and an external LVDT (linearly variable differential transformer, ±0.125-in maximum displacement). The confining pressure is controlled by an air/oil pump and values (in psi) are given by pressure gauge. The axial load is supplied by an electrical hydraulic pump. Values of load are determined within approximately 10 lb, displacement within 50 μin, and confining pressure to within 15 psi.

Compression experiments involving whole rocks were performed on cores containing polished sawcut surfaces, the sawcut being inclined with respect to the core axis by an angle

Fig. 2. Labeled photograph of triaxial-cell apparatus used in the present investigation.

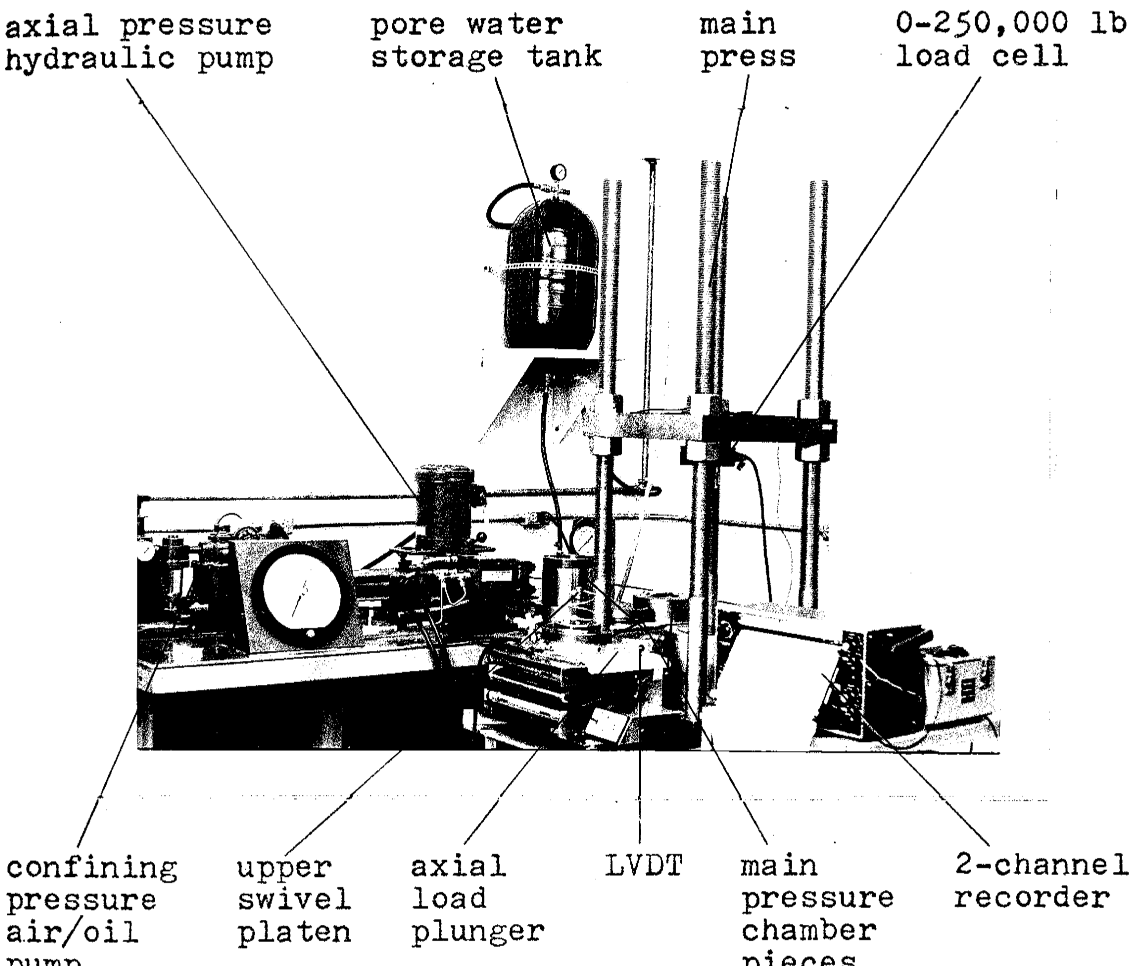
axial pressure hydraulic pump
pore water storage tank
main press
0-250,000 lb load cell
confining pressure air/oil pump
upper swivel platen
axial load plunger
LVDT
main pressure chamber pieces
2-channel recorder

α, usually 45°. For friction experiments, introduction of a thin layer of dry or saturated, controlled gouge (i.e. "controlled" as to grain size, angularity of grains, composition, thickness) along the sawcut was easily facilitated with the apparatus, since plastic electrical tape and Tygon (B44-3) hose was used as a confining jacket. To reduce anomalous friction between the ends of the rock core and metal of the equipment, a thin film of lubricating grease (Dow Corning #4 Compound) was used. A 1/8-in hole was drilled through one half of the core along its axis for the pore-pressure tests (Figure 3). Powdered rock was left in water for approximately two weeks to produce saturated gouge. Figure 4 shows a typical sample configuration prior to an experiment with and without gouge along the sawcut surfaces.

Roughness of the bare sawcut surfaces was controlled by polishing with #600 (relatively fine) and #100 (relatively coarse) grit. Porosity was measured by first weighing the dry core, then evacuating and flooding with distilled water, and finally weighing the wet core. Mineralogy was determined through petrographic analysis.

Problem of partial contact. Jaeger and Cook (1971a, pp. 68-70) have pointed out some problems involved in studying sliding friction with the triaxial-cell apparatus. The most obvious problem, specimen tipping, is usually overcome by

Fig. 3. Diagram of internal parts of triaxial-cell pressure chamber (not to scale). L is axial load, σ_c is confining pressure, and α is sawcut angle.

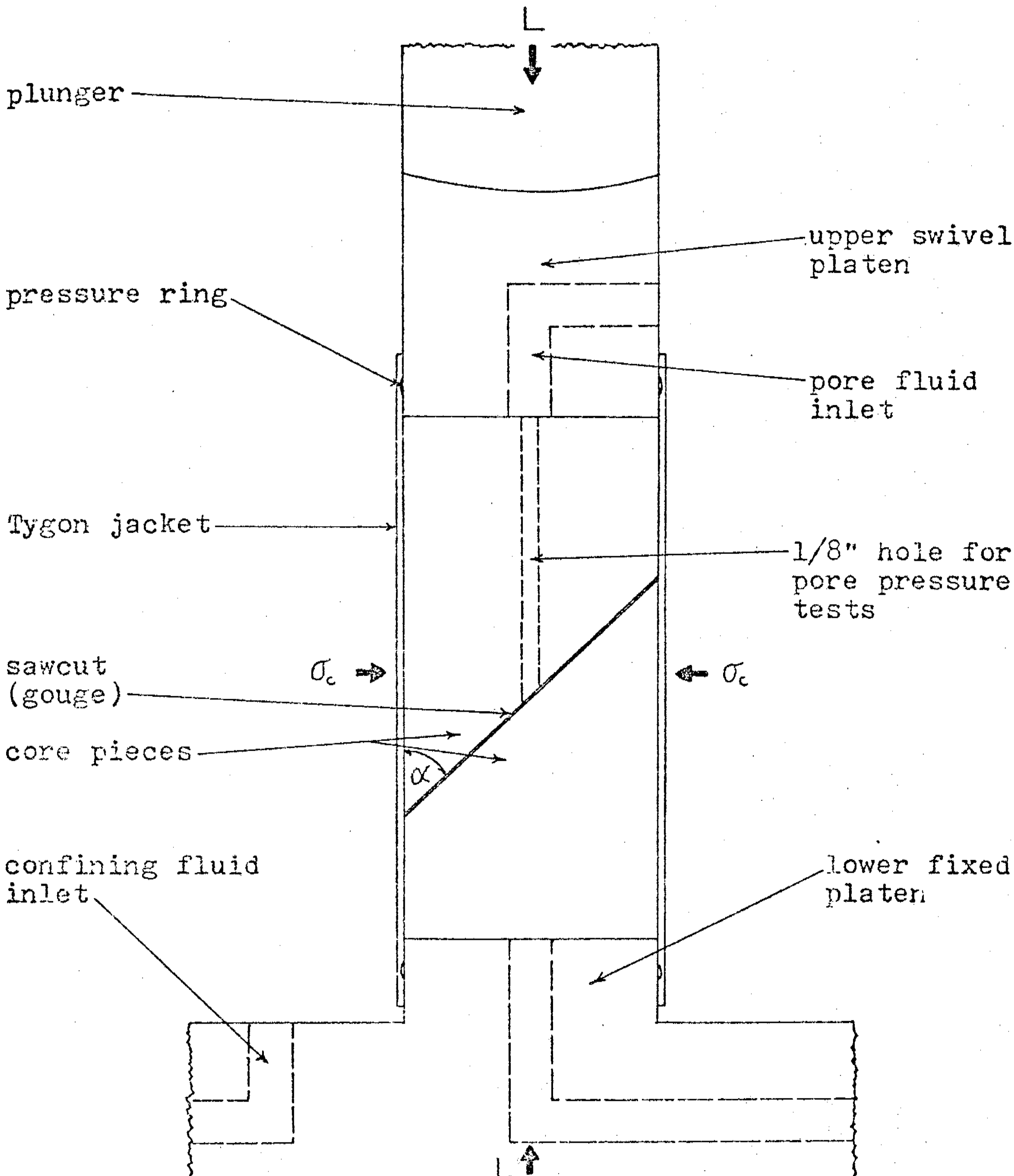
L
plunger
upper swivel platen
pressure ring
pore fluid inlet
Tygon jacket
1/8" hole for pore pressure tests
sawcut (gouge)
σ_c
σ_c
core pieces
α
confining fluid inlet
lower fixed platen
L

Fig. 4. Left: photograph of finished core pieces prior to confinement. Right: pieces with gouge in confining jacket ready for loading into the pressure cell.

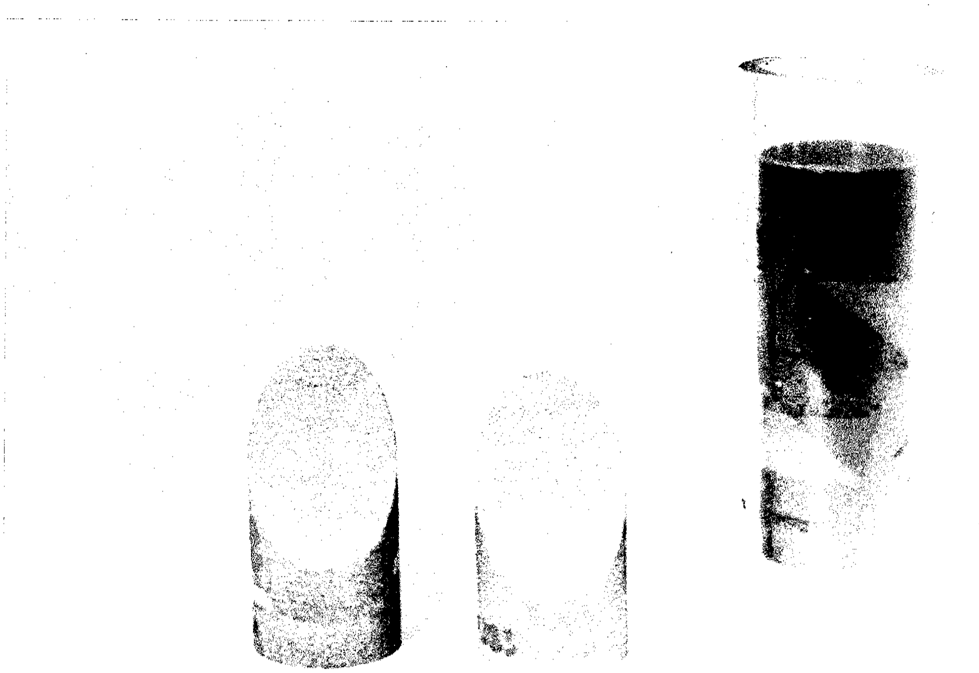

using small displacements during an experiment. One of the major difficulties which is not so apparent is that an axial stress must be calculated from the recorded axial force in order to determine the magnitudes of the shear stresses τ and normal stresses σ acting on the fault or sawcut surface. A certain projected area of contact must be assumed, which is usually the entire end area A_0 of the rock core. The usual assumption is that the entire fault surface is in contact, implying that the two core pieces are perfectly matched during the experiment. This assumption is not likely to be valid due to the possibility that polished surfaces are not really perfectly mated, but rather, there exists a macroscopic contact area A_0' which is supporting the applied forces (see Figure 5).

Several methods have been devised for polishing sawcut surfaces. Among them are the use of polishing grits (e.g. #80 silicon-carbide) or polishing papers containing the grits and a smooth hard surface such as glass. Another polishing tool which has gained wide acceptance within the last few years is the motor-driven grinding wheel, which may be adjusted for various grits and various sawcut angles.

Polishing by hand on polishing paper or loose grit, or by using a grinding wheel, invariably produces poorly matched surfaces. All methods usually give their own set of distinctly different results, each of which are experimentally repro-

Fig. 5. Diagram of cores containing sawcuts exhibiting (a) projected partial contact area A_o' and (b) "perfect" contact over entire surfaces with core cross-sectional area A_o. Note the concentration of axial stress across the smaller area A_o'.

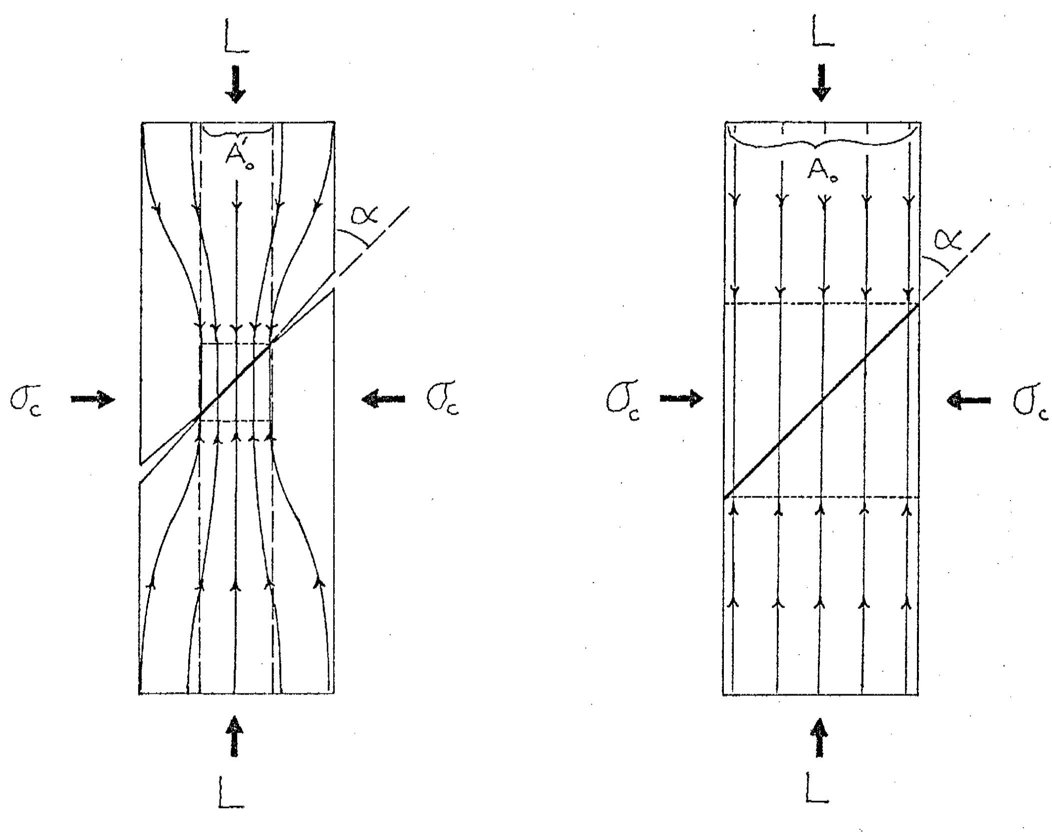

(a) (b)

ducible. For unmatched surfaces, a smaller area of contact A_0' results, and if the larger area A_0 of the core cross-section is used in the calculations, resulting values of τ and σ are much smaller than those calculated from data associated with perfectly matched sawcuts. This relationship may be seen by observing the following equations of shear and normal stress as a function of projected area of contact A_0':

$$\tau = \tau(A_0') = \frac{1}{2}\left(\frac{L}{A_0'} - \sigma_c\right)\sin 2\alpha \tag{1}$$

$$\sigma = \sigma(A_0') = \frac{1}{2}\left(\frac{L}{A_0'} + \sigma_c\right) - \frac{1}{2}\left(\frac{L}{A_0'} - \sigma_c\right)\cos 2\alpha \tag{2}$$

where the axial load L and confining pressure σ_c are measured during the experiment (see also the following section). For the case when the sawcut surfaces are unmatched, $A_0' < A_0$, and thus τ and σ increase accordingly. This condition is shown diagrammatically in Figure 5(a). Figure 5(b) is a diagram of perfectly matched core pieces for which the entire end area A_0 of the core is used to calculate the axial stress σ_a.

An advantage in using smaller contact areas is that for given applied axial loads L, less force is required to obtain large values of τ and σ. However, due to the high buildup of stress along small areas and due to the configuration of the specimens, it is possible that unwanted fracturing may occur at very high stresses.

Coefficients of friction obtained for partial contact using the entire core area A_o are a kind of "average" coefficient because in using A_o the assumption is that there is an average or uniform distribution of stress across the entire surface. Experiments involving reduced areas A_o' which are known to support all applied stresses produce the maximum possible coefficients of friction.

Closeup observations of the sawcuts polished by hand support the contention that only partial contact exists during an experiment. Prior to an experiment when two core pieces are fit together and observed from a side view looking into a light source, the outer portions of the sawcut surfaces transmit light while the central section does not. After an experiment involving approximately 0.01-in maximum displacements, slickensides have been observed only on a small (<20%) portion of the entire sawcut surfaces. Thus, the central part of the polished sawcut is apparently much more "perfectly" matched. Observations on several different sawcut surfaces prepared in the same manner indicate that since there is no detectable variation in actual contact area, an equilibrium is reached during polishing so that a maximum degree of flatness is attained after a certain amount of polishing (usually ~0.5 hr). This is explained as a result of wear of grit material due to continuous polishing, which tends to round the outer edges of the surfaces, because particles become caught under the outer edges, resulting in consistently uneven polishing.

It will be shown that results derived from triaxial-cell friction experiments also tend to support visual observations concerning partial contact. It is possible to eliminate the outer parts of the sawcut surfaces which are known not to be in contact by grinding away this portion and thus controlling that part which is known to be more perfectly mated. Examples of prepared surfaces using this "controlled area" method are shown in Figure 6.

Data gathering. As mentioned above, both fracture and friction are likely to depend upon displacement and displacement rate; thus, experiments are run with both factors uniform. For the friction tests, the easiest method is to displace the specimen from the rest or zero-displacement position by a certain constant distance (at a constant strain rate) and back to the original zero position by alternately increasing the axial load and confining pressure. A diagrammatic explanation of how friction data is obtained in this manner is given in Figure 7. The two sets of data thus obtained represent static and kinetic frictional determinations because of the choice of points on the force-displacement (and confining pressure) record, which were taken such that the axial stress is always greater than the confining stress. Data obtained in this respect tends to reduce the effects of

Fig. 6. Cores showing various controlled-area surface preparations for (left) sandstone, $\alpha=45^{\circ}$, after experiment, (center) limestone, $\alpha=45^{\circ}$, after experiment, and (right) limestone, $\alpha=30^{\circ}$, prior to experiment (1-in dia. cores).

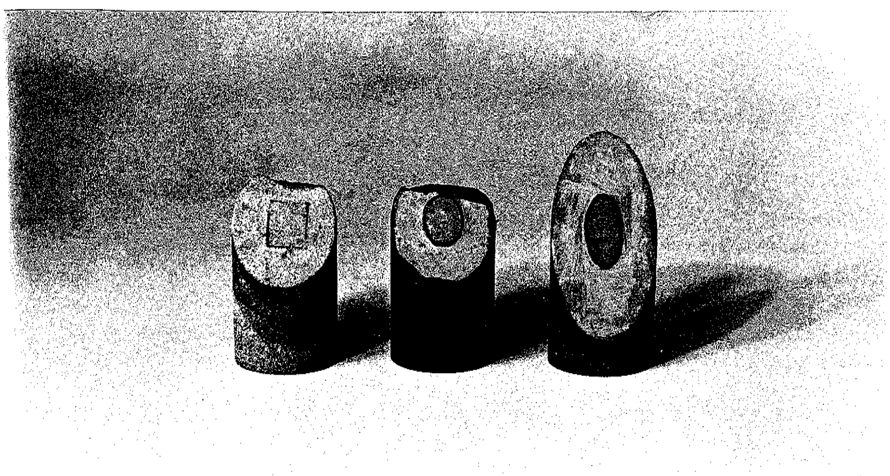

Fig. 7. Diagram of relative positions of core pieces and choice of maximum static (at A and E) and kinetic data (at C) during a typical friction experiment. Note that data are chosen such that axial stress σ_a is always greater than confining pressure σ_c and that controlled displacements are usually $\pm$ 0.01 in (cores not to scale).

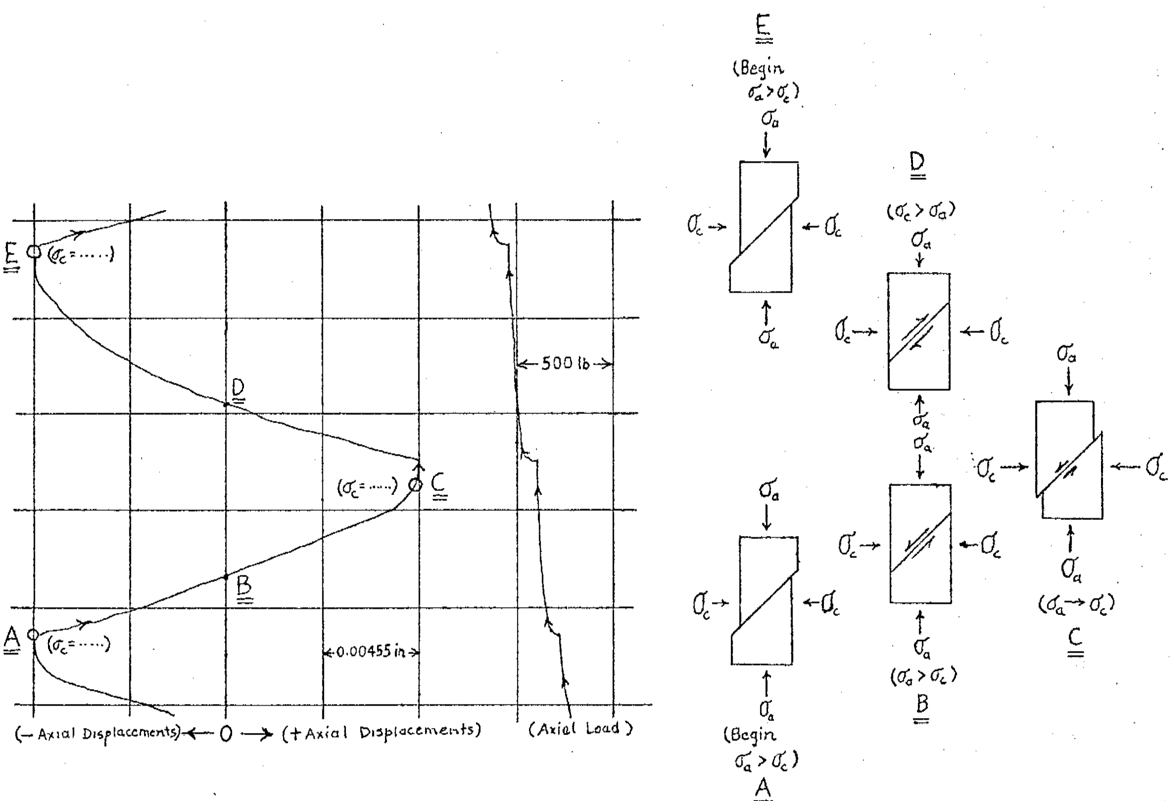
E
(Begin
$\sigma_a > \sigma_c$)
D
($\sigma_c > \sigma_a$)
C
($\sigma_a \rightarrow \sigma_c$)
B
($\sigma_a > \sigma_c$)
A
(Begin
$\sigma_a > \sigma_c$)
(σ_c = ...)
500 lb
0.00455 in
(− Axial Displacements) ← 0 → (+ Axial Displacements)
(Axial Load)

stick-slip, such as large stress drops and displacements, so that stable sliding is likely to dominate. For cases when stick-slip is observed during a cycle, the opposing stress is used to control it.

For fracture experiments, axial stresses and strains, and normal and shear stresses acting on the incipient fracture surface, are calculated directly from recorded values of axial load, displacement, confining pressure, and fracture angle.

An outline of all experiments, involving both the Kelly Limestone and Mesa Verde Sandstone for approximately 60 experimental tests, is given in Figure 8. Some preliminary equipment calibrations and tests involving equipment characteristics, such as a hydrostatic test and machine stiffness, are included.

Fig. 8. Outline of experimentation.

- Preliminary Determinations
  - Equipment Tests
    - LVDT calibration
    - Load-cell calibration
    - Hydrodstatic test
    - Stiffness test
    - Equipment strain correction
  - Optical Stress Analysis
    - Partial contact without gouge (α=45° and 30°)
    - Partial contact with gouge (α=45°)

- Kelly Limestone and Mesa Verde Sandstone
  - Specimen Properties
    - Uncompressed densities and porosities
    - Thin-section studies
    - CO_2 gas pressure and staining tests
  - Fracture Tests
    - Various σ_c
    - Young's modulus
    - Mohr envelopes
  - Friction Tests
    - Without gouge
      - #100 grit roughness
      - Duplicate runs
      - #600 grit roughness
      - Controlled area tests
    - With gouge
      - #80 dry gouge
      - >#230 dry gouge
      - #80 wet gouge
      - >#230 wet gouge
      - Controlled area tests
      - Variations
        - Gouge thickness
          - #80, 1 grain-dia.
          - 1 mm
          - 1.5 mm
        - Fault angle (α)
          - 30°
          - 37.5°
          - 45°
          - 60°
        - Rock type
          - #80 ls. and ss. gouge mixture
        - Pore pressure
          - #80 wet, p=0
          - p≈600 psi
          - p≈1200 psi

Calculations and Presentation of Data

During friction experiments the average normal stress σ and shear stress τ acting at the sliding surfaces in contact are calculated from axial stress σ_a and confining pressure σ_c acting over the same contact area by using a form of Equations 1 and 2:

$$\tau = \frac{\sigma_a - \sigma_c}{2} \sin 2\alpha \qquad (1')$$

$$\sigma = \frac{\sigma_a + \sigma_c}{2} - \frac{\sigma_a - \sigma_c}{2} \cos 2\alpha \qquad (2')$$

(e.g. Byerlee, 1967a, p. 3640; Jaeger and Cook, 1971a, p. 65). The derivation of (1') and (2') is given in Appendix I.

Derivation of an area correction which relates loss of contact area as a function of displacement is also given in Appendix I. For relatively small maximum displacements of ±0.01 in (as in the present study) the correction is shown to be unnecessary.

For fracture experiments involving virgin cores, axial stress σ_a and strain ε_a and Young's modulus E are calculated from axial load L and displacement x with the following equations:

$$\sigma_a = \frac{L}{A_o} \tag{2}$$

$$\varepsilon_a = \frac{x}{l_o} \tag{3}$$

$$E = \frac{\Delta\sigma_a}{\Delta\varepsilon_a} = \frac{\sigma_{a2} - \sigma_{a1}}{\varepsilon_{a2} - \varepsilon_{a1}} \tag{4}$$

where A_o is the core cross-sectional area and l_o the original core length. E is determined for those points on the $\sigma_a(\varepsilon_a)$ curve where $\sigma_a \propto \varepsilon_a$ (linear). Fracture strengths defining the Mohr envelope are calculated from Equation 2 and Equations 1' and 2' for measured fracture angles. As mentioned in a previous section, the general equation of the Mohr envelope is

$$\tau = (A + B_f\sigma)^{1/n} \tag{4'}$$

Nearly all friction data for τ as a function of σ have been assumed to be linear, with possible exceptions being given by Murrell (1965), Maurer (1965), Hobbs (1970), and Edmond and Murrell (1973) who use a power law of the form

$$\tau = \tau_o + B\sigma^n. \tag{5}$$

In the present investigation it will be shown that plotted values of (σ, τ) for a certain experiment exhibit nonlinearity when core end-area A_o is used in the calculations. When corrected areas A_o' are used the data exhibit linearity such that

$$\tau = \tau_0 + B\sigma. \qquad (6)$$

For relatively large-grained rocks with rough surfaces or in the presence of gouge the least-square curves representing (σ, τ) data are likely to intercept the ordinate (τ) at the value τ_0, considered to be a kind of inherent shear strength or cohesion of the asperities or gouge materials. To determine the degree of fit of least-square Equations (4'), (5), or (6) to the experimental data, a correlation coefficient R^2 is calculated according to Walpole (1968, pp. 271, 285-286).

The coefficient of friction μ is calculated using the relationship which Byerlee (1967a) used. The nonlinear case of Equation 5 and the linear case of Equation 6 produce (respectively):

$$\mu = \mu[\sigma(A_o)] \equiv \frac{\tau(A_o)}{\sigma(A_o)} = \frac{\tau_o}{\sigma} + B\sigma^{n-1} \qquad (7)$$

and

$$\mu = \mu[\sigma(A_o')] \equiv \frac{\tau(A_o')}{\sigma(A_o')} = \frac{\tau_o}{\sigma} + B. \qquad (8)$$

For consistency, the coefficient of "internal friction" or resistance to fracture μ_f associated with fracture experiments is calculated using this same concept of $\mu_f = \tau/\sigma$ and Equation 4' such that

$$\mu_f = \mu_f[\sigma(A_o)] \equiv \frac{\tau(A_o)}{\sigma(A_o)} = \left(\frac{A}{\sigma^n} + B_f\sigma^{1-n}\right)^{1/n} \qquad (8')$$

It will be shown that experiments in the present study which involve controlled areas $A_o' = A_c$ on surfaces known to be perfectly matched produce maximum coefficients of friction which are reproducible.[1] Due to the high degree of reproducibility involved in polishing the sawcuts by hand (see above), it is possible to apply a certain area correction such that coefficients are standardized. The high degree of reproducibility also permits the comparison of the effects of such factors as surface roughness on friction, whether experiments are conducted on unmatched, hand-polished sawcuts or on controlled areas known to be perfectly matched.

Standardized areas A_o' are calculated by using average least-square coefficients τ_{oc} and B_c for the controlled-area tests in which

$$\tau = \tau_{oc} + B_c \sigma. \qquad (9)$$

Equivalent tests using unevenly matched sawcut surfaces produce experimental values of L, σ_c, and α which then must be converted by an appropriate standardized area A_o' to account for partial contact. Substituting Equations 1 and 2 in Equation 9 gives

$$\frac{1}{2}\left(\frac{L}{A_c'} - \sigma_c\right)\sin 2\alpha = \tau_{oc} + B_c\left[\frac{1}{2}\left(\frac{L}{A_o'} + \sigma_c\right) - \frac{1}{2}\left(\frac{L}{A_c'} - \sigma_c\right)\cos 2\alpha\right] \qquad (10)$$

---

[1] A less accurate visual determination of A_o' was tried, which produced $\mu \approx 0.65$ as compared to $\mu \approx 0.75$ for the $A_o' = A_c$ method.

and upon solving for A_o':

$$A_o' = A_o'(L, \sigma_c) = \frac{L[B_c(\cos 2\alpha - 1) + \sin 2\alpha]}{\sigma_c B_c(\cos 2\alpha + 1) + \sigma_c \sin 2\alpha + 2\tau_{oc}} \qquad (11)$$

Thus for a particular α, each set of N experimental values (L, σ_c) involving unmatched sawcut surfaces will be associated with a partial contact area A_o'. An average area $(\Sigma A_o')/N$ is thus obtained for a given experiment.

Computer programs are ideal tools for calculating and plotting (σ, τ) and (σ, μ) or (σ, μ_f), with corresponding least-square curves of the forms (5)-(8), or (4), (4'), and (8'), reflecting the various experimental conditions. Several programs were written for this purpose and used throughout the present study. They are given in Appendix III and referenced in later sections of the report.

RESULTS

Equipment Tests

Calibrations. The LVDT was calibrated using a micrometer with accuracy to within 0.0001 in and on several recorder scales. The average of 6 trials is 0.00455 in/v (inches displacement per volt) with an error of ±0.000045 in/v. Throughout the experimentation the most commonly used recorder scale was the 10-v scale, for which calibration was carried out across the entire 10 scale divisions (1 v/division) of the recorder such that the 0.00455 in/v linear response was determined to hold ±10 divisions from a starting position.

The load cell was calibrated using a 0-250,000 lb test gauge which had been factory calibrated. The 50-mv recorder scale was used in conjunction with the load cell, and the average axial force per 50-mv scale division was 500 lb/divition or 500 lb/5mv such that 100,000 lb axial force is equivalent to 1 v on the recorder.

To check the accuracy of the load-cell calibration with respect to the confining-pressure gauge, a "hydrostatic" test was devised. The hydrostatic test consisted of the very same experimental setup as for a friction or fracture test with the exception that no core or upper swivel platen was used. Instead, the confining fluid was used to equalize any applied axial force. If calibration was done properly, load-cell (stress) data and confining-pressure gauge data should be identical. Results of the hydrostatic test, shown in Table 2, indicate a 6% disagreement of data. This "error" may be accounted for as a result of minor equipment friction, such as occurs along mechanical contacts between the plunger and the rubber pressure rings of the triaxial-cell chamber. Most of this error was accounted for in subsequent experimentation by adding 0.01 in^2 to all measured areas prior to the σ_a calculations. Of course, some error (~4%) was due to reading inaccuracies associated with the original data gathering.

<u>Machine stiffness</u>. The stiffness of the equipment was determined for σ_c=0 in the absence of any core. Seven tests were conducted, several of which included effects of a thin film of the lubricating grease between the swivel platen of the cell. Original data for the tests are given in Appendix II.

Two equations relating axial stress to axial strain were determined using the least-square method. They are:

TABLE 2. Results of Hydrostatic Test

Confining Pressure Gage σ_c (psi)	Axial Load Cell L (lb)	σ_a* (psi)	$\frac{\sigma_a}{\sigma_c}$
650	530	675	1.038
1020	820	1044	1.024
1325	1060	1349	1.018
1580	1325	1687	1.068
1990	1675	2132	1.071
2335	1975	2514	1.077
2895	2420	3081	1.064
3525	2900	3692	1.047
4080	3400	4328	1.061
4825	4080	5194	1.076
4950	4170	5308	1.072
5210	4350	5538	1.063
5550	4640	5907	1.064
5935	5000	6365	1.073
		Average:	1.058

* The axial stress σ_a is calculated from: $\sigma_a = L/A_o$, where $A_o = 0.785$ sq. in.

$$\sigma_a = -250(\text{psi}) + 18.5\cdot10^4(\text{psi}/\%)\,\varepsilon_a(\%) \qquad (\sigma_a < 2100 \text{ psi})$$

$$= -17.2(\text{bars}) + 1.28\cdot10^4(\text{bars}/\%)\,\varepsilon_a(\%) \quad (\sigma_a < 145 \text{ bars}) \quad (12)$$

and

$$\sigma_a = -1694(\text{psi}) + 28.33\cdot10^4(\text{psi}/\%)\,\varepsilon_a(\%) \qquad (\sigma_a > 2100 \text{ psi})$$

$$= -116.8(\text{bars}) + 1.95\cdot10^4(\text{bars}/\%)\,\varepsilon_a(\%) \quad (\sigma_a > 145 \text{ bars}) \quad (13)$$

The average Young's modulus for the equipment is thus (for $\sigma_a > 2100$ psi or 145 bars) $E_{equip} = 1.95$ Mbar. This is equivalent to a machine stiffness constant $k = 67.4\cdot10^4$ kg/cm.

The strain that occurs in the equipment during an experiment must be accounted for. The stiffness test is a direct means of determining an equipment strain correction which is used primarily in the fracture tests for determining Young's modulus of the limestone and sandstone. The axial strain ε_a may be obtained from (12) and (13) above such that the equipment strain correction is

$$\varepsilon_{ac} = \frac{\sigma_a + 250(\text{psi})}{18.5\cdot10^4(\text{psi}/\%)} \quad \frac{\sigma_a + 17.2(\text{bars})}{1.28\cdot10^4(\text{bars}/\%)} \quad (\sigma_a < 2100 \text{ psi} = 145 \text{ bars}) \quad (14)$$

$$\varepsilon_{ac} = \frac{\sigma_a + 1694(\text{psi})}{28.33\ 10^4(\text{psi}/\%)} \quad \frac{\sigma_a + 116.8(\text{bars})}{1.95\cdot10^4(\text{bars}/\%)} \quad (\sigma_a < 2100 \text{ psi} = 145 \text{ bars}). \quad (15)$$

Specimen Characteristics

Densities and porosities. Average uncompressed densities for several cores of Kelly Limestone and Mesa Verde Sandstone were determined by measuring the dimensions of the cores with vernier calipers and by weighing. The range of densities for the limestone cores is 2.622-2.711 (±0.005) g/cm^3, with a mean rock density of 2.689 g/cm^3. The range of densities for the sandstone cores is 2.256-2.314 (±0.005) g/cm^3, with a mean rock density of 2.285 g/cm^3. Table 3 presents all density data for cores used in the friction and fracture tests.

Average uncompressed porosities were determined as explained in a previous section on the basis that 1 cm^3 water weighs 1 g at room temperature. The values of mean rock densities are used in calculating average porosities, as shown in Table 4. The mean porosity of the limestone is 1.1 (±0.5)% and the mean sandstone porosity is 12.9 (±0.5)%.

Thin-section study. Two thin sections were made of each rock and photomicrographs were taken to aid in describing textures. Mineralogy, average grain dimensions, and degree of grain roundness were noted. A weighted average grain size for each of the rocks was also calculated and, along

TABLE 3. Uncompressed Density Determinations for Kelly Limestone and Mesa Verde Sandstone Cores Used in Fracture and Friction Experiments*

Sample	L_o (cm)	d_o (in)	M_o (g)	A_o (in^2)	V_o (cm^3)	ρ_o (g/cc)	ρ_m (g/cc)
Mesa Verde Ss.							
1	7.065	0.969	76.622	0.737	33.614	2.279	
2	7.045	0.970	77.182	0.739	33.588	2.298	
3	7.040	0.970	75.622	0.739	33.564	2.253	
4	7.375	0.968	80.600	0.736	35.016	2.302	
5	7.240	0.968	77.550	0.736	34.375	2.256	
6	6.497	1.017	80.575	0.812	34.050	2.311	
7	6.645	1.017	80.575	0.812	34.825	2.314	
8	6.314	1.017	75.027	0.812	33.091	2.267	2.285
Kelly Ls.							
1	6.995	0.969	88.250	0.737	33.281	2.652	
2	6.685	0.968	83.217	0.736	31.740	2.622	
3	6.790	0.968	85.005	0.736	32.239	2.637	
4	6.700	0.968	85.190	0.736	31.811	2.678	
5	5.805	0.973	75.505	0.744	27.847	2.711	
6	5.958	0.974	77.610	0.745	28.640	2.710	
7	6.030	0.975	78.550	0.747	29.046	2.704	
8	5.678	0.974	73.940	0.745	27.294	2.709	
9	6.274	0.975	81.610	0.747	30.221	2.700	
10	5.800	0.973	75.255	0.744	27.823	2.705	
11	5.936	0.973	77.125	0.744	28.476	2.708	
12	5.936	0.973	77.125	0.744	28.476	2.708	
13	5.994	0.975	77.900	0.747	28.872	2.698	
14	5.276	0.973	68.485	0.744	25.310	2.706	2.689

* L_o=average length of core
d_o=average diameter of core
M_o=mass of core
A_o=average cross-sectional core area
V_o=volume of core
ρ_o=density of individual core $=M_o/V_o$
ρ_m=mean density of cores

TABLE 4. Porosity Determinations for Kelly Limestone and Mesa Verde Sandstone Cores Used in Fracture and Friction Experiments*

Sample, ρ_m (g/cm^3)	M_d (g)	M_s (g)	ϕ (%)	ϕ_m (%)
Mesa Verde Sandstone, 2.285				
1	11.055	11.580	10.85	
2	9.698	10. 75	11.24	
3	14.910	15.660	11.49	
4	12.650	13.490	15.17	
5	11.710	12.515	15.71	12.9
Kelly Limestone, 2.689				
1	13.104	13.145	0.84	
2	10.546	10.595	1.25	
3	13.855	13.910	1.07	
4	6.105	6.135	1.32	
5	14.905	14.975	1.26	1.1

* ρ_m=mean density of core (from Table 3) = M_d/V_d
V_d=volume of dry specimen
M_d=mass of dry specimen
M_w=mass of water added during saturation
V_w=volume of water added = M_w (for 1 g H_2O = 1 cm^3 H_2O)
M_s=mass of saturated specimen = M_d+M_w = M_d+V_w
ϕ =porosity of specimen = $(V_w/V_d)100\%$ = $(\rho_m/M_d)(M_s-M_d)100\%$
ϕ_m=mean porosity for all specimens

with related petrographic data, is given in Appendix II.

The Kelly Limestone (Mississippian; Magdalena, N.M.) is a microcrystalline micritic limestone characterized by a high luster and a mosaic of tightly interlocking calcite crystals (Figure 9a). In thin section the calcite is very clear and transparent and has well-defined crystal faces. A few sparry calcite veins (~0.05-0.3 mm wide) are also present and grade texturally into the mosaic of calcite crystals. Staining techniques (Rodgers, 1940; Friedman, 1959) and CO_2 gas pressure tests (Müller and Gastner, 1971) give approximately 93% calcite and 7% dolomite and disseminated organic and detrital minerals. Further analysis, assuming 93% calcite and 7% dolomite, produces calculated densities and porosities which are nearly identical to the measured values in Tables 3 and 4 (see Appendix I). Most mineral grains are subangular, with an average diameter of approximately 0.01 mm (Appendix II).

The Mesa Verde Sandstone (Late Cretaceous; San Antonio, N.M.) is a fine-grained, well-sorted feldspathic (weathered) arenite with compacted, moderately porous texture (Figure 9b). Minerals present include quartz (75.3%), plagioclase (1.1%), microcline (0.7%), weathered feldspars (11.8%), and limonite (1.6%), in addition to some rock particles (0.7%). Most grains are subangular and 0.19 mm in diameter (Appendix II).

Fig. 9. (a) Optical micrograph of Kelly Limestone thin section under plane-polarized light. (b) Optical micrograph of Mesa Verde Sandstone thin section under plane-polarized light.

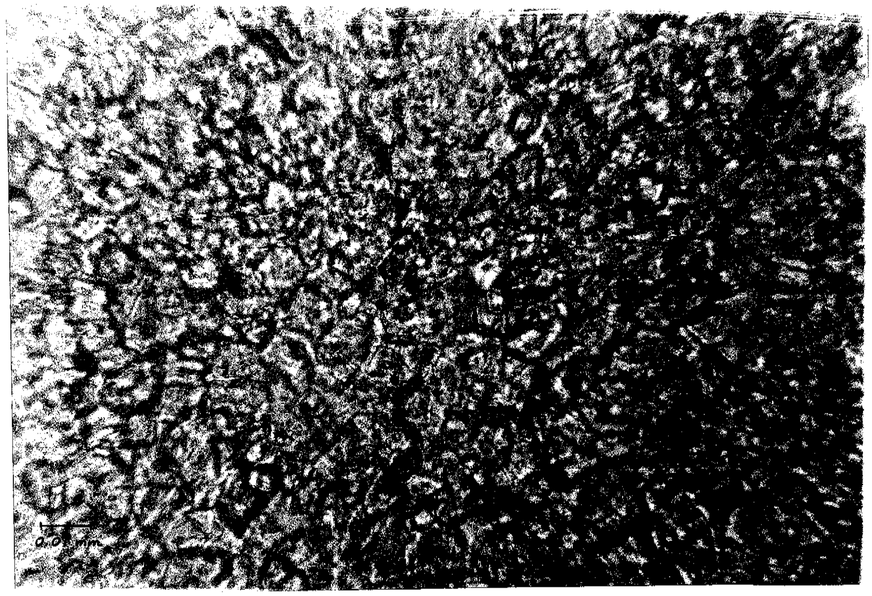

(a)

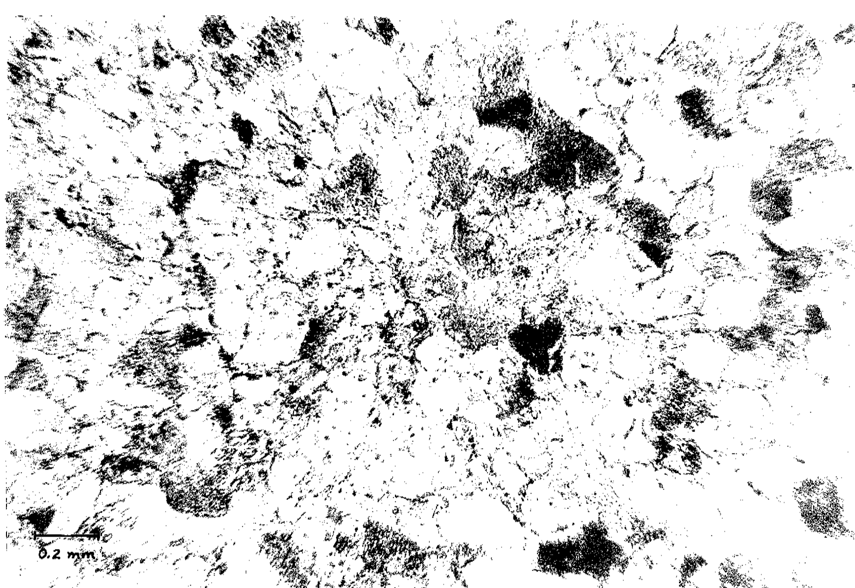

(b)

Optical Stress Analysis

In an effort to observe how applied stresses become concentrated along an irregularly polished sawcut, an optical stress analyzer (Vishay Stress Opticon) was used. In principle, the analyzer allows optical observations of stress-induced changes in birefringence patterns of photoelastic material with the use of optically polarized sheets (for a complete discussion of principles see: Post, 1965; Dally and Riley, 1965; or Durelli and Riley, 1965).

In the absence of gouge, stress trajectories associated with areas of high birefringence concentrate near the more parallel central parts of 30° and 45° sawcuts prepared through polishing by hand on #100 grit paper. Photographs of the birefringence patterns for $\alpha=30^{\circ}$ and $\alpha=45^{\circ}$ given in Figure 10 also show the apparent influence of protruding asperities along the surfaces, which produce local pockets of stress concentration.

In the presence of a thin layer of #80 silicon-carbide grit acting as gouge, the stress birefringence pattern is essentially the same as for the bare-surface tests; see Figure 11. This indicates that gouge becomes compacted only in regions where there is close contact and good surface

Fig. 10. Birefringence patterns in optical stress-sensitive material showing concentration of stress along central part of (a) 30° sawcut and (b) 45° sawcut polished by hand on #100 grit. Dark bands are stress trajectories; note especially those bands and point concentrations along the sawcuts.

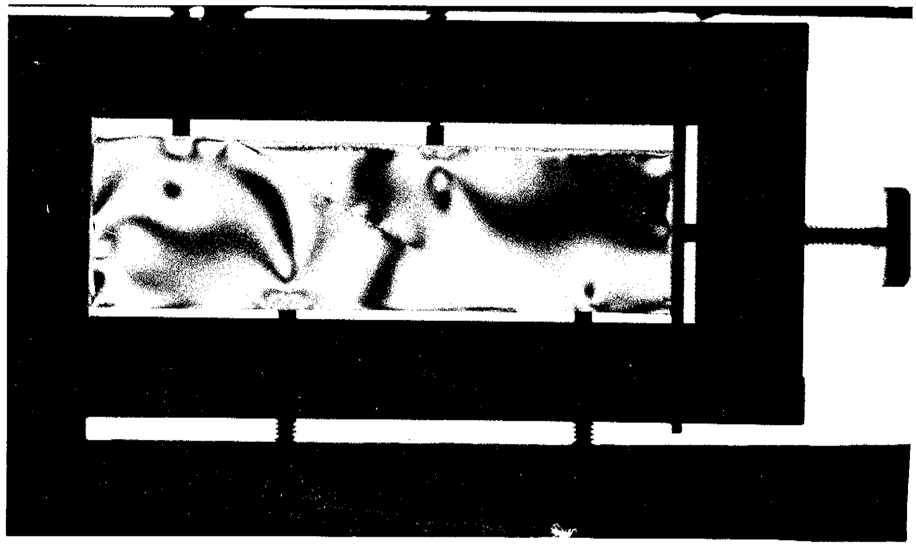

(a)

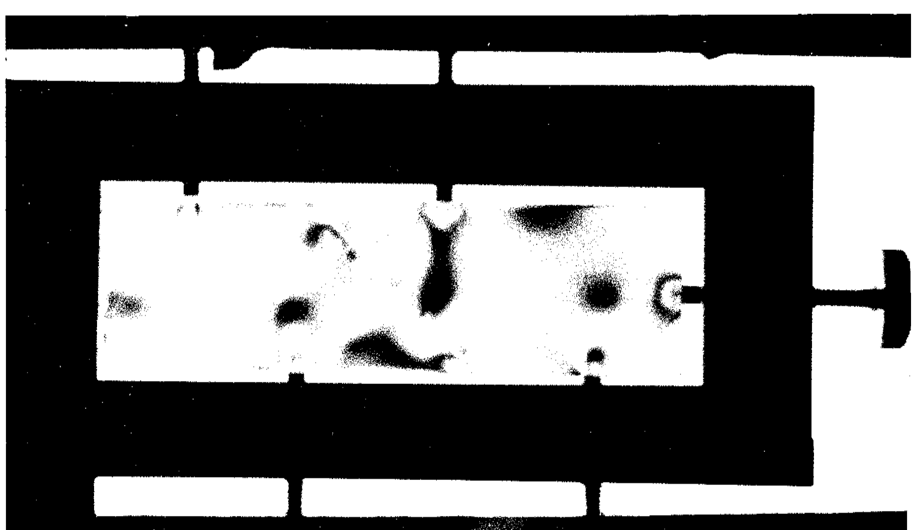

(b)

Fig. 11. Birefringence pattern in optical stress-sensitive material showing concentration of stress along central part of 45° sawcut polished by hand on #100 grit in presence of #80 silicon-carbide grit acting as gouge; note that gouge does not redistribute stress along entire sawcut.

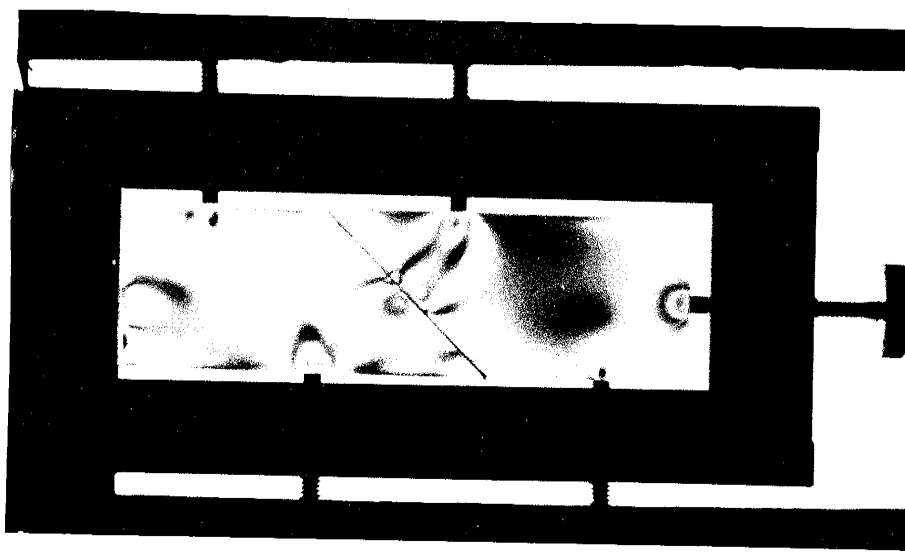

matching of the sawcut surfaces, and that gouge in other unmatched regions (along outer parts of the plastic material) does not support any appreciable stresses. Apparently most applied stress is supported where there occurs the greatest degree of gouge compaction, and the nature of frictional sliding is controlled only by the gouge properties along these restricted areas of the sawcut.

Fracture Tests

Fracture experiments on virgin cores of Kelly Limestone and Mesa Verde Sandstone were carried out at a constant displacement rate of $7 \cdot 10^{-4}$ cm/sec ($\approx 10^{-4}$ sec^{-1} strain rate) in an attempt to obtain an average value of Young's modulus, the fracture-strength (Mohr) envelope, and resistance to fracture μ_f (Equation 8') vs. σ for each of the rock types. Stress vs. strain curves for seven limestone and five sandstone cores are given in Figures 12 and 13 on the basis of original load-displacement data presented in Appendix II (Tables AII-1 to AII-12). Table 5 lists Young's modulus for each test and a resulting average modulus for each rock, in addition to measured fracture angles and (σ, τ) least-square data. Mohr envelopes of τ vs. σ at fracture are presented in Figures 14 and 15, and variations of μ_f as a function of σ are given in Figures 16 and 17.

Fig. 12. Differential stress vs. strain curves for Kelly Limestone; ordinate is given in both psi (10^3) and bars (10^1).

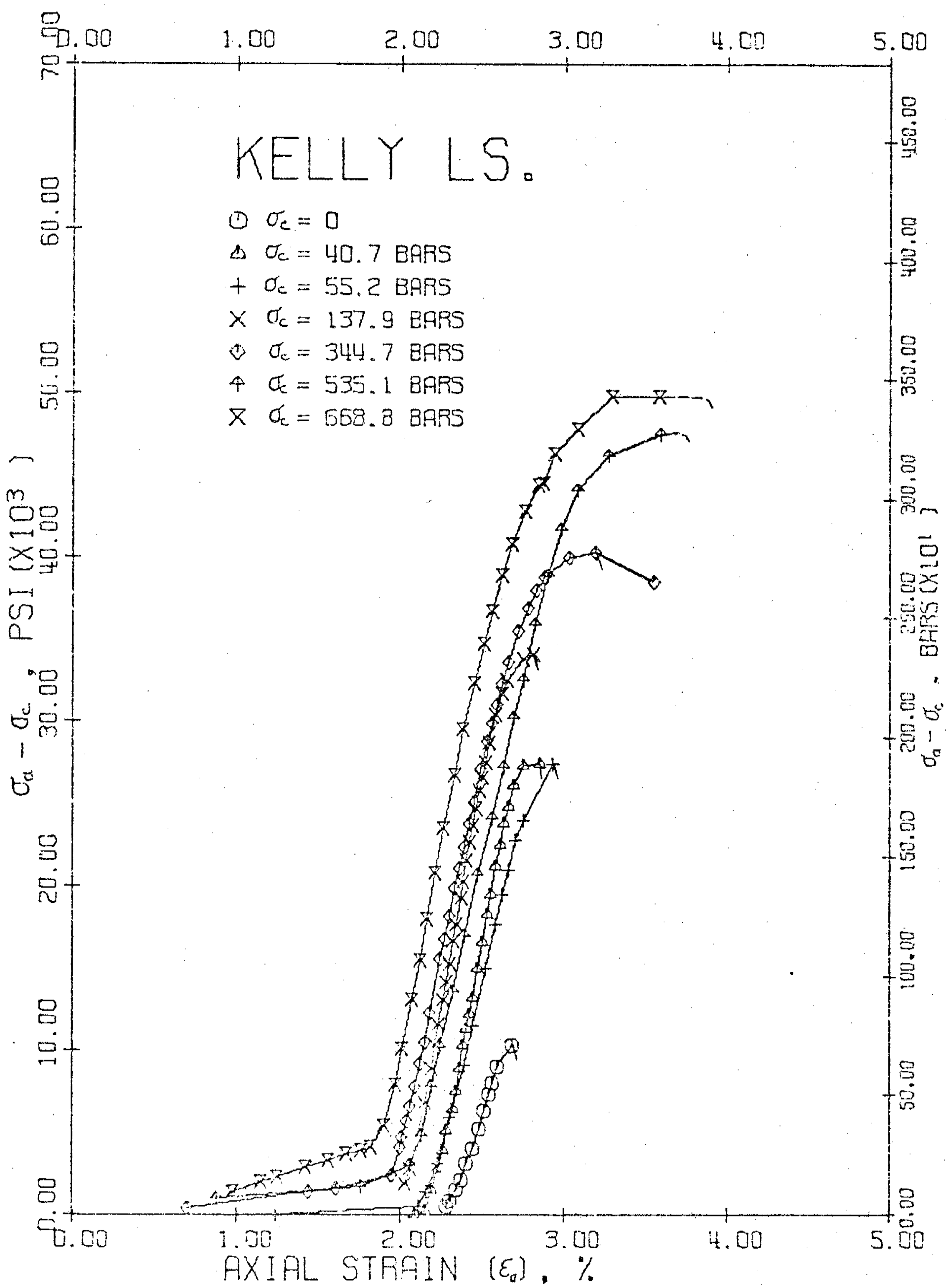
KELLY LS.
σc = 0
σc = 40.7 BARS
σc = 55.2 BARS
σc = 137.9 BARS
σc = 344.7 BARS
σc = 535.1 BARS
σc = 668.8 BARS
σa − σc , PSI (X10³)
σa − σc , BARS (X10¹)
AXIAL STRAIN (εa) , %
0.00
1.00
2.00
3.00
4.00
5.00
10.00
20.00
30.00
40.00
50.00
60.00
70.00
50.00
100.00
150.00
200.00
250.00
300.00
350.00
400.00
450.00

Fig. 13. Differential stress vs. strain curves for Mesa Verde Sandstone.

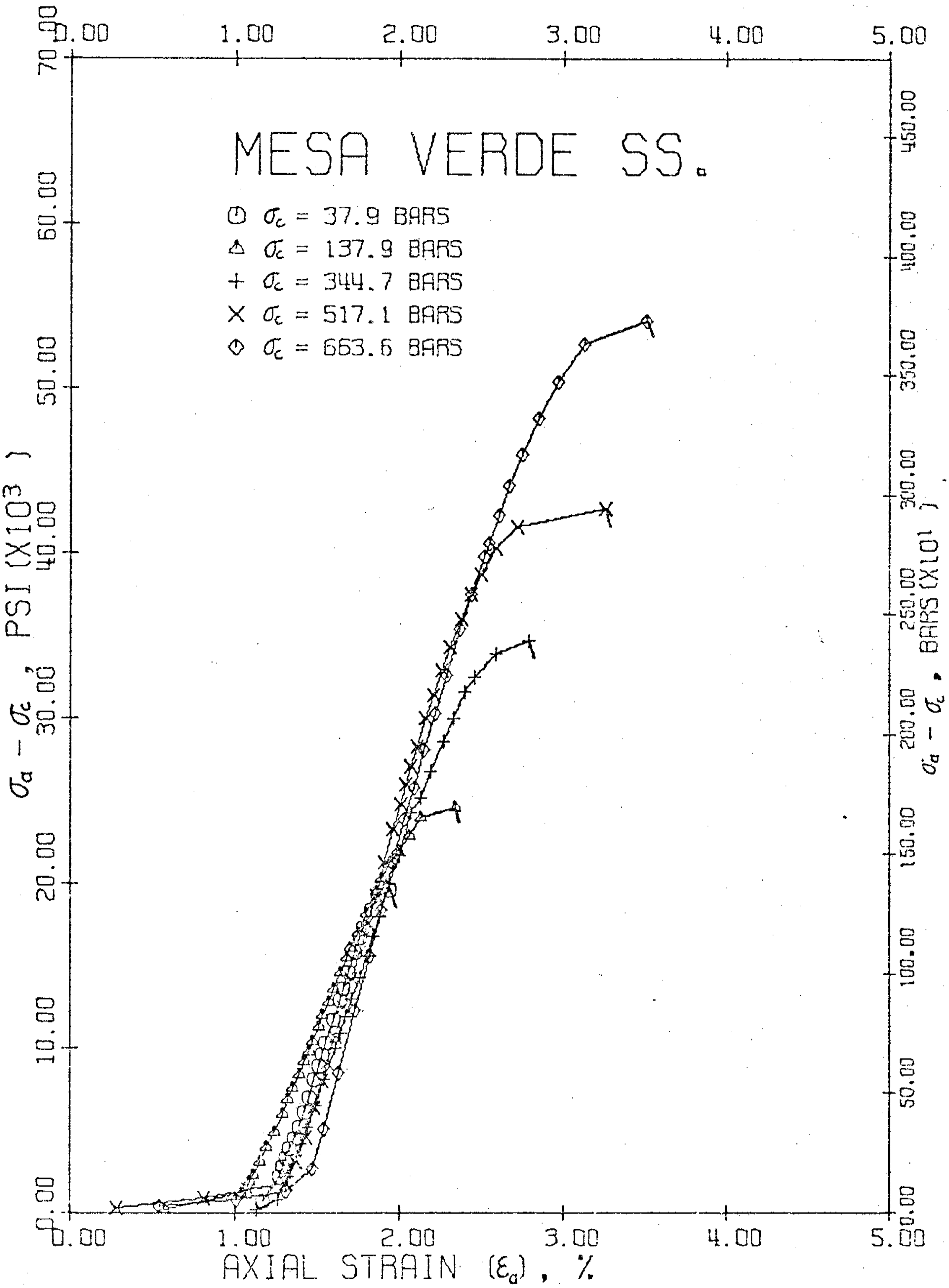

MESA VERDE SS.
○ σ_c = 37.9 BARS
△ σ_c = 137.9 BARS
+ σ_c = 344.7 BARS
× σ_c = 517.1 BARS
◇ σ_c = 663.6 BARS
$\sigma_a - \sigma_c$, PSI (X10^3)
$\sigma_a - \sigma_c$, BARS (X10^1)
AXIAL STRAIN (ε_a), %
0.00
1.00
2.00
3.00
4.00
5.00
10.00
20.00
30.00
40.00
50.00
60.00
70.00
50.00
100.00
150.00
200.00
250.00
300.00
350.00
400.00
450.00

TABLE 5. Mechanical Properties during Deformation and Fracture of Kelly Limestone and Mesa Verde Sandstone

Elastic Deformation			Fracture			Least-Sq. Data		
σ_c (psi)	E (Mbar)	E_{ave} (Mbar)	α_{meas} (deg.)	τ (psi)	σ (psi)	A (psi)	B (psi)	n
Kelly Limestone								
0	0.213		23	3585	1448			
590	0.368		25	10494	5483			
800	0.291		26	10791	6063			
2000	0.379		28	14126	9511			
5000	0.321		38	16703	13881			
7400	0.305		32	21352	20863			
9700	0.345	0.317	35	23107	25286			
						$-2.69 \cdot 10^7$	32000	2.04
Mesa Verde Sandstone								
550	0.211		27	8022	4637			
2000	0.162		29	10444	7789			
5000	0.197		31	15332	14212			
7500	0.238		32	19177	19483			
9625	0.256	0.213	38	26250	30134			
						20650	6.2	1.20

Fig. 14. Mohr envelope for Kelly Limestone; stresses are given in both psi (10^3) and bars (10^1).

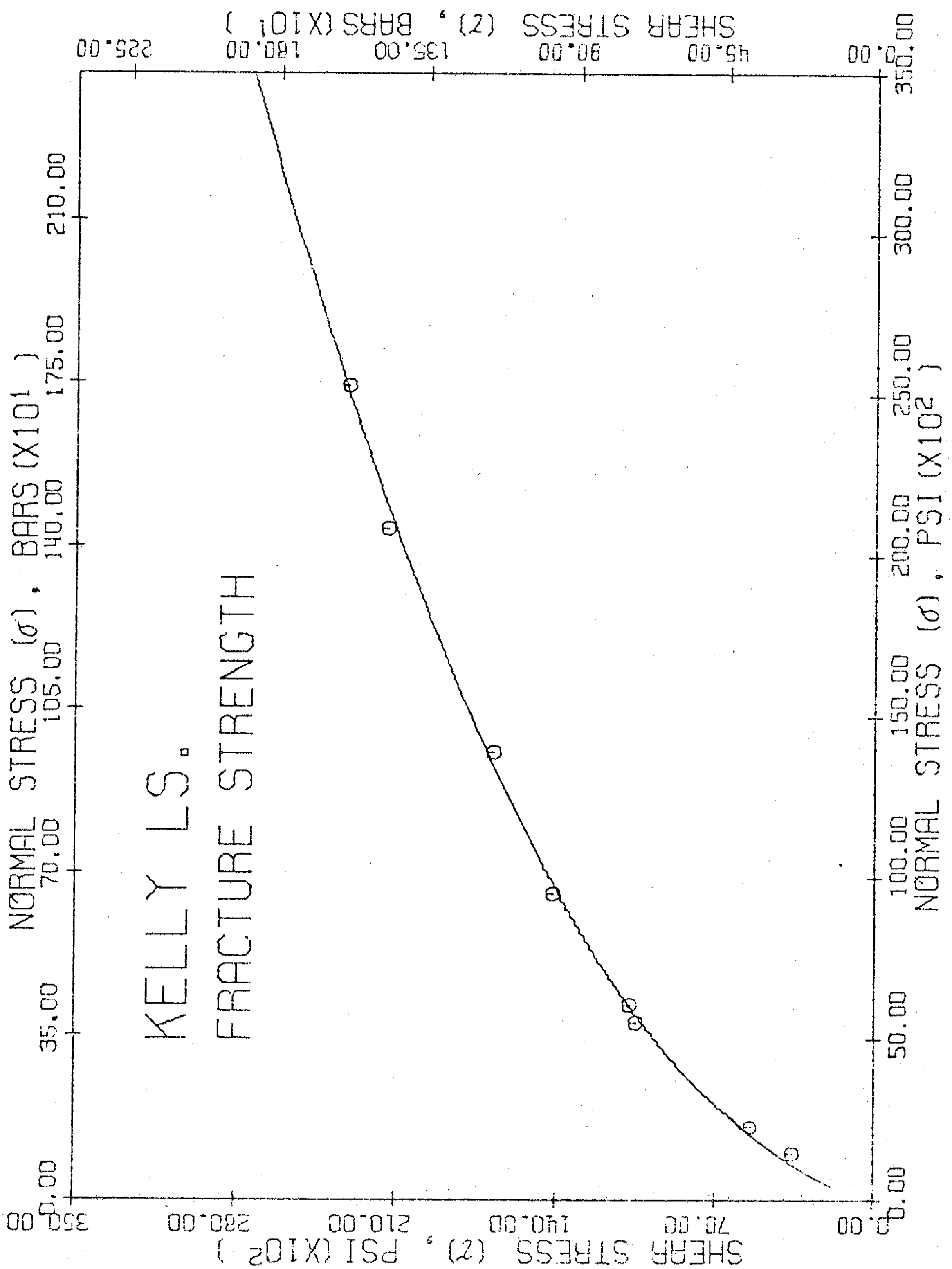
KELLY LS.
FRACTURE STRENGTH
NORMAL STRESS (σ), BARS (X10¹)
0.00
35.00
70.00
105.00
140.00
175.00
210.00
NORMAL STRESS (σ), PSI (X10²)
0.00
50.00
100.00
150.00
200.00
250.00
300.00
350.00
SHEAR STRESS (τ), BARS (X10¹)
0.00
45.00
90.00
135.00
180.00
225.00
SHEAR STRESS (τ), PSI (X10²)
0.00
70.00
140.00
210.00
280.00
350.00

Fig. 15. Mohr envelope for Mesa Verde Sandstone.

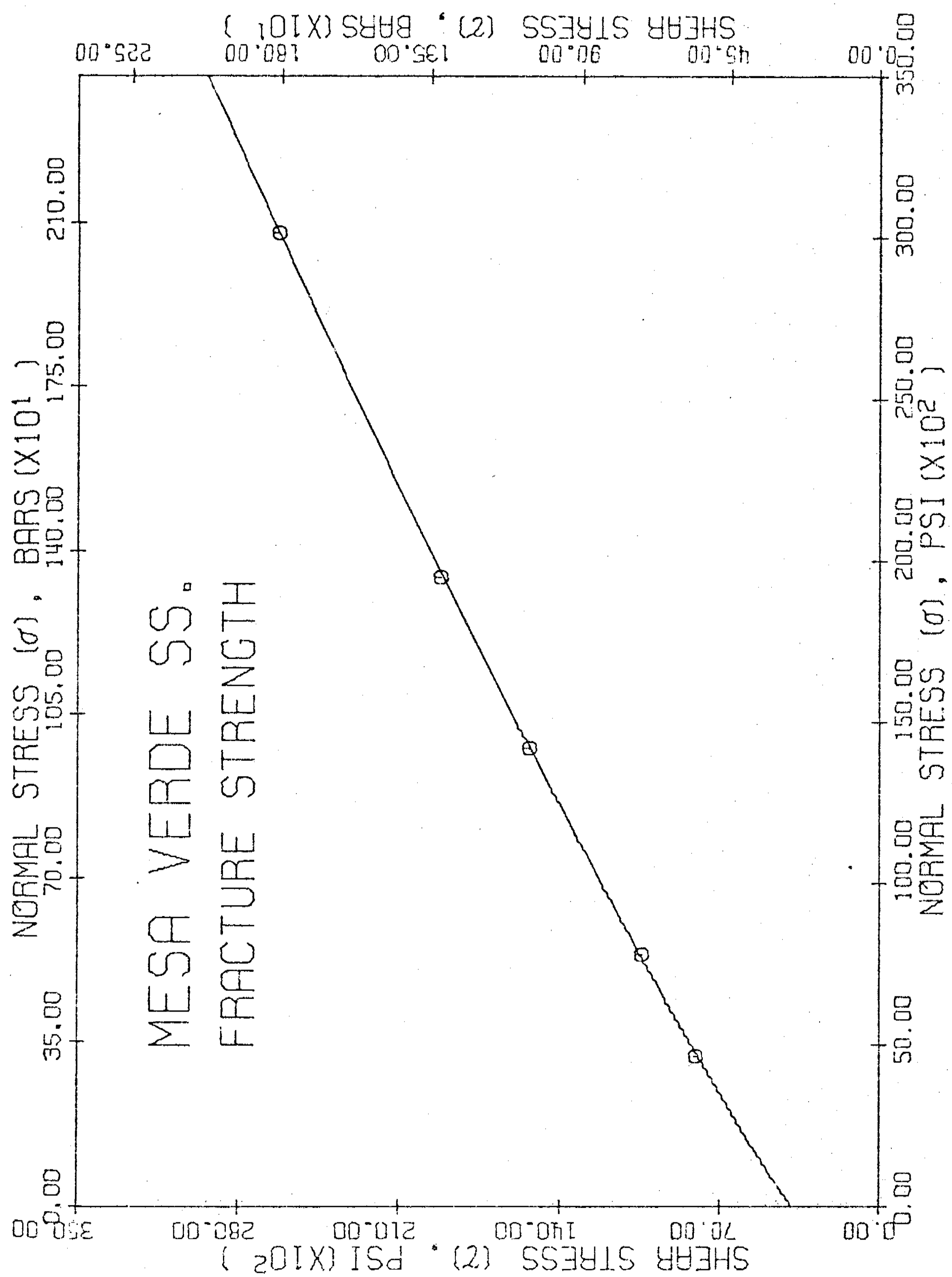
MESA VERDE SS.
FRACTURE STRENGTH
NORMAL STRESS (σ), BARS (X10^1)
0.00
35.00
70.00
105.00
140.00
175.00
210.00
NORMAL STRESS (σ), PSI (X10^2)
0.00
50.00
100.00
150.00
200.00
250.00
300.00
350.00
SHEAR STRESS (τ), BARS (X10^1)
0.00
45.00
90.00
135.00
180.00
225.00
SHEAR STRESS (τ), PSI (X10^2)
0.00
70.00
140.00
210.00
280.00
350.00

Fig. 16. Ratio of $\tau(\sigma)$ to σ at fracture (fracture resistance) vs. σ for Kelly Limestone.

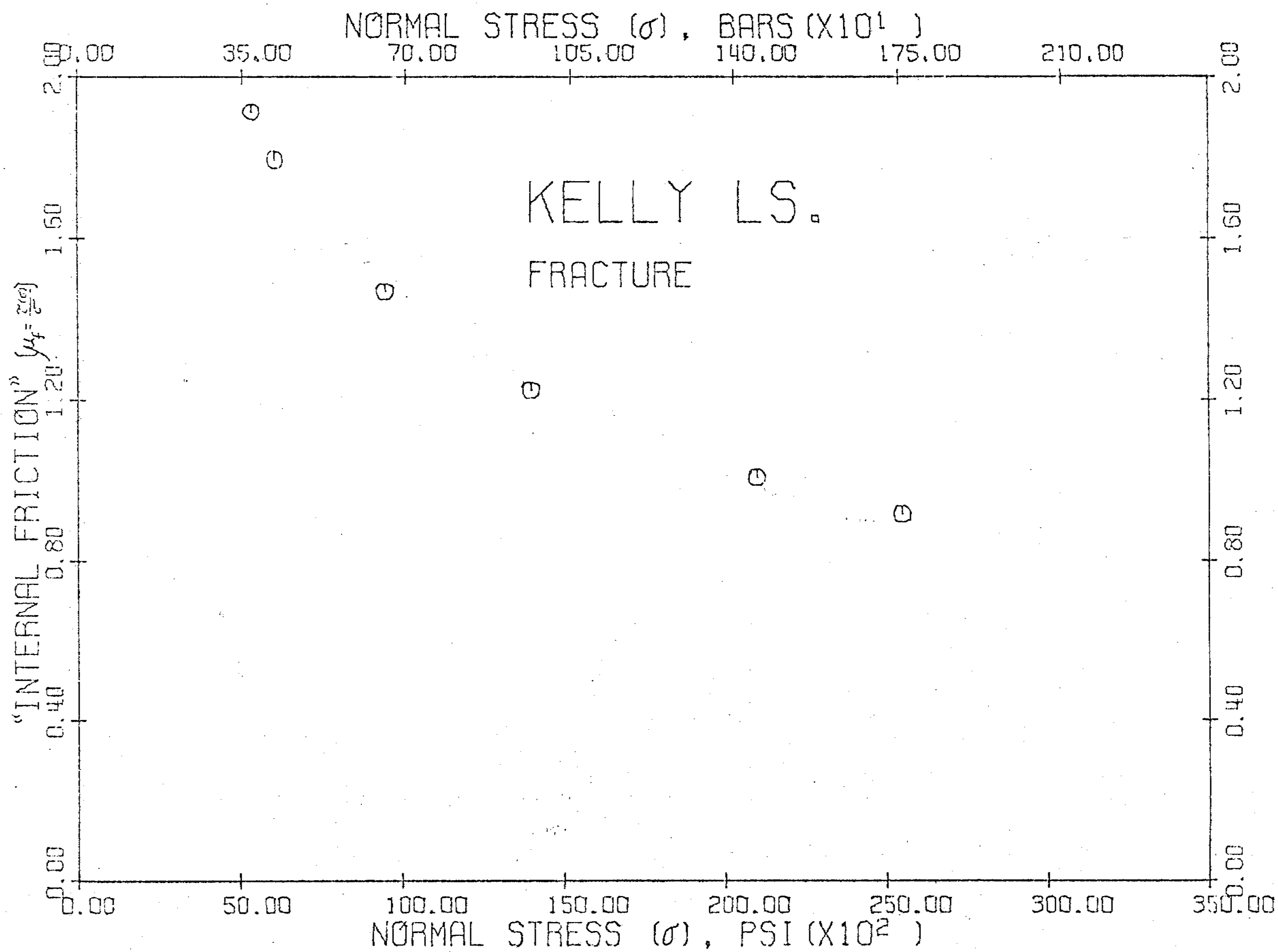
NORMAL STRESS (σ), BARS (X10¹)
0.00
35.00
70.00
105.00
140.00
175.00
210.00
KELLY LS.
FRACTURE
"INTERNAL FRICTION"
0.00
0.40
0.80
1.20
1.60
2.00
NORMAL STRESS (σ), PSI (X10²)
0.00
50.00
100.00
150.00
200.00
250.00
300.00
350.00

Fig. 17. Ratio of $\tau(\sigma)$ to σ at fracture (fracture resistance) vs. σ for Mesa Verde Sandstone.

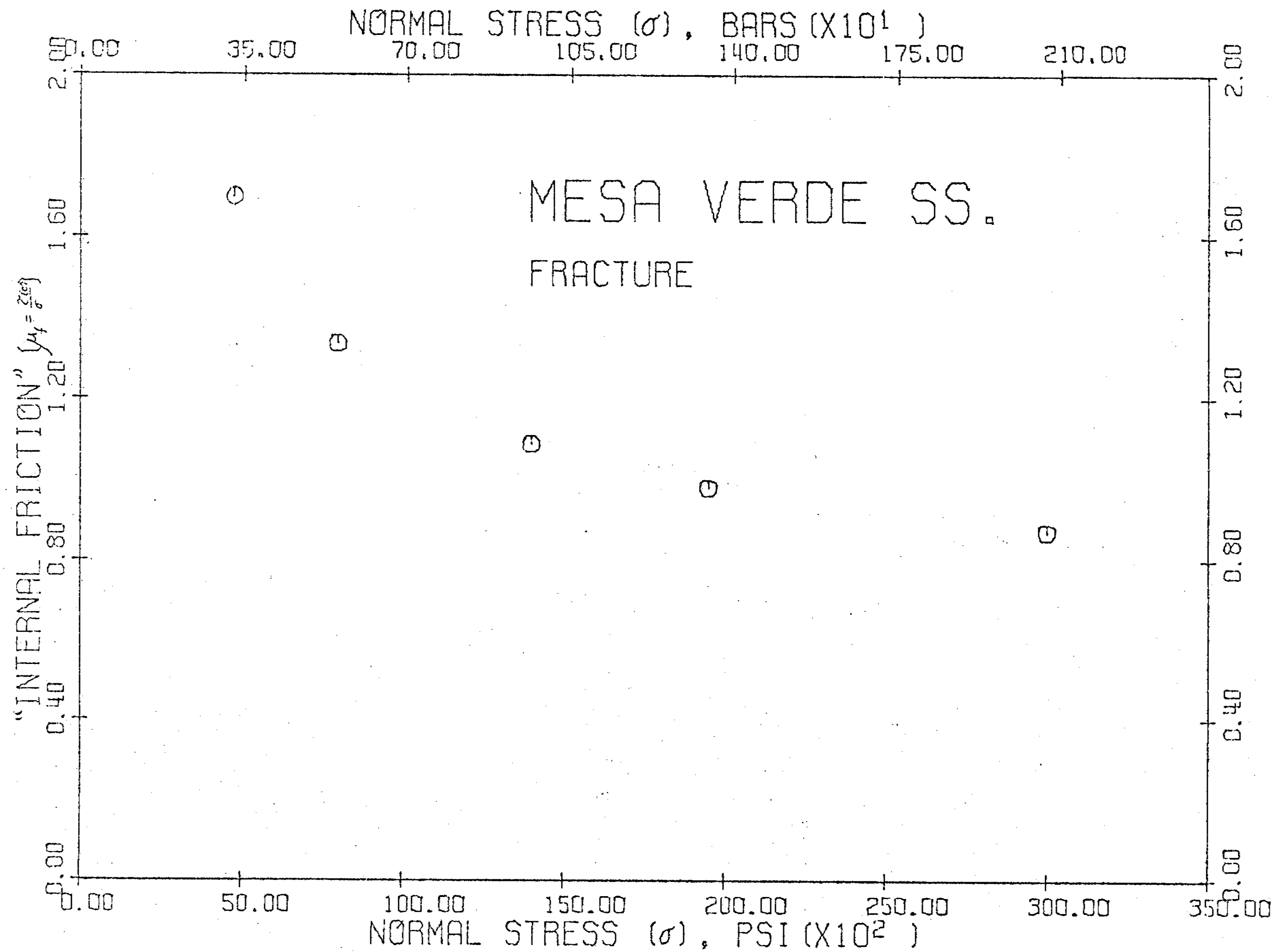
NORMAL STRESS (σ), BARS (X10¹)
0.00 35.00 70.00 105.00 140.00 175.00 210.00
MESA VERDE SS.
FRACTURE
"INTERNAL FRICTION" ($\mu_f = \frac{\tau(\sigma)}{\sigma}$)
0.00 0.40 0.80 1.20 1.60 2.00
0.00 50.00 100.00 150.00 200.00 250.00 300.00 350.00
NORMAL STRESS (σ), PSI (X10²)

Friction Tests without Gouge

Friction experiments were conducted on Kelly Limestone and Mesa Verde Sandstone cores containing sawcuts at $\alpha = 45^{\circ}$ (unless otherwise specified) which were polished on #100- and #600-grit polishing paper. As noted above, all friction experiments were made at constant displacement rates, in this case at approximately $7 \cdot 10^{-4}$ cm/sec ($\approx 10^{-4}$ sec^{-1} strain rate), and at maximum displacements of ±0.01 in.

The graphs of τ vs. σ for the #100 grit, #600 grit, and a #100 grit duplicate test for both the limestone and sandstone involving uncorrected, partial-contact areas (A_o) are given in Figures 18 and 19. Similarly, graphs of the controlled-area (A_c') tests in which different areas (also circular vs. square) are given in Figures 20 and 21, while results of original partial-contact area tests standardized by accounting for partial contact (using A_o') are given in Figures 22 and 23. Least-square curves according to Equations 5, 6, and 9 are also shown for each data set; the least-square constants are presented in Table 6. The equations, computer programs, and original data used in calculating the (σ,τ) values and the least-square curves (including R^2) are given in Appendix II (Tables AII-13 to AII-28) and Appendix III.

Fig. 18. Shear stress vs. normal stress uncorrected for partial contact for sliding experiments without gouge on Kelly Limestone.

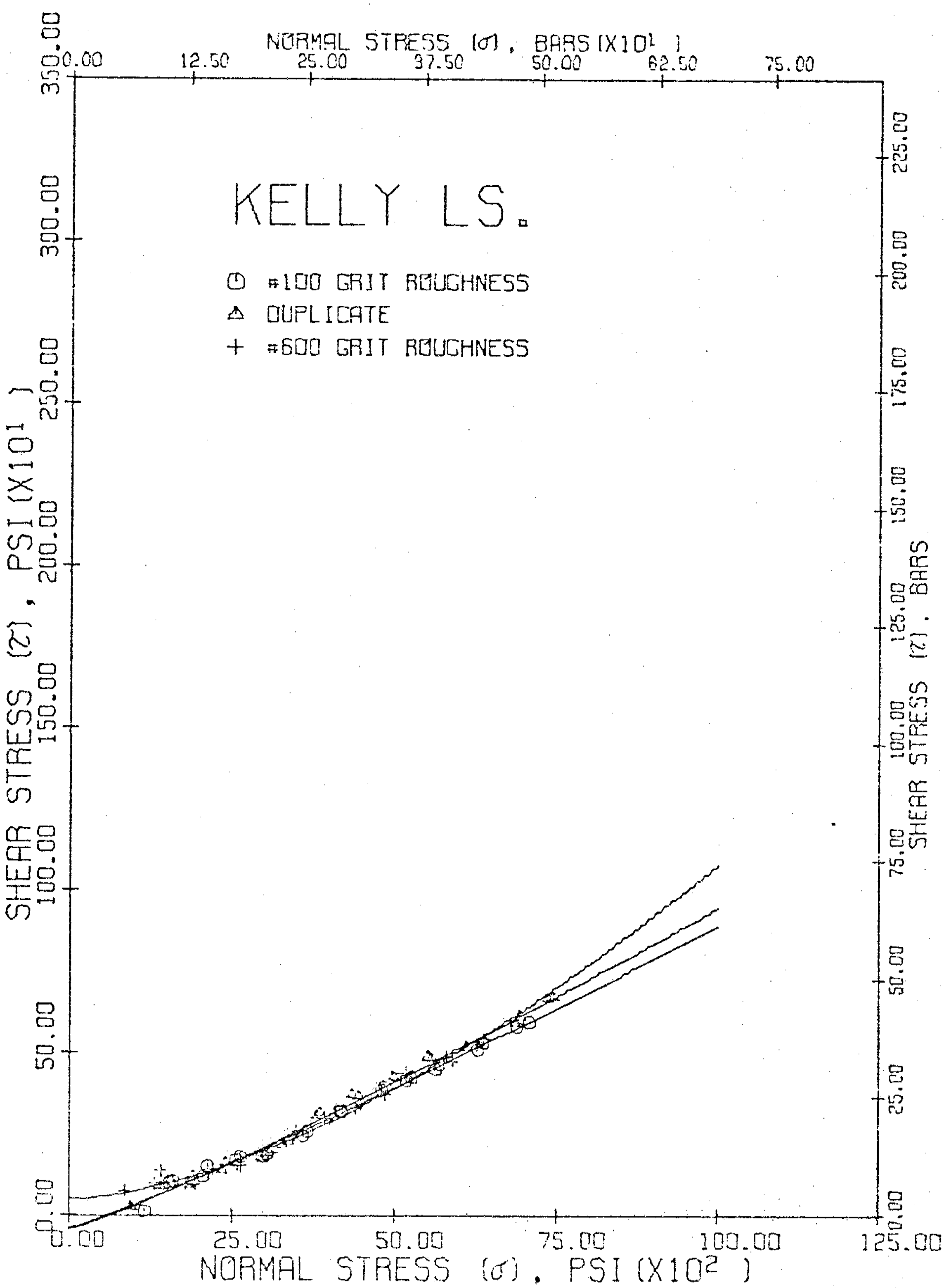
NORMAL STRESS (σ), BARS (X10^1)
0.00
12.50
25.00
37.50
50.00
62.50
75.00
KELLY LS.
#100 GRIT ROUGHNESS
DUPLICATE
#600 GRIT ROUGHNESS
SHEAR STRESS (τ), PSI (X10^1)
350.00
300.00
250.00
200.00
150.00
100.00
50.00
0.00
SHEAR STRESS (τ), BARS
225.00
200.00
175.00
150.00
125.00
100.00
75.00
50.00
25.00
0.00
NORMAL STRESS (σ), PSI (X10^2)
0.00
25.00
50.00
75.00
100.00
125.00

Fig. 19. Shear stress vs. normal stress uncorrected for partial contact for sliding experiments without gouge on Mesa Verde Sandstone.

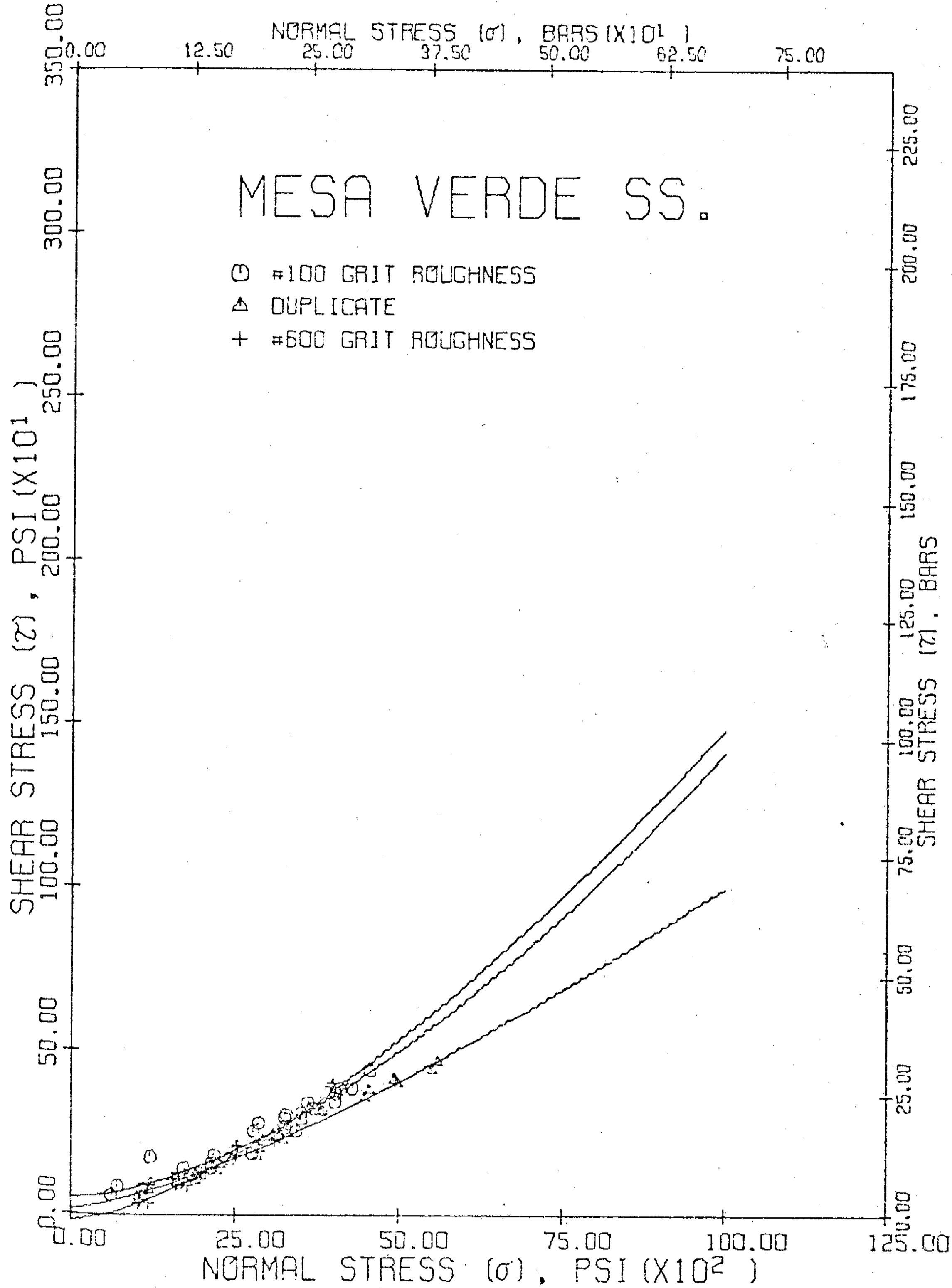
NORMAL STRESS (σ), BARS (X10¹)
0.00
12.50
25.00
37.50
50.00
62.50
75.00
MESA VERDE SS.
#100 GRIT ROUGHNESS
DUPLICATE
#600 GRIT ROUGHNESS
SHEAR STRESS (τ), PSI (X10¹)
0.00
50.00
100.00
150.00
200.00
250.00
300.00
350.00
SHEAR STRESS (τ), BARS
25.00
50.00
75.00
100.00
125.00
150.00
175.00
200.00
225.00
NORMAL STRESS (σ), PSI (X10²)
0.00
25.00
50.00
75.00
100.00
125.00

Fig. 20. Shear stress vs. normal stress for friction experiments involving perfectly-matched controlled surfaces of contact in Kelly Limestone; note negligible difference between tests with and without synthetic limestone gouge.

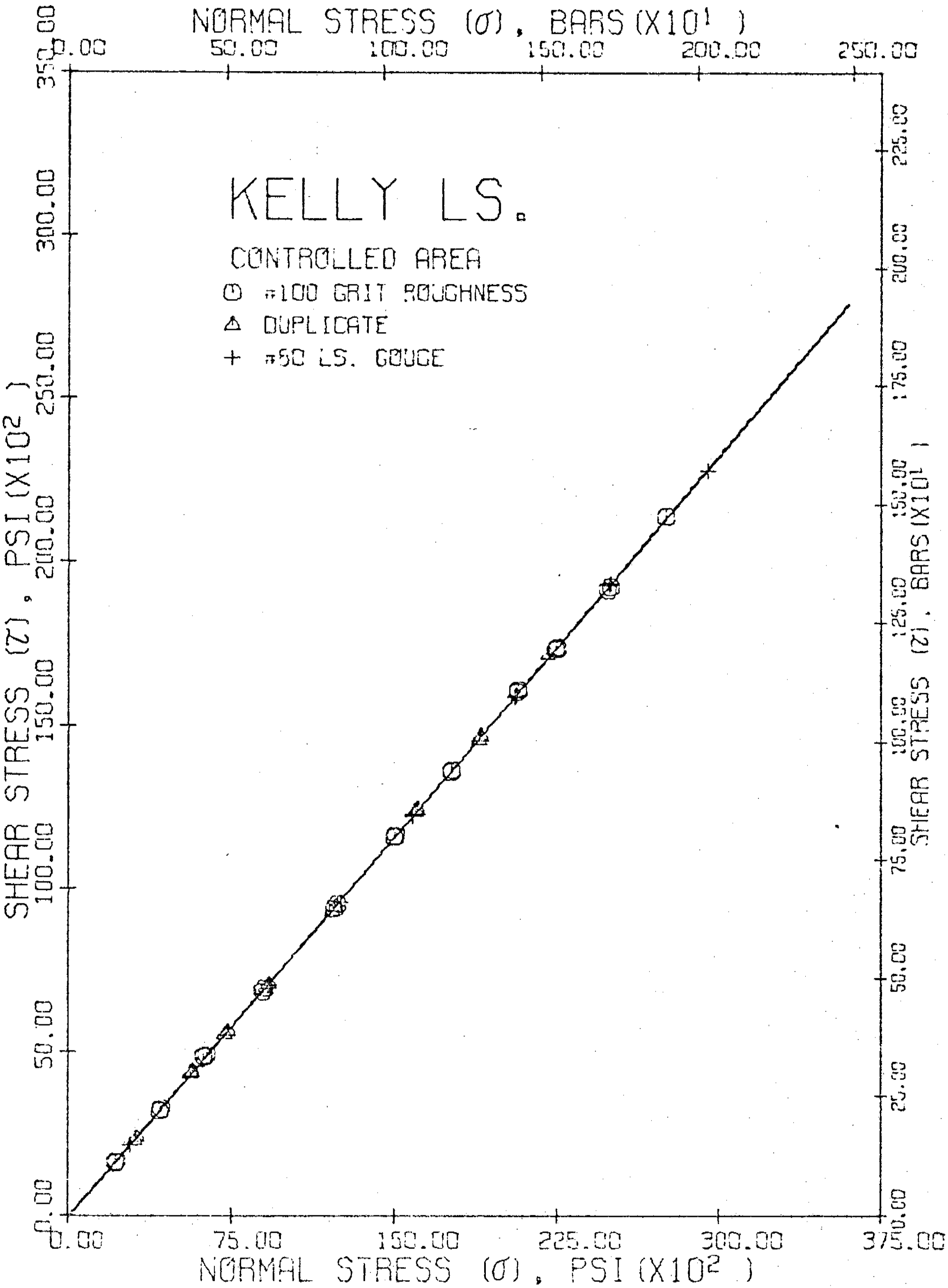
NORMAL STRESS (σ), BARS (X10¹)
0.00
50.00
100.00
150.00
200.00
250.00
KELLY LS.
CONTROLLED AREA
#100 GRIT ROUGHNESS
DUPLICATE
#50 LS. GOUGE
SHEAR STRESS (τ), PSI (X10²)
0.00
50.00
100.00
150.00
200.00
250.00
300.00
350.00
SHEAR STRESS (τ), BARS (X10¹)
25.00
50.00
75.00
100.00
125.00
150.00
175.00
200.00
225.00
NORMAL STRESS (σ), PSI (X10²)
75.00
150.00
225.00
300.00
375.00

Fig. 21. Shear stress vs. normal stress for friction experiments involving perfectly-matched controlled surfaces of contact in Mesa Verde Sandstone; note negligible difference between run with and without synthetic sandstone gouge.

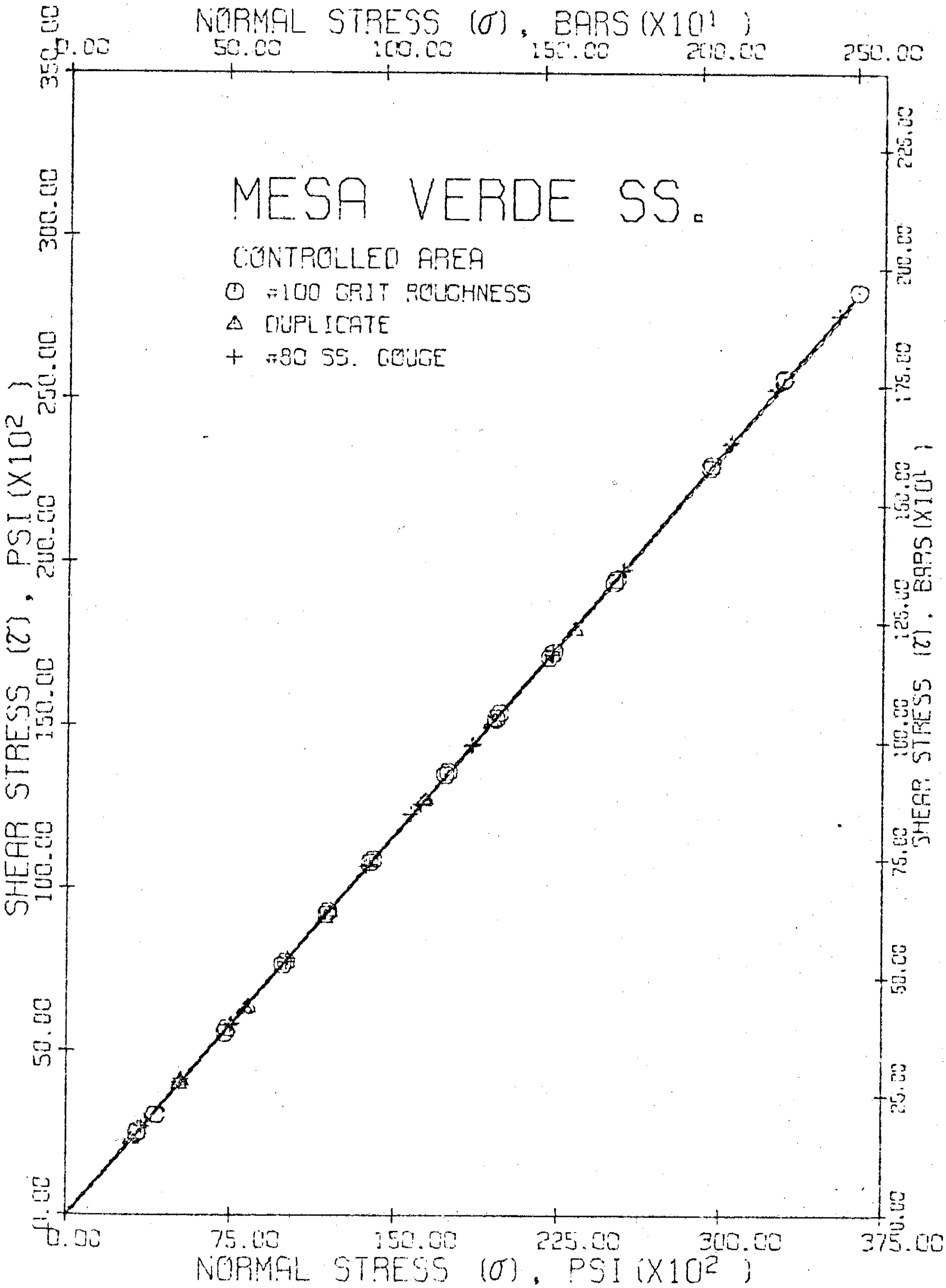
NORMAL STRESS (σ), BARS (X10¹)
0.00
50.00
100.00
150.00
200.00
250.00
MESA VERDE SS.
CONTROLLED AREA
○ #100 GRIT ROUGHNESS
△ DUPLICATE
+ #80 SS. GOUGE
SHEAR STRESS (τ), PSI (X10²)
0.00
50.00
100.00
150.00
200.00
250.00
300.00
350.00
SHEAR STRESS (τ), BARS (X10¹)
0.00
25.00
50.00
75.00
100.00
125.00
150.00
175.00
200.00
225.00
0.00
75.00
150.00
225.00
300.00
375.00
NORMAL STRESS (σ), PSI (X10²)

Fig. 22. Shear stress vs. normal stress, corrected for partial contact, for friction experiments without gouge on Kelly Limestone.

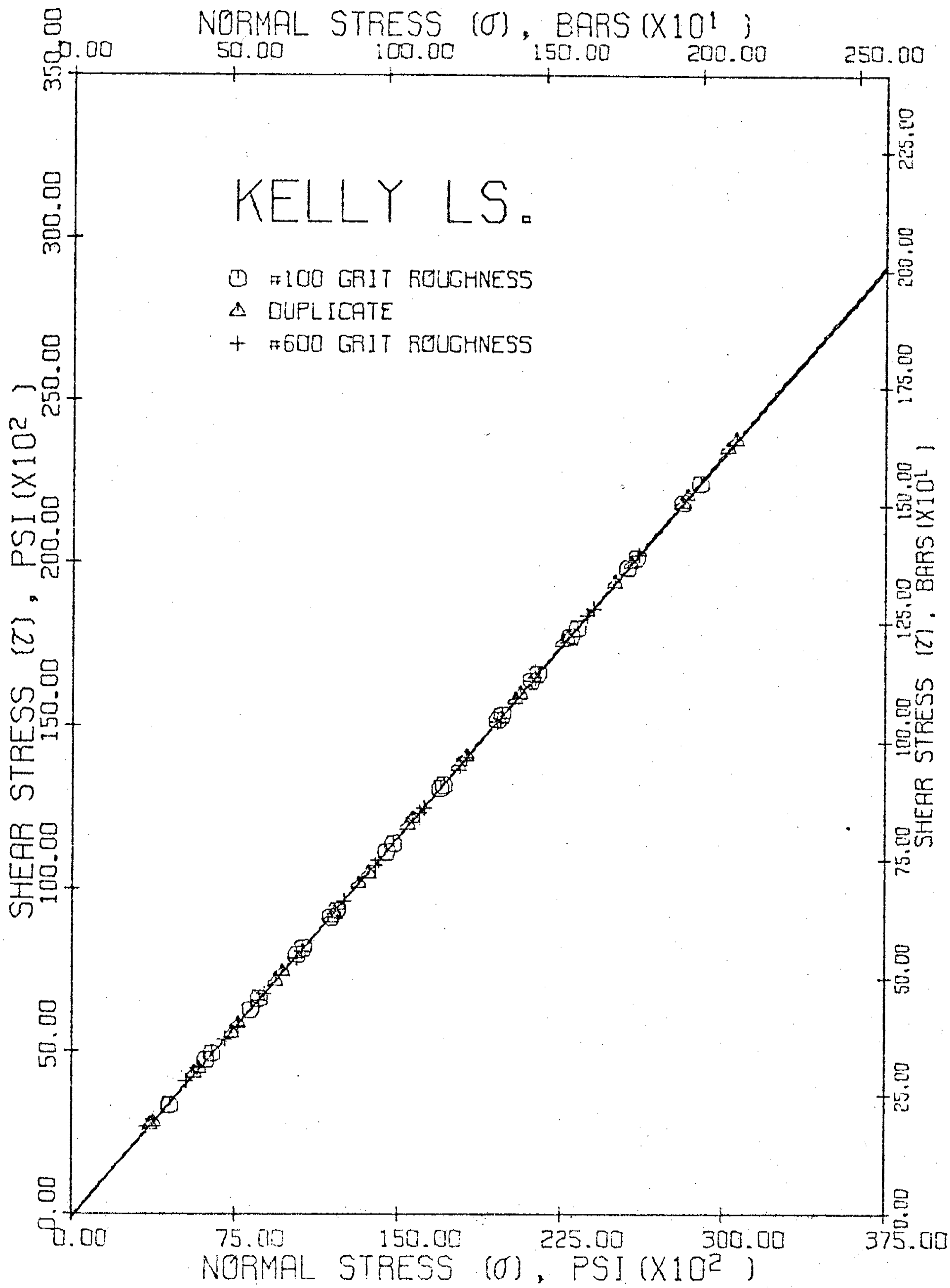
NORMAL STRESS (σ), BARS (X10¹)
0.00
50.00
100.00
150.00
200.00
250.00
KELLY LS.
#100 GRIT ROUGHNESS
DUPLICATE
#600 GRIT ROUGHNESS
SHEAR STRESS (τ), PSI (X10²)
0.00
50.00
100.00
150.00
200.00
250.00
300.00
350.00
SHEAR STRESS (τ), BARS (X10¹)
25.00
75.00
125.00
175.00
225.00
0.00
75.00
150.00
225.00
300.00
375.00
NORMAL STRESS (σ), PSI (X10²)

Fig. 23. Shear stress vs. normal stress, corrected for partial contact, for friction experiments without gouge on Mesa Verde Sandstone.

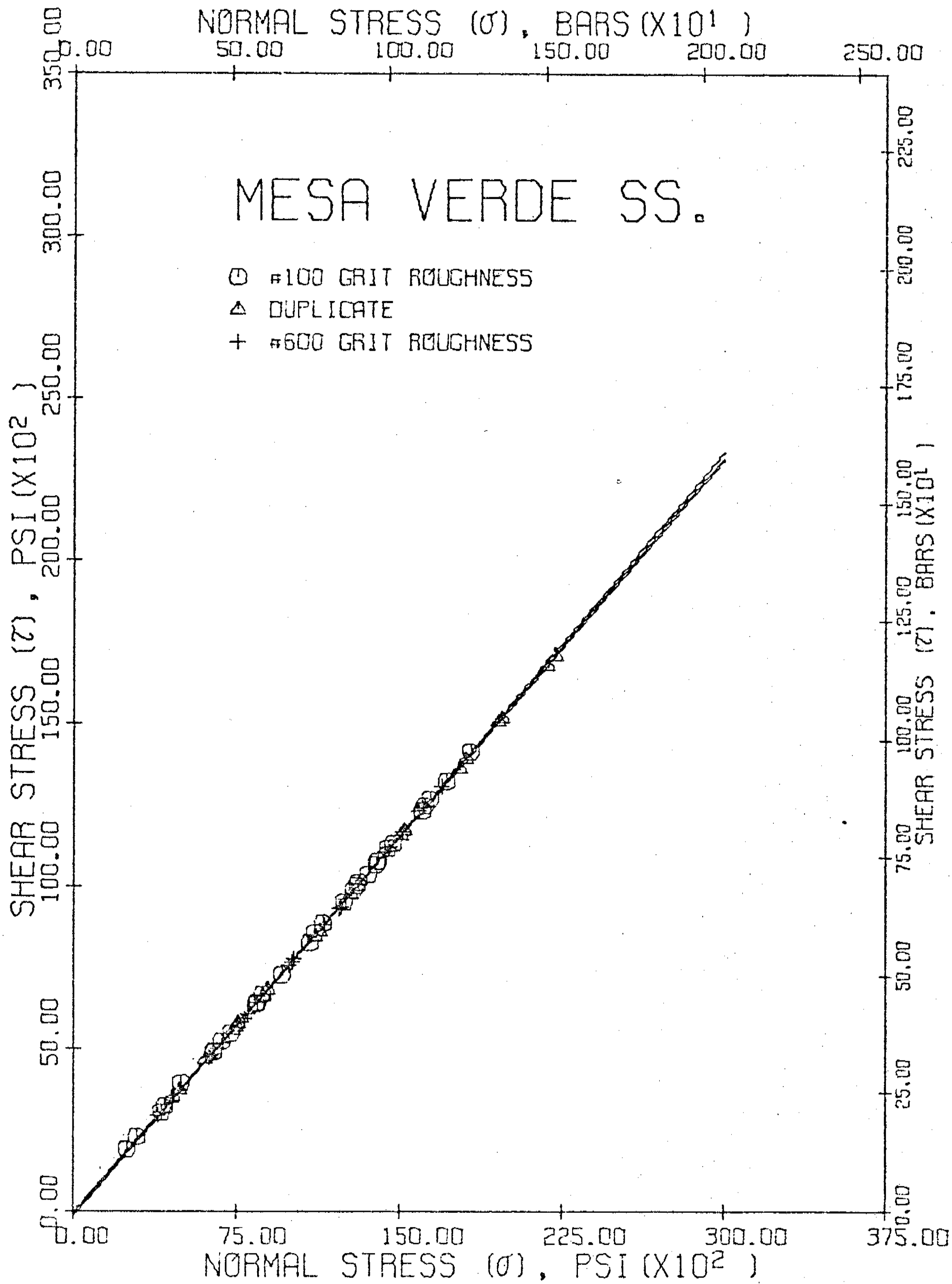
NØRMAL STRESS (σ), BARS (X10¹)
0.00
50.00
100.00
150.00
200.00
250.00
MESA VERDE SS.
⊙ #100 GRIT RØUGHNESS
△ DUPLICATE
+ #600 GRIT RØUGHNESS
SHEAR STRESS (τ), PSI (X10²)
0.00
50.00
100.00
150.00
200.00
250.00
300.00
350.00
SHEAR STRESS (τ), BARS (X10¹)
0.00
25.00
50.00
75.00
100.00
125.00
150.00
175.00
200.00
225.00
NØRMAL STRESS (σ), PSI (X10²)
0.00
75.00
150.00
225.00
300.00
375.00

TABLE 6. Least-Square Data $\tau=\tau_o+B\sigma^n$ for Bare-Surface Friction Experiments on Kelly Limestone and Mesa Verde Sandstone at $\alpha=45^o$ Using Uncorrected, Corrected, and Controlled Surface Areas

Experimental Condition	τ_o (psi)	τ_o (bars)	B <psi>	B <bars>	n	R^{2*} (%)
Kelly Limestone (A_o=0.74; A_o'=0.110; A_c'=0.108 in^2)						
#100 Grit Roughness						
Uncorrected Area	-39	-2.7	0.0372	0.0486	1.100	99.3
Corrected Area	-111	-7.6	0.780		1.000	100.0
Controlled Area	-52	-3.6	0.776		1.000	100.0
Duplicate						
Uncorrected Area	-45	-3.1	0.0348	0.0472	1.114	99.3
Corrected Area	-127	-8.7	0.782		1.000	100.0
Controlled Area	-99	-6.9	0.779		1.000	100.0
#600 Grit Roughness						
Uncorrected Area	49	3.4	0.0005	0.0023	1.580	98.5
Corrected Area	-77	-5.3	0.778		1.000	100.0
Mesa Verde Sandstone (A_o=0.74; A_o'=0.104; A_c'=0.108 and 0.111 in^2						
#100 Grit Roughness						
Uncorrected Area	50	3.5	0.0005	0.0026	1.603	94.4
Corrected Area	-40	-2.8	0.774		1.000	100.0
Controlled Area	-90	-6.2	0.781		1.000	100.0
Duplicate						
Uncorrected Area	16	1.1	0.0052	0.0123	1.319	98.8
Corrected Area	-76	-5.3	0.772		1.000	100.0
Controlled Area	-55	-3.8	0.776		1.000	100.0
#600 Grit Roughness						
Uncorrected Area	-19	-1.3	0.0024	0.0080	1.448	98.7
Corrected Area	-165	-11.4	0.783		1.000	100.0

* R^2 = correlation coefficient (see text)

Coefficients of friction, $\mu=\tau/\sigma$ (Equations 7 and 8), as a function of normal stress σ were determined for each of the cases using the least-square functions representing A_o, A_c', and A_o' (σ,τ) data. Graphs of μ vs. σ using A_o are given in Figures 24 and 25, for A_c' in Figures 26 and 27, and for A_o' in Figures 28 and 29.

Friction Tests with Gouge

Uncompacted limestone and sandstone gouge was formed by crushing respective samples and sieving to obtain #80- and #230-size fractions. The nature of the gouge, such as uniformity of grain size and degree of angularity, was observed under reflected light with a microscope (see "Photography" section). The coarser #80 gouge has grain sizes ranging from 0.0070 in (0.18 mm) to 0.0083 in (0.21 mm), while the finer fraction contains particles less than 0.0024 in (0.061 mm)-diameter, including some clay-sized particles.

Friction experiments for $\alpha=45^{\circ}$ and 1-mm gouge thickness were conducted using dry and wet #80 and >#230 gouge with geometrically unmatched sawcut surfaces and using A_o in calculating τ and σ. Controlled-area tests with #80 dry gouge using A_c' were also run, and equivalent partial-contact areas A_o' were calculated to take into account partial contact during the original runs. The (σ,τ) data for each case (see

Fig. 24. $\mu=\tau(\sigma)/\sigma$ vs. σ, uncorrected for partial contact, for sliding experiments without gouge on Kelly Limestone.

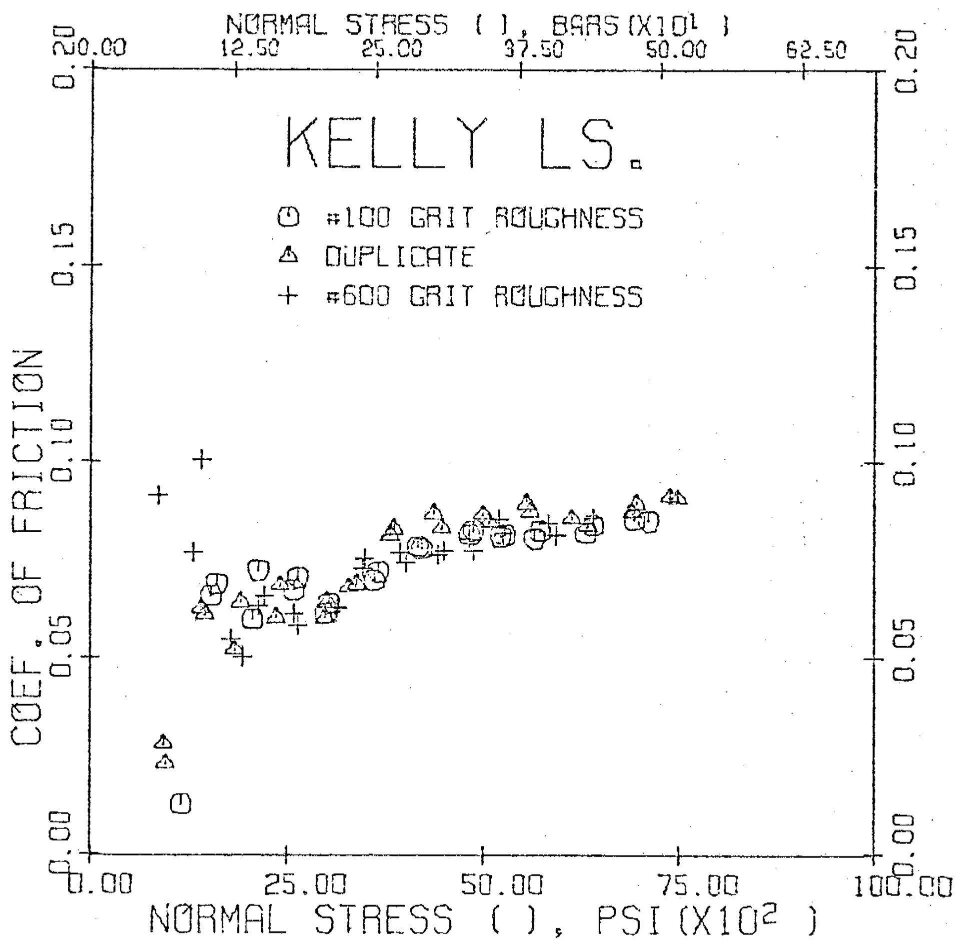
NORMAL STRESS ( ), BARS (X10[1])
0.00
12.50
25.00
37.50
50.00
62.50
KELLY LS.
#100 GRIT ROUGHNESS
DUPLICATE
#600 GRIT ROUGHNESS
COEF. OF FRICTION
0.00
0.05
0.10
0.15
0.20
0.00
25.00
50.00
75.00
100.00
NORMAL STRESS ( ), PSI (X10[2])

Fig. 25. $\mu=\tau(\sigma)/\sigma$ vs. σ, uncorrected for partial contact, for sliding experiments without gouge on Mesa Verde Sandstone.

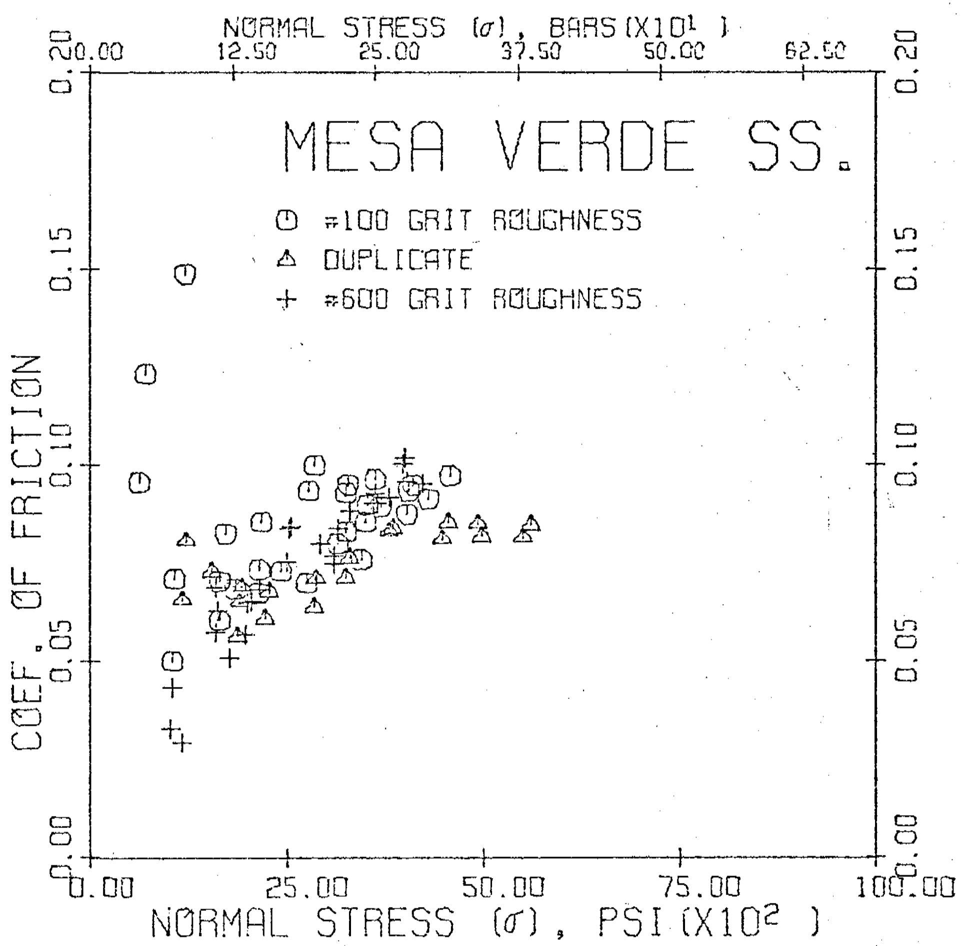
NORMAL STRESS (σ), BARS (X10¹)
0.00
12.50
25.00
37.50
50.00
62.50
MESA VERDE SS.
#100 GRIT ROUGHNESS
DUPLICATE
#600 GRIT ROUGHNESS
COEF. OF FRICTION
0.20
0.15
0.10
0.05
0.00
0.00
25.00
50.00
75.00
100.00
NORMAL STRESS (σ), PSI (X10²)

Fig. 26. $\mu = \tau(\sigma)/\sigma$ vs. σ for friction experiments involving perfectly-matched controlled surfaces of contact in Kelly Limestone; note negligible difference between tests with and without synthetic limestone gouge.

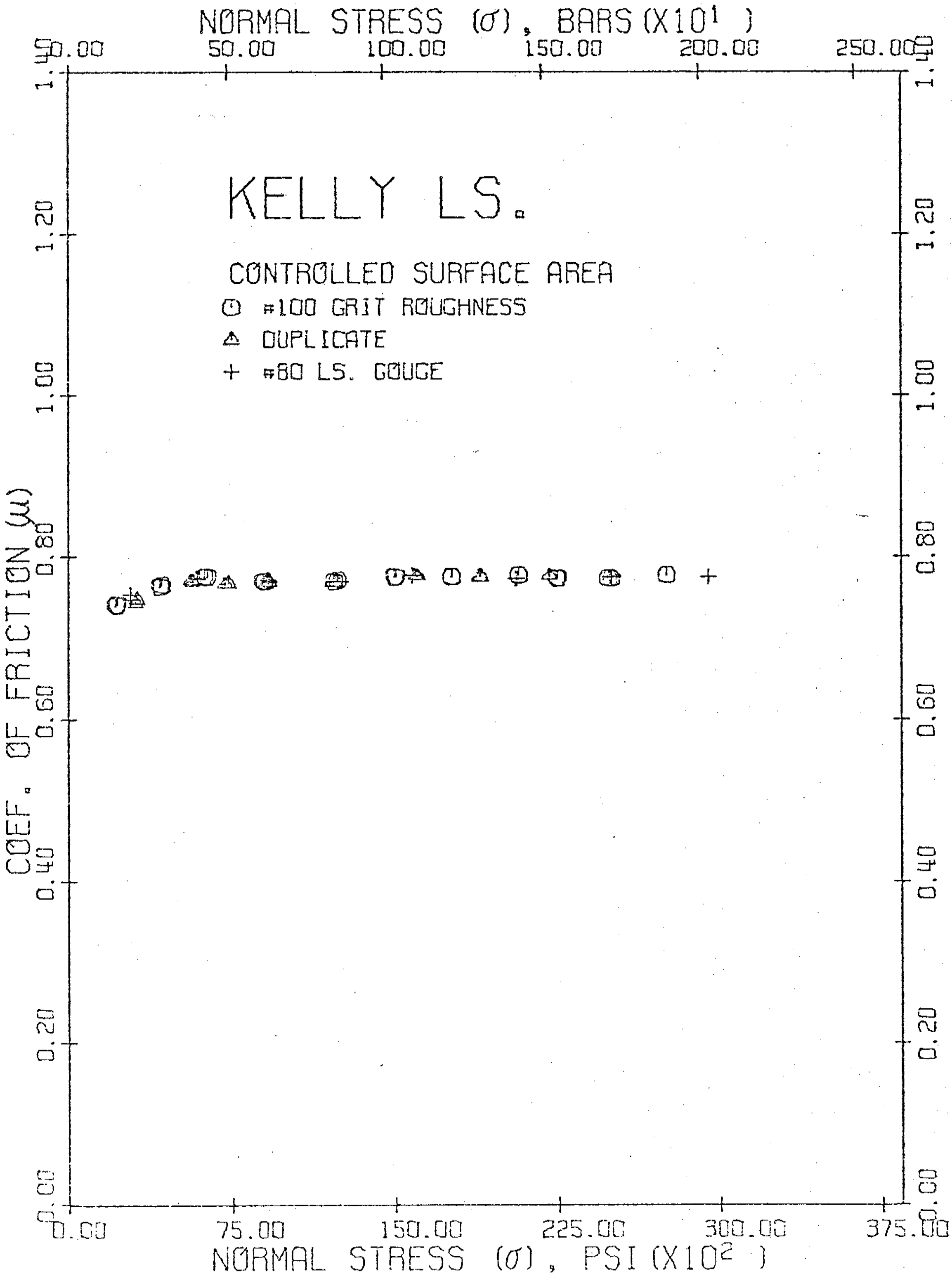
NORMAL STRESS (σ), BARS (X10¹)
0.00
50.00
100.00
150.00
200.00
250.00
1.40
1.20
1.00
0.80
0.60
0.40
0.20
0.00
KELLY LS.
CONTROLLED SURFACE AREA
#100 GRIT ROUGHNESS
DUPLICATE
#80 LS. GOUGE
COEF. OF FRICTION (μ)
0.00
75.00
150.00
225.00
300.00
375.00
NORMAL STRESS (σ), PSI (X10²)

Fig. 27. $\mu=\tau(\sigma)/\sigma$ vs. σ for friction experiments involving perfectly-matched controlled surfaces of contact in Mesa Verde Sandstone; note negligible difference between run with and without synthetic sandstone gouge.

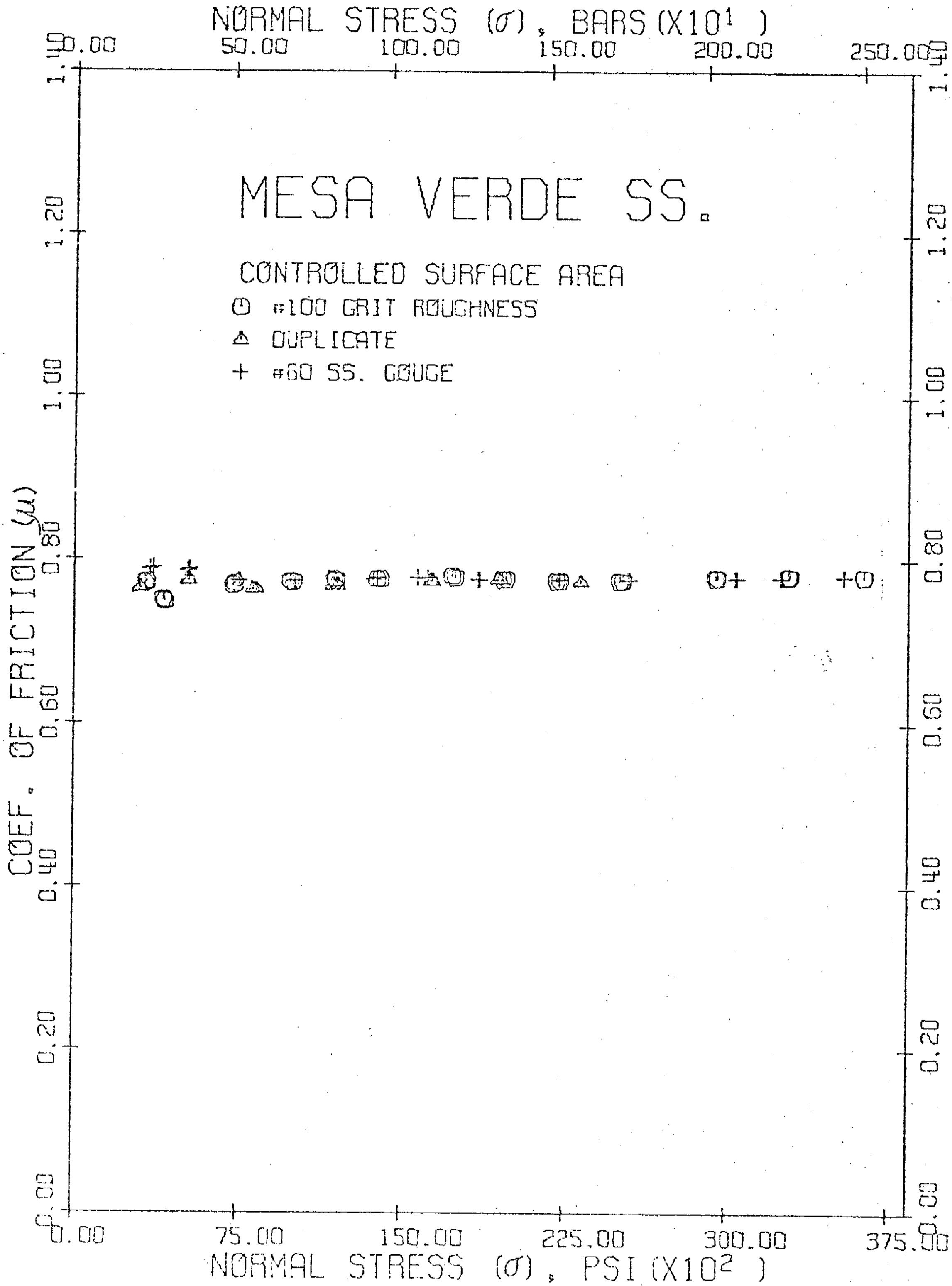
NØRMAL STRESS (σ), BARS (X10¹)
0.00
50.00
100.00
150.00
200.00
250.00
MESA VERDE SS.
CØNTRØLLED SURFACE AREA
#100 GRIT RØUGHNESS
DUPLICATE
#60 SS. GØUGE
COEF. OF FRICTION (μ)
0.00
0.20
0.40
0.60
0.80
1.00
1.20
1.40
0.00
75.00
150.00
225.00
300.00
375.00
NØRMAL STRESS (σ), PSI (X10²)

Fig. 28. $\mu = \tau(\sigma)/\sigma$ vs. σ, corrected for partial contact, for friction experiments without gouge on Kelly Limestone.

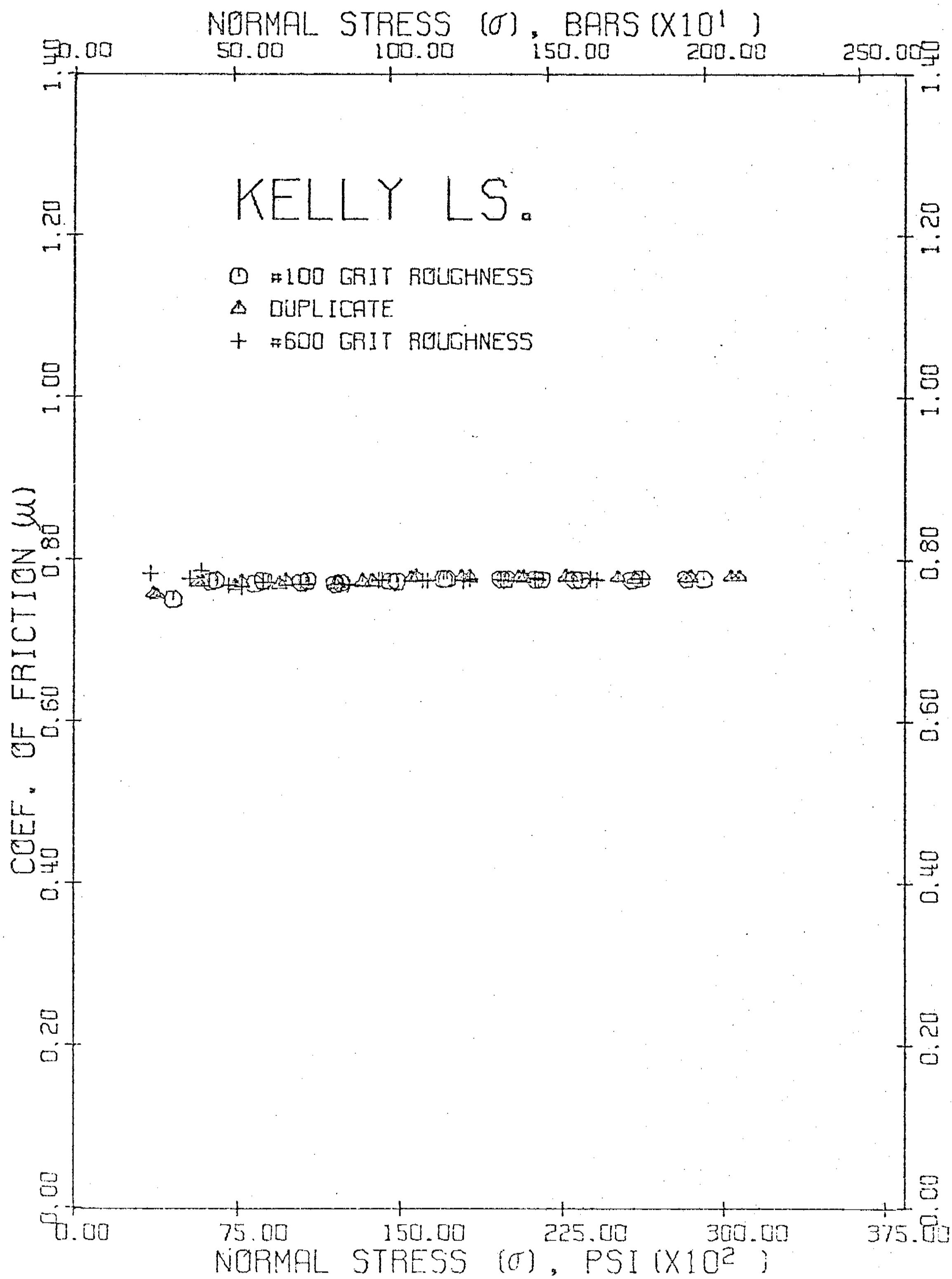
NØRMAL STRESS (σ), BARS (X10¹)
0.00
50.00
100.00
150.00
200.00
250.00
KELLY LS.
#100 GRIT RØUGHNESS
DUPLICATE
#600 GRIT RØUGHNESS
COEF. ØF FRICTIØN (μ)
0.00
0.20
0.40
0.60
0.80
1.00
1.20
1.40
0.00
75.00
150.00
225.00
300.00
375.00
NØRMAL STRESS (σ), PSI (X10²)

Fig. 29. $\mu = \tau(\sigma)/\sigma$ vs. σ, corrected for partial contact, for friction experiments without gouge on Mesa Verde Sandstone.

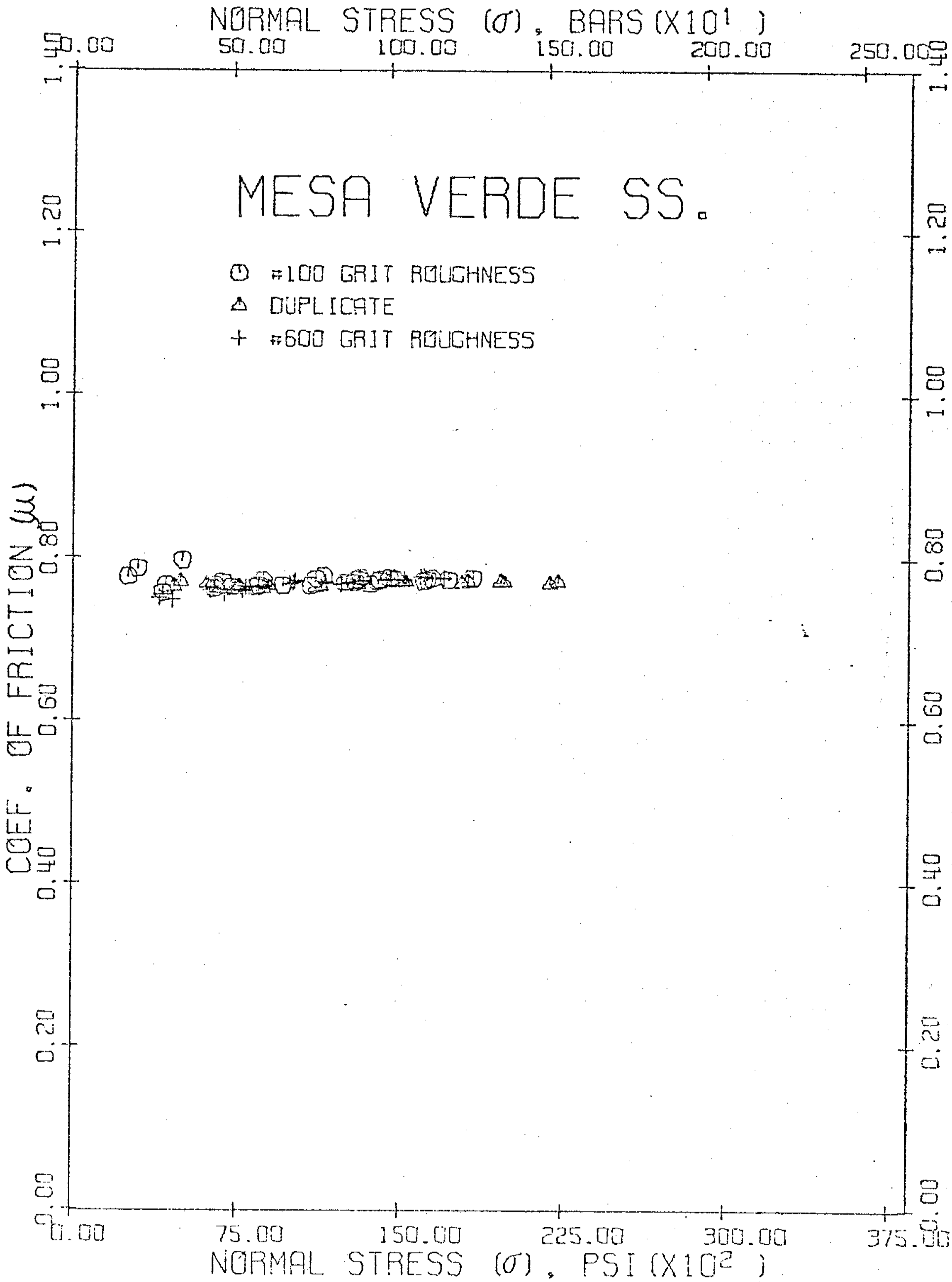
NORMAL STRESS (σ), BARS (X10¹)
0.00
50.00
100.00
150.00
200.00
250.00
MESA VERDE SS.
#100 GRIT ROUGHNESS
DUPLICATE
#600 GRIT ROUGHNESS
COEF. OF FRICTION (μ)
0.00
0.20
0.40
0.60
0.80
1.00
1.20
1.40
0.00
75.00
150.00
225.00
300.00
375.00
NORMAL STRESS (σ), PSI (X10²)

Appendix II Tables II-29 to II-36) were plotted in Figures 30, 31, 20, and 21. Results obtained using uncorrected area A_o are similar to those without gouge (Figures 18 and 19), and are not shown. Corresponding least-square statistics are shown in Table 7.

Friction coefficients (Equation 8) plotted as a function of σ are given in Figures 26 and 27 for controlled-area tests and in Figures 32 and 33 for corrected areas A_o'. Data for frictional experiments involving variations of parameters such as rock type, gouge thickness, and fault angle are presented in the following section.

Variations with Gouge

Rock type. In an effort to gain some insight into the effect of rock type upon sliding friction, two core halves, one limestone and the other sandstone, were pieced together with a 1-mm thick 50-50% (by volume) mixture of #80 limestone and sandstone gouge spread along the 45^o sawcuts. The (σ, τ) data for uncorrected and corrected area cases are given in Appendix II Table AII-37 and least-square data are displayed in Table 8. The original (σ, τ) data for individual limestone and sandstone tests that were run previously are plotted with the gouge-mixture data for comparison in Figure 34. Figure 35 is the corresponding graph of the coefficient of friction vs. normal stress.

Fig. 30. Shear stress vs. normal stress, corrected for partial contact, for friction experiments on Kelly Limestone with various fractions of dry and water-saturated limestone gouge.

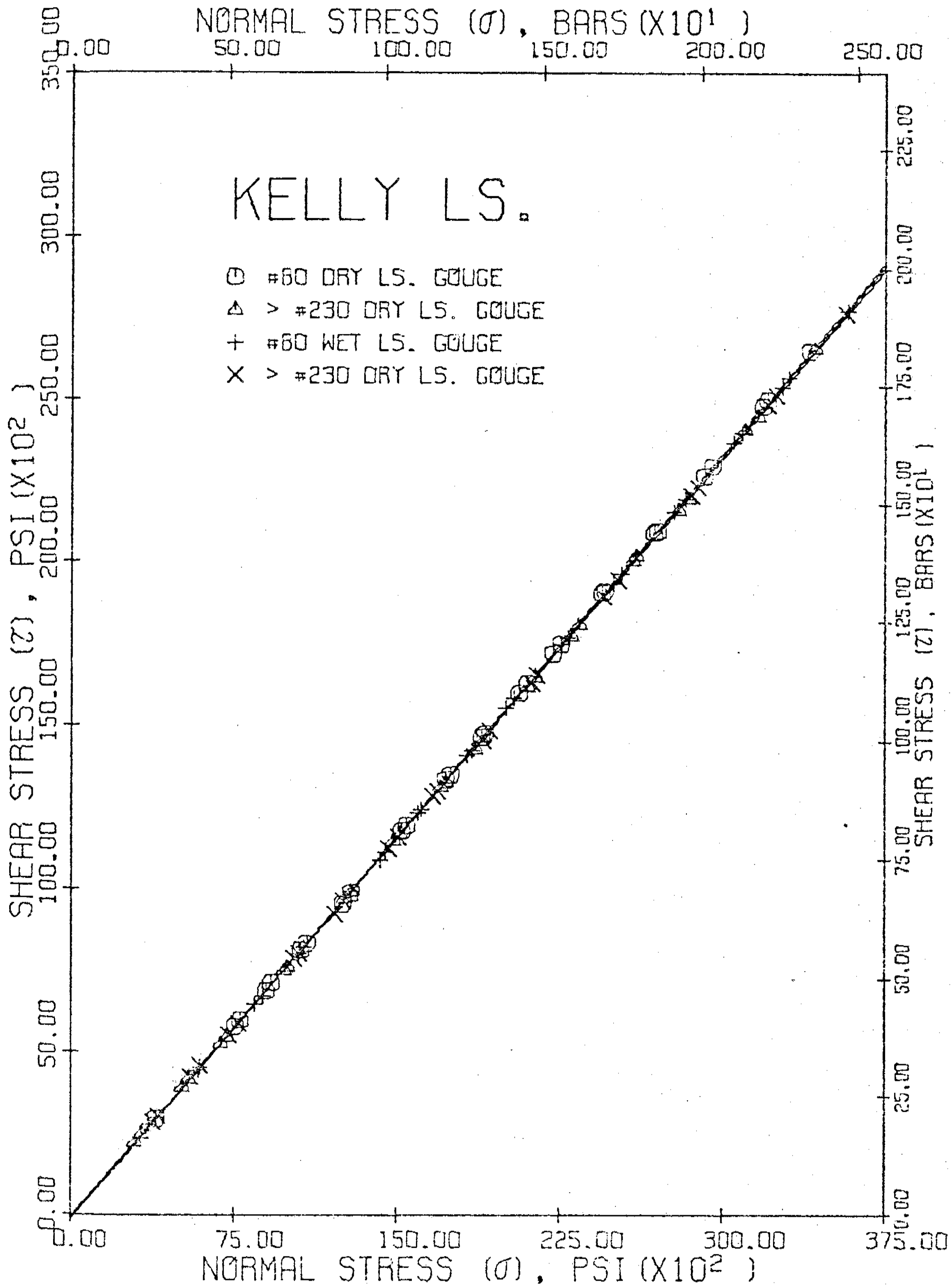
NORMAL STRESS (σ), BARS (X10¹)
0.00
50.00
100.00
150.00
200.00
250.00
KELLY LS.
#60 DRY LS. GOUGE
> #230 DRY LS. GOUGE
+ #60 WET LS. GOUGE
X > #230 DRY LS. GOUGE
SHEAR STRESS (τ), PSI (X10²)
0.00
50.00
100.00
150.00
200.00
250.00
300.00
350.00
SHEAR STRESS (τ), BARS (X10¹)
0.00
25.00
50.00
75.00
100.00
125.00
150.00
175.00
200.00
225.00
NORMAL STRESS (σ), PSI (X10²)
0.00
75.00
150.00
225.00
300.00
375.00

Fig. 31. Shear stress vs. normal stress, corrected for partial contact, for friction experiments on Mesa Verde Sandstone with various fractions of dry and water-saturated sandstone gouge.

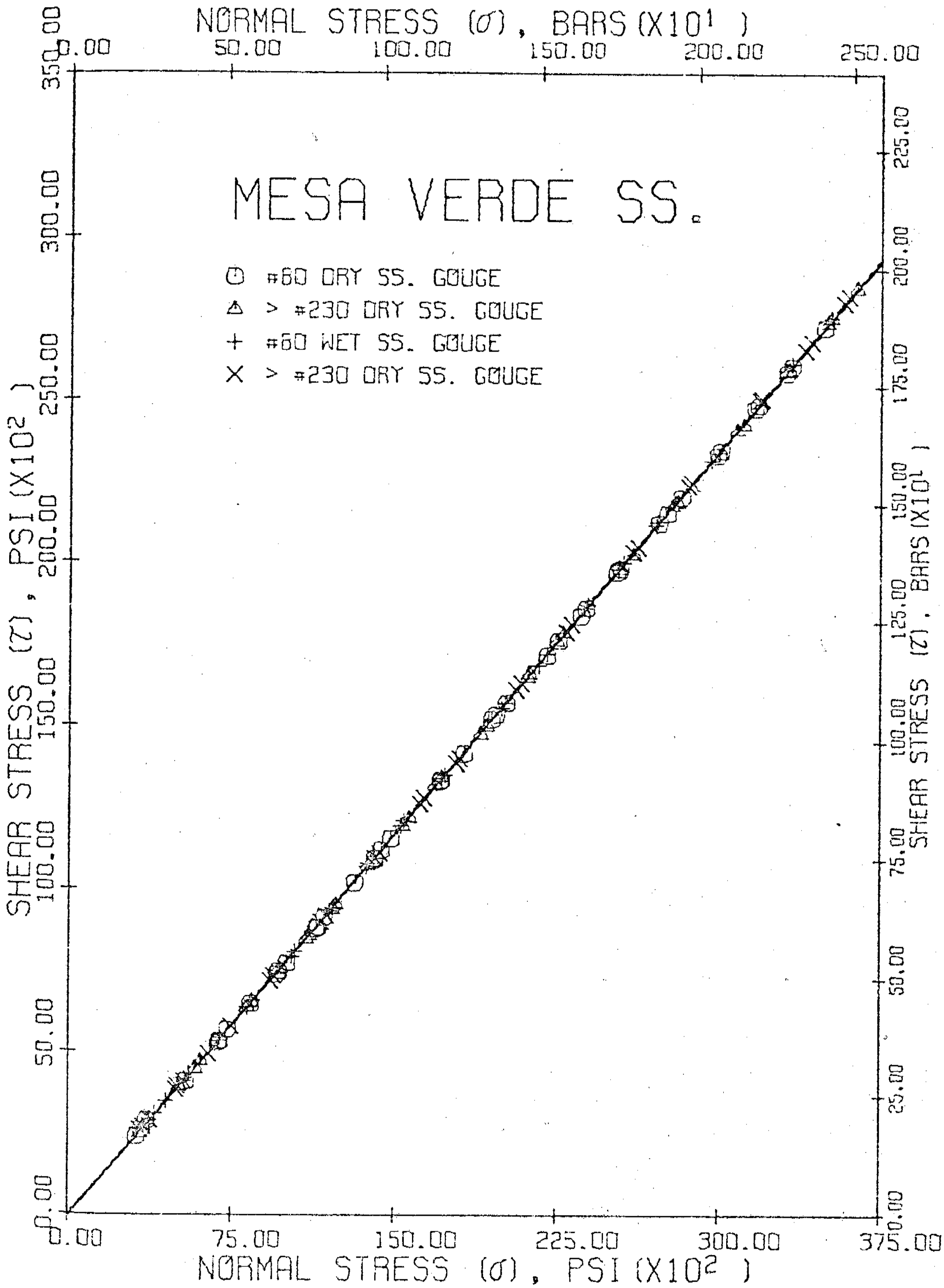

NØRMAL STRESS (σ), BARS (X10¹)
0.00
50.00
100.00
150.00
200.00
250.00
MESA VERDE SS.
#60 DRY SS. GOUGE
> #230 DRY SS. GOUGE
#60 WET SS. GOUGE
> #230 DRY SS. GOUGE
SHEAR STRESS (τ), PSI (X10²)
350.00
300.00
250.00
200.00
150.00
100.00
50.00
0.00
SHEAR STRESS (τ), BARS (X10¹)
225.00
200.00
175.00
150.00
125.00
100.00
75.00
50.00
25.00
0.00
0.00
75.00
150.00
225.00
300.00
375.00
NØRMAL STRESS (σ), PSI (X10²)

TABLE 7. Least-Square Data $\tau=\tau_0+B\sigma^n$ for Friction Experiments with Various Size-Fractions of 1-mm Thick Limestone and Sandstone Gouge at $\alpha=45^o$

Experimental Condition	τ_0 (psi)	τ_0 (bars)	B <psi>	B <bars>	n	R^2 (%)
Kelly Limestone (A_o=0.74; A_o'=0.111; A_c'=0.108 in^2)						
#80 Dry Gouge						
Uncorrected Area	-30	-2.0	0.0238	0.0363	1.159	99.5
Corrected Area	-140	-9.6	0.782		1.000	100.0
Controlled Area	-62	-4.3	0.777		1.000	100.0
#230 Dry Gouge						
Uncorrected Area	19	1.3	0.00678	0.0143	1.278	99.4
Corrected Area	-71	-4.9	0.775		1.000	100.0
#80 Wet Gouge						
Uncorrected Area	0	0.0	0.0161	0.0269	1.192	99.5
Corrected Area	-93	-6.4	0.779		1.000	100.0
#230 Wet Gouge						
Uncorrected Area	35	2.4	0.00398	0.0097	1.334	99.6
Corrected Area	-69	-4.7	0.775		1.000	100.0
Mesa Verde Sandstone (A_o=0.74; A_o'=0.109; A_c'=0.108 in^2)						
#80 Dry Gouge						
Uncorrected Area	21	1.4	0.00786	0.0162	1.271	99.4
Corrected Area	-82	-5.7	0.783		1.000	100.0
Controlled Area	-3	-0.2	0.778		1.000	100.0
#230 Dry Gouge						
Uncorrected Area	19	1.3	0.0118	0.0215	1.225	99.3
Corrected Area	-70	-4.9	0.783		1.000	100.0
#80 Wet Gouge						
Uncorrected Area	19	1.3	0.0186	0.0299	1.179	99.3
Corrected Area	-51	-3.5	0.784		1.000	100.0
#230 Wet Gouge						
Uncorrected Area	28	2.0	0.00838	0.0170	1.265	99.6
Corrected Area	-66	-4.6	0.784		1.000	100.0

Fig. 32. $\mu = \tau(\sigma)/\sigma$ vs. σ, corrected for partial contact, for friction experiments on Kelly Limestone with various fractions of dry and water-saturated limestone gouge.

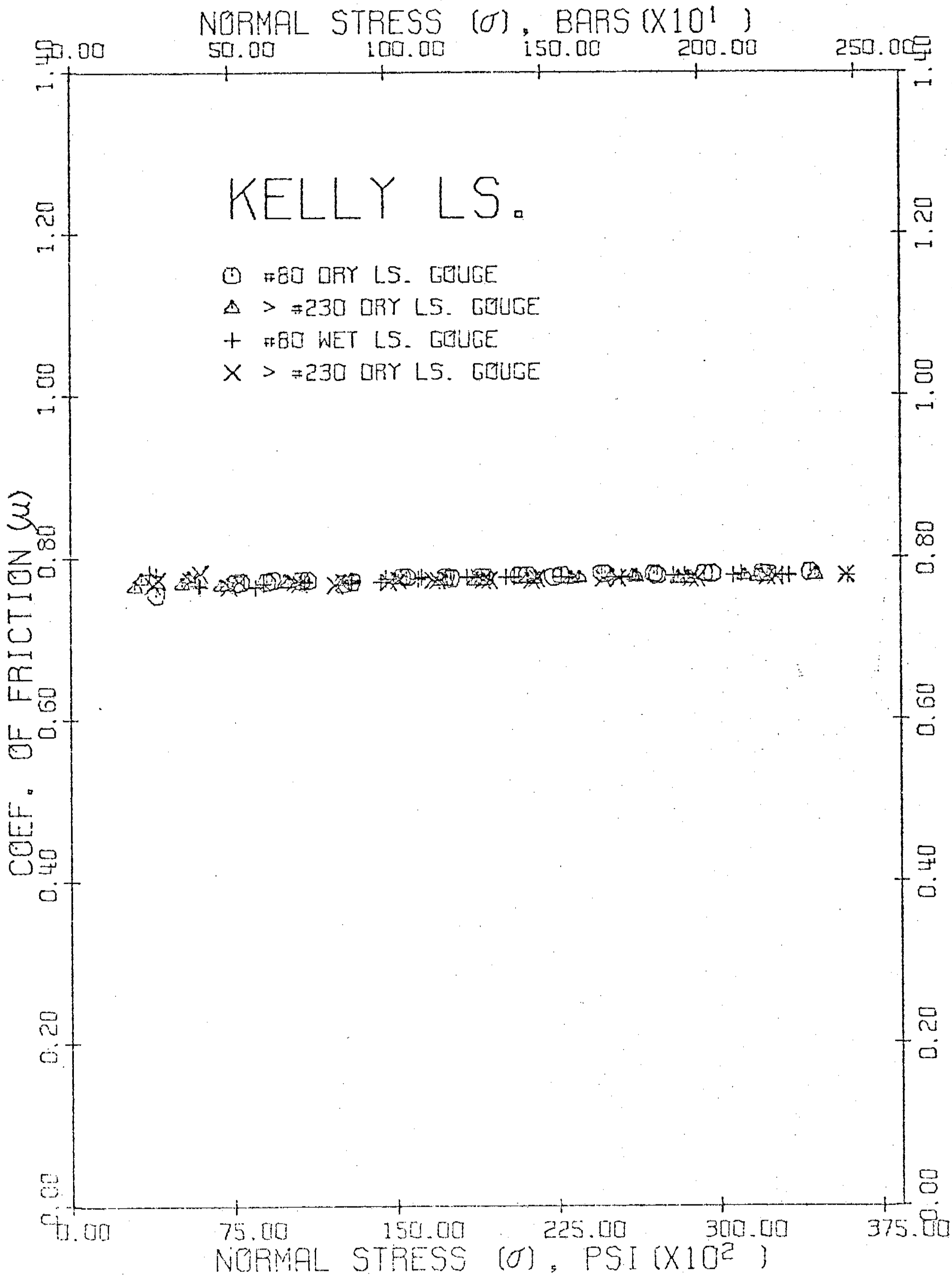
NORMAL STRESS (σ), BARS (X10¹)
0.00
50.00
100.00
150.00
200.00
250.00
KELLY LS.
⊙ #80 DRY LS. GOUGE
△ > #230 DRY LS. GOUGE
+ #80 WET LS. GOUGE
X > #230 DRY LS. GOUGE
COEF. OF FRICTION (μ)
1.40
1.20
1.00
0.80
0.60
0.40
0.20
0.00
0.00
75.00
150.00
225.00
300.00
375.00
NORMAL STRESS (σ), PSI (X10²)

Fig. 33. $\mu = \tau(\sigma)/\sigma$ vs. σ, corrected for partial contact, for friction experiments on Mesa Verde Sandstone with various fractions of dry and water-saturated sandstone gouge.

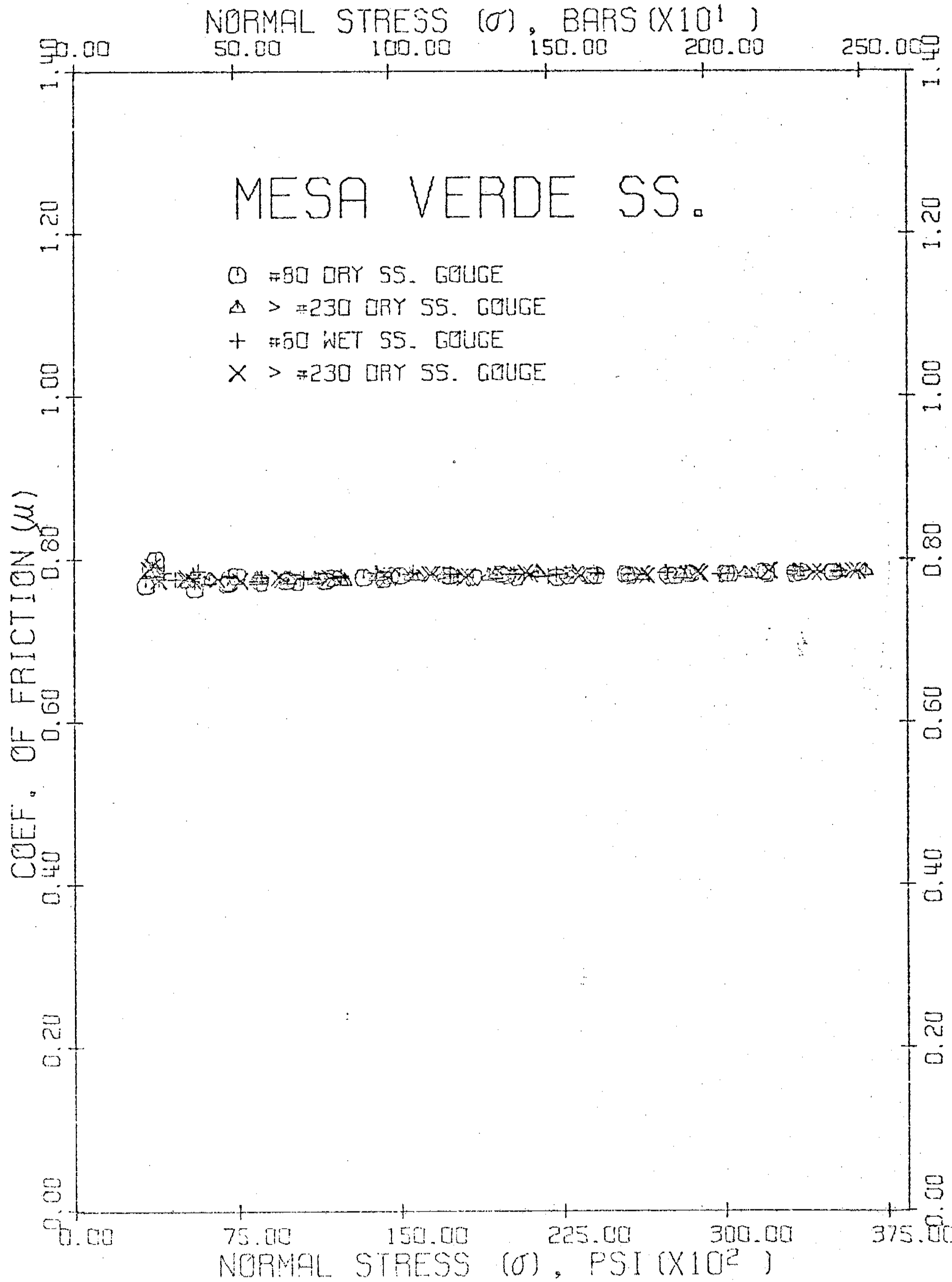
NORMAL STRESS (σ), BARS (X10¹)
0.00
50.00
100.00
150.00
200.00
250.00
MESA VERDE SS.
#80 DRY SS. GOUGE
> #230 DRY SS. GOUGE
#60 WET SS. GOUGE
> #230 DRY SS. GOUGE
COEF. OF FRICTION (μ)
0.00
0.20
0.40
0.60
0.80
1.00
1.20
1.40
0.00
75.00
150.00
225.00
300.00
375.00
NORMAL STRESS (σ), PSI (X10²)

TABLE 8. Least-Square Data $\tau=\tau_0+B\sigma^n$ for Friction Experiments with a Mixture of 1-mm Thick 50% #80 Dry Limestone Gouge and 50% #80 Dry Sandstone Gouge for $\alpha=45^o$

Experimental Condition	τ_0 (psi)	(bars)	B <psi>	<bars>	n	R^2 (%)
#80 Dry Limestone Gouge						
Uncorrected Area (0.74)*	-30	-2.0	0.0238	0.0363	1.159	99.5
Corrected Area (0.111)	-140	-9.6	0.782		1.000	100.0
Controlled Area (0.108)	-62	-4.3	0.777		1.000	100.0
#80 Dry Sandstone Gouge						
Uncorrected Area (0.74)	21	1.4	0.00786	0.0162	1.271	99.4
Corrected Area (0.109)	-82	-5.7	0.783		1.000	100.0
Controlled Area (0.108)	-3	-0.2	0.778		1.000	100.0
Mixture						
Uncorrected Area (0.74)	28	2.0	0.00711	0.0151	1.281	99.7
Corrected Area (0.109)	-86	-5.9	0.779		1.000	100.0

* Areas are in sq.-in.

Fig. 34. Shear stress vs. normal stress, corrected for partial contact, for friction experiments on Kelly Limestone, Mesa Verde Sandstone, and both limestone and sandstone with respective #80 gouge fractions.

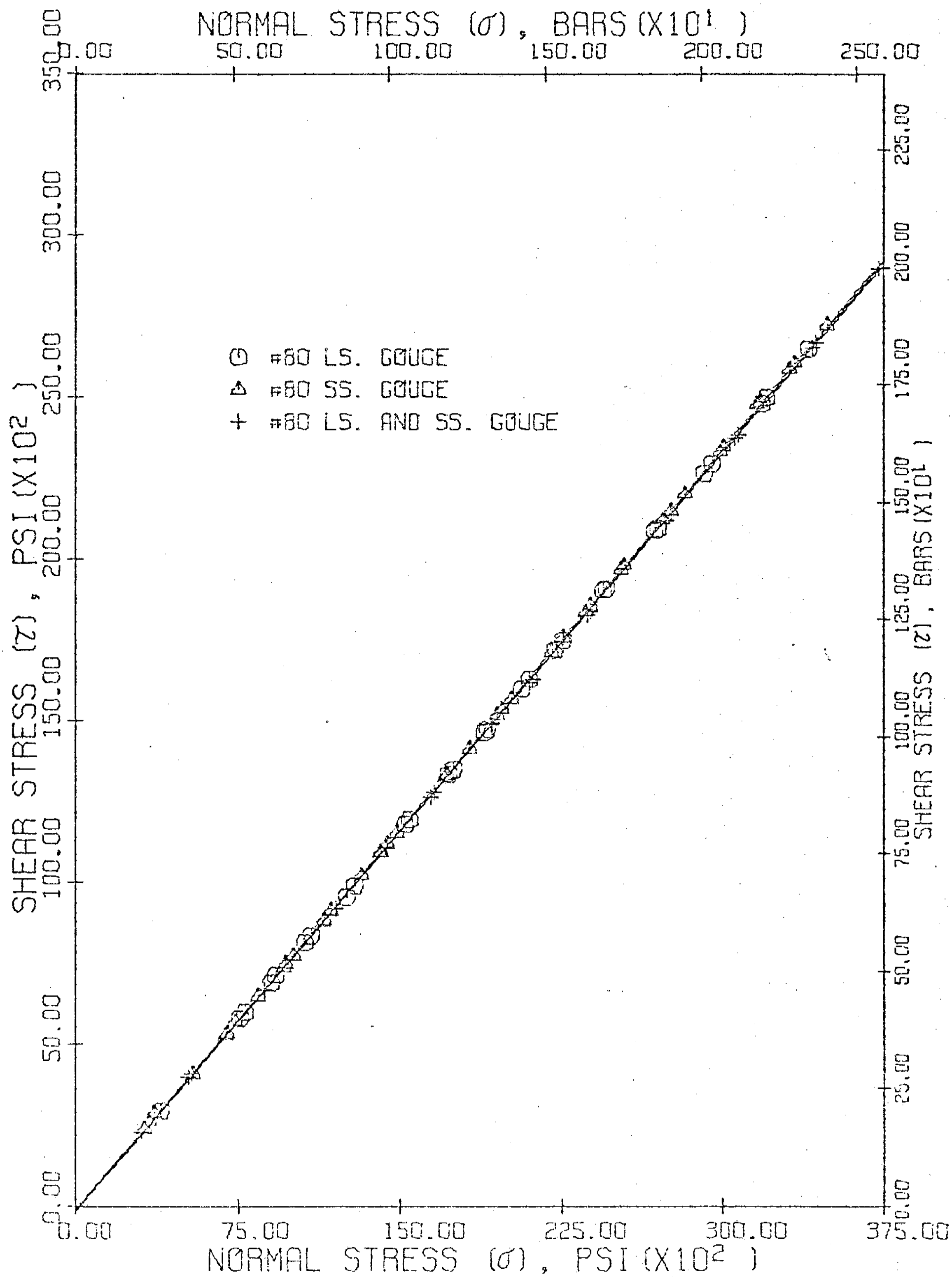
NØRMAL STRESS (σ), BARS (X10¹)
0.00
50.00
100.00
150.00
200.00
250.00
SHEAR STRESS (τ), PSI (X10²)
0.00
50.00
100.00
150.00
200.00
250.00
300.00
350.00
SHEAR STRESS (τ), BARS (X10¹)
25.00
50.00
75.00
100.00
125.00
150.00
175.00
200.00
225.00
⊙ #80 LS. GØUGE
△ #80 SS. GØUGE
+ #80 LS. AND SS. GØUGE
0.00
75.00
150.00
225.00
300.00
375.00
NØRMAL STRESS (σ), PSI (X10²)

Fig. 35. $\mu = \tau(\sigma)/\sigma$ vs. σ, corrected for partial contact, for friction experiments on Kelly Limestone, Mesa Verde Sandstone, and both limestone and sandstone with respective #80 gouge fractions.

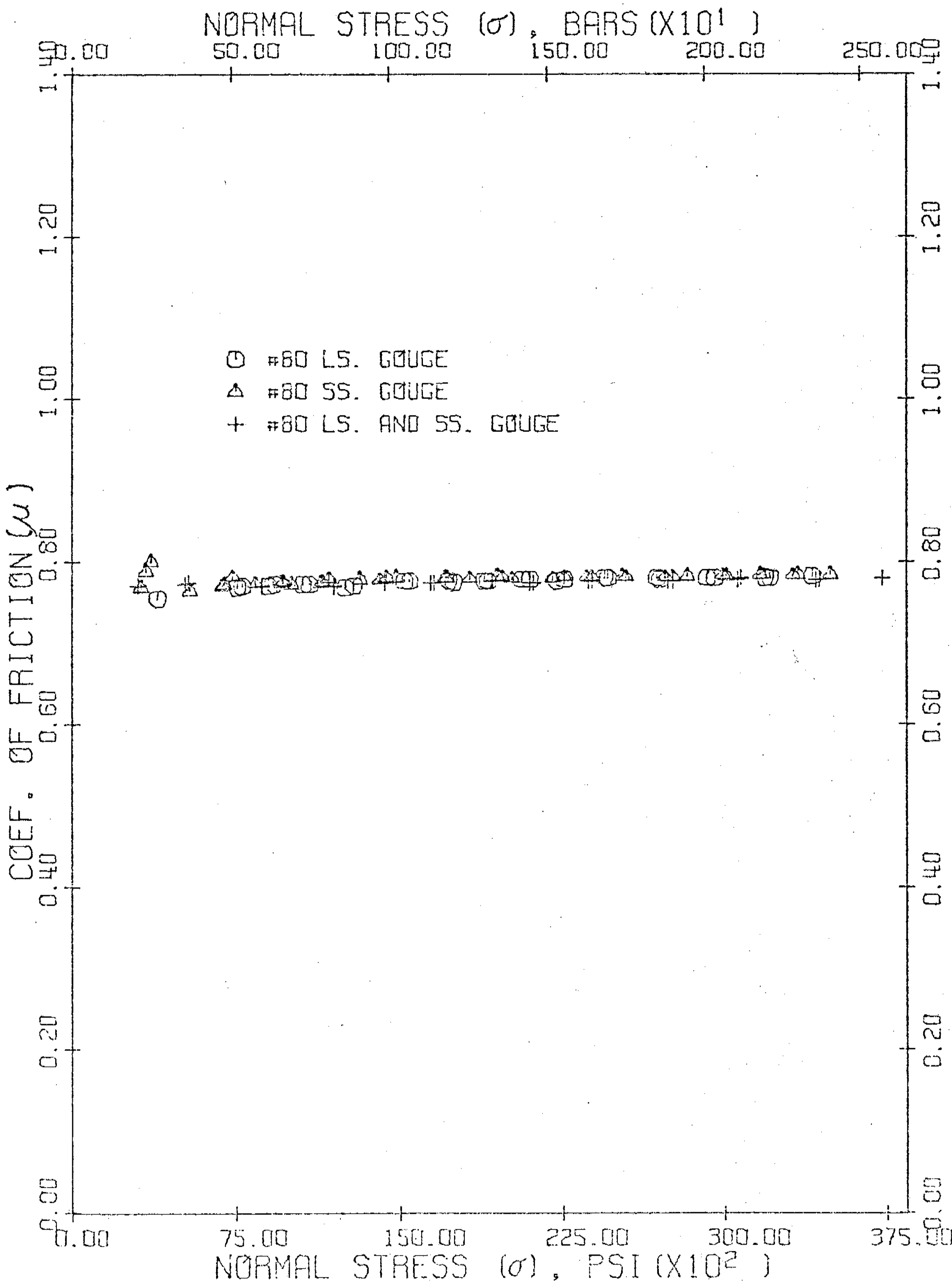
NØRMAL STRESS (σ), BARS (X10¹)
0.00
50.00
100.00
150.00
200.00
250.00
1.40
1.20
1.00
0.80
0.60
0.40
0.20
0.00
COEF. ØF FRICTIØN (μ)
○ #80 LS. GØUGE
△ #80 SS. GØUGE
+ #80 LS. AND SS. GØUGE
0.00
75.00
150.00
225.00
300.00
375.00
NØRMAL STRESS (σ), PSI (X10²)

Gouge thickness. The effect of gouge thickness on friction is given in Appendix II Tables AII-38 to AII-41, Table 9, and Figures 36-39. Gouge thicknesses of approximately 1 grain-diameter (#80 gouge), 1.0 mm, and 1.5 mm were used. After the experiments, gouge thicknesses of approximately half the original thicknesses resulted, due to compaction.

Fault angle. To determine if friction is a function of fault (sawcut) angle α, the angle of the sawcut (containing #80 gouge, 1-mm thick) was varied such that α=30°, 37.5°, 45°, and 60°. Least-square regression data are presented in Table 10, and (σ, τ) data are shown in Appendix II Tables AII-42 to AII-47 and plotted in Figures 40 and 41 for corrected area A_o' (see also Appendix I).

Coefficients of friction vs. normal stress are plotted in Figures 42 and 43 for both rock types. An additional graph involving μ at σ=36,000 psi (s.53 kb) vs. σ for A_o' taking into account partial contact is presented in Figure 44.

TABLE 9. Least-Square Data $\tau=\tau_o+B\sigma^n$ for Friction Experiments with Various Thicknesses of #80 Dry Limestone and #80 Dry Sandstone Gouge for $\alpha=45^o$

Experimental Condition	τ_o (psi)	τ_o (bars)	B ⟨psi⟩	B ⟨bars⟩	n	R^2 (%)
Kelly Limestone (A_o=0.74; A_δ'=0.111; A_c'=0.108 in^2)						
1 Grain-Dia. Thick						
Uncorrected Area	34	2.3	0.0130	0.0225	1.207	99.3
Corrected Area	-30	-2.1	0.776		1.000	100.0
1.0-mm Thick						
Uncorrected Area	-30	-2.0	0.0238	0.0363	1.159	99.5
Corrected Area	-140	-9.6	0.782		1.000	100.0
Controlled Area	-62	-4.3	0.777		1.000	100.0
1.5-mm Thick						
Uncorrected Area	1	0.1	0.00951	0.0182	1.242	99.5
Corrected Area	-111	-7.7	0.777		1.000	100.0
Mesa Verde Sandstone (A_o 0.74; A_δ' 0.109; A_c' 0.108 in^2)						
1 Grain-Dia. Thick						
Uncorrected Area	84	5.8	0.00148	0.0047	1.430	97.3
Corrected Area	-8	-0.5	0.777		1.000	100.0
1.0-mm Thick						
Uncorrected Area	21	1.4	0.00786	0.0162	1.271	99.4
Corrected Area	-82	-5.7	0.783		1.000	100.0
Controlled Area	-3	-0.2	0.778		1.000	100.0
1.5-mm Thick						
Uncorrected Area	26	1.8	0.00349	0.0088	1.344	99.3
Corrected Area	-83	-5.7	0.778		1.000	100.0

Fig. 36. Shear stress vs. normal stress, corrected for partial contact, for friction experiments on Kelly Limestone involving various thicknesses of #80 limestone gouge.

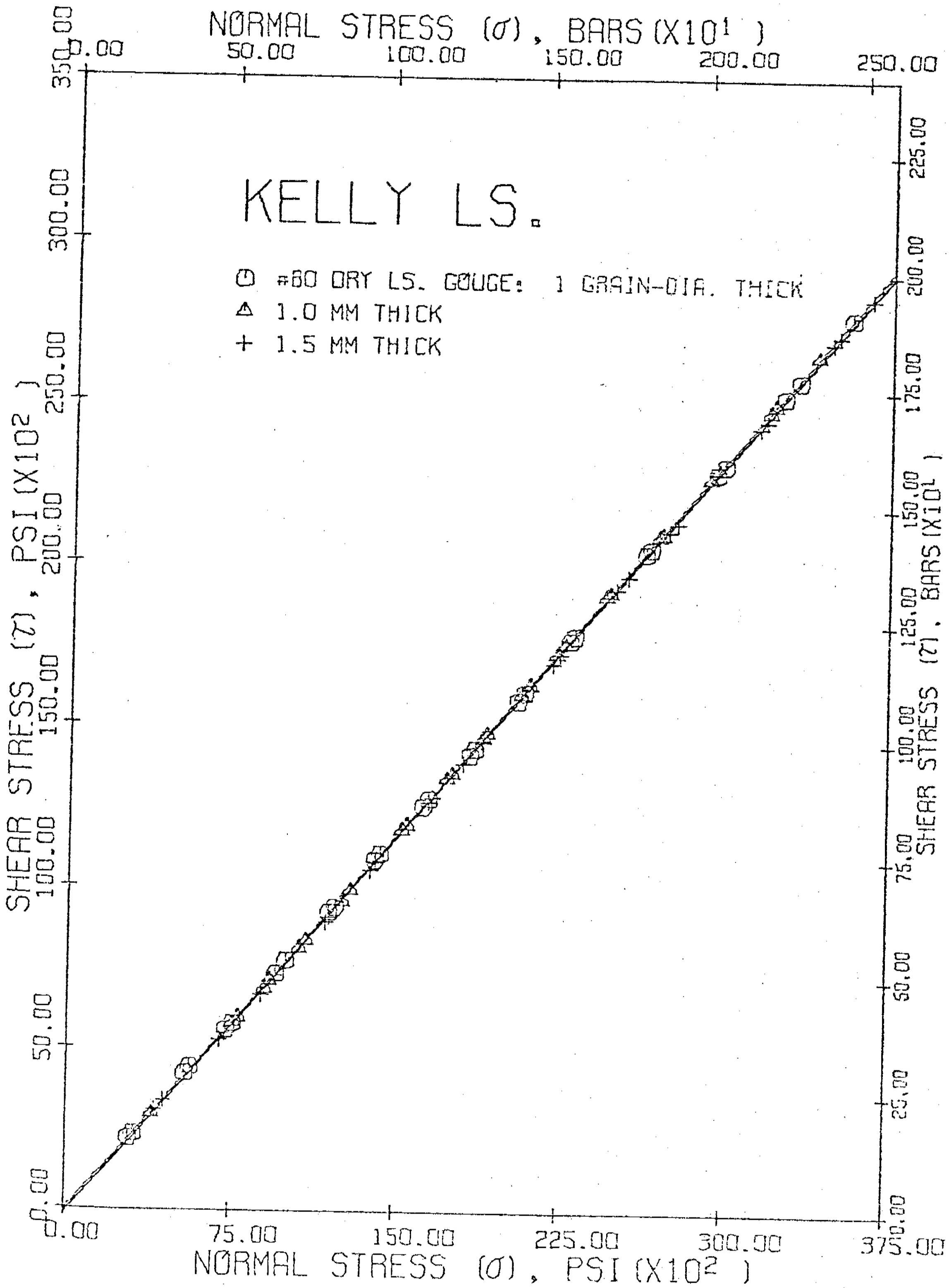
NØRMAL STRESS (σ), BARS (X10¹)
0.00
50.00
100.00
150.00
200.00
250.00
KELLY LS.
#60 DRY LS. GØUGE: 1 GRAIN-DIA. THICK
1.0 MM THICK
1.5 MM THICK
SHEAR STRESS (τ), PSI (X10²)
0.00
50.00
100.00
150.00
200.00
250.00
300.00
350.00
SHEAR STRESS (τ), BARS (X10¹)
25.00
50.00
75.00
100.00
125.00
150.00
175.00
200.00
225.00
0.00
75.00
150.00
225.00
300.00
375.00
NØRMAL STRESS (σ), PSI (X10²)

Fig. 37. Shear stress vs. normal stress, corrected for partial contact, for friction experiments on Mesa Verde Sandstone involving various thicknesses of #80 sandstone gouge.

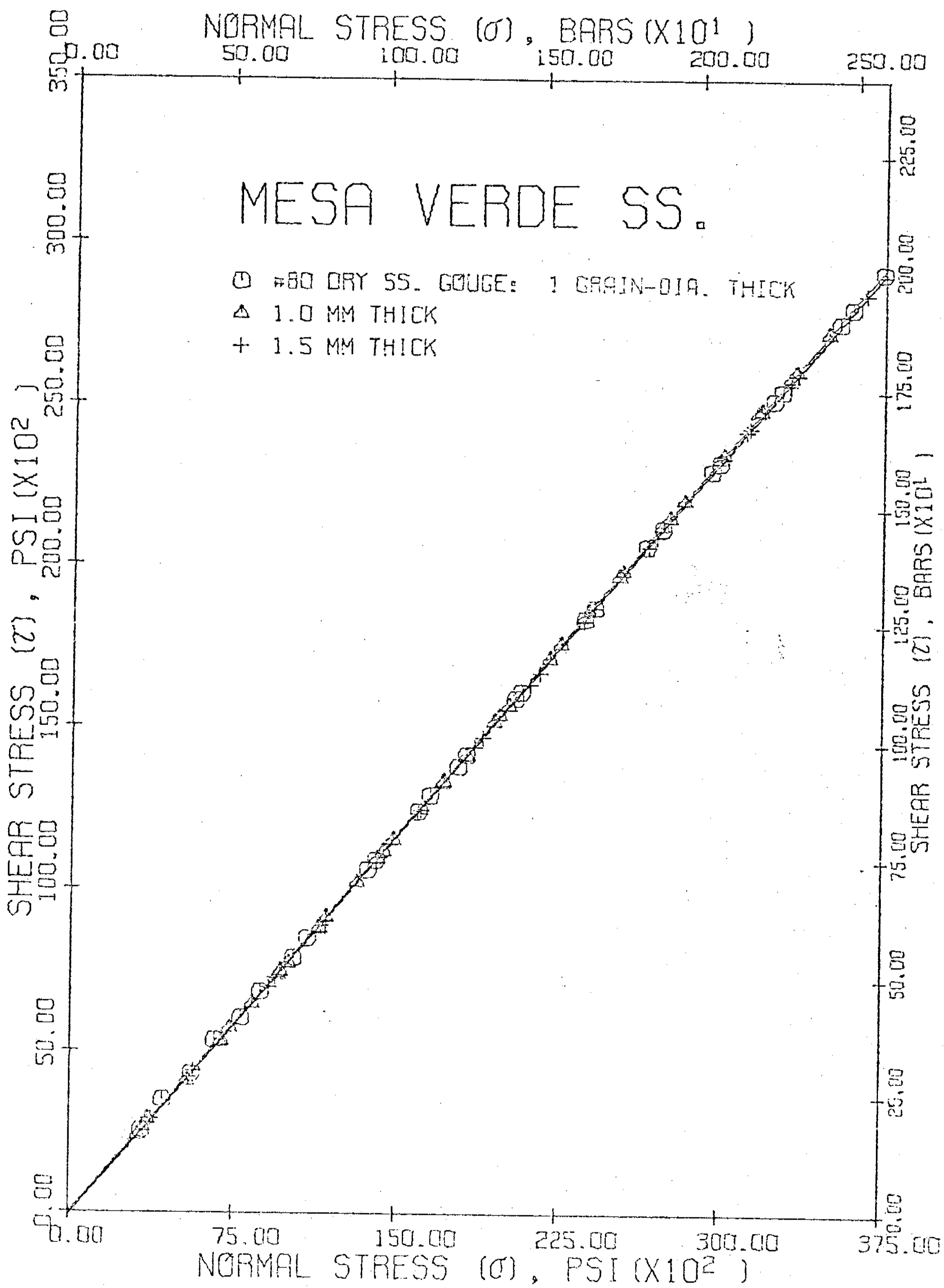
NØRMAL STRESS (σ), BARS (X10¹)
0.00
50.00
100.00
150.00
200.00
250.00
MESA VERDE SS.
#80 DRY SS. GOUGE: 1 GRAIN-DIA. THICK
1.0 MM THICK
1.5 MM THICK
SHEAR STRESS (τ), PSI (X10²)
0.00
50.00
100.00
150.00
200.00
250.00
300.00
350.00
SHEAR STRESS (τ), BARS (X10¹)
0.00
25.00
50.00
75.00
100.00
125.00
150.00
175.00
200.00
225.00
0.00
75.00
150.00
225.00
300.00
375.00
NØRMAL STRESS (σ), PSI (X10²)

Fig. 38. $\mu=\tau(\sigma)/\sigma$ vs. σ, corrected for partial contact, for friction experiments on Kelly Limestone involving various thicknesses of #80 limestone gouge.

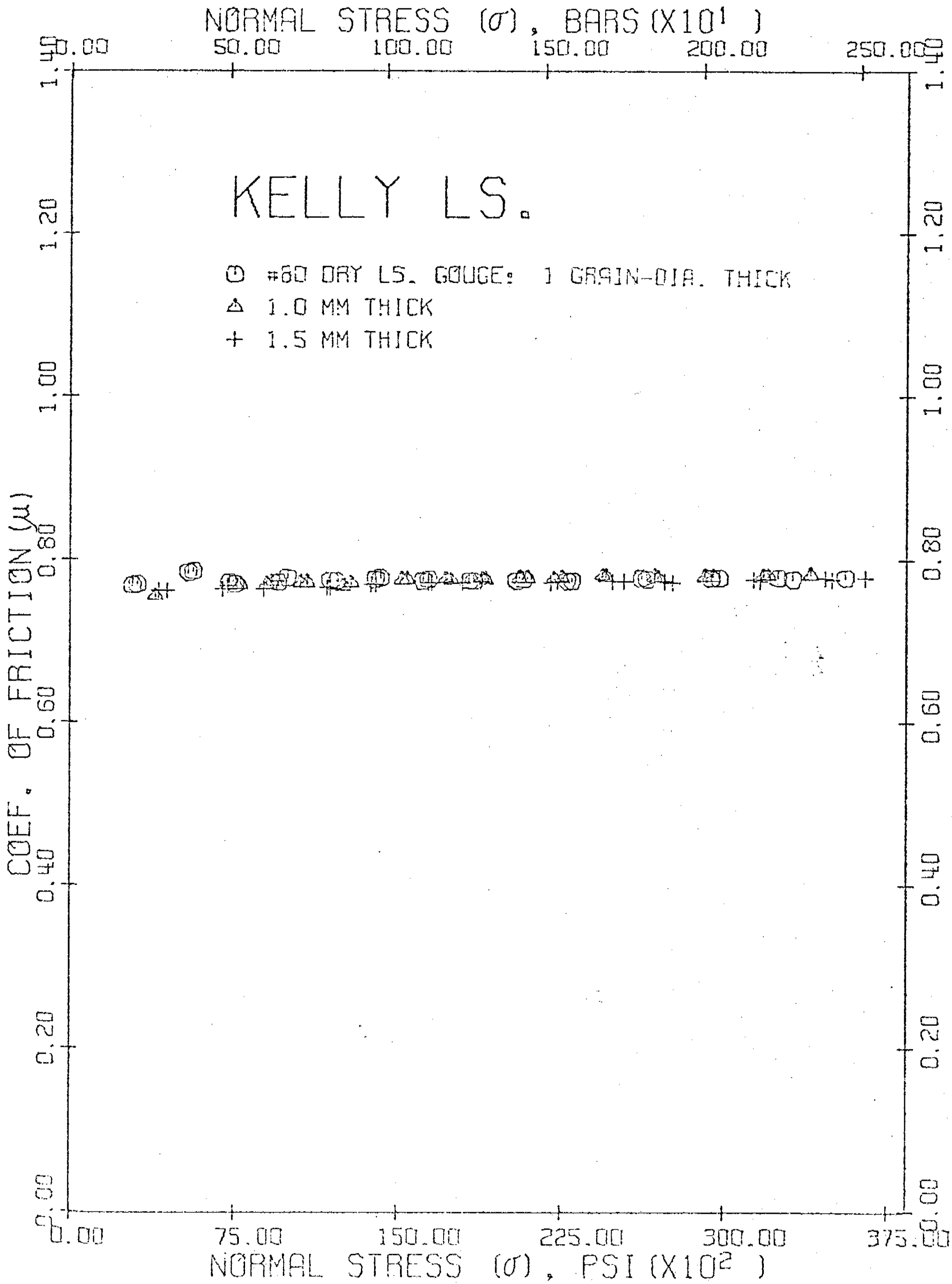
NORMAL STRESS (σ), BARS (X10¹)
0.00
50.00
100.00
150.00
200.00
250.00
1.40
1.20
1.00
0.80
0.60
0.40
0.20
0.00
KELLY LS.
#60 DRY LS. GOUGE: 1 GRAIN-DIA. THICK
1.0 MM THICK
1.5 MM THICK
COEF. OF FRICTION (μ)
0.00
75.00
150.00
225.00
300.00
375.00
NORMAL STRESS (σ), PSI (X10²)

Fig. 39. $\mu = \tau(\sigma)/\sigma$ vs. σ, corrected for partial contact, for friction experiments on Mesa Verde Sandstone involving various thicknesses of #80 sandstone gouge.

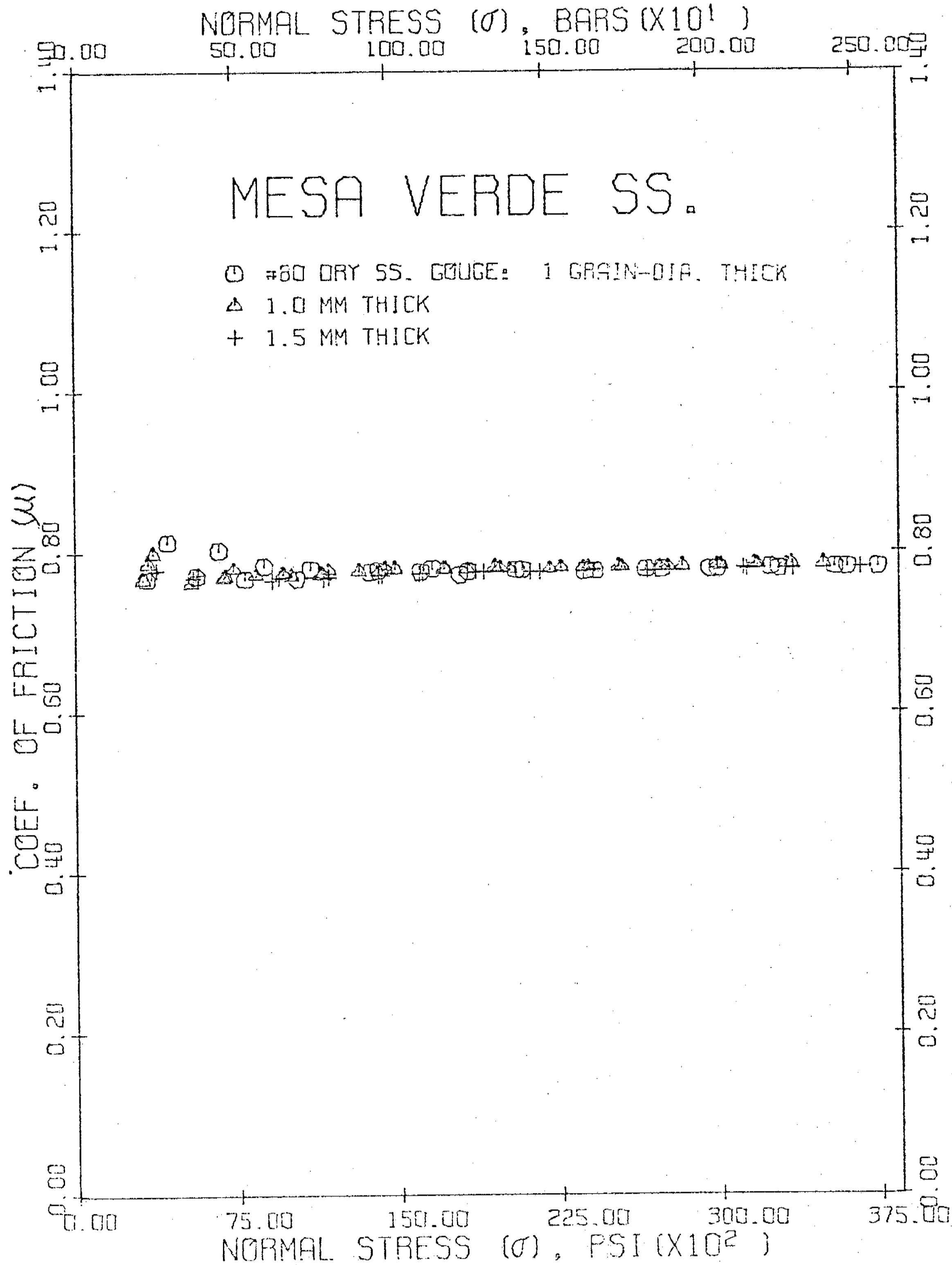
NORMAL STRESS (σ), BARS (X10¹)
0.00
50.00
100.00
150.00
200.00
250.00
1.40
1.20
1.00
0.80
0.60
0.40
0.20
0.00
MESA VERDE SS.
#60 DRY SS. GOUGE: 1 GRAIN-DIA. THICK
1.0 MM THICK
1.5 MM THICK
COEF. OF FRICTION (μ)
0.00
75.00
150.00
225.00
300.00
375.00
NORMAL STRESS (σ), PSI (X10²)

TABLE 10. Least-Square Data $\tau=\tau_0+B\sigma^n$ for Friction Experiments with 1.0-mm Thick Dry Limestone and Sandstone Gouge at Various Sawcut Angles (α)

Experimental Condition	τ_0 (psi)	τ_0 (bars)	B <psi>	B <bars>	n	R^2 (%)
Kelly Limestone (A_0=0.74)*						
$\alpha=30^\circ$						
Uncorrected Area	18	1.2	0.00003	0.0003	1.827	98.5
Corrected Area (0.326)	-113	-7.8	0.491		1.000	100.0
$\alpha=37.5^\circ$						
Uncorrected Area	20	1.4	0.00006	0.0005	1.754	99.5
Corrected Area (0.219)	-104	-7.2	0.670		1.000	100.0
$\alpha=45^\circ$						
Uncorrected Area	-30	-2.0	0.0238	0.0363	1.159	99.5
Corrected Area (0.111)	-140	-9.6	0.782		1.000	100.0
Controlled Area (0.108)	-62	-4.3	0.777		1.000	100.0
$\alpha=60^\circ$						
Uncorrected Area	-14	-1.0	0.00603	0.0120	1.257	99.2
Corrected Area (0.079)	-76	-5.3	0.510		1.000	100.0
Mesa Verde Sandstone (A_0=0.74)						
$\alpha=30^\circ$						
Uncorrected Area	17	1.2	0.00095	0.0033	1.472	99.4
Corrected Area (0.320)	-118	-8.2	0.521		1.000	100.0
$\alpha=37.5^\circ$						
Uncorrected Area	-9	-0.6	0.00125	0.0042	1.450	99.4
Corrected Area (0.215)	-144	-9.9	0.687		1.000	100.0
$\alpha=45^\circ$						
Uncorrected Area	21	1.4	0.00786	0.0162	1.271	99.4
Corrected Area (0.109)	-82	-5.7	0.783		1.000	100.0
Controlled Area (0.108)	-3	-0.2	0.778		1.000	100.0
$\alpha=60^\circ$						
Uncorrected Area	23	1.6	0.00355	0.0083	1.320	99.5
Corrected Area (0.078)	-48	-3.3	0.510		1.000	100.0

* All areas are in sq.-in.

Fig. 40. Shear stress vs. normal stress, corrected for partial contact, for friction experiments on Kelly Limestone involving various sawcut angles (α) with #80 limestone gouge.

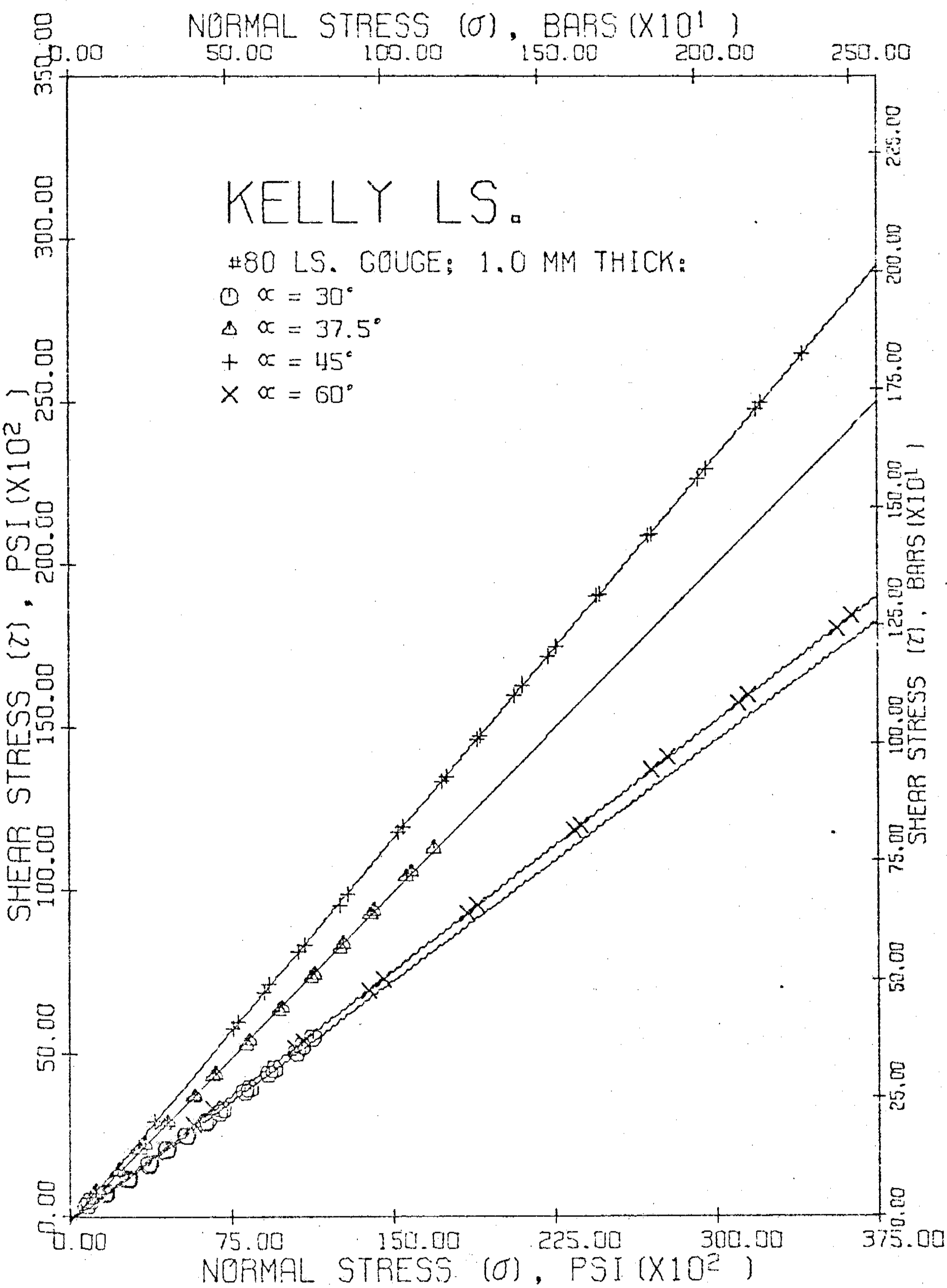
NØRMAL STRESS (σ), BARS (X10¹)
0.00
50.00
100.00
150.00
200.00
250.00
KELLY LS.
#80 LS. GØUGE; 1.0 MM THICK:
○ α = 30°
△ α = 37.5°
+ α = 45°
× α = 60°
SHEAR STRESS (τ), PSI (X10²)
0.00
50.00
100.00
150.00
200.00
250.00
300.00
350.00
SHEAR STRESS (τ), BARS (X10¹)
0.00
25.00
50.00
75.00
100.00
125.00
150.00
175.00
200.00
225.00
0.00
75.00
150.00
225.00
300.00
375.00
NØRMAL STRESS (σ), PSI (X10²)

Fig. 41. Shear stress vs. normal stress, corrected for partial contact, for friction experiments on Mesa Verde Sandstone involving various sawcut angles (α) with #80 sandstone gouge.

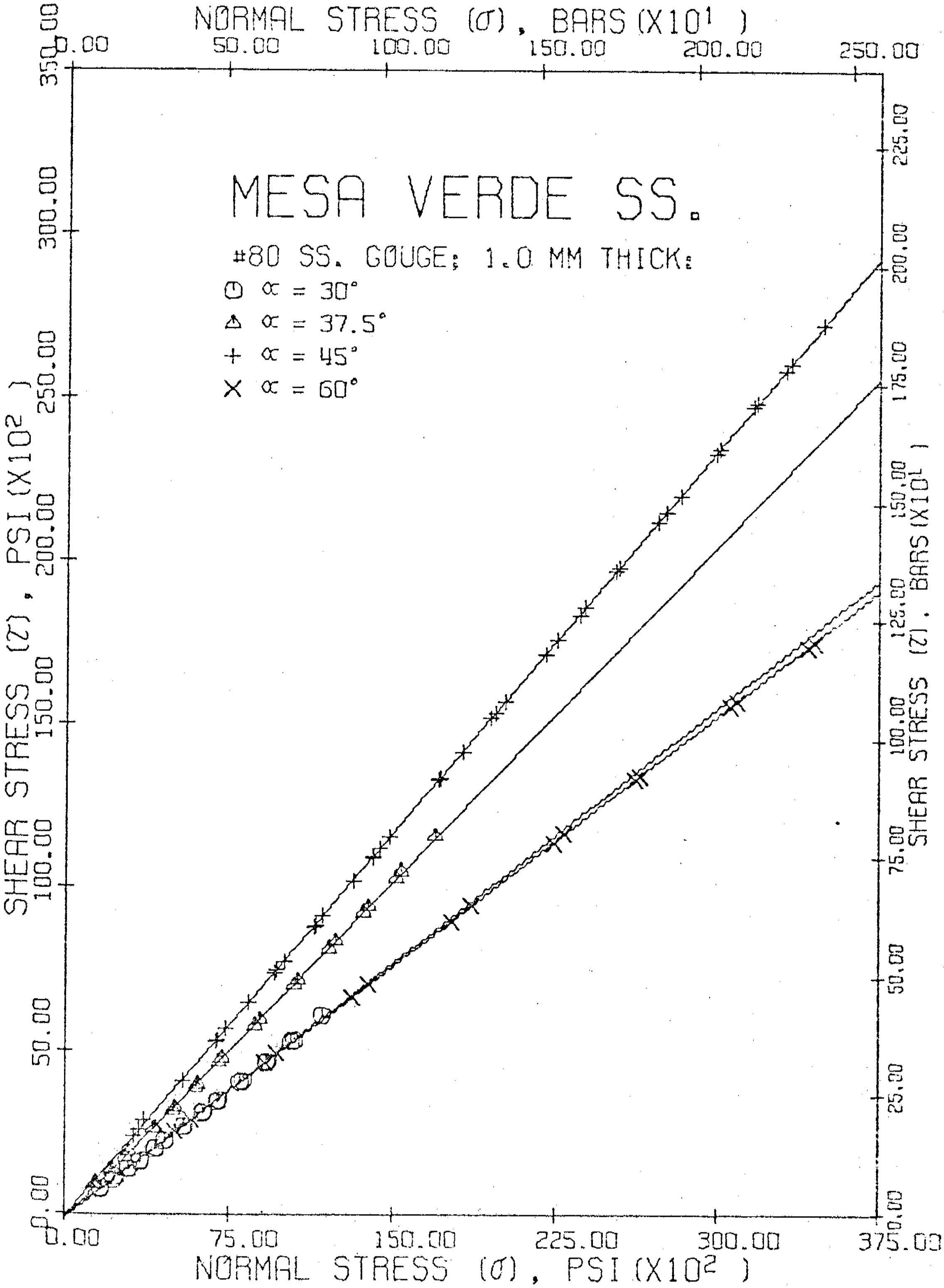

NORMAL STRESS (σ), BARS (X10¹)
0.00
50.00
100.00
150.00
200.00
250.00
MESA VERDE SS.
#80 SS. GOUGE; 1.0 MM THICK:
α = 30°
α = 37.5°
α = 45°
α = 60°
SHEAR STRESS (τ), PSI (X10²)
0.00
50.00
100.00
150.00
200.00
250.00
300.00
350.00
SHEAR STRESS (τ), BARS (X10¹)
25.00
50.00
75.00
100.00
125.00
150.00
175.00
200.00
225.00
NORMAL STRESS (σ), PSI (X10²)
0.00
75.00
150.00
225.00
300.00
375.00

Fig. 42. $\mu = \tau(\sigma)/\sigma$ vs. σ, corrected for partial contact, for friction experiments on Kelly Limestone involving various sawcut angles (α) with #80 sandstone gouge.

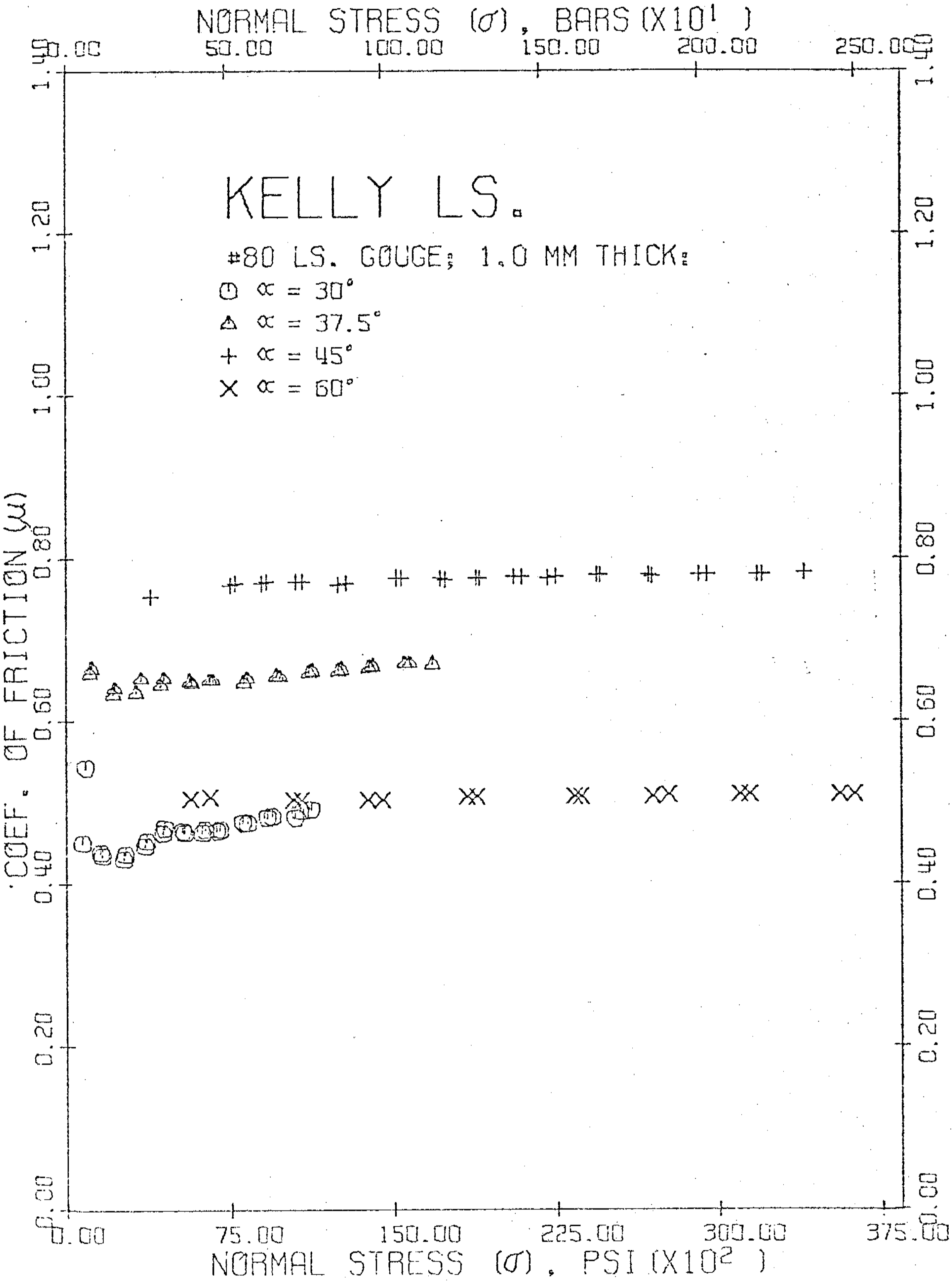
NORMAL STRESS (σ), BARS (X10[1])
0.00
50.00
100.00
150.00
200.00
250.00
KELLY LS.
#80 LS. GOUGE; 1.0 MM THICK:
α = 30°
α = 37.5°
α = 45°
α = 60°
COEF. OF FRICTION (μ)
0.00
0.20
0.40
0.60
0.80
1.00
1.20
1.40
0.00
75.00
150.00
225.00
300.00
375.00
NORMAL STRESS (σ), PSI (X10[2])

Fig. 43. $\mu = \tau(\sigma)/\sigma$ vs. σ, corrected for partial contact, for friction experiments on Mesa Verde Sandstone involving various sawcut angles (α) with #80 sandstone gouge.

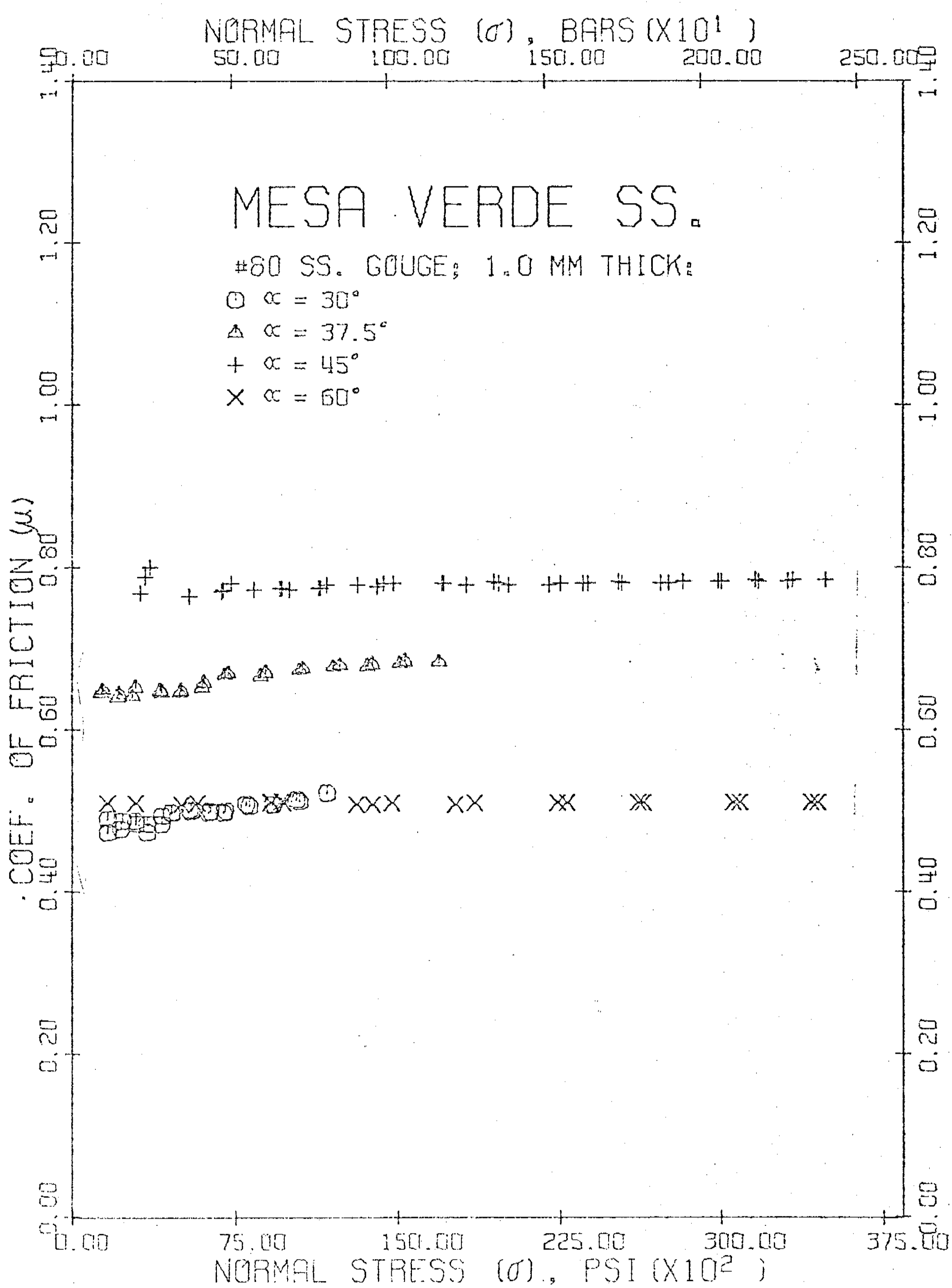
NORMAL STRESS (σ), BARS (X10¹)
0.00
50.00
100.00
150.00
200.00
250.00
MESA VERDE SS.
#60 SS. GOUGE; 1.0 MM THICK:
α = 30°
α = 37.5°
α = 45°
α = 60°
COEF. OF FRICTION (μ)
0.00
0.20
0.40
0.60
0.80
1.00
1.20
1.40
0.00
75.00
150.00
225.00
300.00
375.00
NORMAL STRESS (σ), PSI (X10²)

Fig. 44. $\mu = \tau(2.53 \text{ kb})/2.53$ kb vs. α, corrected for partial contact, for friction experiments on both Kelly Limestone and Mesa Verde Sandstone with #80 gouge.

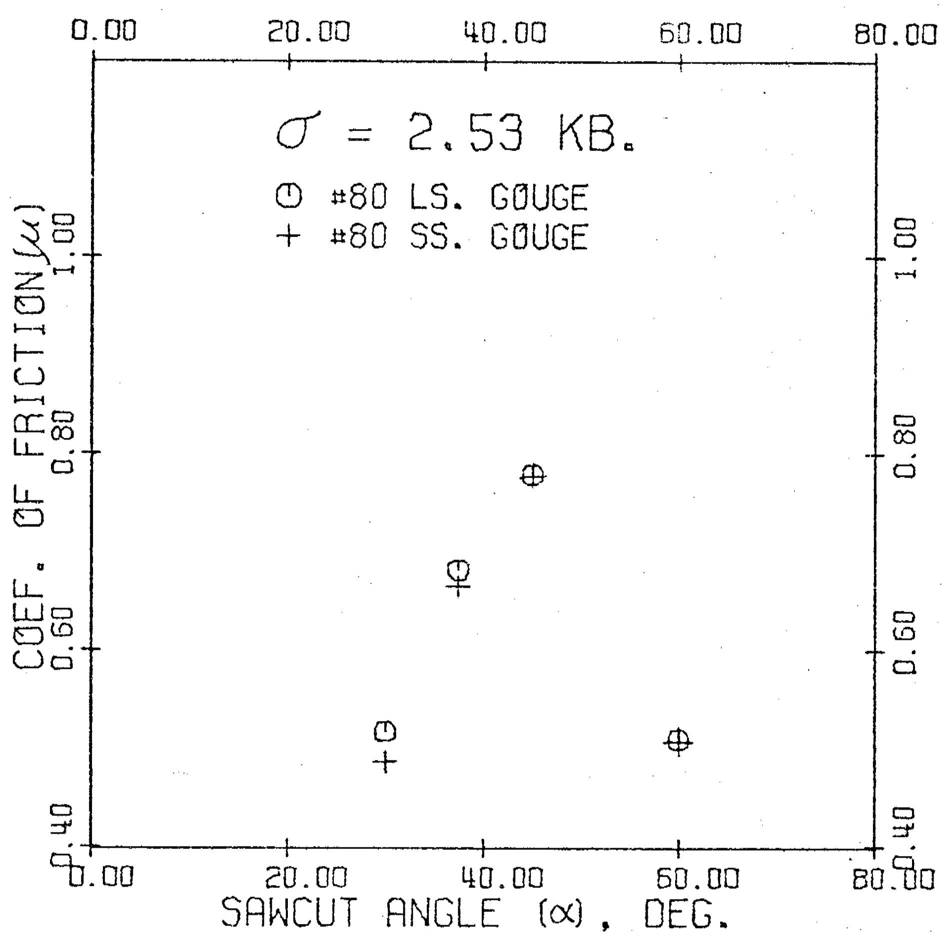
σ = 2.53 KB.
⊖ #80 LS. GØUGE
+ #80 SS. GØUGE
COEF. ØF FRICTIØN (μ)
SAWCUT ANGLE (α), DEG.
0.00
20.00
40.00
60.00
80.00
0.40
0.60
0.80
1.00

Pore pressure. Three separate experiments were conducted with water-saturated gouge for both rock types (with $\alpha=45^{o}$ and 1.0-mm gouge thickness), each corresponding to different values of water pore-pressure p in the gouge. The #80 wet gouge tests presented above represent the case p=0 and are used in comparison to the other tests with variable p.

The limestone pore-pressure friction tests represent data for p=0, 550 psi (37.9 bars), and 1260 psi (86.9 bars), while the sandstone pore-pressure experiments represent p 0, 500 psi (34.5 bars), and 1150 psi (79.3 bars). Basic (σ, τ) data are presented in Appendix II Tables AII-48 to AII-51, least-square data are presented in Table 11, and graphs of τ vs. σ are given in Figures 45 and 46. The corresponding friction function (Equation 8) is plotted in Figures 47 and 48.

Sandstone data were further analyzed separately by considering static and kinetic data, as shown in Appendix II Tables AII-52 to AII-55 and Table 11. Figures 49 and 50 show the variations of as a function of for this data at the two highest pore pressures. Corresponding coefficients of friction as a function of normal stress are presented in Figure 51.

TABLE 11. Least-Square Data $\tau=\tau_0+B\sigma^n$ for Friction Experiments with 1.0-mm Thick Limestone and Sandstone Gouge at $\alpha=45^\circ$ for Various Pore Pressures (p)

Experimental Condition	τ_0 (psi)	(bars)	B <psi>	<bars>	n	(%)
Kelly Limestone (A_0 0.74; A_0' 0.111 in^2)						
p=0						
Uncorrected Area	0	0.0	0.0161	0.0269	1.192	99.5
Corrected Area	-93	-6.4	0.779		1.000	100.0
p=550 psi=37.9 bars						
Uncorrected Area	-61	-4.2	0.0254	0.0362	1.133	99.5
Corrected Area	-162	-11.1	0.775		1.000	100.0
p=1260 psi=86.9 bars						
Uncorrected Area	34	2.3	0.00088	0.0033	1.491	99.6
Corrected Area	-168	-11.6	0.776		1.000	100.0
Mesa Verde Sandstone (A_0 0.74; A_0' 0.109 in^2)						
p=0						
Uncorrected Area	19	1.3	0.0186	0.0300	1.179	99.3
Corrected Area	-51	-3.6	0.784		1.000	100.0
p=500 psi=34.5 bars						
Uncorrected Area	113	7.8	0.00042	0.0019	1.564	95.0
Corrected Area	11	0.8	0.775		1.000	100.0
Static Data						
Uncorrected Area	49	3.4	0.00098	0.0036	1.482	99.4
Corrected Area	-97	-6.7	0.779		1.000	100.0
Kinetic Data						
Uncorrected Area	188	13.0	0.00006	0.0005	1.756	96.9
Corrected Area	141	9.7	0.770		1.000	100.0
p=1150 psi=79.3 bars						
Uncorrected Area	114	7.9	0.00118	0.0038	1.433	86.8
Corrected Area	40	2.8	0.772		1.000	100.0
Static Data						
Uncorrected Area	89	6.2	0.00003	0.0003	1.855	98.7
Corrected Area	-99	-6.8	0.775		1.000	100.0
Kinetic Data						
Uncorrected Area	120	8.3	0.0587		1.000	95.0
Corrected Area	200	13.8	0.768		1.000	100.0

Fig. 45. Shear stress vs. normal stress, corrected for partial contact, for friction experiments on Kelly Limestone involving #80 limestone gouge with various water pore-pressures (p).

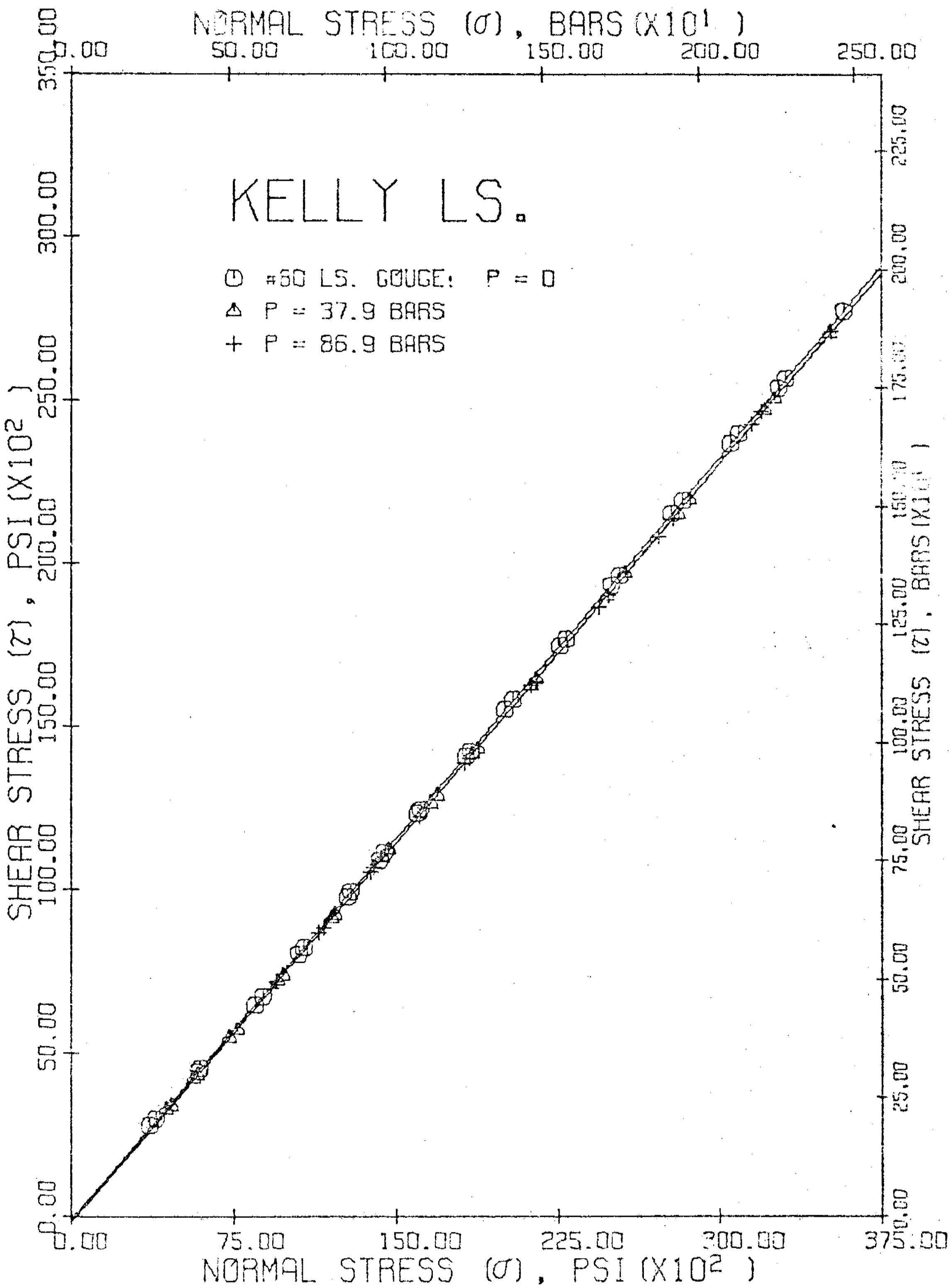
NORMAL STRESS (σ), BARS (X10¹)
0.00
50.00
100.00
150.00
200.00
250.00
KELLY LS.
○ #60 LS. GOUGE: P = 0
△ P = 37.9 BARS
+ P = 86.9 BARS
SHEAR STRESS (τ), PSI (X10²)
0.00
50.00
100.00
150.00
200.00
250.00
300.00
350.00
SHEAR STRESS (τ), BARS (X10¹)
25.00
50.00
75.00
100.00
125.00
175.00
200.00
225.00
NORMAL STRESS (σ), PSI (X10²)
75.00
150.00
225.00
300.00
375.00

Fig. 46. Shear stress vs. normal stress, corrected for partial contact, for friction experiments on Mesa Verde Sandstone involving #80 sandstone gouge with various water pore-pressures.

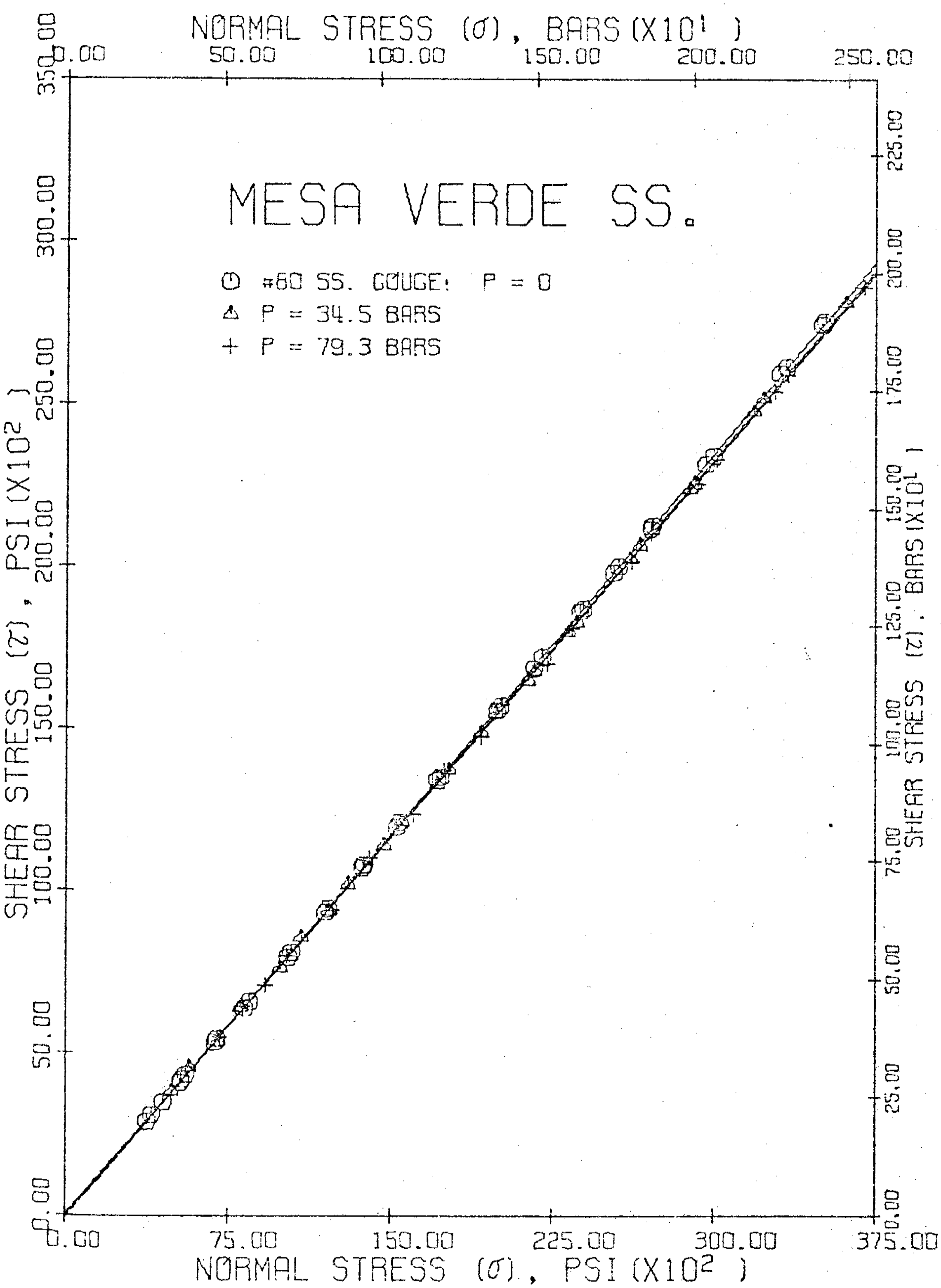
NØRMAL STRESS (σ), BARS (X10¹)
0.00
50.00
100.00
150.00
200.00
250.00
MESA VERDE SS.
#60 SS. GØUGE: P = 0
P = 34.5 BARS
P = 79.3 BARS
SHEAR STRESS (τ), PSI (X10²)
0.00
50.00
100.00
150.00
200.00
250.00
300.00
350.00
SHEAR STRESS (τ), BARS (X10¹)
0.00
25.00
50.00
75.00
100.00
125.00
150.00
175.00
200.00
225.00
0.00
75.00
150.00
225.00
300.00
375.00
NØRMAL STRESS (σ), PSI (X10²)

Fig. 47. $\mu=\tau(\sigma)/\sigma$ vs. σ', corrected for partial contact, for friction experiments on Kelly Limestone involving 1-mm thick #80 limestone gouge at $\alpha=45^{\circ}$ with various water pore-pressures (p).

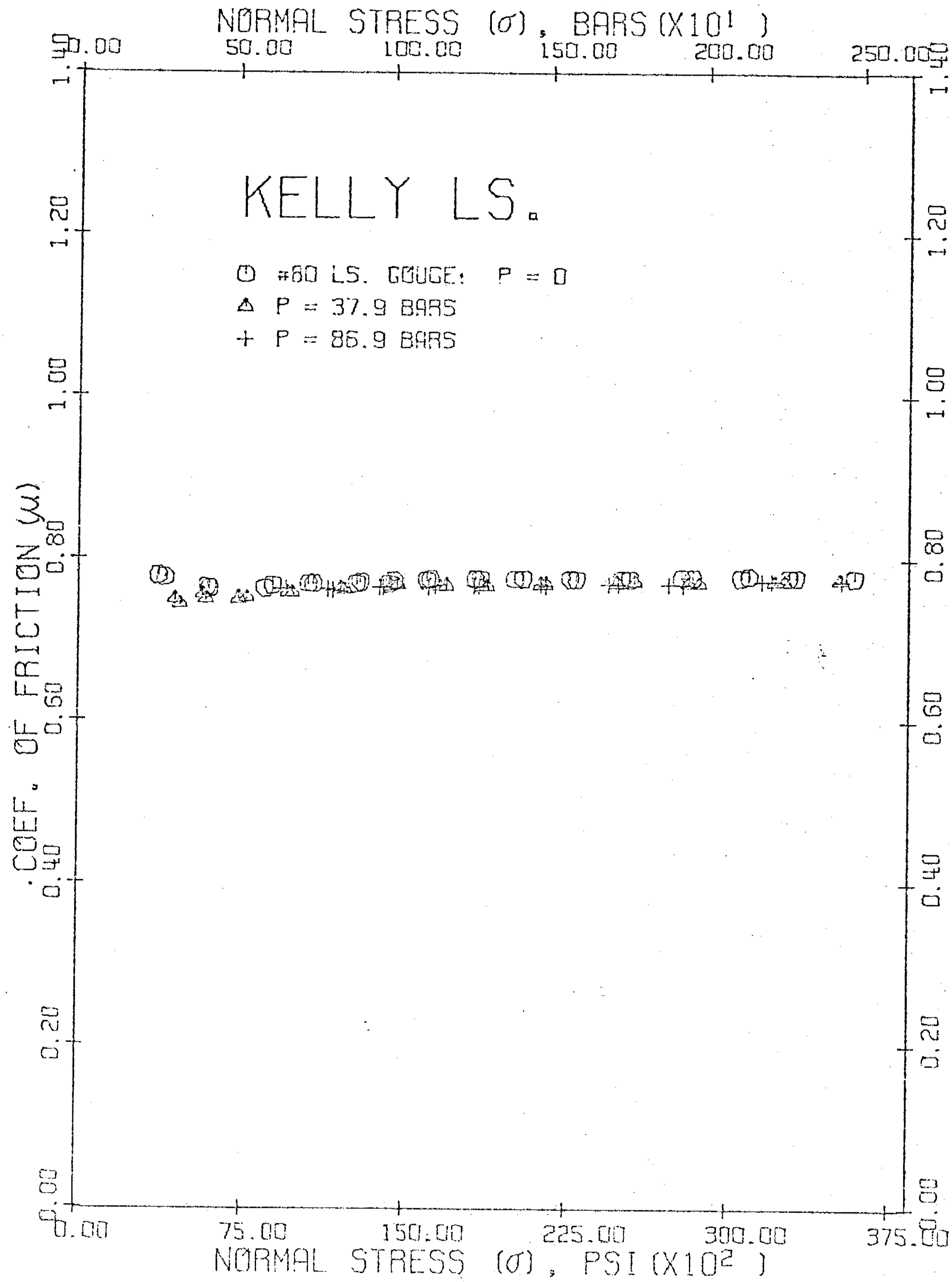
NØRMAL STRESS (σ), BARS (X10¹)
0.00
50.00
100.00
150.00
200.00
250.00
KELLY LS.
#60 LS. GØUGE: P = 0
P = 37.9 BARS
P = 86.9 BARS
COEF. ØF FRICTION (μ)
0.00
0.20
0.40
0.60
0.80
1.00
1.20
1.40
0.00
75.00
150.00
225.00
300.00
375.00
NØRMAL STRESS (σ), PSI (X10²)

Fig. 48. $\mu=\tau(\sigma)/\sigma$ vs. σ, corrected for partial contact, for friction experiments on Mesa Verde Sandstone involving 1-mm thick #80 sandstone gouge at $\alpha=45^{\circ}$ with various water pore-pressures (p).

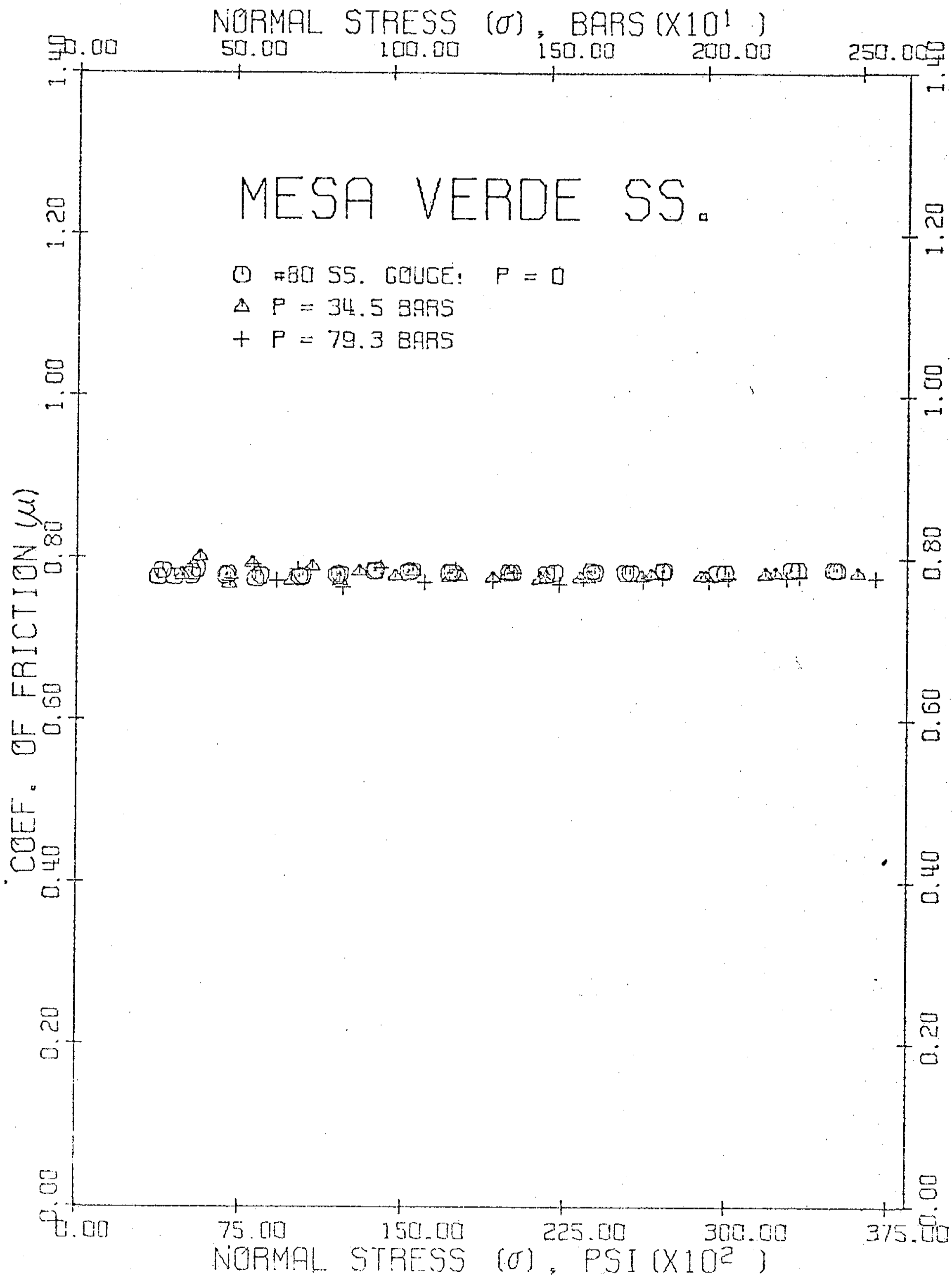
NORMAL STRESS (σ), BARS (X10¹)
0.00
50.00
100.00
150.00
200.00
250.00
MESA VERDE SS.
#80 SS. GOUGE: P = 0
P = 34.5 BARS
P = 79.3 BARS
COEF. OF FRICTION (μ)
0.00
0.20
0.40
0.60
0.80
1.00
1.20
1.40
0.00
75.00
150.00
225.00
300.00
375.00
NORMAL STRESS (σ), PSI (X10²)

Fig. 49. Shear stress vs. normal stress, corrected for partial contact, for static and kinetic data of friction experiment on Mesa Verde Sandstone involving 1-mm thick #80 sandstone gouge at $\alpha=45^{\circ}$ with p=34.5 bars.

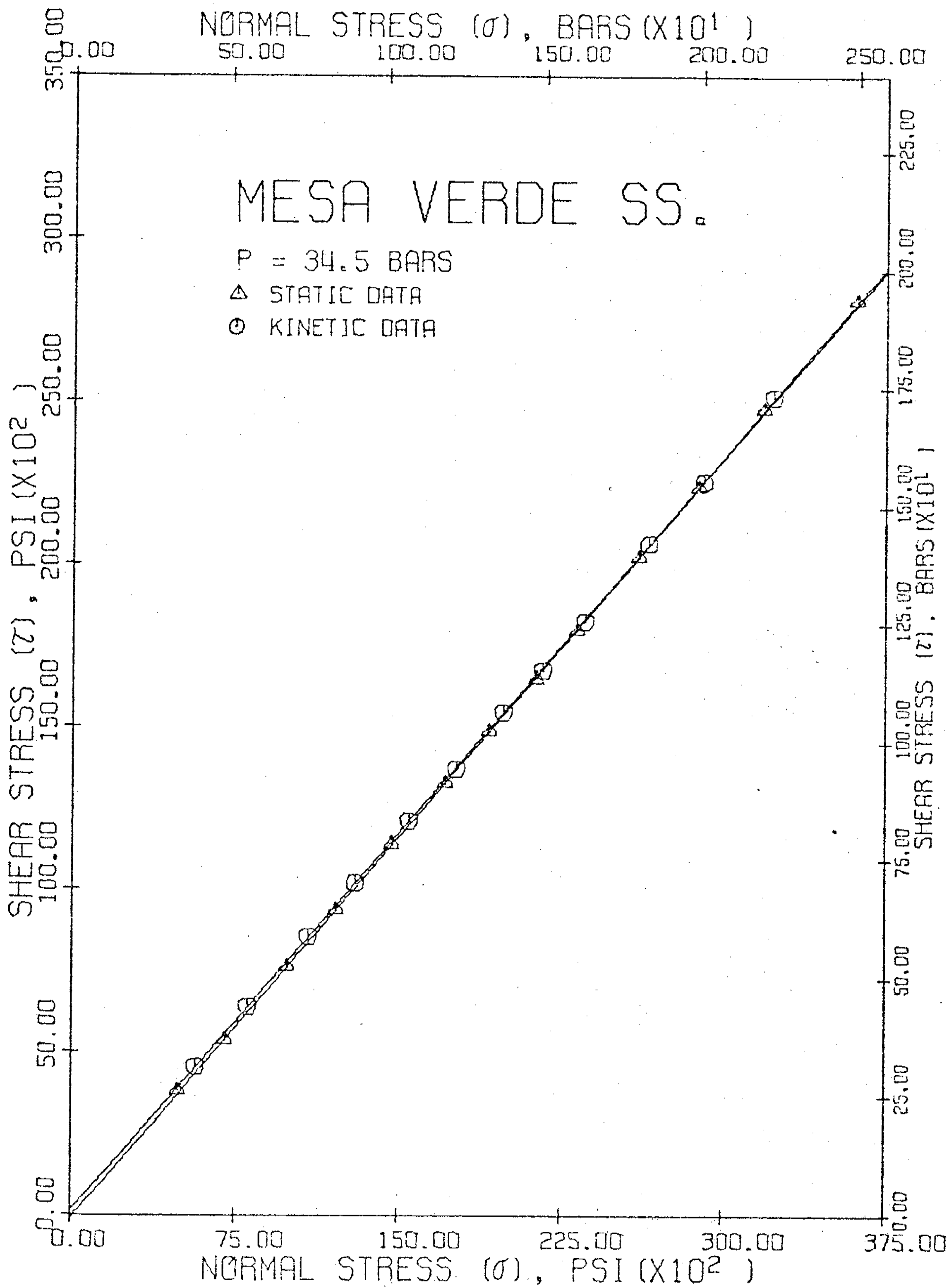
NØRMAL STRESS (σ), BARS (X10¹)
0.00
50.00
100.00
150.00
200.00
250.00
MESA VERDE SS.
P = 34.5 BARS
STATIC DATA
KINETIC DATA
SHEAR STRESS (τ), PSI (X10²)
0.00
50.00
100.00
150.00
200.00
250.00
300.00
350.00
SHEAR STRESS (τ), BARS (X10¹)
0.00
25.00
50.00
75.00
100.00
125.00
150.00
175.00
200.00
225.00
0.00
75.00
150.00
225.00
300.00
375.00
NØRMAL STRESS (σ), PSI (X10²)

Fig. 50. Shear stress vs. normal stress, corrected for partial contact, for static and kinetic data of friction experiment on Mesa Verde Sandstone involving 1-mm thick #80 sandstone gouge at $\alpha=45^{\circ}$ with p=79.3 bars.

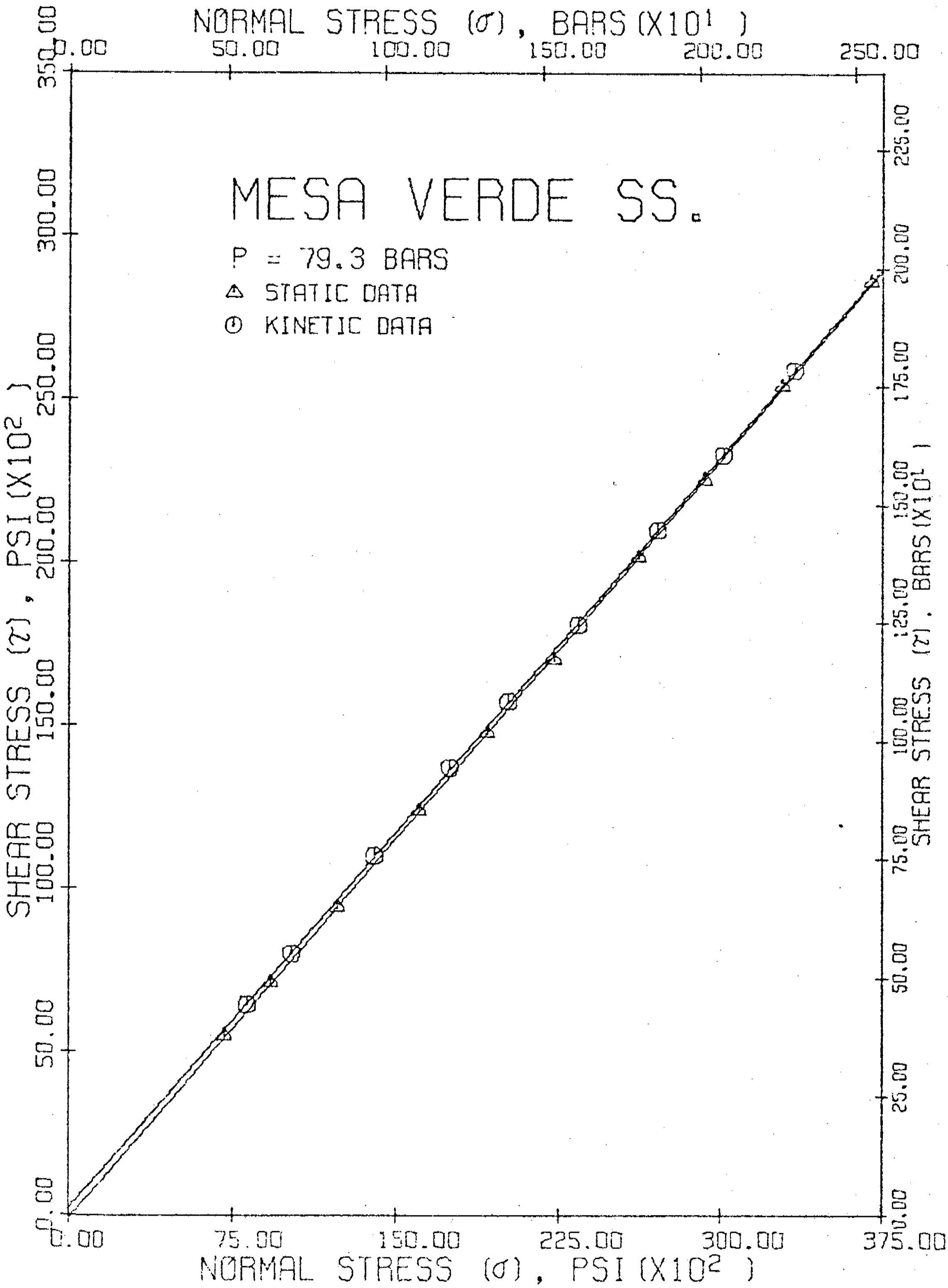
NORMAL STRESS (σ), BARS (X10¹)
0.00
50.00
100.00
150.00
200.00
250.00
MESA VERDE SS.
P = 79.3 BARS
STATIC DATA
KINETIC DATA
SHEAR STRESS (τ), PSI (X10²)
0.00
50.00
100.00
150.00
200.00
250.00
300.00
350.00
SHEAR STRESS (τ), BARS (X10¹)
0.00
25.00
50.00
75.00
100.00
125.00
150.00
175.00
200.00
225.00
NORMAL STRESS (σ), PSI (X10²)
0.00
75.00
150.00
225.00
300.00
375.00

Fig. 51. $\mu = \tau(\sigma)/\sigma$ vs. σ, corrected for partial contact, for static and kinetic data of friction experiments on Mesa Verde Sandstone involving 1-mm thick #80 sandstone gouge at $\alpha = 45^{\circ}$ with p=34.5 and 79.3 bars.

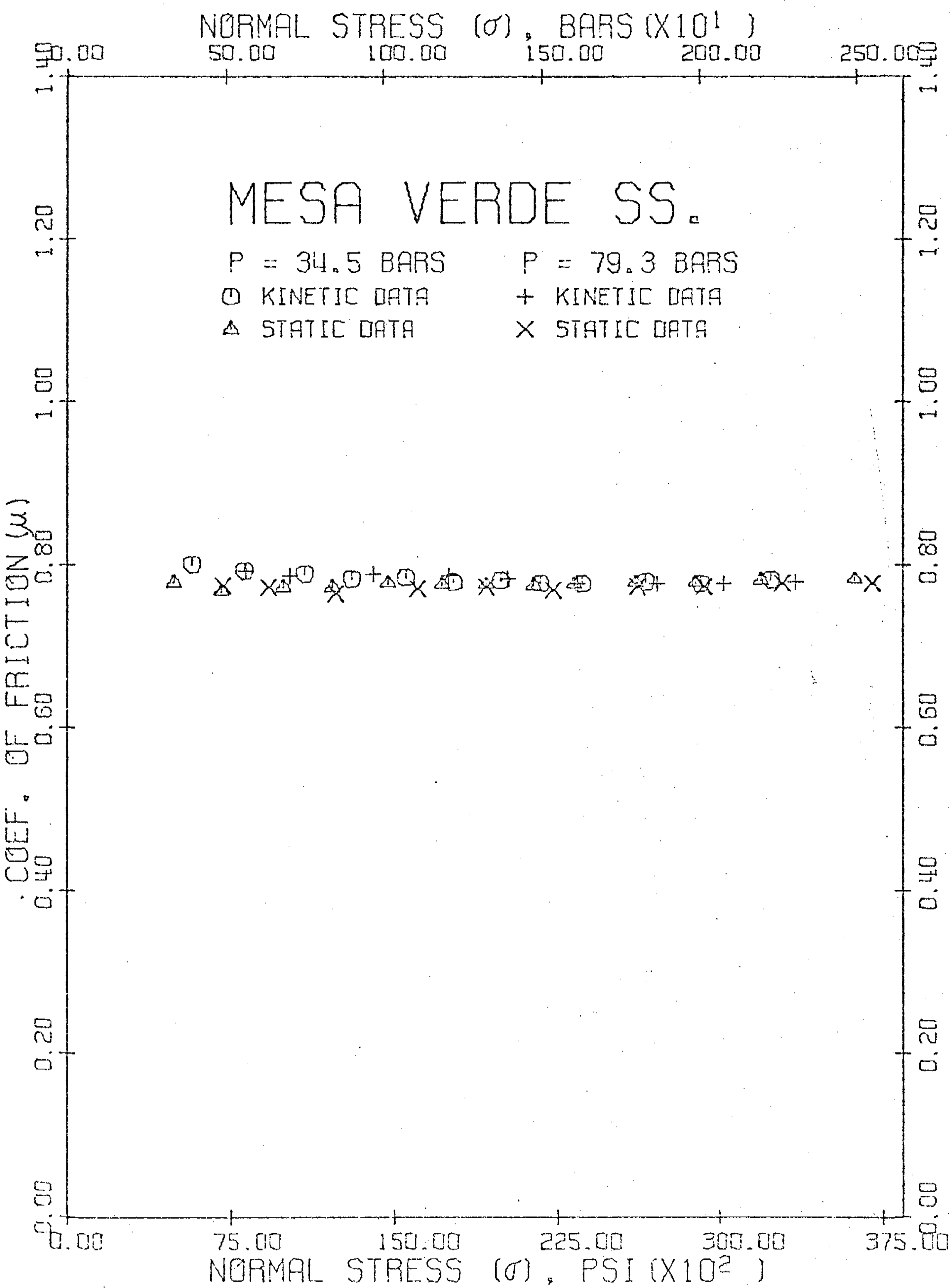
NORMAL STRESS (σ), BARS (X10¹)
0.00
50.00
100.00
150.00
200.00
250.00
MESA VERDE SS.
P = 34.5 BARS
P = 79.3 BARS
KINETIC DATA
STATIC DATA
KINETIC DATA
STATIC DATA
COEF. OF FRICTION (μ)
0.00
0.20
0.40
0.60
0.80
1.00
1.20
1.40
0.00
75.00
150.00
225.00
300.00
375.00
NORMAL STRESS (σ), PSI (X10²)

Visual Observations

Photographs under reflected light were taken of post-run gouge for the dry and water-saturated gouge tests and of some shear surfaces and deformed cores produced during the fracture experiments.

To obtain a visual comparison between features of the gouge in friction experiments and structural makeup of gouge formed during fracture experiments, photomicrographs under reflected light of fault zones in fractured specimens were taken. Photomicrographs were also taken of the sawcut surfaces and of the gouge before and after each friction experiment to aid in describing the nature of sliding and its effect on gouge generation and on textural changes in pre-existing gouge.

All photographs are given in Figures 52-69, and correspond to the order in which the experimental data were presented in previous sections.

Fig. 52. (a) Fractured limestone cores representing (left to right) σ_c=550, 800, and 2000 psi; note jointing associated with major faults. (b) Fault surface of limestone core for σ_c=800 psi showing layer of gouge. (1-in dia. cores.)

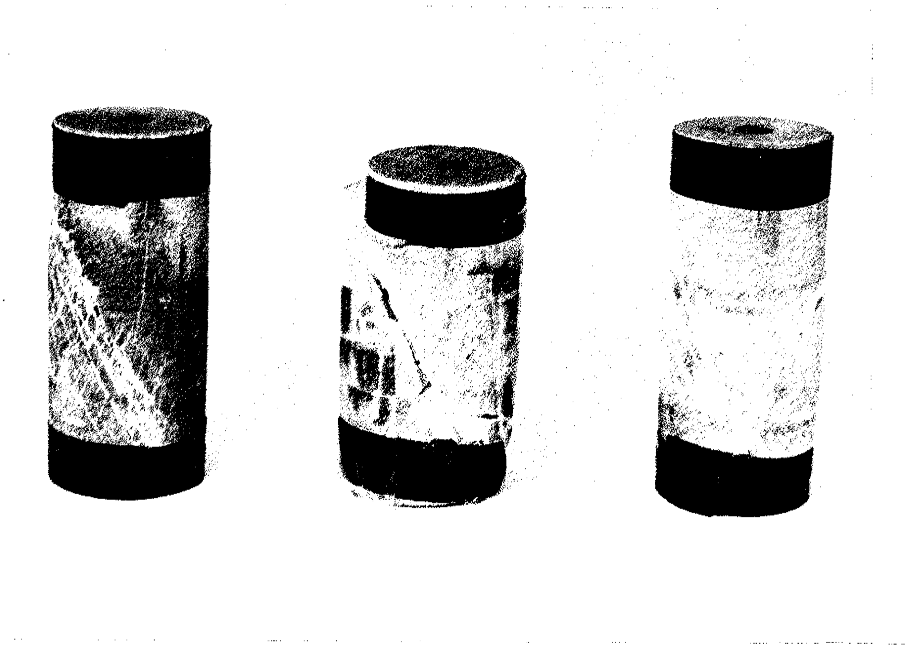

(a)

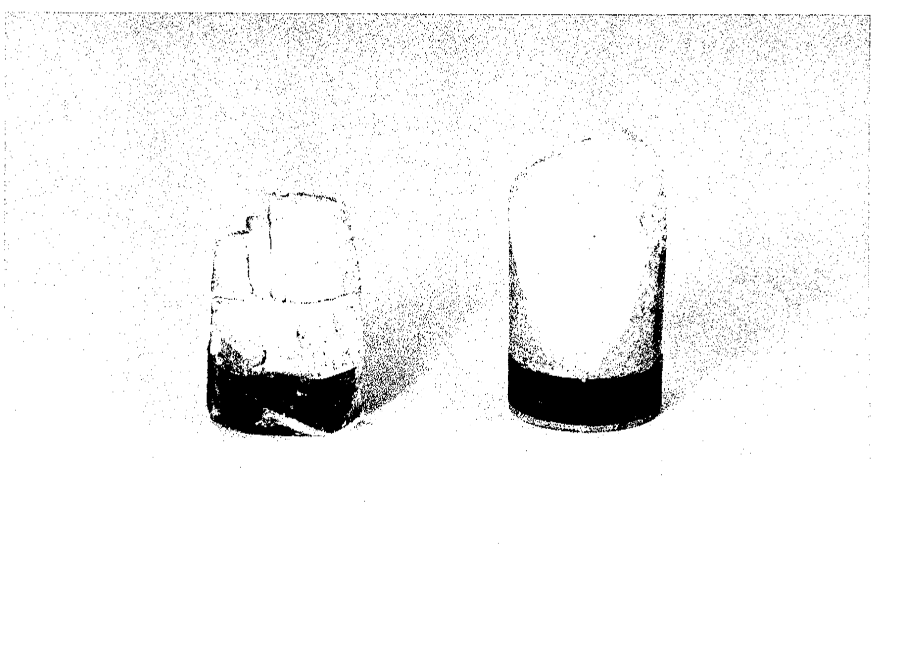

(b)

Fig. 53. (a) Fractured limestone cores representing (left) σ_c=5000 psi and (right) σ_c=9700 psi. (b) Magnified view of jointing in barrel-shaped specimen for σ_c=9700 psi of (a) above; note possibility of segregated "plastic" flow bands around primary calcite grains, which may explain macroscopic ductile behavior.

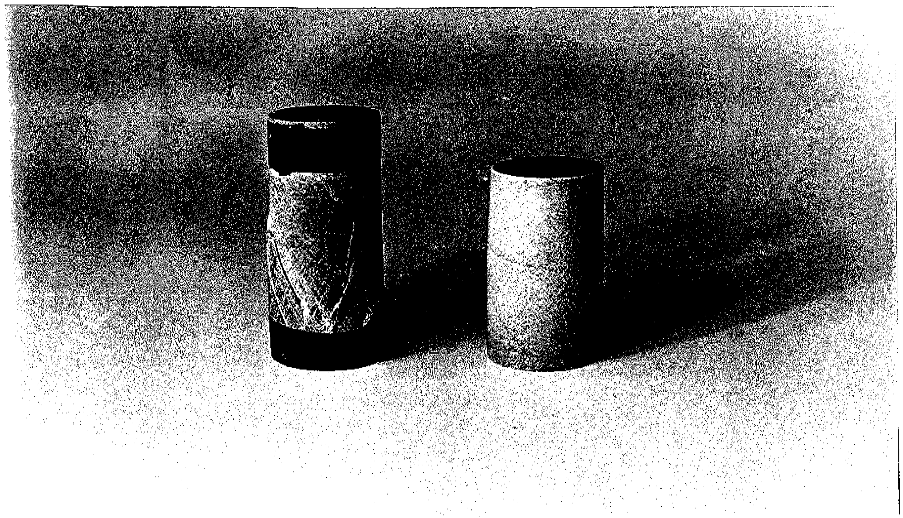

(a)

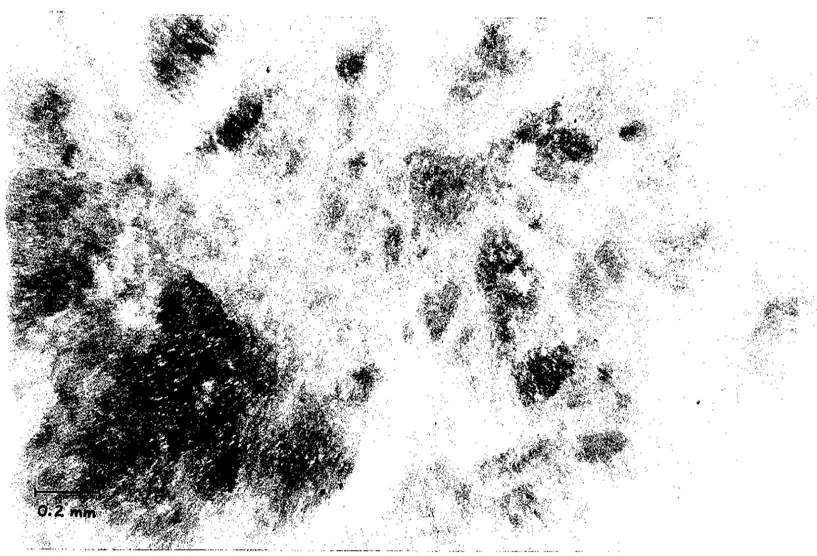

(b)

Fig. 54. (a) Fractured sandstone cores representing (left to right) σ_c=590 and 2000 psi; note clean, well-defined fault surfaces. (b) Fault surface of sandstone core for σ_c=2000 psi showing minor amounts of gouge. Fractures at higher σ_c appear similar to that at σ_c=2000 psi. (1-in dia. cores.)

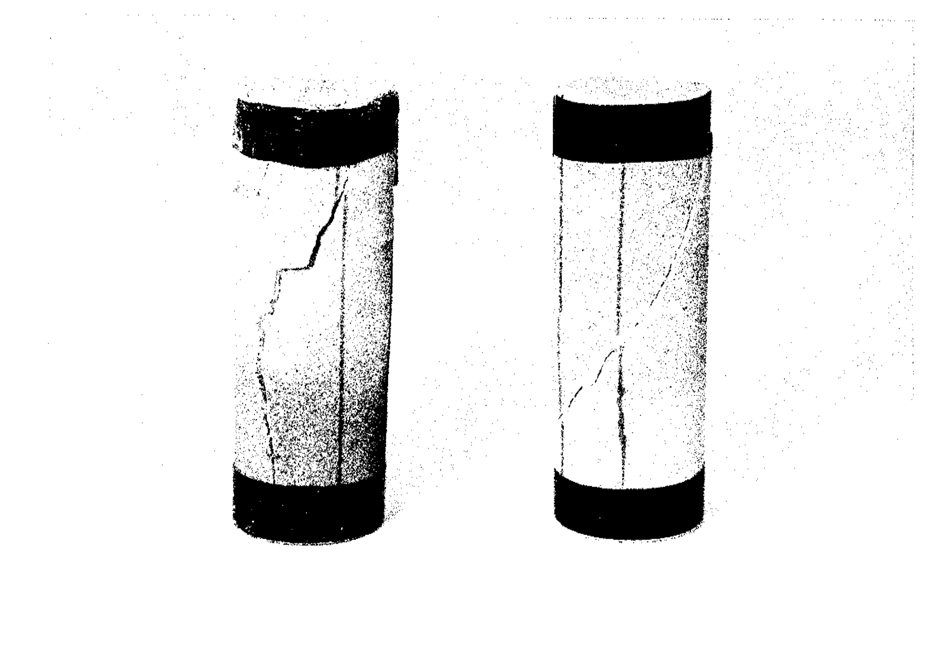

(a)

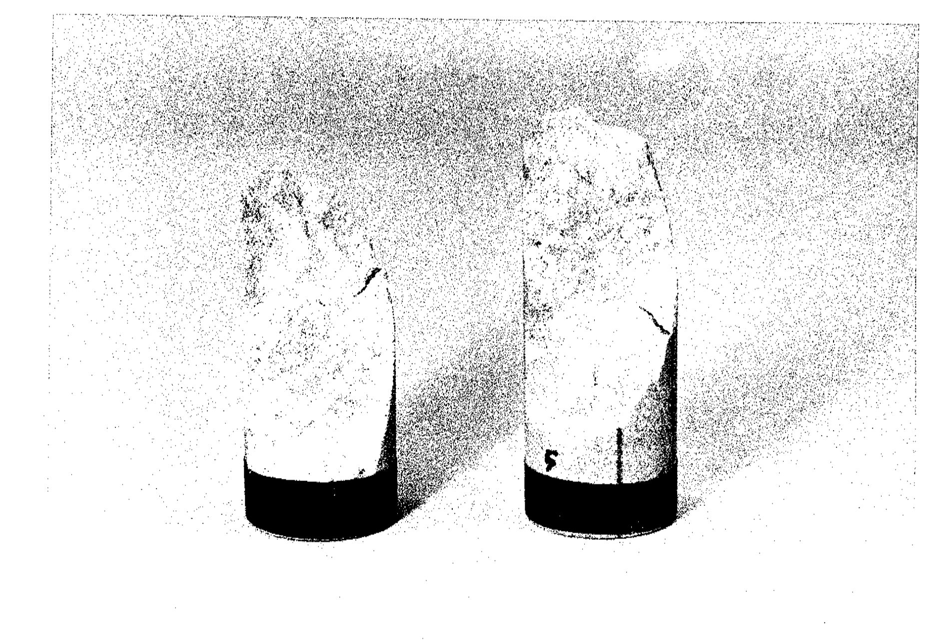

(b)

Fig. 55. Magnified plan views of limestone fracture surfaces for (a) σ_c=800 psi and (b) σ_c=590 psi displaying abundance of puffy, cotton-like gouge (reflected light).

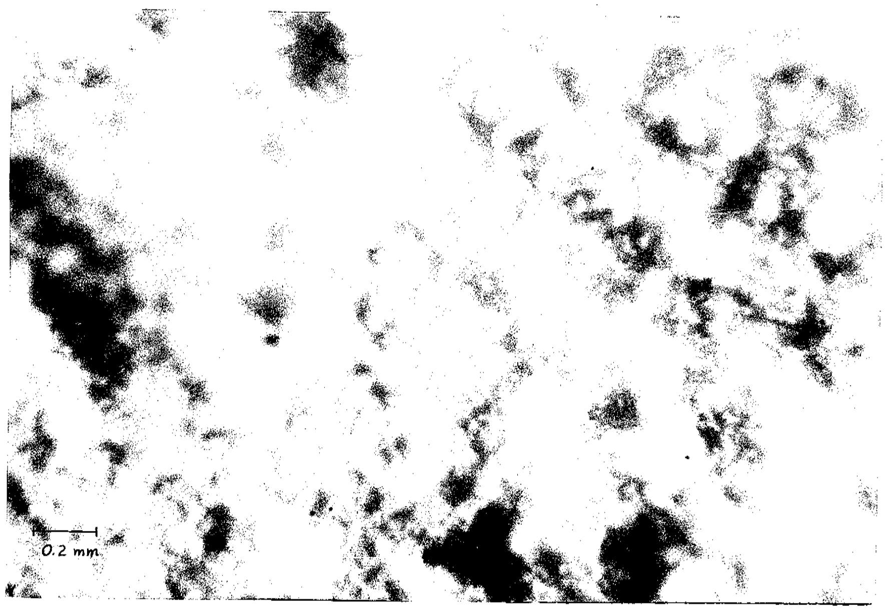

(a)

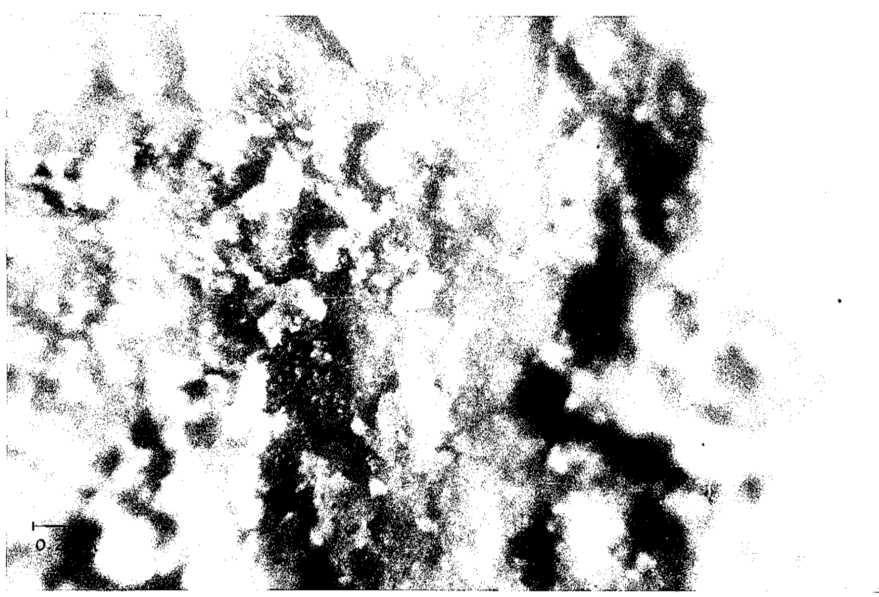

(b)

Fig. 56. Magnified cross-sectional views of fault systems in fractured limestone for σ_c=2000 psi (a) along a wide gouge zone and (b) along the same fault but near outer edge of core (reflected light).

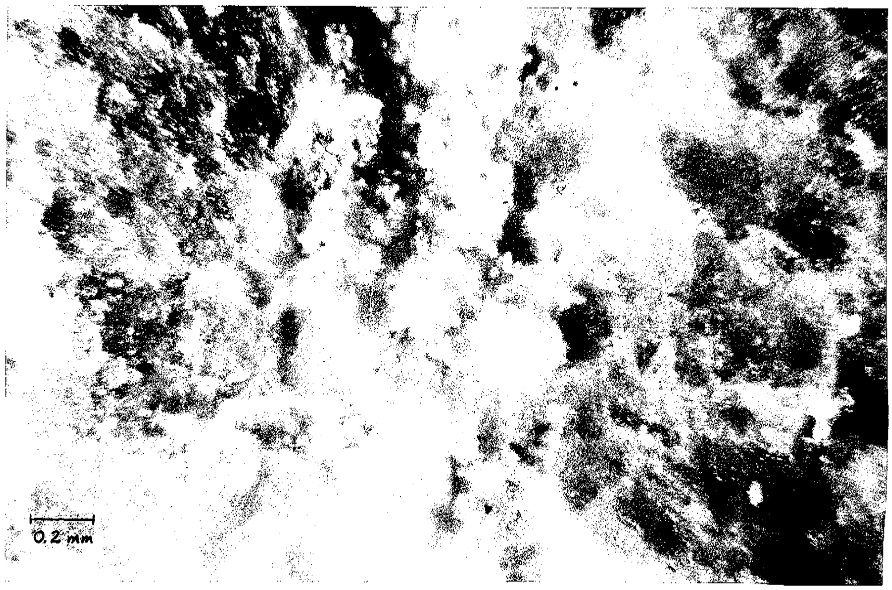

(a)

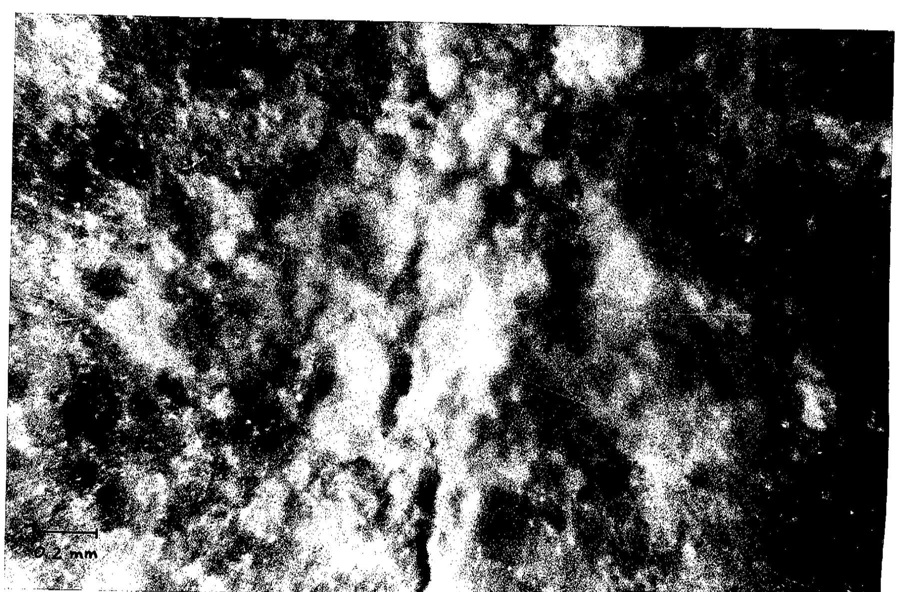

(b)

Fig. 57. Magnified plan views of sandstone fracture surfaces for (a) σ_c=590 psi and (b) σ_c=2000 psi (reflected light).

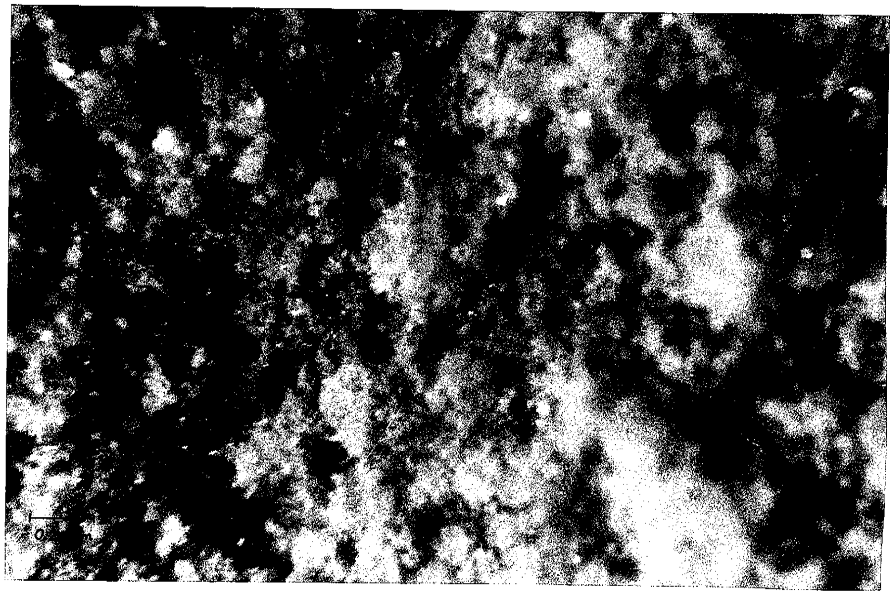

(a)

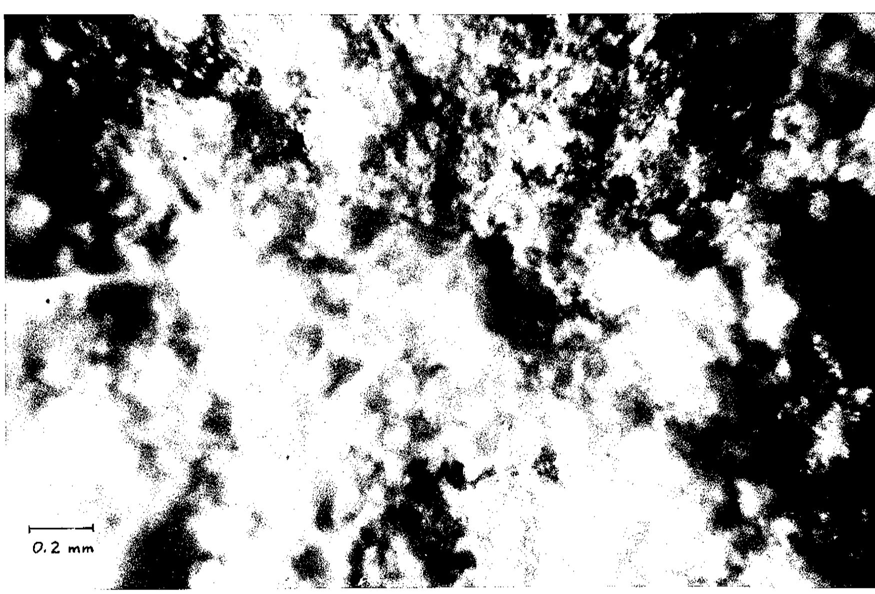

(b)

Fig. 58. (a) Side view of core containing sawcut at $\alpha=45^{\circ}$ polished by hand on #100 grit; note obvious partial contact between surfaces. (b) Appearance of polished surface after friction experiment showing slickensides over central part of surface.

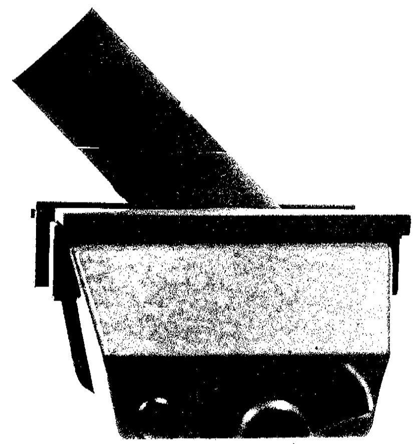

(a)

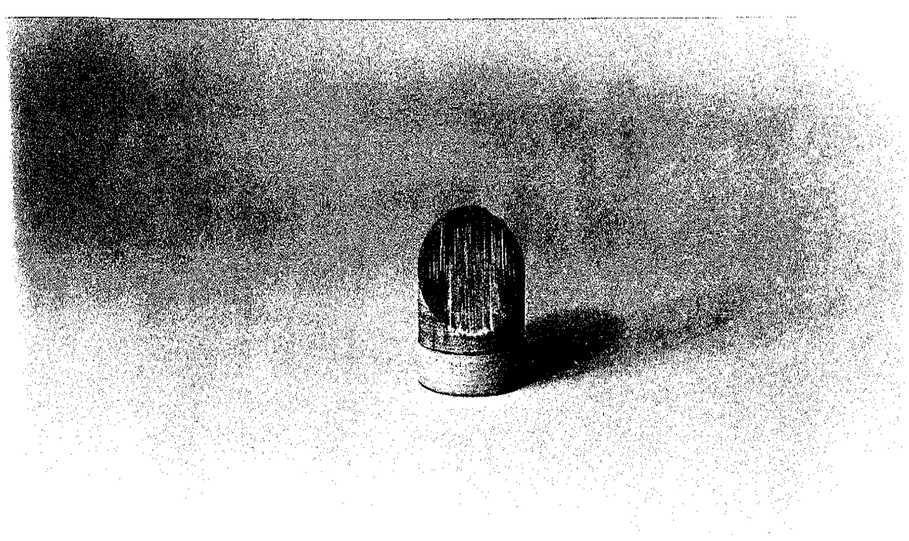

(b)

Fig. 59. Magnified plan views of limestone sawcut surfaces prepared on #100 grit (a) prior to a friction experiment and (b) after an experiment; note reduction of original furrows oriented left to right by sliding in vertical direction and presence of strewn gouge especially in right half of (b) (eflected light

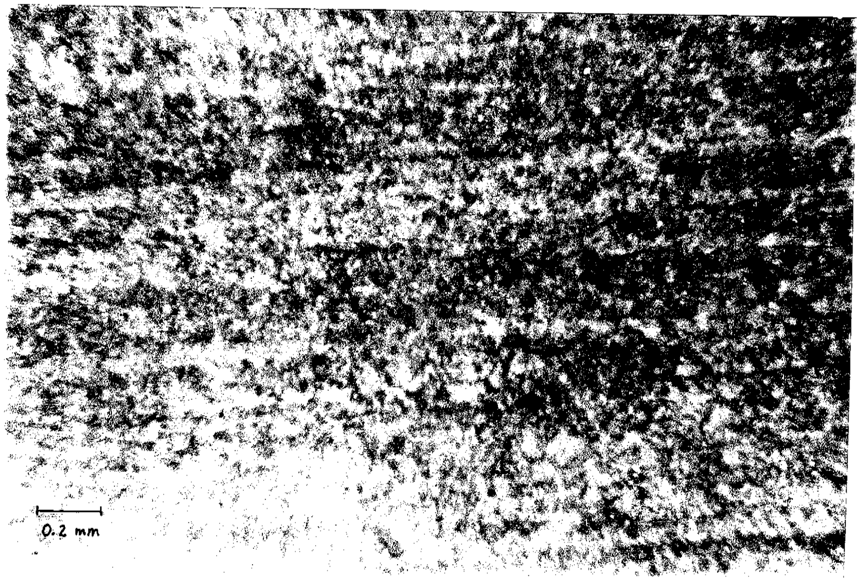

(a)

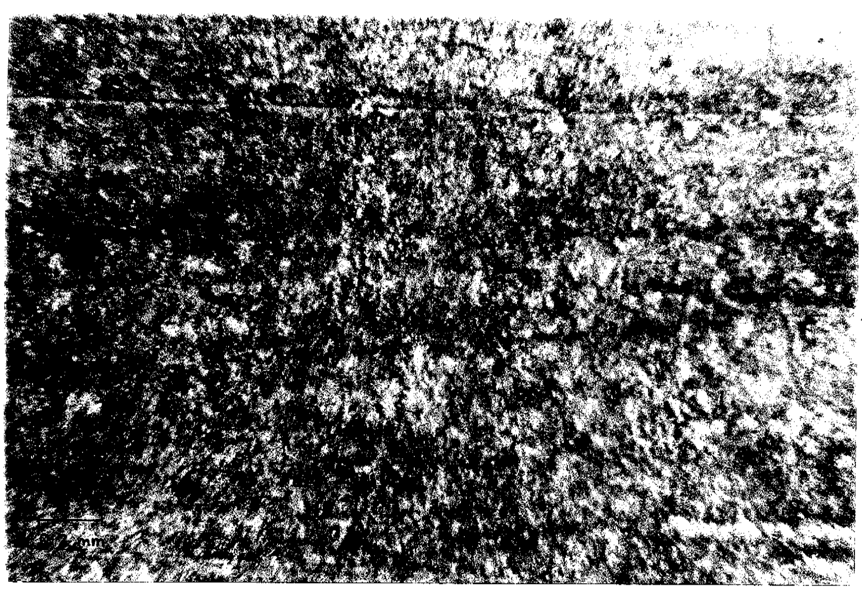

(b)

Fig. 60. Magnified plan views of limestone sawcut surfaces prepared on #600 grit (a) prior to a friction experiment and (b) after an experiment; note little observed difference between (a) and (b) (reflected light).

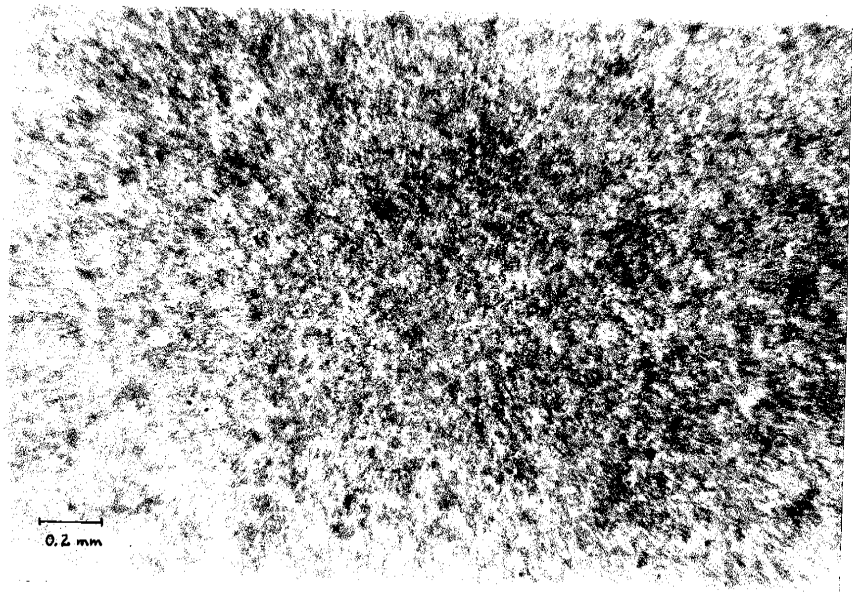

(a)

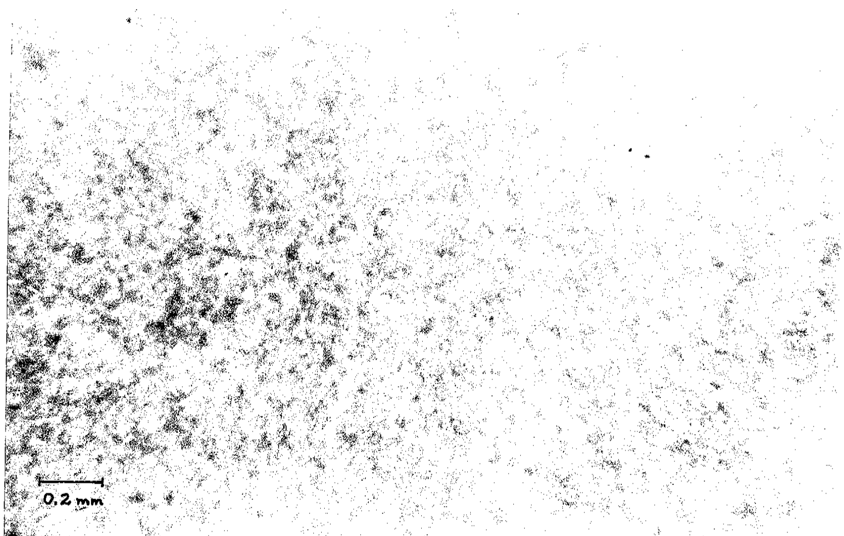

(b)

Fig. 61. Appearance of #80 synthetic limestone gouge used in friction experiments (reflected light).

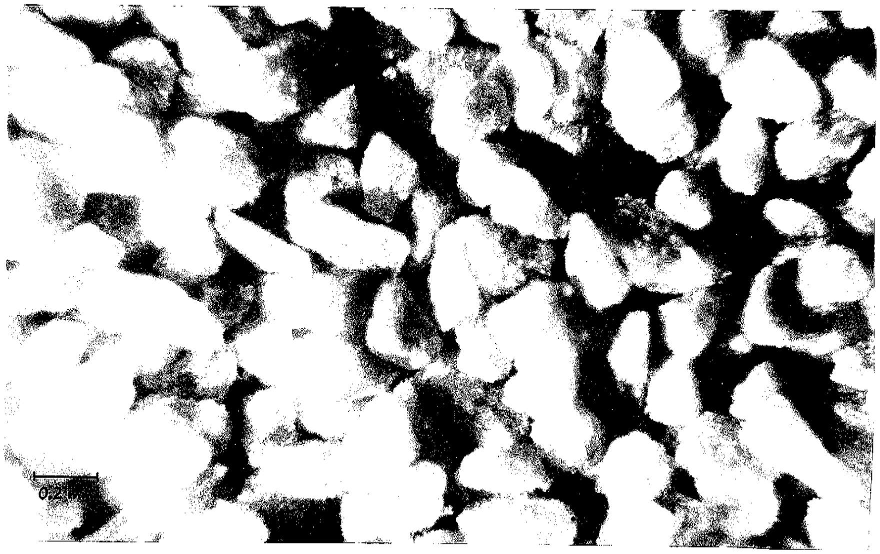

(a)

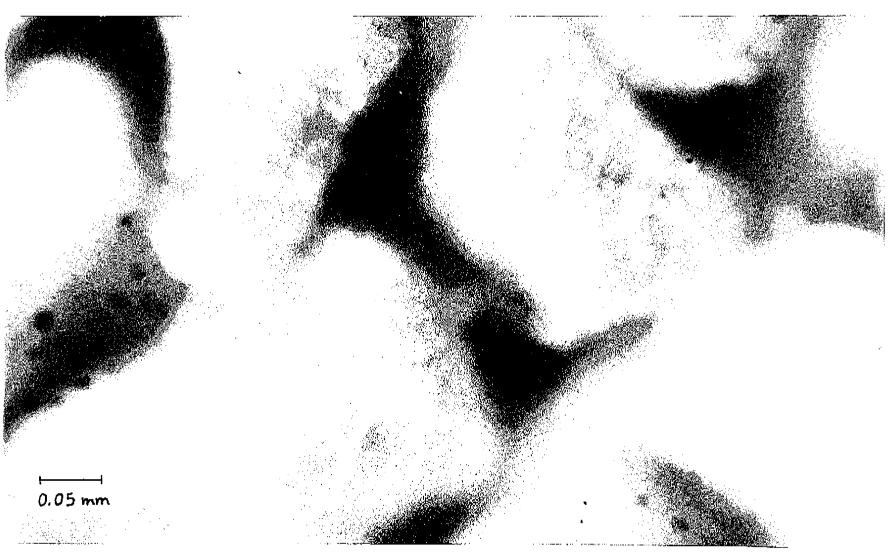

(b)

Fig. 62. Appearance of #80 synthetic sandstone gouge used in friction experiments (reflected light).

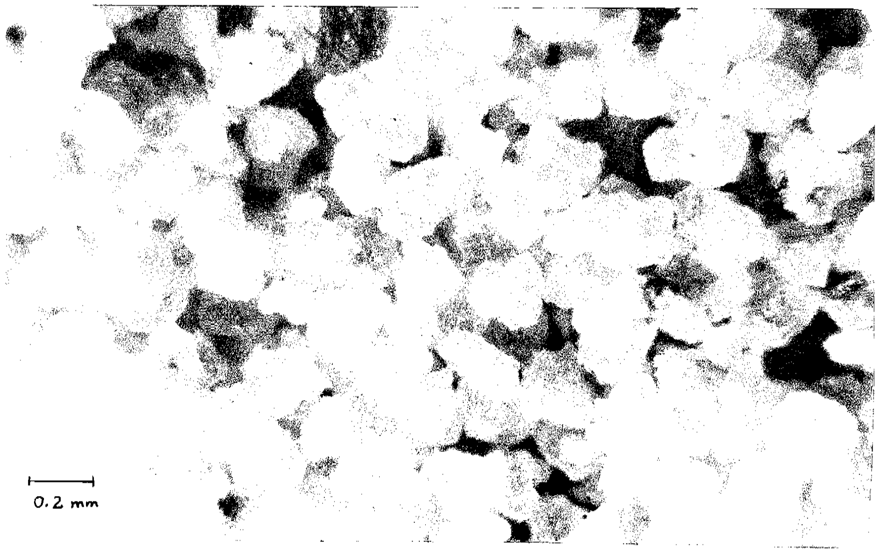

(a)

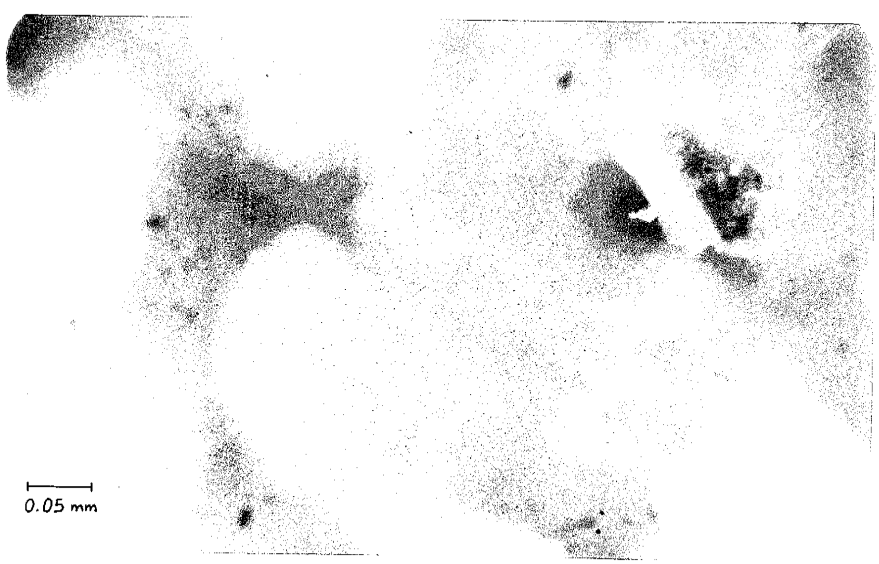

(b)

Fig. 63. Appearance of sandstone sawcut surfaces (a) without gouge and (b) with #80 gouge after friction experiments. Note indication of stress concentration near center of sawcut in core piece on left in (b), exemplifying partial contact. (1-in dia. cores.)

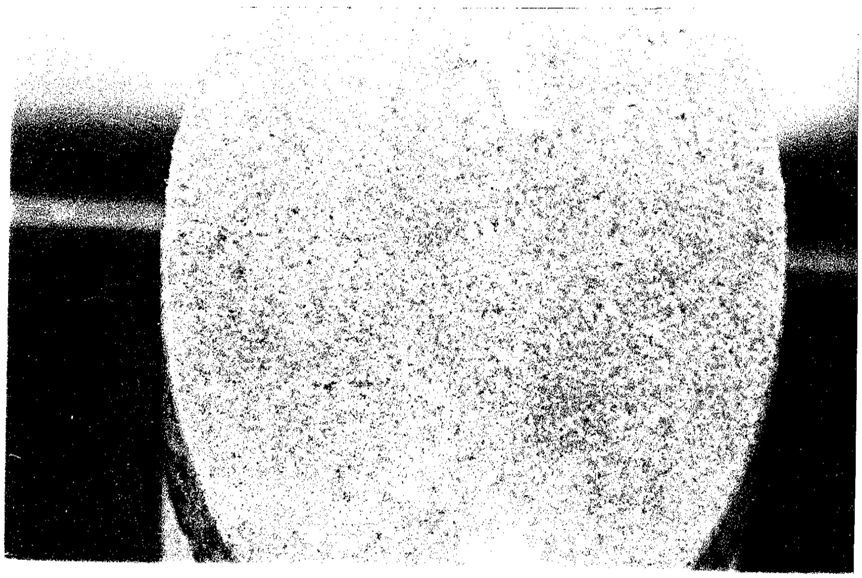

(a)

(b)

Fig. 64. Appearance of (a) >#230 sandstone gouge and (b) #80 wet sandstone gouge after friction experiments. Note vertically oriented slickensides (in direction of relative movement) in gouge of (a). Unmagnified limestone gouge appears very much like the sandstone gouge and is not shown. (1-in dia. cores.)

(a)

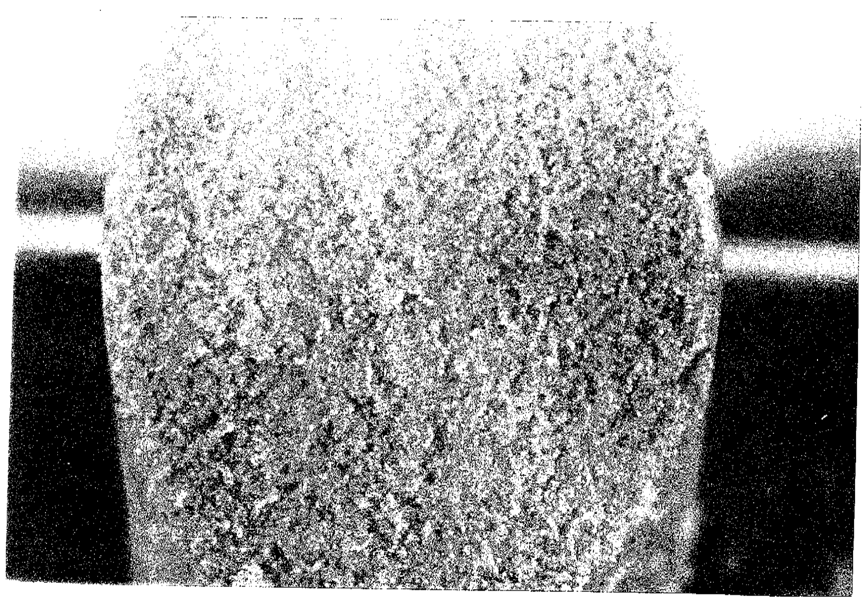

(b)

Fig. 65. Appearance of #80 limestone gouge in regions along sawcut surfaces which were not perfectly mated (reflected light).

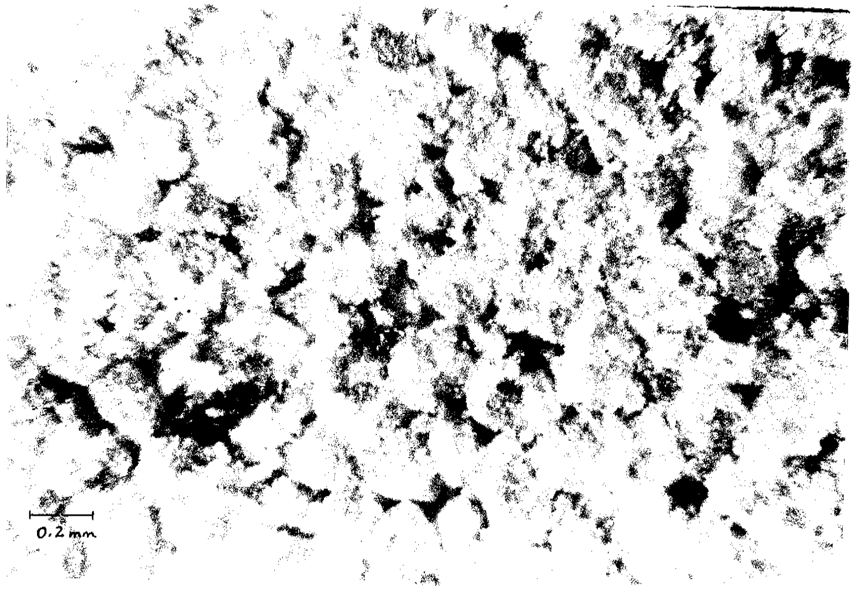

(a)

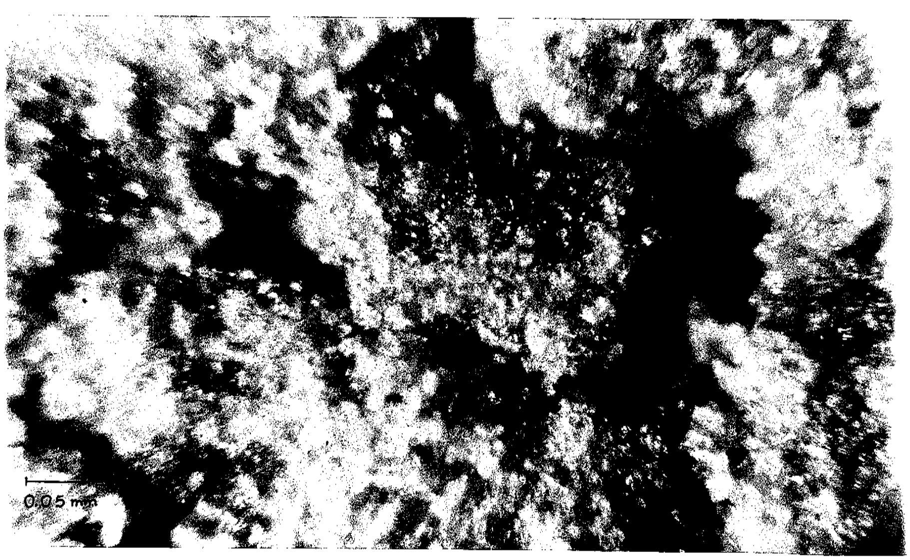

(b)

Fig. 66. (a) Appearance of #80 limestone gouge in regions along sawcut surfaces which were perfectly mated showing large relict primary gouge particles (center) embedded in a very fine-grained secondary gouge matrix (reflected light; 1-cm scale bar = 0.23 mm). (b) Closeup of (a); note extreme degree of cataclasis (compare with Figure 65; reflected light).

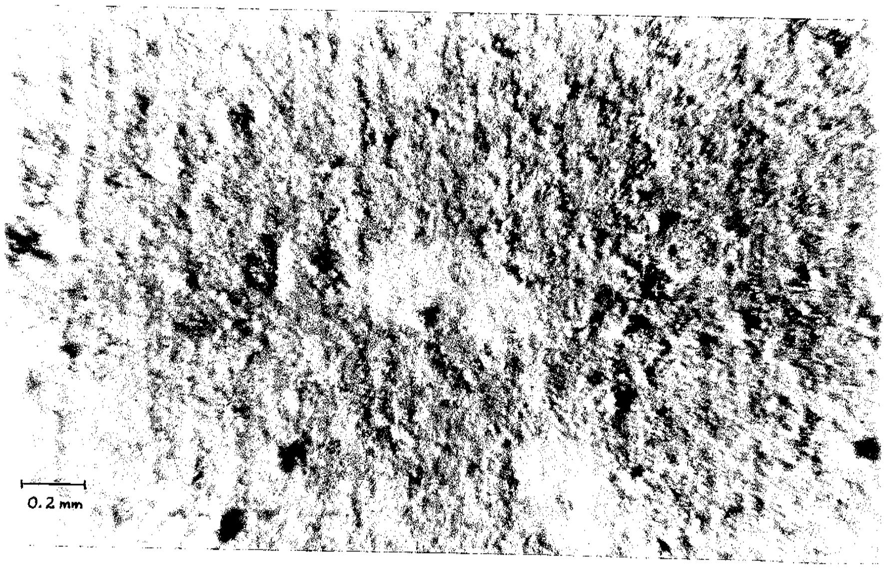

(a)

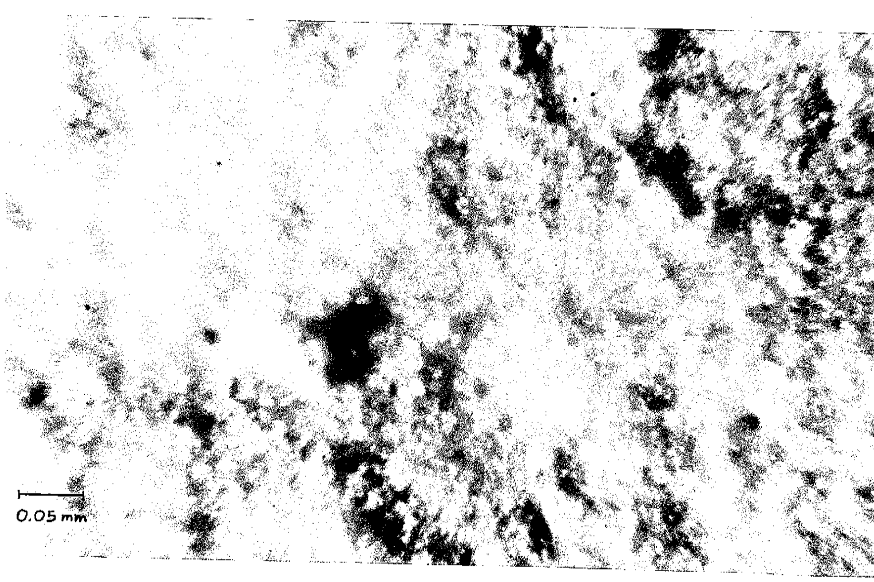

(b)

Fig. 67. Appearance of #80 sandstone gouge in regions along sawcut surfaces which were not perfectly mated (reflected light).

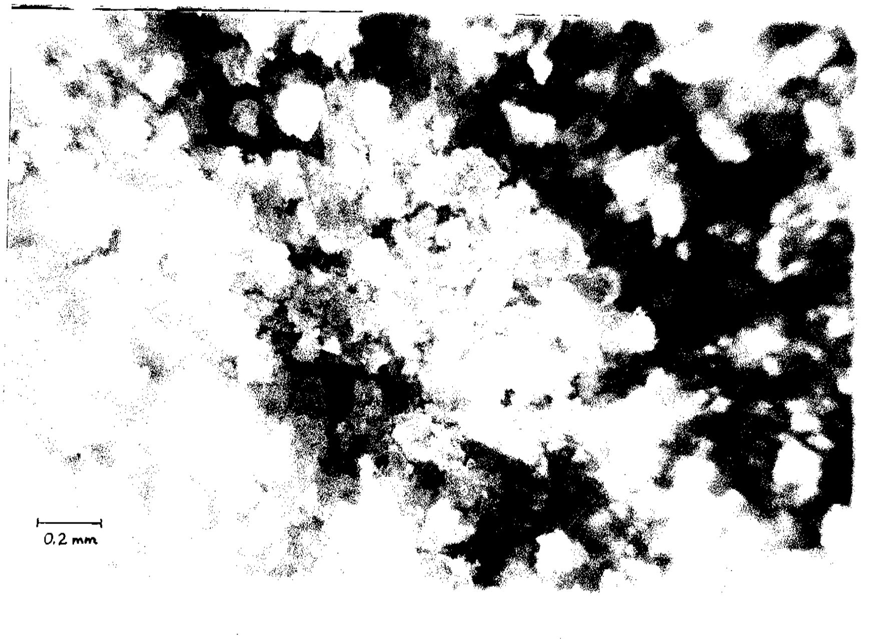

(a)

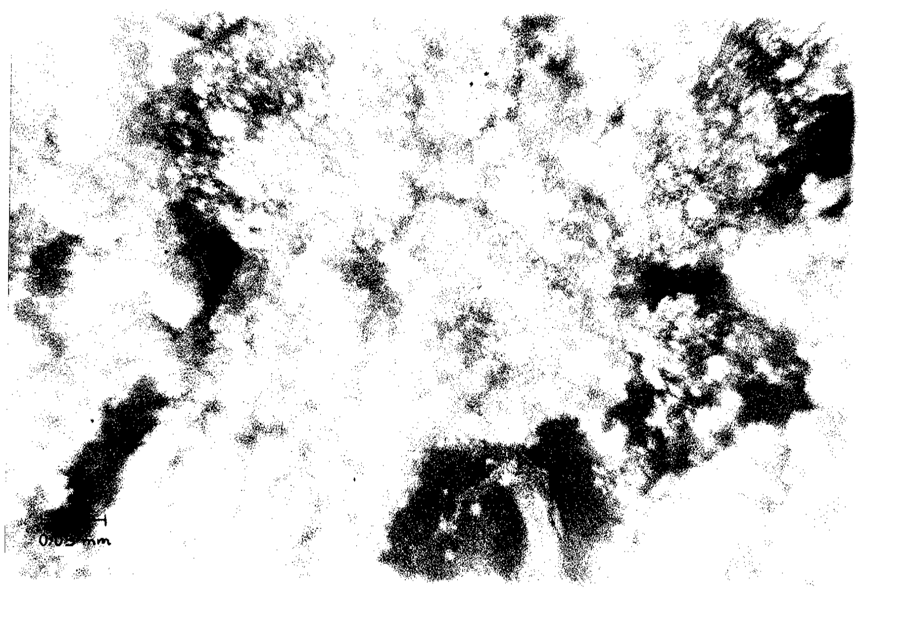

(b)

Fig. 68. Appearance of #80 sandstone gouge in regions along sawcut surfaces which were perfectly mated showing greater degree of cataclasis than shown in Figure 67 (reflected light).

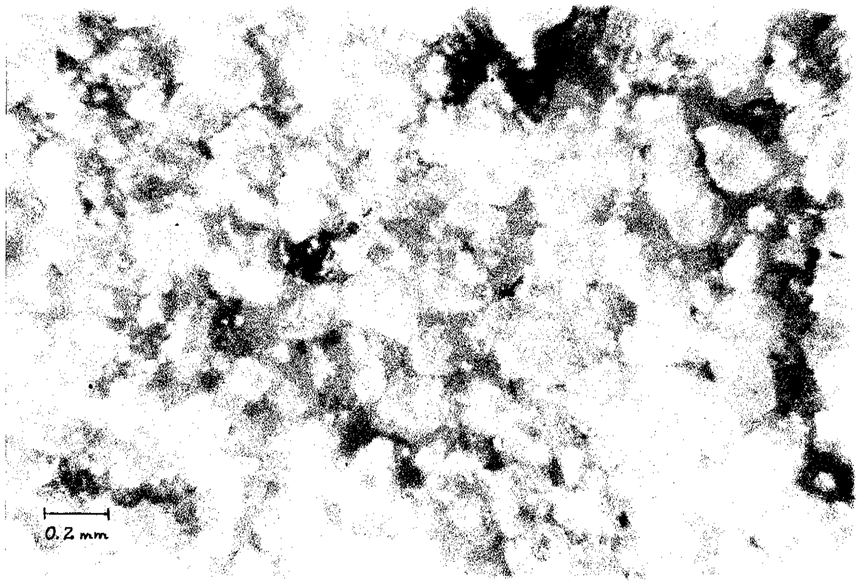

(a)

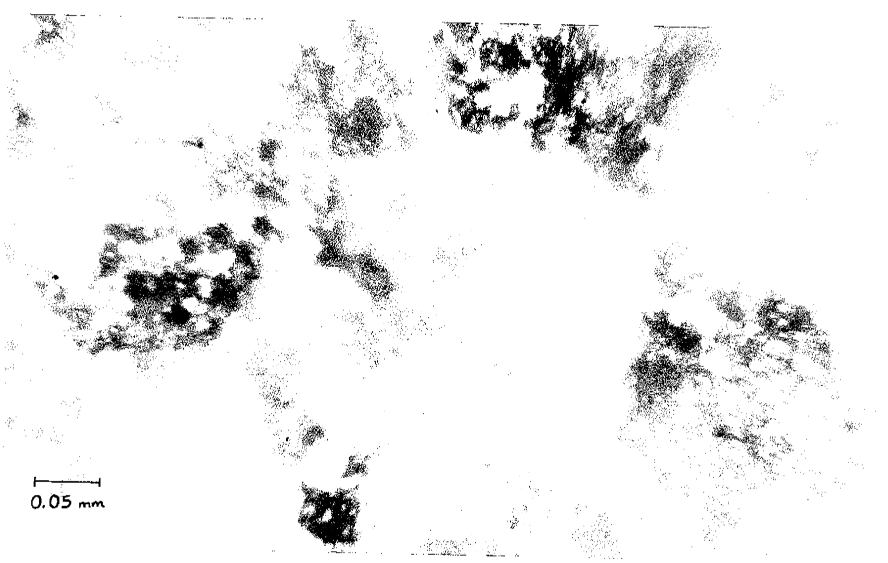

(b)

Fig. 69. Appearance of #80 limestone and sandstone gouge mixture; larger quartz grains are nearly masked by abundant secondary limestone gouge and minor secondary sandstone gouge (reflected light).

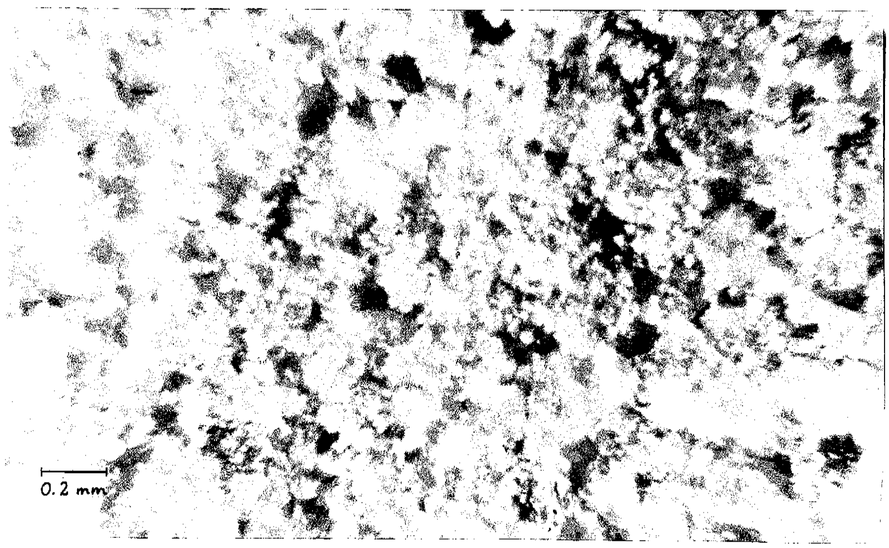

(a)

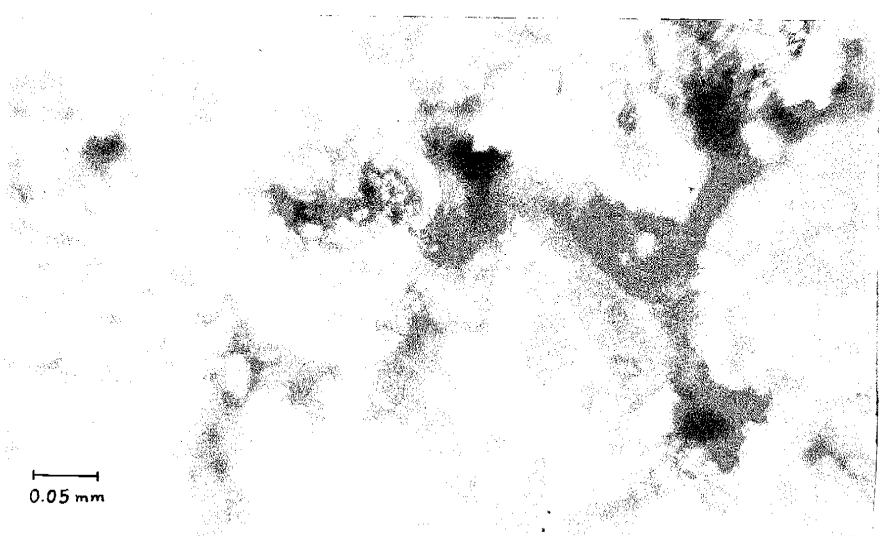

(b)

DISCUSSION OF RESULTS

Fracture Mechanics

The mechanical properties of each of the two rock types studied in the present investigation are quite different. The average value of Young's modulus for the Kelly Limestone is much greater than for the Mesa Verde Sandstone (Table 5). The purely elastic deformation of the limestone gives way to a ductile behavior at high stresses near fracture (Figure 12). At low confining pressure σ_c the limestone fails in a brittle manner along a single inclined shear fracture (Figure 52). The amount of ductile deformation and the ultimate strength (fracture strength) increase progressively with increasing confining pressure until fully ductile deformation occurs with apparent work-hardening (e.g. Nabarro et al., 1964), resulting in barrel-shaped specimens (Figure 53a). This ductility is mainly due to sliding across a multitude of intersecting shear planes, and thus, as a whole, is not true plastic deformation; however, microscopic observations indicate segregated plastic flow around primary calcite grains (Figure 53b). The near absence of ductility in the sandstone is expressed by the constant amount of nonelastic strain for any σ_c, which is not associated with small-scale fracturing. This reflects the fact that quartz and feldspar do not deform by intragranular flow unless stresses are in excess of 50 kb (Christie et al., 1964; Seifert, 1969). The coefficient of "internal friction" or fracture resistance μ_f[1] for the limestone (Figure 16) is more variable (1.75-0.825) than the sandstone (Figure 17; 1.46-0.865) for the stresses investigated. The difference in μ_f is much less at normal stresses greater than 15,000 psi (~1 kb) and in fact the two have identical fracture resistance (μ_f=0.890) at σ=26,4000 psi (1.8 kb). At normal stresses greater than 26,400 psi, the limestone has less resistance to fracture than the sandstone.

The change of μ_f in the limestone is a result of its low inherent shear strength (at σ=0) and of the increase in ductility at higher stresses. It would appear that the influence of inherent shear strength on the fracture process becomes less for normal stresses greater than about 5000 psi (350 bars), above which μ_f changes little; however, for stresses less than this amount, there is a rapid increase in resistance to fracture (Figure 14), possibly due to a work-hardening of the limestone at these stresses.

---

[1] This is different than the classical coefficient of internal friction μ_i in the Coulomb criterion. In the present investigation, the coefficient of "internal friction" or fracture resistance μ_f is intended to be defined such that $\mu_f=\tau(\sigma)/\sigma$ at fracture, analogous to the definition of μ.

Fracture strengths of the limestone (Figure 14) and sandstone (Figure 15) appear to be reflections of the inherent shear strengths of constituent minerals and of the nature of cementation. The sandstone, although the more porous and less cemented of the two rocks, still retains a higher value of inherent shear strength (at $\sigma=0$), approximately 4000 psi (276 bars) as opposed to near zero for the limestone. This behavior may be explained by considering the fact that quartz has a higher shear strength, 25,000 bars (minimum) at $\sigma_c=0$, than the calcite, 140 bars (minimum) at $\sigma_c=0$ (Handin, 1966). An important fact is that for both minerals, especially calcite, shear strength depends upon the crystallographic orientation with respect to applied stress, and thus values of shear strength may be quite variable (Handin, 1966). Similarly, an explanation of the work-hardening nature of the limestone and the production of many small cracks throughout the core during the ductile stage, rather than one individual shear fracture, involves a possible redistribution of internal stress due to an inherent strength variability between individual calcite crystals. Indeed, a small crack may develop and begin to grow to a certain stage and then stop growing due to hardening associated with a redistribution of stress, then other weaker parts of the rock may start "cracking," or, perhaps certain highly stressed points will deform plastically, as might be the case shown in Figure 53b.

In an analogous sense, the small-scale fracture processes in both rocks reflect the influence of the internal chemical structure of constituent minerals. The apparent weak nature of the limestone at very low stresses and during the ductile stage is likely a result of slip associated with certain crystallographic directions in the calcite ($CaCO_3$) structure (e.g. Berry and Mason, 1959). Thus, the fracture pattern associated with ductility may well be an expression of the different $CaCO_3$ cleavages. On the other hand, the Si-O bonding in the quartz (SiO_2) structure is much stronger, as evidenced by the mineral's lack of cleavage, and thus, it does not deform as easily. Hence, an explanation of the mechanical behavior of the limestone is much more dependent upon the internal structure and orientation of calcite grains than is the behavior of the sandstone upon the quartz structure.

Sliding Friction

Definition of μ. Several definitions of the coefficient of sliding friction μ used by some investigators involve the assumption that μ is constant over any range of normal stress σ for a particular experiment. For example, the plot of τ

vs. σ usually produces the equation $\tau=\tau_0+\mu\sigma$, where $\mu=(\tau-\tau_0)/\sigma$ is thus the slope of the curve (e.g. Jaeger and Cook, 1971a). However, experiments by Maurer (1965) and Murrell (1965) produce results which appear to follow the relation $\tau=\mu\sigma^n$, where $\mu=\tau/\sigma^n$ is a constant. When μ is treated in these ways, "Ammonton's law," $\mu=\tau/\sigma$, is interpreted such that τ and σ, or τ and σ^n, are linearly related by a constant μ (Bowden and Tabor, 1950). Thus, a consistent and physically reasonable definition of μ which takes into account various shapes of the $\tau(\sigma)$ curve is lacking.

The classical definition $\mu=\tau/\sigma$ has been used in the present study. The author has found that the physical behavior of μ for a particular experiment may be explained when the entire function $\tau=\tau(\sigma)$ is considered in the definition of μ. $\tau=\tau(\sigma)$ may produce <u>any</u> functional relation between τ and σ, but $\mu=\tau(\sigma)/\sigma$ will always involve an implicit relationship $\tau=\tau(\sigma)=\mu\sigma$ and thus consistency is achieved. Byerlee (1967a) has also recognized the advantages in this definition, the most important of which is that μ need not be restricted as constant during an experiment, but instead, will reflect the "resistance to sliding" at any normal stress.

Effect of sawcut preparation. Introduction of a layer of uncompacted gouge along the hand-polished sawcut surfaces produces the same type of results as found for bare surfaces. When the entire core area (A_o) is used to calculate τ and σ, resulting values of μ are nearly an order of magnitude less than values of μ obtained when a controlled, predetermined flat surface area (A_c') is used. This is contrary to the idea that gouge acts as a cushion to reduce the centralized concentration of stress such that the stress becomes uniformly distributed across the entire surface area. Instead, stress is concentrated along those areas which are more closely fitted, causing the gouge in these areas to become compacted to the extent that individual particles are sheared and produce a secondary gouge matrix (compare Figures 65 and 66).

Experiments with gouge on hand-polished sawcuts and on controlled surfaces of various size each gave consistent results. It is the uniformity in polishing which has permitted using a correction term to account for partial contact so that maximum coefficients of friction are obtained. As an example, Handin and Engelder (1973) obtained values of $\mu\,(=B) = 0.68\text{-}0.86$ using entire core cross-sectional areas, which are comparable to those obtained in the present investigation when partial contact is taken into account. This implies that they were able to produce nearly "perfectly" matched sawcut surfaces with their method of grinding.

On the other hand, for the case when μ of pre-faulted cores is determined, "perfect" fit of adjacent core pieces exists only prior to initial displacement, and when displacement occurs, there exist areas of partial contact, until at greater stresses and displacements, enough gouge has been formed and compacted to fill open areas. When entire core cross-sectional areas are used to calculate μ, one would expect values of μ to be high for initial displacement, then become minimized for subsequent small displacements, and finally increase and approach a "residual" value at very large cumulative displacements.

Thus the somewhat fictitious behavior of μ, caused by conditions inherent in the triaxial apparatus which require that actual contact areas be known, exemplifies the possibility that values of μ calculated using entire core cross-sectional areas may not be valid if maximum coefficients of friction are desired. This would account for the seemingly contradictory effects of certain factors on friction reported in the literature (see Table 1), depending upon the methods of determining μ. Methods which involve recording values of applied forces only, and not both forces and stresses as in the triaxial apparatus, may thus avoid the problem of actual contact area, since μ may be calculated directly from the shear and normal forces (i.e. $\mu=F_s/F_n$, where F_s=shearing force and F_n= normal force). The author proposes that the particular method used to study friction and whether partial contact is accounted for be indicated when results are given in published form. Unless otherwise noted, throughout the following discussions of friction, coefficients of sliding friction are based on calculations involving actual contact areas and are thus maximum coefficients.

Experimental behavior of μ. Results of the friction experiments may be understood through an analogy with the mechanical interaction of individual grains along fault zones consisting of either polished sawcuts or sawcuts containing gouge particles. For tests on polished surfaces of Kelly Limestone and Mesa Verde Sandstone, surface roughness does not appear to affect resistance to sliding (Figures 22, 23, 28, and 29). As pointed out above, the inherent shear strength of the limestone is very low, and as a result it would take a relatively low applied stress to deform the sliding surface such that equilibrium is reached in the early stages of an experiment. The surface of the sandstone, on the other hand, is probably more responsive to the #100-grit polish, which causes plucking of quartz grains, and thus is a very rough surface as compared to the limestone. The #600-grit polish is not as abrasive and does not tend to pluck grains; instead, it cuts into and flattens the rounded quartz grains, permitting more microscopic surfaces of contact, rather than the point contacts present in the #100-grit experiment. The increase in coefficient of friction with normal stress for both surface roughnesses (Figures 28 and 29) is likely a result of interlocking of asperities and ploughing at very high stresses (>1 kb) when enough gouge is generated such that a maximum "residual" coefficient $\mu_{\text{"res"}}$ is reached.

By introducing uncompacted synthetic limestone and sandstone gouge between the sawcut surfaces (polished on #100 grit) the coefficient of friction is not appreciably changed. In addition, absolute values of friction coefficients are essentially identical for both limestone and sandstone gouge, seemingly independent of gouge type, gouge grain-size, or whether or not water is present (Figures 32, 33, and 35).

The behavior of μ as a function of σ is a direct result of the interplay of the two terms in the expression $\tau = \tau_0/\sigma + B$ (Equation 8). Depending upon the magnitude of σ, either one or the other of the terms may dominate. In a physical sense, especially in the presence of gouge, this may be explained by considering grain interactions in response to applied stress. For example, the originally uncompacted gouge becomes compacted due to a reorientation and rearrangement of grains by the initial application of confining stresses. In order for displacement to occur, glide surfaces must be overcome first. This adds to the resistance to sliding such that friction may increase quite rapidly at relatively low stresses. Thus, the first term, τ_o/σ, will dominate at very low normal stress σ. At higher stresses, sliding surfaces are established in the gouge and the rapid increase in resistance to sliding is reduced until movement is constrained strictly by sliding resistance along established glide surfaces.

During a friction experiment there is a mechanical interaction of original gouge particles that produces a secondary finer gouge which clusters about the larger parent grains, as shown in the photomicrographs of Figures 66, 68, and 69. Once gliding planes have been established at higher stresses such that newly formed gouge has filled voids left in the original synthetic gouge, the resistance to sliding is essentially uniform ($\mu \rightarrow \mu_{\text{"res"}}$) and a mechanical system is set up which responds only to changes in applied stresses.

Under the microscope the finer secondary gouge appearing around the larger synthetic-gouge particles tends to hide the original parent grains almost completely, particularly in the limestone gouge (e.g. Figures 66 and 68). This is in agreement with the concept that more secondary limestone gouge will have been formed at a given normal stress than secondary sandstone gouge of the same size, due to the different shear strengths of the respective minerals. The new gouge is characterized by a seemingly homogeneous, very fine-grained (<0.005 mm) cataclastic matrix of elongated grains and aggregates oriented in a direction nearly perpendicular to the direction of the applied axial stress but within the plane of the sawcut. This relationship is similar to, although much more prominant than, that found in gouge generated as a result of fracture of previously intact specimens which were allowed to continue to slide after fracture (e.g. for the limestone run at σ_c=344.7 bars).

Effect of gouge thickness and fault angle on μ. The possibility that a buildup of gouge with time along an active fault might affect the mechanical nature of the system has been investigated by varying the #80-size gouge thickness between the sawcut surfaces. Figures 38 and 39 suggest that a common "residual" resistance to sliding is reached at high stresses such that gouge thickness has little influence on the mechanical response of the system to various applied stresses. As usual, there is a gradual filling of interstices in the original synthetic gouge by freshly generated gouge of much smaller grain size due to natural compaction and grinding together of gouge particles.

Figures 42 and 43 indicate a change in the resistance to sliding depending upon the angle between applied stress and sliding surface. A maximum resistance to sliding is established for fault angles near 45^{o} in both the limestone and sandstone. If the fault angle is oriented near 30^{o} or 60^{o} to the maximum applied stress (axial stress), a minimum resistance to sliding is observed (see Figure 44).

An attempt to explain the relationship in Fugure 44 must account for the unique behavior of the fault system (core pieces and gouge) at $\alpha=45^{o}$. A possible explanation, at least for angles much greater than 45^{o}, is that there may exist a slight misalignment of core pieces (e.g. Jaeger and Cook, 1971a, pp. 68-69), thus concentrating the applied axial load on a part of the entire sliding surface. At $\alpha=45^{o}$, there is a uniform distribution of applied stresses due to the equant positioning of the fault angle between directions of confining stress and axial load, and thus, specimen tipping is unlikely (especially for maximum displacements of 0.01 in).

Stick-slip behavior appears to be directly related to the friction process. Humston (1972) has discovered that specimens (not containing gouge) with pre-cut angles of 30^{o}, 35^{o}, and 37^{o} produce stick-slip continuously with no noticeable specimen fracturing. But for specimens with pre-cut surfaces of 40^{o}, new macroscopic faulting was produced in the specimens with minor stick-slip occuring before faulting, and for pre-cut surfaces at 45^{o} faulting occurred without any stick-slip. He concluded that (Humston, 1972, p. 58):

> "at some angle between 37^{o} (stick-slip) and 40^{o} (faulting), there is a value of the coefficient of friction that is too great to allow slip on the cut surface."

Although Humston did not offer an explanation for this behavior, it is possible that at α=40^{o} maximum resistance to sliding occurs, due to a maximum mechanical interaction (bonding) of asperities produced by interlocking grains. For other angles, it is likely that more secondary gouge is produced for a given normal stress, due to increased point-contact of corners of grains, thus reducing the resistance to sliding. Microscopic examination of the gouge tends to confirm this behavior.

The preferred direction of fracture at approximately 30^{o} for both the limestone and sandstone also supports the idea that less friction develops near 30^{o}, than at 45^{o}, as shown in Figure 70a. However, it is also possible that a combination of compressional stresses may produce less friction near α=60^{o}, as predicted by friction experiments (Figure 70b).

Influence of pore pressure on μ. Friction experiments with uncompacted gouge involving pore-water pressure p produce results (Table 11; Figures 45-48) which indicate a slight reduction in the coefficient of friction with increasing pore pressure, especially as seen in the sandstone data. The limestone data do not show a uniform reduction in μ with the higher pore pressure (p=86.9 bars), because the gouge particles become sheared and compacted so thghtly with secondary gouge that water cannot circulate along the fault sur-

Figure 70. Diagrams illustrating preferred orientations of less resistance to sliding at (a) $\alpha=30^{\circ}$ and (b) $\alpha=60^{\circ}$, as determined from friction experiments using the conventional triaxial apparatus.

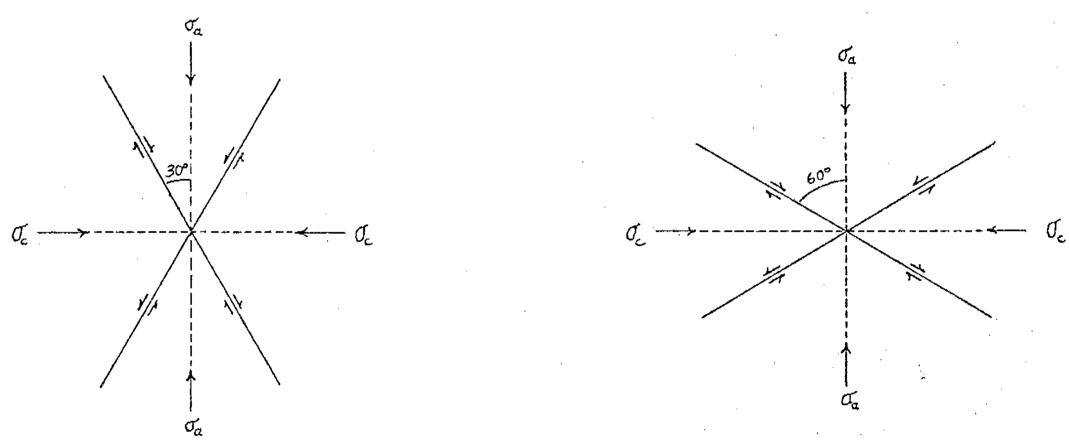

σ_a
30°
σ_c
σ_c
σ_a
σ_a
60°
σ_c
σ_c
σ_a

(a) (b)

face. In the sandstone, the shear strength of the quartz particles is higher and the degree of compaction with secondary gouge is less, so that water is more free to circulate, thus producing a more effective reduction in the coefficient of friction at higher pore pressures. In addition, the pore pressure does not appear to reduce the inherent shear strength of the gouge, which tends to disagree with studies of Handin et al. (1963) and Colback and Wiid (1965).

The fact that the slopes of the various $\tau(\sigma)$ curves are different at different p is indicative that an effective-stress law (of any form) does not hold for either rock under the pore pressures studied. This may be expected when gouge compaction is considered, as fluid-pressure equilibration apparently was not reached. Some additional tests were conducted at higher pore pressures, but the relationship was unchanged.

The sandstone displays a segregation of kinetic and static friction data at higher pore pressures (Figures 49-51), with a reduction of this segregation at progressively higher normal stresses. At relatively low normal stress, the difference between μ_s and μ_k is at a maximum, but at high normal stress (>7500 psi) μ_s and μ_k approach one another, probably due to the influence of secondary gouge buildup (as described by Swolfs, 1971; see preliminary discussion of μ_k in presence of fluids in "Previous Investigations" section). This behavior of μ_k and μ_s under the influence of pore pressure is a possible mechanism for explaining the water-induced increase in magnitude of stick-slip events observed by Handin and Engelder (1973). The present study would predict a gradual reduction of these stress drops at increasing normal stress to the point where stick-slip is absent altogether.

The kinetic data reflect increasing positive values of τ_o with increasing p. Engelder (personal communication, 1973) has attempted to explain this as being due to the way in which data is obtained. He has noticed that for kinetic data calculated from stress drops during stick-slip events in dry cores, τ_o increases with increasing displacement. On the other hand, he has observed that τ_o associated with the initiation of sliding (static data) is usually negative. The physical explanation for this is lacking and seems to be contrary to common sense, as one is likely to expect the gouge to have a higher cohesion prior to sliding than during sliding. Apparently, there is a certain amount of furrowing and an increased asperity interaction during sliding that does not exist at the initiation of sliding. Another explanation is that for low values of normal stress where data are scarce, usually for $\sigma < 4000$ psi, there exists a local curvature of the (σ, τ) plot which has been hidden by the linear approximation of the overall data trend, which is weighted by (σ, τ)

values for σ>4000 psi. This would occur as a result of the increase in compaction of the originally uncompacted gouge at initially low σ, thus causing an increase in cohesion.

Friction Versus Fracture

Problems of scale. Most theoretical principles of elastic and plastic behavior of rocks are based upon a macroscopic view of the material so that structural discontinuities in the rock are smoothed out. As yet no one has been able to explain in quantitative terms the relationship between stress and strain in the crystal aggregate and the deformation mechanisms of individual crystals at elevated stresses, although several attempts have been made (e.g. Swanson, 1969; Morland, 1971; McGarr, 1971). It is therefore important to discuss those factors which are responsible for structural inhomogeneities in a rock mass.

The mechanical behavior of the Kelly Limestone and Mesa Verde Sandstone are likely a reflection of inherent nonhomogeneous properties, for the shape of their respective stress-strain curves and fracture-strength curves are apparently influenced by cracks and pores, and especially by the friction acting along them. As mentioned above, the frictional behavior of the two rocks appears to be related to the shear strengths of interlocking asperities along the fault surfaces, which in turn are a function of the overall rock strenghts. However, there does exist a problem of scale, as exemplified by the behavior of the limestone during deformation. On the one scale at certain applied stresses the limestone is observed to undergo permanent deformation in an apparently uniform manner so that it may be said to be ductile, while on a finer scale, microscopic observations reveal that the mechanism of deformation is small-scale fracturing (jointing) and relative movement on the fractures (cataclasis).

One of the most obvious sources of structural discontinuity in rocks is due to the absence of material around grains, producing intergranular cracks and pores that reflect an overall or bulk porosity. The compaction (volume decrease) associated with porous rocks at low stresses is usually considered to be due to the closing of pre-existing cracks and pores. However, some rocks may have very low porosity, which implies that any appreciable strain release will be associated with movement in fissures along grain boundaries, with the possibility that slip regions within one grain may be transferred to another across their common boundary (such as proposed by dislocation theory; e.g. McGarr, 1971). Indeed, the parabolic (n=2) nature of the Kelly Limestone Mohr envelope suggests that elliptical Griffith cracks or flaws may play an important part in the mechanical behavior of the rock. On the other hand, very porous materials, such as the extreme case of, say, unconsolidated sands, there exists the possibility of pure frictional sliding associated with appreciable rotations of grains. It is interesting to note that, in general, corresponding Mohr envelopes usually differ to the extent that most consolidated rock materials have an inherent strength (τ_0) and a curved Mohr envelope, while for unconsolidated materials, the Mohr envelope is linear and passes through the origin ($\tau_0=0$; see, for example, Ramsay, 1967, pp. 290-291, or Jaeger and Cook, 1971a, pp. 384-390).

"Residual" strength. The purely linear case (Coulomb criterion) associated with fracture of poorly consolidated rocks affords some interesting analogies with the linear curve which results from pure frictional sliding on a pre-existing plane of weakness. The near linear nature of the Mohr envelope and the $\tau=\tau(\sigma)$ linear friction curve (Equation 6) associated with the Mesa Verde Sandstone imply that microscopic processes leading to the formation of macrofractures and those processes associated with the initiation of slip along a pre-existing fault surface are quite similar. An obvious difference between the two conditions is the apparent lack of purely frictional displacements during the fracture process so that an additional "residual" shear strength $\tau_{\text{"res"}}$

of interlocking brittle grains must be overcome before appreciable strain resulting in macrofracture can occur.[1] That is, from Equations 4' and 6,

$$\tau_{"res"} = \tau_f(\sigma) - \tau(\sigma) = (A_f + B_f\ )^{1/n} - (\tau_o + B\sigma) \qquad (16)$$

where τ_f is the shear stress needed to produce failure and τ is the shear stress needed to cause pure frictional sliding on a pre-existing surface at a particular normal stress.

A possible factor which influences the magnitude of $\tau_{"res"}$ is that of dilatancy, whereby a period of permanent volume increase occurs in a rock at a finite time before fracture, when many cracks and voids open and perhaps ultimately coalesce in the region of the incipient macrofracture. The magnitude of the weakening effect of dilatancy for a particular rock may well be characteristic of only that rock and may then reflect the variability of corresponding Mohr envelopes. Thus, to explain the mechanical behavior of dilatancy for rocks could conceivably explain the behavior of corresponding Mohr envelopes.

In the present study, the friction and fracture data for the limestone and sandstone may be used to exemplify the existence of a "residual" shear strength associated with the fracture process as compared with frictional sliding along a pre-existing surface. For the Mesa Verde Sandstone, the dif-

---

1 $\tau_{"res"}$ is in no way directly related to $\mu_{"res"}$ used above.

ference between the shear strength needed to produce fracture and that needed to produce pure sliding at a particular normal stress is (from Equation 16 and Tables 5 and 10):

$$\tau_{\text{"res"}} = (2.1\cdot10^{4} + 6.2\ )^{1/1.2} - (-144 + 0.687\sigma)$$
$$= (8.3\cdot10^{2} + 3.6\ )^{1/1.2} - (-9.9 + 0.687\sigma). \quad (17)$$

Similarly, for the Kelly Limestone,

$$\tau_{\text{"res"}} = (-2.7\cdot10^{7} + 3.2\cdot10^{4}\ )^{1/2.0} - (-104 + 0.670\sigma)$$
$$= (-1.2\cdot10^{5} + 2.0\cdot10^{3}\ )^{1/2.0} - (-7.2 + 0.670\sigma).(18)$$

Both (17) and (18) have been graphed in Figure 71 for the range of normal stress investigated. There is a greater "residual" shear stress that must be overcome in the limestone than exists in the sandstone for 2500 psi$\lesssim\sigma\lesssim$26,000 psi, which is due to the work-hardening nature of the limestone. At $\sigma\gtrsim$26,000 psi, of the two rocks the sandstone reflects the greatest discrepancy between fracture and sliding-friction processes, while the limestone appears to be sliding on pre-existing planes of weakness. This near frictional behavior of the limestone during fracture at very high normal stress is to be expected because it corresponds to the ductile regime, during which the rock becomes jointed. The observed existence of gouge along these joints favors a pure sliding mechanism associated with failure during the ductile stage.

Values of μ_f for each of the rocks also reflect similarity between pure frictional sliding and fracture processes. At high normal stress, such as for σ=30,000 psi, each rock

Fig. 71. Graph of shear stress at fracture minus shear stress to cause sliding vs. normal stress for Kelly Limestone and Mesa Verde Sandstone.

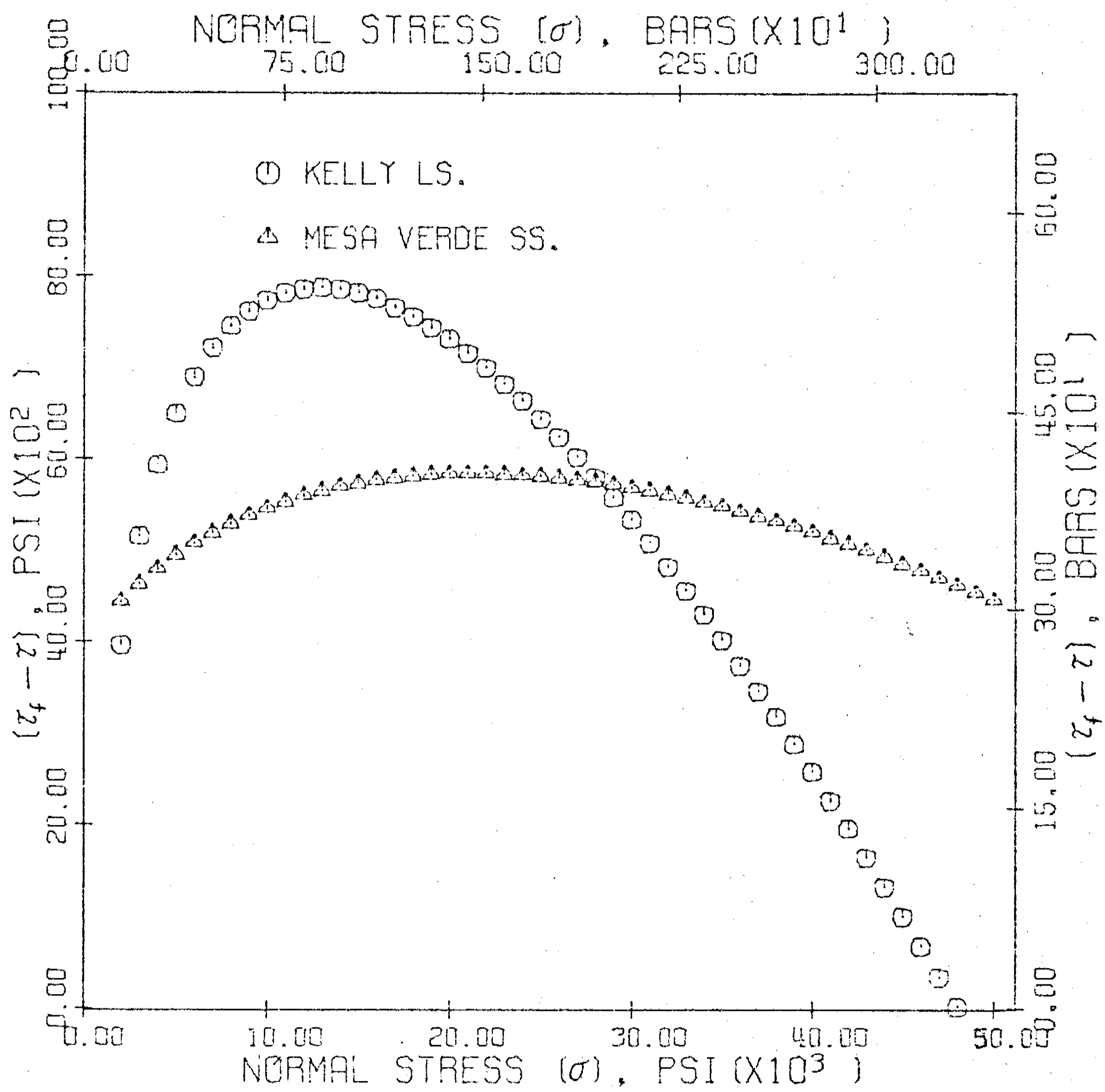

NORMAL STRESS (σ), BARS (X10¹)
0.00
75.00
150.00
225.00
300.00
⊙ KELLY LS.
△ MESA VERDE SS.
(τ_f − τ), PSI (X10²)
0.00
20.00
40.00
60.00
80.00
100.00
(τ_f − τ), BARS (X10¹)
0.00
15.00
30.00
45.00
60.00
0.00
10.00
20.00
30.00
40.00
50.00
NORMAL STRESS (σ), PSI (X10³)

retains a "resistance to fracture" which is nearly the same as the maximum resistance to sliding. For example, $\mu_{f,ls} \simeq 0.84$ and $\mu_{f,ss} \simeq 0.87$, while $\mu_{ls} \simeq \mu_{ss} \simeq 0.78$ at $\sigma = 30{,}000$ psi. At even greater σ, μ_f for both rocks decreases and μ increases, suggesting that perhaps the two will eventually be identical. The fact that fracture processes and pure frictional-sliding processes are closely related and that the "resistance to fracture" and the resistance to sliding may be nearly the same implies that a fractured rock mass is capable of supporting as much external stress as an unfractured rock.

Friction and the brittle-ductile transition. Murrell (1965), Byerlee (1968), and Edmond and Murrell (1973) have been able to experimentally confirm Orowan's (1960) ideas that a brittle rock will eventually become ductile ("flow" in a cataclastic sense) at a certain confining pressure (or normal stress), and that subsequent deformation will be due to an overall frictional behavior. The assumption, which appears to hold in the present study, is that there exists a transition between brittle fracture and ductility at the intersection of the Mohr envelope and the frictional stress curve. In other words, for the present study this transition occurs in the limestone when

$$(-2.7 \cdot 10^7 + 3.2 \cdot 10^4 \sigma)^{1/2.0} = -104 + 0.670\sigma \ \langle psi \rangle \quad (19)$$

or

$$\sigma_{ls} \simeq 48{,}000 \text{ psi} \simeq 3.3 \text{ kb.}$$

Similarly, for the sandstone,

$$(-2.1 \cdot 10^4 + 6.2\ )^{1/1.2} = -144 + 0.687\sigma \quad \langle\text{psi}\rangle \qquad (20)$$

or

$$\sigma_{ss} \simeq 89{,}300 \text{ psi} \simeq 6.1 \text{ kb.}$$

Thus the theoretical value of $\sigma_{ls} \simeq 48{,}000$ psi defining the transition between brittle and ductile behavior is the same as that value in Figure 94 for which $\tau_{\text{"res"}} = \tau_f - \tau = 0$, as is the case for the sandstone at $\sigma_{ss} \simeq 89{,}300$ psi.

The fact that ductility associated with fracture in the limestone was observed below $\sigma \simeq 48{,}000$ psi is suggestive that an intragranular plasticity may indeed exist at lower normal stresses in localized regions where there are high concentrations of internal stress. The observed lack of ductility in the sandstone for the range $\sigma \lesssim 25{,}000$ psi is to be expected, as intragranular plastic flow would require stress concentrations in excess of 725,000 psi, as indicated by Christie et al., 1964, and Seifert, 1969, on studies of quartz and feldspar.

Microscopic observations. Microscopic examinations of the fractured cores tend to support the above explanations of the mechanical and frictional behavior of the two rocks. As previously mentioned, the limestone cores contained many more fracture-related joint systems that the sandstone, especially at high stresses (e.g. Figure 53). This observation suggests that a considerable amount of strain developed due to opening of (Griffith?) cracks in the limestone, and thus, also permitted frictional forces to play an important role in the fracture processes. Both the sandstone and especially the limestone cement was noticeably affected by the fracture tests, as intermittent pockets of gouge formed throughout most of the cores, especially along the cracks associated with the major fracture systems (Figure 56). In addition, the weak cementation in the sandstone supports the experimental results for which $\mu_{f,ss} < \mu_{f,ls}$ throughout most of the range of normal stress used in the study.

For the condition of slip along a pre-existing sawcut surface, asperities and gouge fragments tend to become sheared after very little displacement and a layer of finer grained gouge forms as a result. As evidenced by microscopic observations, these gouge particles are apparently free to rotate such that they display a preferred orientation, whereas gouge grains along fractures do not generally show appreciable rounding or an obvious preferred orientation. Thus, a microscopic distinction between pure sliding friction and "internal friction" during the formation of fractures can be made, based upon the relative degree of freedom for grains to rotate under applied external stresses.

A diagram of stages of gouge formation during the pure frictional sliding and fracture processes as inferred from microscopic observations is given in Figure 72. The diagram summarizes relative degrees of cataclasis from the initiation of fracture in virgin rocks to the post-fracture stage involving an immature gouge zone (A-C). There is a greater degree of cataclasis involved in the later stages of gouge generation during the frictional sliding process (D-F), which produces a more mature gouge zone. It is possible to follow the process of gouge generation and cataclasis from the initial pre-fracture dilatancy stage to the final stages of frictional sliding involving a very mature gouge system (A-F).

Figure 72. Diagram of stages of gouge formation during the fracture and frictional-sliding processes as inferred from microscopic observations.

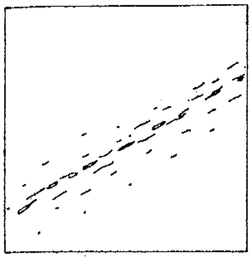

A
During Dila-
tancy: cracks
begin to open

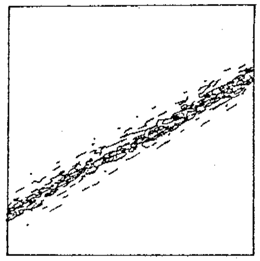

B
Formation of
Major Fracture:
coalescence of
cracks

C
Post Fracture:
brecciated
gouge zone due
to shearing of
grains between
cracks

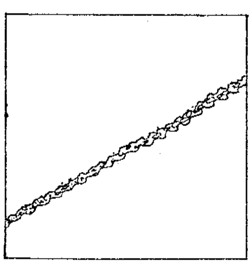

D
Prior to Initi-
ation of Sliding:
asperities causing
very irregular
surface

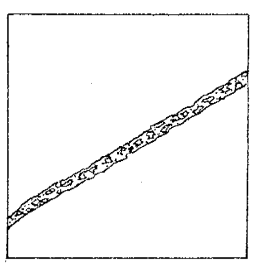

E
After Initiation
of Sliding: as-
perities are
sheared and form
brecciated gouge

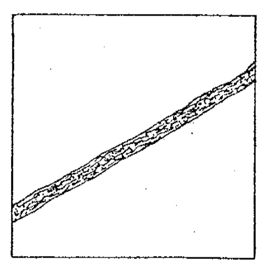

F
Subsequent Slid-
ing: gouge grains
become compacted
and rounded due
to rotations,
forming secon-
dary gouge matrix

Applications

<u>Role of cohesion in overthrust faulting and landsliding</u>. Hsü (1969) has suggested that the shearing resistance to faulting is not due to friction alone, as proposed by Hubbert and Rubey (1959), but also includes the cohesion term τ_o (Coulomb criterion). Results of the present investigation indicate that a large cohesion at $\sigma=0$ is associated with the fracture of the Mesa Verde Sandstone (Figure 15), while the Kelly Limestone has almost no cohesion at $\sigma=0$ (Figure 14). However, for both rocks, especially the limestone, the rate of change of resistance to fracture decreases with increasing normal stress (Figures 16 and 17), thus exemplifying the importance of a "variable" cohesion term, depending upon the relative magnitudes of applied stresses. The fact that ductility (cataclastic flow) associated with fracture in the limestone occurs prior to the brittle-ductile transition predicted by Orowan (1960) is evidence that an additional or "residual" strength must be overcome before frictional sliding can occur uniquely.

As indicated by friction experiments in the present study, after a sliding surface is produced in either of the rocks, a gouge or surface-asperity cohesion term τ_o does exist and, indeed, influences the resistance to sliding. In the presence of pore-water pressure along the sliding surface, τ_o tends to increase with increasing pore pressure <u>during</u> sliding and, thus, adds to the resistance to sliding (μ_k). Results of the present study, therefore, tend to support Hsü's contention that τ_o should be taken into account when considering overthrust faulting and landsliding.

<u>Active faults</u>. For an active fault, such as the San Andreas fault (e.g. Brune et al., 1969; Eaton et al., 1970; Wood and Allen, 1973), it is likely that certain factors, such as direction of principal stresses, pore-water pressure, and gouge character, influence stability of the fault. It is possible that fault stability may change with time or space as a function of changes in the physical regime of the influencing factors. For example, percolating solutions may change the degree of cementation and compaction of the fault gouge, or there may be a change in the local hydrology, which could cause the pressure along the fault zone to change.

A specific example of the existence of planes of weakness at certain directions in a rock mass may be applied to the San Andreas fault. If the San Andreas fault is considered a primary fault, its right-lateral nature and general strike, N45W north of the Salton Sea (Elders et al., 1972, Figure 6), imply that $\sigma_a = \sigma_1$ is oriented approximately N15W and $\sigma_c = \sigma_3$ is compressional and oriented N75E (see the case of

Figure 93a).

In view of current ideas on plate tectonics, it may be more justifiable to consider the pre-existence of faults and the relative sliding resistance along them. Results of friction experiments for various fault angles indicate that resistance to sliding is less at angles near 30^{o} and 60^{o} to σ_1 than at 45^{o} and suggest that on a regional scale secondary active faults associated with the San Andreas should not be oriented in dir ctions approximately 45^{o} to σ_1 or, in other words, in a direction N30E. However, from friction experiments for $\alpha=60^{o}$, indicated in Figure 93b, σ_1 is oriented approximately 60^{o} with respect to the fault so that σ_1 is directed N15E and σ_3 is directed N75E. The case $\alpha=60^{o}$ is supported by actual examples of orientations and relative movements of the San Andreas fault and intersecting faults such as the Garlock fault (see Elders et al., 1972, Figure 1; or Richter, 1958, Figure 14-4, p. 196).

Earthquake mechanism. From the present study on the effect of pore pressure on coefficients of friction, it is possible to postulate diminishing effect of stick-slip with depth in the earth. The fact that pore pressure tends to enlarge the difference between μ_s and μ_k at relatively low normal stress only (<1 kb), may very well explain the existence of large-magnitude (high stress-drop) earthquakes near the surface of the earth (Press and Brace, 1966; Bolt et al., 1968).

Results of the present investigation concerning similarities between fracture and frictional processes tend to support current ideas on the prediction of earthquakes. Because rock masses containing faults are capable of supporting as much stress as intact rocks, it is quite possible that before a seismic event there may be a substantial change in the hydraulics near the region of the hypocenter due to precursory dilatancy (e.g. Nur and Booker, 1972; Whitcomb et al., 1973; Sibson, 1973; Hammond, 1973; Scholz et al., 1973). Indeed, a dynamic decrease in pore pressure could increase the possibility that seismic events will occur due to the change in the magnitude of stress drops associated with stick-slip events. For example, foreshocks may be explained as a result of minor readjustments of stresses (after dilation) ultimately causing localized gradual increases in pore pressure in various parts of the dilatant volume, until at a certain point (in time or space) very large stress drops dominate, which produce the major event(s). Aftershocks may be explained as those events produced by changes in permeability when fluid pressure is reduced in certain parts of the changing volume but temporarily maintained in confined regions, thus causing internal-pressure imbalances, which result in local crustal instabilities.

SUMMARY AND CONCLUSIONS

By defining μ_f as the ratio of shear stress $\tau(\sigma)$ to normal stress σ at fracture and μ as the ratio of $\tau(\sigma)$ to σ for pure frictional sliding, a direct comparison of the two processes is possible.

The mechanical behavior of both the Kelly Limestone and Mesa Verde Sandstone are related to small-scale structural inhomogeneities in the rocks. Calcite glide planes appear to control deformation leading to ductility and fracture in the limestone, while weak cementation of the sandstone is a controlling factor during its deformation.

For frictional sliding experiments on the Kelly Limestone and Mesa Verde Sandstone using a conventional triaxial apparatus, maximum values of coefficients of friction μ obtained when partial contact between sliding surfaces is taken into account are nearly an order of magnitude greater than those values obtained when entire fault-surface areas are used (~0.78 vs. ~0.1, respectively). The implication is that, when maximum coefficients of friction are desired, actual contact area should be considered.

Results of friction experiments reflect mechanical properties of individual particles along sliding surfaces, whether the sliding surfaces be polished sawcuts or sawcuts containing gouge. At low σ, values of μ for both rocks are observed to vary hyperbolically with σ, a behavior which is explained as a result of the filling by freshly generated gouge of open areas along fault surfaces. Surface roughness does not affect friction in the limestone, but does in the sandstone, which may be explained as due to the relative degrees of cementation and porosities of the rocks.

Gouge type, grain size, and thickness do not influence the resistance to sliding, especially at relatively high stresses, due to the mechanical buildup of a fresh secondary gouge matrix that produces a steady-state condition of sliding equilibrium. The fact that gouge does not significantly reduce the coefficient of friction is indicative that friction experiments concerned with coefficients of friction need not involve gouge.

Sawcut angle affects res stance to sliding in a similar manner found in stick-slip experiments (Humston, 1972). Lower values of μ are found to exist near α=30°, which is in agreement with preferred faulting along planes of weakness at these angles for originally intact rocks.

The influence of fluid pore-pressure upon sliding friction, especially in the sandstone-gouge experiments, is the most interesting of the factors studied. The maximum difference between μ_s and μ_k occurs for high pore pressures at relatively low normal stresses, a discovery which may be used to explain observed increases in magnitude of stress drops related to stick-slip events at high pore pressures (Handin and Engelder, 1973). The effect of pore pressure on τ_o during sliding tends to support Hsü's (1969) contention that τ_o should be taken into account when considering overthrust faulting and landsliding. Foreshocks and aftershocks associated with major earthquakes and the shallow nature of most earthquakes can be explained as a result of the influence of dilatancy-related pore pressure changes on fault stability.

The similarity of mechanical processes associated with the fracture of rocks and the pure frictional sliding of rocks implies that frictional processes play an important part in the fracture process, especially at very high stresses (>2.5 kb). One observed difference between fracture and sliding processes is the relative degree of freedom for grains to rotate along incipient or pre-existing fault surfaces. The observed ductile behavior of the limestone for normal stresses (or confining pressures) less than that predicted by Orowan's (1960) theory of brittle-ductile transition, based upon fracture and friction equivalence, may be explained by the existence of small-scale, intragranular plastic flow in segregated regions where there are abnormal stress concentrations. The fact that a rock mass containing planes of weakness is capable of supporting as much stress as unfractured rocks is indicative that such processes as dilatancy and ductility may occur in fractured rock masses.

APPENDIX I

DERIVATION OF EQUATIONS 1' AND 2'

Derivation of normal stress σ and shear stress τ acting on a fault or sawcut surface whose normal is oriented at an angle θ with respect to horizontal or x-axis:

Sign convention--

Normal stresses + if compressional (directed toward origin).

Shear stresses + if directed clockwise with respect to origin, or if directed toward the origin.

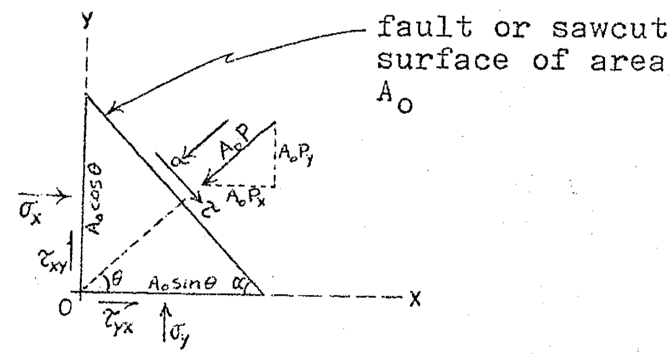

Conditions for equilibrium--

ΣForces in x direction = ΣForces in y direction = 0

$$A_oP_x - \tau_{yx}A_o\sin\theta - \sigma_xA_o\cos\theta = 0$$

$$P_x = \tau_{yx}\sin\theta + \sigma_x\cos\theta \qquad (A1)$$

and

$$A_oP_y - \tau_{xy}A_o\cos\theta - \sigma_yA_o\sin\theta = 0$$

$$P_y = \tau_{xy}\cos\theta + \sigma_y\sin\theta \qquad (A2)$$

Resolving A_oP_x and A_oP_y to σ and τ directions--

$$\cancel{A_o}\sigma = P_x\cancel{A_o}\cos\theta + P_y\cancel{A_o}\sin\theta \qquad (A3)$$

and

$$\not{A}_o \tau = P_x \not{A}_o \sin\theta - P_y \not{A}_o \cos\theta \qquad (A4)$$

Substituting (A3) and (A4) into (A1) and (A2) gives

$$\sigma = \sigma_x \cos^2\theta + \sigma_y \sin^2\theta + (\tau_{xy} + \tau_{yx})\cos\theta\sin\theta \qquad (A5)$$

and

$$\tau = -\frac{\sigma_y - \sigma_x}{2}\sin 2\theta - \tau_{xy}\cos^2\theta + \tau_{yx}\sin^2\theta \qquad (A6)$$

Choose x- and y-axes in directions of principal stresses σ_1 and σ_3, respectively--

$$\begin{matrix} \sigma_x = \sigma_1 \\ \sigma_y = \sigma_3 \end{matrix} \quad \text{and} \quad \left.\begin{matrix} \tau_{xy} = \tau_{13} \\ \tau_{yx} = \tau_{31} \end{matrix}\right\} = 0 \text{ (no shear stresses)}$$

Substituting these conditions into (A5) and (A6) produces

$$\sigma = \sigma_1 \cos^2\theta + \sigma_3 \sin^2\theta = \frac{\sigma_1 + \sigma_3}{2} + \frac{\sigma_1 - \sigma_3}{2}\cos 2\theta \qquad (A7)$$

$$\tau = -\frac{\sigma_3 - \sigma_1}{2}\sin 2\theta = \frac{\sigma_1 - \sigma_3}{2}\sin 2\theta \qquad (A8)$$

For the triaxial apparatus, maximum principal stress (directed along x-axis) equals the axial stress; i.e. $\sigma_1 = \sigma_a$. Thus $\alpha = 90 - \theta$ is the acute angle which σ_a makes with the fault or sawcut surface. Substituting $\sigma_1 = \sigma_a$, $\sigma_3 = \sigma_c$, and $\theta = 90 - \alpha$ into (A7) and (A8) gives

$$\sigma = \frac{\sigma_a + \sigma_c}{2} + \frac{\sigma_a - \sigma_c}{2}\cos 2(90-\alpha) = \frac{\sigma_a + \sigma_c}{2} - \frac{\sigma_a - \sigma_c}{2}\cos 2\alpha \qquad (2')$$

and

$$\tau = \frac{\sigma_a - \sigma_c}{2}\sin 2(90-\alpha) = \frac{\sigma_a - \sigma_c}{2}\sin 2\alpha. \qquad (1')$$

DETERMINATION OF CORRECTION FOR REDUCTION IN CONTACT AREA WITH DISPLACEMENT

d = original dia. of core

$a = \sqrt{2}d/2$ = semi-major axis

$b = d/2$ = semi-minor oxis

e = displacement along sawcut

A_a = actual area of contact

$A = \frac{1}{2}$ area not in contact

$A_e = \pi ab$ = area of ellipse

f = fraction of area in contact

$= A_a/A_e = (A_e - 2A_o)/A_e$

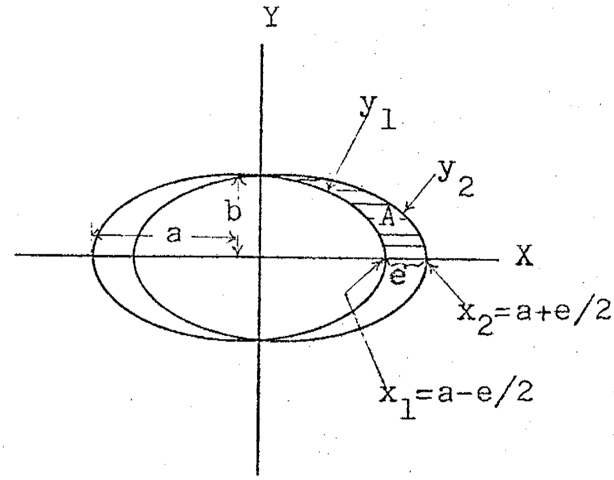

$$y_1 = (b/a)[a^2 - (x - e/2)^2]^{\frac{1}{2}}$$

$$y_2 = (b/a)[a^2 - (x + e/2)^2]^{\frac{1}{2}}$$

Derivation of A:

$$A = \int_0^{x_2} y_2 dx - \int_0^{x_1} y_1 dx$$

$$= \int_0^{a+e/2} (b/a)[a^2 - (x - e/2)^2]^{\frac{1}{2}} dx - \int_0^{a-e/2} (b/a)[a^2 - (x + e/2)^2]^{\frac{1}{2}} dx$$

(let $x' = x - e/2 \Rightarrow dx = dx'$) (let $x' = x + e/2 \Rightarrow dx = dx'$)

$$= (b/a)\left[\int_{-e/2}^{a} + \int_{a}^{e/2}\right][a^2 - x'^2]^{\frac{1}{2}} dx'$$

$$A = (b/a)\left[(e/2)(a^2 - e^2/4)^{\frac{1}{2}} + a^2 \sin^{-1}(e/2a)\right]$$

For 0.00910-in max. axial displacement, $e = (0.00910)(1.414) =$

0.0129", d=1" $\Rightarrow$ a=0.707" and b=0.500"--

$$A_o = 0.707[(0.00645)(0.707) + (0.500)(0.00912)]$$
$$= (0.707)(0.00912)$$
$$= 0.00645"$$

and

$$f = [1.11 - 2(0.00645)]/1.11 = 1.097/1.11$$
$$= \underline{\underline{99\%}}$$

NUMERICAL COMPARISON OF POROSITY-DENSITY-COMPOSITION RELATION FOR KELLY LIMESTONE

Derivation of density of solid material in rock mass--

V_{solid} = volume of solid material in rock mass

V_{void} = volume of voids   volume of space around solid material

M_{solid} = mass of solid material in rock mass

ϕ = fractional rock porosity $V_{void}/(V_{void} \quad V_{solid})$

ρ_{rk} = bulk density of rock mass

ρ_{solid} = density of solid material in rock mass = M_{solid}/V_{solid}

$$V_{void} = V_{solid}\ \phi/(1 - \phi)$$

$$\rho_{rk} = M_{solid}/(V_{solid} + V_{void})$$

$$\rho_{rk}[(V_{solid}/M_{solid}) + (V_{void}/M_{solid})] = 1$$

$$\rho_{rk}\{(V_{solid}/M_{solid}) + (V_{solid}/M_{solid})[\phi/(1 - \phi)]\} = 1$$

$$\rho_{rk}\{1/\rho_{solid} + (1/\rho_{solid})[\phi/(1 - \phi)]\} = 1$$

or

$$\rho_{solid} = \rho_{rk}\ 1/(1 - \phi) \qquad \text{(a)}$$

By assuming the limestone is bimineralic, i.e. it is essentially composed of calcite and dolomite, it is possible to calculate the respective weight percentages from the following data:

ρ_{ca} = 2.71 (c.g.s.) and ρ_{dol} = 2.85 (c.g.s.)   (Berry and Mason, 1959)

$$\rho_{1s} = 2.69 \text{ (c.g.s.) and } \phi = 0.011 \qquad \text{(Tables 3 and 4)}$$

$$\rho_{solid} = 2.69[1/(1 - 0.011)] = 2.72 \text{ (c.g.s.)} \qquad \text{(Equation a)}$$

M_{ca} = mass of calcite in solid material

M_{dol} = mass of dolomite in solid material

x = fraction of solid material which is dolomite

$$= M_{dol}/M_{solid} = M_{dol}/(M_{dol} + M_{ca})$$

$$\Rightarrow M_{dol}/M_{ca} = x/(1 - x)$$

$$\rho_{solid} = (M_{ca} + M_{dol})/[(M_{ca}/\ _{ca}) + (M_{dol}/\ _{dol})]$$

$$= [1 + (M_{dol}/M_{ca})]/[1/\rho_{ca} + (1/\rho_{dol})(M_{dol}/M_{ca})]$$

$$= [1 + x/(1 - x)]/\{1/\rho_{ca} + (1/\rho_{dol})[x/(1 - x)]\}$$

and solving for x,

$$x = [(\rho_{solid}/\rho_{ca}) - 1]/\rho_{solid}\ (1/\rho_{ca}) - (1/\rho_{dol})] \qquad \text{(b)}$$

Substituting values of ρ_{solid}, ρ_{ca}, and ρ_{dol} given above, Equation b becomes

$$x = [(2.72/2.71) - 1]/2.72[(1/2.71) - (1/2.85)]$$

$$= \underline{\underline{0.075}}$$

This is in very good agreement with the value of 7% dolomite obtained from CO_2 gas pressure tests.

EXAMPLE OF PARTIAL-CONTACT AREA CORRECTION FOR $\alpha=30^{\circ}$

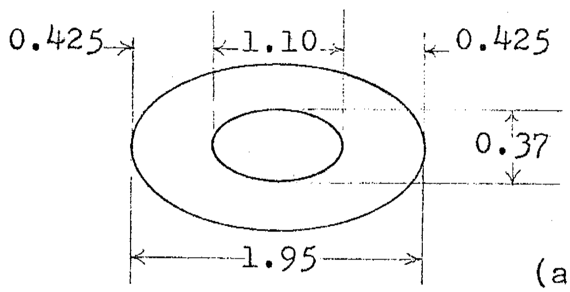

(all dimensions in inches)

$A_o' = \pi(0.37)(1.10)/4 = 0.320$ in^2 (sandstone)

$0.111/0.109 = A_o'/0.320 \Longrightarrow A_o' = 0.326$ in^2 (limestone)

(0.111 in^2 and 0.109 in^2 obtained from Tables AII-21 and AII-22 respectively)

APPENDIX II

THIN-SECTION STUDY

Kelly Limestone (Mississippian; Magdalena Mountains, N.M.)

Mineral	Wt. %	Method*	Dia. (mm)	Round.
Calcite--crystalline	93		0.01	Subang.
veins			>0.05	Subang.
Dolomite (+ organics and detritus)	7		0.02	Ang.
		Average:	0.01	Subang.

* The method of determining wt. % involves determination of CO_2 gas pressure after 15 sec reaction of 1 g limestone with 5 ml concentrated HCl (Muller and Gastner, 1971); results agree with lizarine-red staining tests (Rodgers, 1940; Friedman, 1959)

Texture:

Microcrystalline micritic limestone; high luster; sparry calcite veins (0.05-0.3 mm wide) grade texturally into calcite mosaic.

Comments:

Tightly interlocking calcite rhombs.

Mesa Verde Sandstone (Late Cretaceous; San Antonio, N.M.)

Mineral	Modal Analysis Count	%	S.D. (±%)*	Grain Parameters Dia. (mm)	Round.
Quartz	556	75.3	1.6	0.2	Subang.
Plagioclase	8	1.1	0.4	0.15	Subang.
Microcline	5	0.7	0.3	0.15	Angular
Weathered Felds.	87	11.8	1.2	0.15	Subang.
Rock Particles	5	0.7	0.3	0.13	Subrou.
Limonite	12	1.6	0.5	0.02	Subang.
Void Space	65	8.8	1.0	--	--
Total:	738	100.0		Average: 0.19**	Subang.

* S.D. Standard deviation; calculated from (Chayes, 1956, pp. 39-40):

$$S.D. = 100\sqrt{pq/n}$$

where: p = decimal fraction of a given constituent
q = 1 - p
n = number of counts

** Weighted average diameter; calculated as follows:

$$\begin{array}{ll} (75.3)(0.2) & 15.06 \\ (1.1)(0.15) & 0.165 \\ (0.7)(0.15) & 0.105 \\ (1.6)(0.02) & 0.032 \\ (0.7)(0.13) & 0.091 \\ (\underline{11.8})(0.15) & \underline{1.77} \\ 91.2 & 17.223 \end{array} \Rightarrow 17.223/91.2 = 0.189 \text{ mm}$$

("fine-grained")

Texture:

Well-sorted feldspathic arenite with compacted, moderately porous texture.

Comments:

Plag.-- albite twin.; microcl.-- polysynth. twin.; qtz.-lim. cmt.

Original Experimental Data

TABLE AII-0. Experimental Data for Determination of Machine Stiffness k and Equipment Strain Corrections ε_{equip}

Load L (lb)	Displacement x (in)	Axial Stress σ_a (psi)	Axial Strain ε_a (l_o 5.888")
530	0.000319	675	0.0000542
1075	0.000547	1369	0.0000929
1560	0.000730	1987	0.000124
2130	0.000889	2713	0.000151
2750	0.00107	3503	0.000182
3130	0.00116	3987	0.000197
3680	0.00132	4688	0.000224
4230	0.00145	5389	0.000246
4800	0.00160	6115	0.000272
590	0.000274	752	0.0000465
1075	0.000467	1369	0.0000793
1600	0.000650	2038	0.000110
2010	0.000752	2561	0.000128
2810	0.000969	3580	0.000185
3200	0.00109	4076	0.000185
3520	0.00116	4484	0.000197
4200	0.00132	5350	0.000224
4840	0.00147	6166	0.000250
550	0.000364	701	0.0000618
1025	0.000546	1306	0.0000927
1560	0.000751	1987	0.000128
2065	0.000910	2631	0.000155
2520	0.00105	3210	0.000178
3050	0.00118	3885	0.000200
3825	0.00125	4873	0.000212
4840	0.00164	6166	0.000279
1410	0.000878	1796	0.000149
1980	0.00108	2522	0.000183
2490	0.00123	3172	0.000209
3060	0.00140	3898	0.000238
3550	0.00153	4522	0.000260
3975	0.00166	5064	0.000282
4440	0.00177	5656	0.000301
4850	0.00189	6178	0.000321

TABLE AII-0. (Continued)

Load L (lb)	Displacement x (in)	Axial Stress σ_a (psi)	Axial Strain ε_a (l_o 5.888")
450	0.000308	573	0.0000523
1025	0.000593	1306	0.000101
1500	0.000775	1911	0.000132
2060	0.000946	2624	0.000161
2500	0.00106	3185	0.000180
3070	0.00123	3911	0.000209
3500	0.00133	4459	0.000226
4660	0.00162	5936	0.000275
475	0.000353	605	0.0000560
1090	0.000627	1389	0.000106
1500	0.000787	1911	0.000134
2050	0.000958	2611	0.000163
2630	0.00115	3350	0.000195
3250	0.00132	4140	0.000224
3780	0.00145	4815	0.000246
4280	0.00157	5452	0.000267
540	0.000137	688	0.0000233
1060	0.000365	1350	0.0000620
1525	0.000513	1943	0.0000871
2040	0.000684	2599	0.000116
2700	0.000878	3439	0.000149
3130	0.000992	3987	0.000168
3560	0.00112	4535	0.000190
4200	0.00128	5350	0.000217
4520	0.00135	5758	0.000229
4825	0.00143	6146	0.000243

Ave. Linear Least-square Fit:
(<2100 psi--)
$A = -250$ psi
$B = 18.5 \cdot 10^6$ psi $= 1.28$ Mbar
(>2100 psi--)
$A = -1694$ psi
$B = 28.33 \cdot 10^6$ psi $= 1.954$ Mbar

Note: neglegable difference between tests with and without lubricating grease between metal pieces.

TABLE AII- 1. RECORDED VALUES AXIAL LOAD AND DISPLACEMENT WITH CALCULATED DATA FOR STRESS-STRAIN FRACTURE TEST ON A KELLY LIMESTONE CORE*

AXIAL LOAD (LB)	AXIAL DISPL. (IN)	AXIAL STRESS (PSI)	AXIAL STRESS (BARS)	$(\sigma_a - \sigma_c)$ (PSI)	$(\sigma_a - \sigma_c)$ (BARS)	EQUIP. STRAIN (PERCENT)	AXIAL STRAIN (PERCENT)
350.0	0.0020	468.5	32.3	468.5	32.3	0.00	2.28
600.0	0.0025	803.2	55.4	803.2	55.4	0.01	2.30
1120.0	0.0035	1499.3	103.4	1499.3	103.4	0.01	2.34
1600.0	0.0043	2141.9	147.7	2141.9	147.7	0.01	2.37
2340.0	0.0051	3132.5	216.0	3132.5	216.0	0.02	2.40
3010.0	0.0061	4029.5	277.8	4029.5	277.8	0.02	2.44
3890.0	0.0072	5207.5	359.0	5207.5	359.0	0.02	2.48
4715.0	0.0080	6311.9	435.2	6311.9	435.2	0.03	2.51
5445.0	0.0087	7289.2	502.6	7289.2	502.6	0.03	2.54
5960.0	0.0093	7978.6	550.1	7978.6	550.1	0.03	2.56
6705.0	0.0102	8975.9	618.9	8975.9	618.9	0.04	2.59
7710.0	0.0123	10321.3	711.6	10321.3	711.6	0.04	2.68

* CONFINING P: σ_c = 0.0 PSI; AREA OF CORE: AO = 0.747 SQ. IN.

TABLE AII- 2. RECORDED VALUES AXIAL LOAD AND DISPLACEMENT WITH CALCULATED DATA FOR STRESS-STRAIN FRACTURE TEST ON A KELLY LIMESTONE CORE*

AXIAL LOAD (LB)	AXIAL DISPL. (IN)	AXIAL STRESS (PSI)	AXIAL STRESS (BARS)	$(\sigma_a - \sigma_c)$ (PSI)	$(\sigma_a - \sigma_c)$ (BARS)	EQUIP. STRAIN (PERCENT)	AXIAL STRAIN (PERCENT)
470.0	0.0186	630.9	43.5	40.9	2.8	0.00	2.09
590.0	0.0199	791.9	54.6	201.9	13.9	0.00	2.15
1520.0	0.0210	2040.3	140.7	1450.3	100.0	0.01	2.19
2510.0	0.0222	3369.1	232.3	2779.1	191.6	0.02	2.23
3380.0	0.0230	4536.9	312.8	3946.9	272.1	0.02	2.26
4220.0	0.0236	5664.4	390.5	5074.4	349.9	0.02	2.28
5240.0	0.0245	7033.6	484.9	6443.6	444.3	0.03	2.32
6000.0	0.0251	8053.7	555.3	7463.7	514.6	0.03	2.34
7090.0	0.0257	9516.8	656.2	8926.8	615.5	0.04	2.36
8085.0	0.0264	10852.3	748.2	10262.3	707.6	0.04	2.38
8835.0	0.0269	11859.1	817.7	11269.1	777.0	0.05	2.40
9500.0	0.0274	12751.7	879.2	12161.7	838.5	0.05	2.42
10255.0	0.0280	13765.1	949.1	13175.1	908.4	0.05	2.44
11645.0	0.0289	15630.9	1077.7	15040.9	1037.0	0.06	2.47
12800.0	0.0296	17181.2	1184.6	16591.2	1143.9	0.06	2.50
14050.0	0.0305	18859.1	1300.3	18269.1	1259.6	0.07	2.53
14950.0	0.0311	20067.1	1383.6	19477.1	1342.9	0.07	2.55
16250.0	0.0319	21812.1	1503.9	21222.1	1463.2	0.08	2.58
17200.0	0.0327	23087.2	1591.8	22497.2	1551.1	0.09	2.61
18150.0	0.0333	24362.4	1679.7	23772.4	1639.0	0.09	2.63
18900.0	0.0340	25369.1	1749.1	24779.1	1708.5	0.09	2.66
19850.0	0.0350	26644.3	1837.1	26054.3	1796.4	0.10	2.69
20750.0	0.0363	27852.3	1920.3	27262.3	1879.7	0.10	2.75
20850.0	0.0388	27986.6	1929.6	27396.6	1888.9	0.10	2.85

* CONFINING P: σ_c = 590.0 PSI; AREA OF CORE: AO = 0.745 SQ. IN.

TABLE AII- 3. RECORDED VALUES AXIAL LOAD AND DISPLACEMENT WITH CALCULATED DATA FOR STRESS-STRAIN FRACTURE TEST ON A KELLY LIMESTONE CORE*

AXIAL LOAD (LB)	AXIAL DISPL. (IN)	AXIAL STRESS (PSI)	AXIAL STRESS (BARS)	$(\sigma_a - \sigma_c)$ (PSI)	$(\sigma_a - \sigma_c)$ (BARS)	EQJIP. STRAIN (PERCENT)	AXIAL STRAIN (PERCENT)
610.0	0.0166	818.8	56.5	18.8	1.3	0.00	1.24
970.0	0.0360	1302.0	89.8	502.0	34.6	0.00	2.11
1650.0	0.0372	2214.8	152.7	1414.8	97.5	0.01	2.16
2940.0	0.0390	3946.3	272.1	3146.3	216.9	0.02	2.23
4980.0	0.0409	6684.6	460.9	5884.6	405.7	0.03	2.30
7360.0	0.0430	9879.2	681.1	9079.2	626.0	0.04	2.39
9190.0	0.0445	12335.6	850.5	11535.6	795.3	0.05	2.44
11790.0	0.0465	15825.5	1091.1	15025.5	1036.0	0.06	2.52
13750.0	0.0480	18456.4	1272.5	17656.4	1217.4	0.07	2.58
15100.0	0.0491	20268.5	1397.5	19468.5	1342.3	0.07	2.62
16250.0	0.0500	21812.1	1503.9	21012.1	1448.7	0.08	2.66
17550.0	0.0512	23557.0	1624.2	22757.0	1569.0	0.09	2.70
18450.0	0.0524	24765.1	1707.5	23965.1	1652.3	0.09	2.75
21000.0	0.0567	28187.9	1943.5	27387.9	1888.3	0.10	2.93

* CONFINING P: σ_c = 800.0 PSI; AREA OF CORE: AO = 0.745 SQ. IN.

TABLE AII- 4. RECORDED VALUES AXIAL LOAD AND DISPLACEMENT WITH CALCULATED DATA FOR STRESS-STRAIN FRACTURE TEST ON A KELLY LIMESTONE CORE*

AXIAL LOAD (LB)	AXIAL DISPL. (IN)	AXIAL STRESS (PSI)	AXIAL STRESS (BARS)	$(\sigma_a - \sigma_c)$ (PSI)	$(\sigma_a - \sigma_c)$ (BARS)	EQUIP. STRAIN (PERCENT)	AXIAL STRAIN (PERCENT)
2900.0	0.0129	3882.2	267.7	1882.2	129.8	0.01	2.03
3560.0	0.0137	4765.7	328.6	2765.7	190.7	0.02	2.06
6550.0	0.0161	8768.4	604.6	6768.4	466.7	0.03	2.15
8145.0	0.0172	10903.6	751.8	8903.6	613.9	0.04	2.19
9240.0	0.0179	12369.5	852.8	10369.5	714.9	0.04	2.21
10170.0	0.0185	13614.5	938.7	11614.5	800.8	0.05	2.23
11270.0	0.0193	15087.0	1040.2	13087.0	902.3	0.05	2.26
12135.0	0.0199	16245.0	1120.0	14245.0	982.2	0.06	2.28
12960.0	0.0205	17349.4	1196.2	15349.4	1058.3	0.06	2.30
14000.0	0.0210	18741.6	1292.2	16741.6	1154.3	0.07	2.32
14700.0	0.0216	19678.7	1356.8	17678.7	1218.9	0.07	2.34
15900.0	0.0223	21285.1	1467.6	19285.1	1329.7	0.07	2.37
16680.0	0.0228	22329.3	1539.5	20329.3	1401.7	0.08	2.38
17600.0	0.0234	23560.9	1624.5	21560.9	1486.6	0.08	2.40
18450.0	0.0240	24698.8	1702.9	22698.8	1565.0	0.09	2.42
19200.0	0.0245	25702.8	1772.1	23702.8	1634.2	0.09	2.44
19950.0	0.0251	26706.8	1841.4	24706.8	1703.5	0.09	2.46
20800.0	0.0256	27844.7	1919.8	25844.7	1781.9	0.10	2.48
21400.0	0.0261	28647.9	1975.2	26647.9	1837.3	0.10	2.50
22050.0	0.0267	29518.1	2035.2	27518.1	1897.3	0.10	2.52
22900.0	0.0273	30656.0	2113.6	28656.0	1975.8	0.11	2.54
24240.0	0.0283	32449.8	2237.3	30449.8	2099.4	0.11	2.58
25150.0	0.0293	33668.0	2321.3	31668.0	2183.4	0.12	2.62
25800.0	0.0301	34538.2	2381.3	32538.2	2243.4	0.12	2.65
26770.0	0.0326	35836.7	2470.8	33836.7	2333.0	0.13	2.75
26950.0	0.0342	36077.6	2487.5	34077.6	2349.6	0.13	2.81

* CONFINING P: σ_c = 2000.0 PSI; AREA OF CORE: AO = 0.747 SQ. IN.

TABLE AII- 5. RECORDED VALUES AXIAL LOAD AND DISPLACEMENT WITH CALCULATED DATA FOR STRESS-STRAIN FRACTURE TEST ON A KELLY LIMESTONE CORE*

AXIAL LOAD (LB)	AXIAL DISPL. (IN)	AXIAL STRESS (PSI)	AXIAL STRESS (BARS)	$(\sigma_a - \sigma_c)$ (PSI)	$(\sigma_a - \sigma_c)$ (BARS)	EQUIP. STRAIN (PERCENT)	AXIAL STRAIN (PERCENT)
4030.0	0.0093	5416.7	373.5	416.7	28.7	0.00	0.70
4735.0	0.0263	6364.2	438.8	1364.2	94.1	0.01	1.44
4920.0	0.0302	6612.9	455.9	1612.9	111.2	0.01	1.61
5470.0	0.0380	7352.1	506.9	2352.1	162.2	0.01	1.95
6750.0	0.0394	9072.6	625.5	4072.6	280.8	0.02	2.00
7240.0	0.0397	9731.2	670.9	4731.2	326.2	0.02	2.01
7960.0	0.0403	10698.9	737.7	5698.9	392.9	0.03	2.04
8630.0	0.0408	11599.5	799.8	6599.5	455.0	0.03	2.06
9505.0	0.0417	12775.5	880.8	7775.5	536.1	0.03	2.09
10540.0	0.0425	14166.7	976.8	9166.7	632.0	0.04	2.12
11500.0	0.0432	15457.0	1065.7	10457.0	721.0	0.04	2.15
12880.0	0.0442	17311.8	1193.6	12311.8	848.9	0.05	2.18
15300.0	0.0458	20564.5	1417.9	15564.5	1073.1	0.06	2.24
16250.0	0.0465	21841.4	1505.9	16841.4	1161.2	0.07	2.27
17270.0	0.0473	23212.4	1600.4	18212.4	1255.7	0.07	2.30
18540.0	0.0482	24919.4	1718.1	19919.4	1373.4	0.08	2.33
19440.0	0.0489	26129.0	1801.5	21129.0	1456.8	0.08	2.36
20400.0	0.0497	27419.4	1890.5	22419.4	1545.8	0.09	2.39
21460.0	0.0505	28844.1	1988.7	23844.1	1644.0	0.09	2.42
22400.0	0.0512	30107.5	2075.8	25107.5	1731.1	0.09	2.45
23900.0	0.0525	32123.7	2214.8	27123.7	1870.1	0.10	2.49
25150.0	0.0534	33803.8	2330.7	28803.8	1985.9	0.11	2.53
25950.0	0.0541	34879.0	2404.8	29879.0	2060.1	0.11	2.56
26800.0	0.0550	36021.5	2483.6	31021.5	2138.9	0.12	2.59
27750.0	0.0558	37298.4	2571.6	32298.4	2226.9	0.12	2.62
28750.0	0.0568	38642.5	2664.3	33642.5	2319.6	0.12	2.66
30160.0	0.0584	40537.6	2795.0	35537.6	2450.2	0.13	2.72

TABLE AII- 5. (CONTINUED)

31170.0	0.0597	41895.2	2888.6	36895.2	2543.8	0.14	2.78
31970.0	0.0610	42970.4	2962.7	37970.4	2618.0	0.14	2.83
32600.0	0.0623	43817.2	3021.1	38817.2	2676.3	0.14	2.88
33470.0	0.0658	44986.6	3101.7	39986.6	2757.0	0.15	3.03
33700.0	0.0694	45295.7	3123.0	40295.7	2778.3	0.15	3.19
32400.0	0.0775	43548.4	3002.5	38548.4	2657.8	0.14	3.55

* CONFINING P: σ_c = 5000.0 PSI; AREA OF CORE: AO = 0.744 SQ. IN.

TABLE AII- 6. RECORDED VALUES AXIAL LOAD AND DISPLACEMENT WITH CALCULATED DATA FOR STRESS-STRAIN FRACTURE TEST ON A KELLY LIMESTONE CORE*

AXIAL LOAD (LB)	AXIAL DISPL. (IN)	AXIAL STRESS (PSI)	AXIAL STRESS (BARS)	$(\sigma_a - \sigma_c)$ (PSI)	$(\sigma_a - \sigma_c)$ (BARS)	EQUIP. STRAIN (PERCENT)	AXIAL STRAIN (PERCENT)
6320.0	0.0052	8483.2	584.9	963.2	66.4	0.01	0.88
6900.0	0.0211	9261.7	638.6	1741.7	120.1	0.01	1.76
7810.0	0.0266	10483.2	722.8	2963.2	204.3	0.02	2.06
9210.0	0.0280	12362.4	852.4	4842.4	333.9	0.02	2.13
11400.0	0.0293	15302.0	1055.0	7782.0	536.5	0.03	2.19
13200.0	0.0303	17718.1	1221.6	10198.1	703.1	0.04	2.24
15710.0	0.0319	21087.2	1453.9	13567.2	935.4	0.05	2.32
18250.0	0.0334	24496.6	1689.0	16976.6	1170.5	0.07	2.39
21050.0	0.0351	28255.0	1948.1	20735.0	1429.6	0.08	2.47
23550.0	0.0369	31610.7	2179.5	24090.7	1661.0	0.09	2.56
25880.0	0.0384	34738.3	2395.1	27218.3	1876.6	0.10	2.63
28130.0	0.0397	37758.4	2603.3	30238.4	2084.9	0.11	2.69
29820.0	0.0408	40026.8	2759.7	32506.8	2241.3	0.12	2.75
32320.0	0.0424	43382.5	2991.1	35862.5	2472.6	0.13	2.82
34600.0	0.0440	46442.9	3202.1	38922.9	2683.6	0.14	2.90
36660.0	0.0456	49208.1	3392.8	41688.1	2874.3	0.15	2.98
38460.0	0.0476	51624.2	3559.4	44104.2	3040.9	0.16	3.08
40020.0	0.0511	53718.1	3703.7	46198.1	3185.2	0.17	3.27
41000.0	0.0569	55033.6	3794.4	47513.6	3275.9	0.17	3.59

* CONFINING P: σ_c = 7520.0 PSI; AREA OF CORE: AO = 0.745 SQ. IN.

TABLE AII- 7. RECORDED VALUES AXIAL LOAD AND DISPLACEMENT WITH CALCULATED DATA FOR STRESS-STRAIN FRACTURE TEST ON A KELLY LIMESTONE CORE*

AXIAL LOAD (LB)	AXIAL DISPL. (IN)	AXIAL STRESS (PSI)	AXIAL STRESS (BARS)	$(\sigma_a - \sigma_c)$ (PSI)	$(\sigma_a - \sigma_c)$ (BARS)	EQUIP. STRAIN (PERCENT)	AXIAL STRAIN (PERCENT)
8250.0	0.0231	11088.7	764.5	1388.7	95.7	0.01	0.98
8680.0	0.0271	11666.7	804.4	1966.7	135.6	0.01	1.15
8950.0	0.0295	12029.6	829.4	2329.6	160.6	0.01	1.25
9360.0	0.0335	12580.6	867.4	2880.6	198.6	0.02	1.42
9700.0	0.0368	13037.6	898.9	3337.6	230.1	0.02	1.56
9940.0	0.0394	13360.2	921.2	3660.2	252.4	0.02	1.67
10120.0	0.0416	13602.1	937.8	3902.1	269.0	0.02	1.76
10300.0	0.0429	13844.1	954.5	4144.1	285.7	0.02	1.82
11200.0	0.0451	15053.8	1037.9	5353.8	369.1	0.02	1.90
13100.0	0.0468	17607.5	1214.0	7907.5	545.2	0.03	1.97
14750.0	0.0480	19825.3	1366.9	10125.3	698.1	0.04	2.01
16960.0	0.0497	22795.7	1571.7	13095.7	902.9	0.05	2.07
18770.0	0.0510	25228.5	1739.4	15528.5	1070.6	0.06	2.12
20610.0	0.0522	27701.6	1910.0	18001.6	1241.2	0.07	2.16
22700.0	0.0536	30510.8	2103.6	20810.8	1434.8	0.08	2.21
24700.0	0.0550	33198.9	2289.0	23498.9	1620.2	0.09	2.26
27100.0	0.0567	36424.7	2511.4	26724.7	1842.6	0.10	2.33
29150.0	0.0583	39180.1	2701.4	29480.1	2032.6	0.11	2.38
31260.0	0.0600	42016.1	2896.9	32316.1	2228.1	0.12	2.45
33000.0	0.0616	44354.8	3058.2	34654.8	2389.4	0.13	2.51
34500.0	0.0629	46371.0	3197.2	36671.0	2528.4	0.14	2.56
36150.0	0.0646	48588.7	3350.1	38888.7	2681.3	0.14	2.62
37550.0	0.0662	50470.4	3479.8	40770.4	2811.0	0.15	2.68
39040.0	0.0682	52473.1	3617.9	42773.1	2949.1	0.16	2.76
40270.0	0.0702	54126.3	3731.9	44426.3	3063.1	0.16	2.84
40350.0	0.0710	54233.9	3739.3	44533.9	3070.5	0.16	2.87
41700.0	0.0727	56048.4	3864.4	46348.4	3195.6	0.17	2.94

TABLE AII- 7. (CONTINUED)

42800.0	0.0760	57526.9	3966.3	47826.9	3297.5	0.17	3.08
44240.0	0.0811	59462.4	4099.8	49762.4	3431.0	0.18	3.29
44300.0	0.0878	59543.0	4105.3	49843.0	3436.5	0.18	3.58

* CONFINING P: σ_c = 9700.0 PSI; AREA OF CORE: AO = 0.744 SQ. IN.

TABLE AII- 8. RECORDED VALUES AXIAL LOAD AND DISPLACEMENT WITH CALCULATED DATA FOR STRESS-STRAIN FRACTURE TEST ON A MESA VERDE SANDSTONE TEST CORE*

AXIAL LOAD (LB)	AXIAL DISPL. (IN)	AXIAL STRESS (PSI)	AXIAL STRESS (BARS)	$(\sigma_a - \sigma_c)$ (PSI)	$(\sigma_a - \sigma_c)$ (BARS)	EQUIP. STRAIN (PERCENT)	AXIAL STRAIN (PERCENT)
910.0	0.0122	1236.4	85.2	686.4	47.3	0.01	0.42
2020.0	0.0154	2744.6	189.2	2194.6	151.3	0.01	0.52
2490.0	0.0162	3383.2	233.3	2833.2	195.3	0.02	0.54
2870.0	0.0168	3899.5	268.9	3349.5	230.9	0.02	0.56
3280.0	0.0175	4456.5	307.3	3906.5	269.3	0.02	0.58
3710.0	0.0183	5040.8	347.5	4490.8	309.6	0.02	0.61
4250.0	0.0192	5774.5	398.1	5224.5	360.2	0.02	0.64
4890.0	0.0202	6644.0	458.1	6094.0	420.2	0.03	0.67
5560.0	0.0212	7554.3	520.9	7004.3	482.9	0.03	0.70
6370.0	0.0223	8654.9	596.7	8104.9	558.8	0.03	0.73
6970.0	0.0232	9470.1	652.9	8920.1	615.0	0.04	0.76
7500.0	0.0239	10190.2	702.6	9640.2	664.7	0.04	0.78
8010.0	0.0246	10883.1	750.4	10333.1	712.4	0.04	0.80
9050.0	0.0260	12296.2	847.8	11746.2	809.9	0.05	0.85
9880.0	0.0272	13423.9	925.5	12873.9	887.6	0.05	0.89
10440.0	0.0280	14184.8	978.0	13634.8	940.1	0.05	0.91
11150.0	0.0290	15149.5	1044.5	14599.5	1006.6	0.06	0.94
12020.0	0.0302	16331.5	1126.0	15781.5	1088.1	0.06	0.98
12720.0	0.0313	17282.6	1191.6	16732.6	1153.7	0.07	1.01
13130.0	0.0320	17839.7	1230.0	17289.7	1192.1	0.07	1.03
13980.0	0.0335	18994.6	1309.6	18444.6	1271.7	0.07	1.08
14600.0	0.0346	19837.0	1367.7	19287.0	1329.8	0.07	1.12
15000.0	0.0356	20380.4	1405.2	19830.4	1367.3	0.08	1.15
14850.0	0.0367	20176.6	1391.1	19626.6	1353.2	0.08	1.19

* CONFINING P: σ_c = 550.0 PSI; AREA OF CORE: AO = 0.736 SQ. IN.

TABLE AII- 9. RECORDED VALUES AXIAL LOAD AND DISPLACEMENT WITH CALCULATED DATA FOR STRESS-STRAIN FRACTURE TEST ON A MESA VERDE SANDSTONE TEST CORE*

AXIAL LOAD (LB)	AXIAL DISPL. (IN)	AXIAL STRESS (PSI)	AXIAL STRESS (BARS)	$(\sigma_a - \sigma_c)$ (PSI)	$(\sigma_a - \sigma_c)$ (BARS)	EQUIP. STRAIN (PERCENT)	AXIAL STRAIN (PERCENT)
1600.0	0.0164	2173.9	149.9	173.9	12.0	0.00	0.57
2340.0	0.0300	3179.3	219.2	1179.3	81.3	0.01	1.04
2865.0	0.0313	3892.7	268.4	1892.7	130.5	0.01	1.09
3160.0	0.0321	4293.5	296.0	2293.5	158.1	0.01	1.11
3725.0	0.0332	5061.1	349.0	3061.1	211.1	0.02	1.15
4390.0	0.0345	5964.7	411.2	3964.7	273.4	0.02	1.19
5085.0	0.0360	6909.0	476.4	4909.0	338.5	0.02	1.24
5880.0	0.0374	7989.1	550.8	5989.1	412.9	0.03	1.29
6570.0	0.0386	8926.6	615.5	6926.6	477.6	0.03	1.32
7070.0	0.0395	9606.0	662.3	7606.0	524.4	0.03	1.35
7675.0	0.0406	10428.0	719.0	8428.0	581.1	0.04	1.39
8245.0	0.0415	11202.4	772.4	9202.4	634.5	0.04	1.42
8655.0	0.0424	11759.5	810.8	9759.5	672.9	0.04	1.45
9100.0	0.0432	12364.1	852.5	10364.1	714.6	0.04	1.47
9760.0	0.0442	13260.9	914.3	11260.9	776.4	0.05	1.51
10300.0	0.0449	13994.6	964.9	11994.6	827.0	0.05	1.53
10870.0	0.0461	14769.0	1018.3	12769.0	880.4	0.05	1.57
11490.0	0.0472	15611.4	1076.4	13611.4	938.5	0.05	1.60
12190.0	0.0484	16562.5	1141.9	14562.5	1004.0	0.06	1.64
12900.0	0.0495	17527.2	1208.5	15527.2	1070.6	0.06	1.68
13325.0	0.0502	18104.6	1248.3	16104.6	1110.4	0.06	1.70
14000.0	0.0517	19021.7	1311.5	17021.7	1173.6	0.07	1.75
14880.0	0.0533	20217.4	1393.9	18217.4	1256.0	0.07	1.80
15800.0	0.0550	21467.4	1480.1	19467.4	1342.2	0.07	1.86
16400.0	0.0562	22282.6	1536.3	20282.6	1398.4	0.08	1.89
17050.0	0.0577	23165.8	1597.2	21165.8	1459.3	0.08	1.94
17650.0	0.0591	23981.0	1653.4	21981.0	1515.5	0.08	1.99

TABLE AII- 9. (CONTINUED)

18350.0	0.0612	24932.1	1719.0	22932.1	1581.1	0.09	2.06
19100.0	0.0633	25951.1	1789.3	23951.1	1651.4	0.09	2.13
19600.0	0.0694	26630.4	1836.1	24630.4	1698.2	0.09	2.34

* CONFINING P: σ_c = 2000.0 PSI; AREA OF CORE: AO = 0.736 SQ. IN.

TABLE AII-10. RECORDED VALUES AXIAL LOAD AND DISPLACEMENT WITH CALCULATED DATA FOR STRESS-STRAIN FRACTURE TEST ON A MESA VERDE SANDSTONE TEST CORE*

AXIAL LOAD (LB)	AXIAL DISPL. (IN)	AXIAL STRESS (PSI)	AXIAL STRESS (BARS)	$(\sigma_a - \sigma_c)$ (PSI)	$(\sigma_a - \sigma_c)$ (BARS)	EQUIP. STRAIN (PERCENT)	AXIAL STRAIN (PERCENT)
4250.0	0.0208	5234.0	360.9	234.0	16.1	0.00	0.83
4700.0	0.0241	5788.2	399.1	788.2	54.3	0.01	0.96
5850.0	0.0258	7204.4	496.7	2204.4	152.0	0.01	1.02
7500.0	0.0279	9236.5	636.8	4236.5	292.1	0.02	1.10
8270.0	0.0290	10184.7	702.2	5184.7	357.5	0.02	1.14
9320.0	0.0303	11477.8	791.4	6477.8	446.6	0.03	1.19
10620.0	0.0317	13078.8	901.8	8078.8	557.0	0.03	1.24
12200.0	0.0335	15024.6	1035.9	10024.6	691.2	0.04	1.31
12910.0	0.0344	15899.0	1096.2	10899.0	751.5	0.04	1.34
13700.0	0.0353	16871.9	1163.3	11871.9	818.5	0.05	1.37
14650.0	0.0364	18041.9	1243.9	13041.9	899.2	0.05	1.41
15700.0	0.0376	19335.0	1333.1	14335.0	988.4	0.06	1.46
16700.0	0.0388	20566.5	1418.0	15566.5	1073.3	0.06	1.50
17710.0	0.0399	21810.3	1503.8	16810.3	1159.0	0.07	1.54
18640.0	0.0410	22955.7	1582.7	17955.7	1238.0	0.07	1.58
20300.0	0.0427	25000.0	1723.7	20000.0	1378.9	0.08	1.64
21700.0	0.0444	26724.1	1842.6	21724.1	1497.8	0.08	1.70
23800.0	0.0464	29310.3	2020.9	24310.3	1676.1	0.09	1.77
24550.0	0.0479	30234.0	2084.6	25234.0	1739.8	0.10	1.83
25820.0	0.0495	31798.0	2192.4	26798.0	1847.7	0.10	1.89
27320.0	0.0516	33645.3	2319.8	28645.3	1975.0	0.11	1.97
28460.0	0.0533	35049.3	2416.6	30049.3	2071.8	0.11	2.03
29740.0	0.0552	36625.6	2525.2	31625.6	2180.5	0.12	2.10
30480.0	0.0568	37536.9	2588.1	32536.9	2243.3	0.12	2.16
31550.0	0.0601	38854.7	2678.9	33854.7	2334.2	0.13	2.29
32260.0	0.0652	39729.1	2739.2	34729.1	2394.5	0.13	2.49

* CONFINING P: σ_c = 5000.0 PSI; AREA OF CORE: AO = 0.812 SQ. IN.

TABLE AII-11. RECORDED VALUES AXIAL LOAD AND DISPLACEMENT WITH CALCULATED DATA FOR STRESS-STRAIN FRACTURE TEST ON A MESA VERDE SANDSTONE TEST CORE*

AXIAL LOAD (LB)	AXIAL DISPL. (IN)	AXIAL STRESS (PSI)	AXIAL STRESS (BARS)	$(\sigma_a - \sigma_c)$ (PSI)	$(\sigma_a - \sigma_c)$ (BARS)	EQUIP. STRAIN (PERCENT)	AXIAL STRAIN (PERCENT)
6320.0	0.0073	7783.3	536.6	283.3	19.5	0.00	0.28
6830.0	0.0210	8411.3	579.9	911.3	62.8	0.01	0.81
7210.0	0.0278	8879.3	612.2	1379.3	95.1	0.01	1.08
7560.0	0.0339	9310.3	641.9	1810.3	124.8	0.01	1.31
8600.0	0.0356	10591.1	730.2	3091.1	213.1	0.02	1.37
9800.0	0.0371	12069.0	832.1	4569.0	315.0	0.02	1.43
11300.0	0.0386	13916.3	959.5	6416.3	442.4	0.03	1.48
12600.0	0.0400	15517.2	1069.9	8017.2	552.8	0.03	1.53
13450.0	0.0409	16564.0	1142.0	9064.0	624.9	0.04	1.56
14760.0	0.0423	18177.3	1253.3	10677.3	736.2	0.04	1.61
16200.0	0.0437	19950.7	1375.6	12450.7	858.4	0.05	1.66
17600.0	0.0452	21674.9	1494.4	14174.9	977.3	0.06	1.71
18960.0	0.0465	23349.8	1609.9	15849.8	1092.8	0.06	1.76
20410.0	0.0480	25135.5	1733.0	17635.5	1215.9	0.07	1.81
21800.0	0.0494	26847.3	1851.1	19347.3	1333.9	0.07	1.86
23400.0	0.0509	28817.7	1986.9	21317.7	1469.8	0.08	1.91
25010.0	0.0525	30800.5	2123.6	23300.5	1606.5	0.09	1.96
26240.0	0.0537	32315.3	2228.1	24815.3	1710.9	0.09	2.01
27170.0	0.0547	33460.6	2307.0	25960.6	1789.9	0.10	2.04
28080.0	0.0556	34581.3	2384.3	27081.3	1867.2	0.10	2.07
29100.0	0.0567	35837.4	2470.9	28337.4	1953.8	0.11	2.11
30450.0	0.0582	37500.0	2585.5	30000.0	2068.4	0.11	2.16
31620.0	0.0596	38940.9	2684.9	31440.9	2167.8	0.12	2.21
32800.0	0.0609	40394.1	2785.1	32894.1	2268.0	0.12	2.26
33980.0	0.0624	41847.3	2885.3	34347.3	2368.2	0.13	2.31
35300.0	0.0642	43472.9	2997.3	35972.9	2480.2	0.13	2.38
36510.0	0.0660	44963.1	3100.1	37463.1	2583.0	0.14	2.44

TABLE AII-11. (CONTINUED)

37510.0	0.0677	46194.6	3185.0	38694.6	2667.9	0.14	2.50
38780.0	0.0701	47758.6	3292.8	40258.6	2775.7	0.15	2.59
39900.0	0.0734	49137.9	3387.9	41637.9	2870.8	0.15	2.72
40740.0	0.0874	50172.4	3459.3	42672.4	2942.2	0.16	3.26

* CONFINING P: σ_c = 7500.0 PSI; AREA OF CORE: AO = 0.812 SQ. IN.

TABLE AII-12. RECORDED VALUES AXIAL LOAD AND DISPLACEMENT WITH CALCULATED DATA FOR STRESS-STRAIN FRACTURE TEST ON A MESA VERDE SANDSTONE TEST CORE*

AXIAL LOAD (LB)	AXIAL DISPL. (IN)	AXIAL STRESS (PSI)	AXIAL STRESS (BARS)	$(\sigma_a - \sigma_c)$ (PSI)	$(\sigma_a - \sigma_c)$ (BARS)	EQUIP. STRAIN (PERCENT)	AXIAL STRAIN (PERCENT)
8100.0	0.0142	9975.4	687.8	350.4	24.2	0.00	0.54
8500.0	0.0265	10468.0	721.7	843.0	58.1	0.01	1.01
8850.0	0.0344	10899.0	751.5	1274.0	87.8	0.01	1.31
10010.0	0.0389	12327.6	850.0	2702.6	186.3	0.02	1.47
11940.0	0.0409	14704.4	1013.8	5079.4	350.2	0.02	1.54
14750.0	0.0436	18165.0	1252.4	8540.0	588.8	0.04	1.63
17800.0	0.0465	21921.2	1511.4	12296.2	847.8	0.05	1.73
20450.0	0.0491	25184.7	1736.4	15559.7	1072.8	0.06	1.82
22720.0	0.0512	27980.3	1929.2	18355.3	1265.6	0.07	1.89
25100.0	0.0534	30911.3	2131.3	21286.3	1467.6	0.08	1.96
27210.0	0.0555	33509.9	2310.4	23884.9	1646.8	0.09	2.03
28800.0	0.0571	35468.0	2445.4	25843.0	1781.8	0.10	2.09
30600.0	0.0589	37684.7	2598.3	28059.7	1934.6	0.11	2.15
32400.0	0.0609	39901.5	2751.1	30276.5	2087.5	0.11	2.22
34320.0	0.0630	42266.0	2914.1	32641.0	2250.5	0.12	2.29
36600.0	0.0655	45073.9	3107.7	35448.9	2444.1	0.13	2.37
38250.0	0.0675	47105.9	3247.8	37480.9	2584.2	0.14	2.44
40120.0	0.0697	49408.9	3406.6	39783.9	2743.0	0.15	2.52
40800.0	0.0706	50246.3	3464.4	40621.3	2800.7	0.15	2.55
42160.0	0.0724	51921.2	3579.8	42296.2	2916.2	0.16	2.61
43600.0	0.0742	53694.6	3702.1	44069.6	3038.5	0.16	2.67
45180.0	0.0764	55640.4	3836.3	46015.4	3172.6	0.17	2.75
46980.0	0.0792	57857.1	3989.1	48232.1	3325.5	0.18	2.85
48700.0	0.0824	59975.4	4135.1	50350.4	3471.5	0.18	2.97
50600.0	0.0869	62315.3	4296.5	52690.3	3632.9	0.19	3.13
51750.0	0.0969	63731.5	4394.1	54106.5	3730.5	0.20	3.51

* CONFINING P: σ_c = 9625.0 PSI; AREA OF CORE: AO = 0.812 SQ. IN.

TABLE AII-13. RECORDED VALUES OF AXIAL LOAD L AND CONFINING PRESSURE σ_c AND CALCULATED VALUES OF SHEAR STRESS τ AND NORMAL STRESS σ FOR CONTROLLED-AREA FRICTIUN TESTS

RECORDED DATA		CALCULATED DATA CONTROLLED AREA (AC')			
L	σ_c	τ		σ	
(LB)	(PSI)	(PSI)	(BARS)	(PSI)	(BARS)
LS. #100 GRIT ROUGHNESS; ALPHA=45 (AC'=0.108 SQ. IN.)					
410	570	1613	111	2183	150
420	580	1654	114	2234	154
795	990	3185	219	4175	287
815	1010	3268	225	4278	294
1200	1410	4850	334	6260	431
1215	1430	4910	338	6339	437
1705	2070	6858	472	8928	615
1725	2100	6936	478	9036	623
2335	2825	9397	647	12222	842
2370	2860	9542	657	12402	855
2870	3375	11599	799	14974	1032
2885	3400	11656	803	15056	1038
3370	3980	13611	938	17591	1212
3380	4000	13648	941	17648	1216
3970	4640	16059	1107	20699	1427
3975	4650	16077	1108	20727	1429
4295	5105	17331	1194	22436	1546
4310	5125	17391	1199	22516	1552
4750	5680	19150	1320	24830	1712
4770	5710	19228	1325	24938	1719
5285	6180	21377	1473	27557	1900

TABLE AII-14. RECORDED VALUES OF AXIAL LOAD L AND CONFINING PRESSURE σ_c AND CALCULATED VALUES OF SHEAR STRESS τ AND NORMAL STRESS σ FOR CONTROLLED-AREA FRICTION TESTS

RECORDED DATA		CALCULATED DATA CONTROLLED AREA (AC')			
L (LB)	σ_c (PSI)	τ (PSI)	τ (BARS)	σ (PSI)	σ (BARS)
LS. #100 GRIT ROUGHNESS; ALPHA=45; DUPLICATE (AC'=0.108 SQ. IN.)					
575	790	2267	156	3057	210
600	810	2372	163	3182	219
1070	1300	4303	296	5603	386
1090	1325	4383	302	5708	393
1375	1700	5515	380	7215	497
1400	1725	5618	387	7343	506
1725	2120	6926	477	9046	623
1760	2150	7073	487	9223	635
2325	2830	9348	644	12178	839
2350	2865	9447	651	12312	848
3065	3605	12387	854	15992	1102
3080	3625	12446	858	16071	1108
3615	4280	14596	1006	18876	1301
3635	4300	14678	1012	18978	1308
4245	5000	17152	1182	22152	1527

TABLE AII-15. RECORDED VALUES OF AXIAL LOAD L AND CONFINING PRESSURE σ_c AND CALCULATED VALUES OF SHEAR STRESS τ AND NORMAL STRESS σ FOR CONTROLLED-AREA FRICTION TESTS

RECORDED DATA		CALCULATED DATA CONTROLLED AREA (AC')			
L	σ_c	τ		σ	
(LB)	(PSI)	(PSI)	(BARS)	(PSI)	(BARS)
LS. #80 DRY GOUGE; 1-MM THICK; ALPHA=45 (AC'=0.108 SQ. IN.)					
535	700	2126	146	2826	194
540	725	2137	147	2862	197
1130	1345	4558	314	5903	407
1140	1360	4597	317	5957	410
1750	2115	7044	485	9159	631
1755	2135	7057	486	9192	633
2365	2865	9516	656	12381	853
2390	2900	9614	662	12514	862
3030	3540	12257	845	15797	1089
3040	3560	12294	847	15854	1093
3940	4680	15900	1096	20580	1418
3950	4700	15937	1098	20637	1422
4775	5620	19296	1330	24916	1717
4790	5645	19353	1334	24998	1723
5645	6645	22811	1572	29456	2030

TABLE AII-16. RECORDED VALUES OF AXIAL LOAD L AND CONFINING PRESSURE σ_c AND CALCULATED VALUES OF SHEAR STRESS τ AND NORMAL STRESS σ FOR CONTROLLED-AREA FRICTION TESTS

RECORDED DATA		CALCULATED DATA CONTROLLED AREA (AC')			
L	σ_c	τ		σ	
(LB)	(PSI)	(PSI)	(BARS)	(PSI)	(BARS)
SS. #100 GRIT ROUGHNESS; ALPHA=45 (AC'=0.108 SQ. IN.)					
615	740	2477	170	3217	221
635	760	2559	176	3319	228
766	1010	3041	209	4051	279
775	1035	3070	211	4105	283
1385	1590	5567	383	7257	500
1410	1700	5677	391	7377	508
1900	2260	7666	528	9926	684
1920	2280	7748	534	10028	691
2280	2670	9220	635	11890	819
2300	2700	9298	641	11998	827
2665	3120	10777	743	13897	958
2690	3150	10878	750	14028	967
3330	3830	13501	930	17331	1194
3350	3860	13579	936	17439	1202
3765	4395	15233	1050	19628	1353
3800	4420	15382	1060	19802	1365
4235	4980	17116	1180	22096	1523
4270	5015	17261	1190	22276	1535
4800	5650	19397	1337	25047	1726
4825	5675	19500	1344	25175	1735
5655	6530	22915	1579	29445	2030
5680	6565	23013	1586	29578	2039
6310	7200	25612	1765	32812	2262
6325	7230	25667	1769	32897	2268
6975	7980	28301	1951	36281	2501

TABLE AII-17. RECORDED VALUES OF AXIAL LOAD L AND CONFINING PRESSURE σ_c AND CALCULATED VALUES OF SHEAR STRESS τ AND NORMAL STRESS σ FOR CONTROLLED-AREA FRICTION TESTS

RECORDED DATA		CALCULATED DATA CONTROLLED AREA (AC')			
L	σ_c	τ		σ	
(LB)	(PSI)	(PSI)	(BARS)	(PSI)	(BARS)
SS. #100 GRIT ROUGHNESS; ALPHA=45; DUPLICATE (AC'=0.111 SQ. IN.)					
580	700	2262	156	2962	204
590	710	2302	158	3012	207
1015	1170	3987	274	5157	355
1035	1190	4067	280	5257	362
1605	1950	6254	431	8204	565
1625	1970	6334	436	8304	572
2325	2760	9092	626	11852	817
2365	2800	9253	637	12053	831
3225	3705	12674	873	16379	1129
3235	3720	12712	876	16432	1132
3835	4370	15089	1040	19459	1341
3850	4400	15142	1044	19542	1347
4570	5280	17945	1237	23225	1601

TABLE AII-18. RECORDED VALUES OF AXIAL LOAD L AND CONFINING PRESSURE σ_c AND CALCULATED VALUES OF SHEAR STRESS τ AND NORMAL STRESS σ FOR CONTROLLED-AREA FRICTION TESTS

RECORDED DATA		CALCULATED DATA CONTROLLED AREA (AC')			
L (LB)	σ_c (PSI)	τ (PSI)	τ (BARS)	σ (PSI)	σ (BARS)
SS. #80 DRY GOUGE; 1-MM THICK; ALPHA=45 (AC'=0.108 SQ. IN.)					
665	730	2713	187	3443	237
700	760	2860	197	3620	249
1000	1110	4074	280	5184	357
1020	1125	4159	286	5284	364
1440	1705	5814	400	7519	518
1445	1710	5834	402	7544	520
1925	2280	7772	535	10052	693
1945	2290	7859	541	10149	699
2640	3075	10684	736	13759	948
2660	3090	10769	742	13859	955
3030	3500	12277	846	15777	1087
3110	3600	12598	868	16198	1116
3560	4150	14406	993	18556	1279
3565	4155	14427	994	18582	1281
4250	4980	17185	1184	22165	1528
4275	5005	17289	1192	22294	1537
4875	5675	19731	1360	25406	1751
4890	5690	19793	1364	25483	1757
5835	6770	23628	1629	30398	2095
5850	6790	23688	1633	30478	2101
6240	7185	25296	1744	32481	2239
6250	7200	25335	1746	32535	2243
6805	7810	27599	1902	35409	2441

TABLE AII-19. DETERMINATION OF AVERAGE CORRECTION AREA FROM $\tau = A + B\sigma$ FIT OF CONTROLLED-AREA FRICTION EXPERIMENTS*

LOAD (LB)	CONFINING P. (PSI)	CALCULATED AREA (SQ. IN.)
KELLY LS. #100 GRIT ROUGHNESS; ALPHA=45		
860.0	1140.0	0.102
1200.0	1430.0	0.112
1250.0	1480.0	0.112
1600.0	1930.0	0.109
1675.0	1970.0	0.111
2020.0	2400.0	0.109
2075.0	2450.0	0.110
2320.0	2790.0	0.107
2370.0	2835.0	0.108
2825.0	3340.0	0.109
2880.0	3390.0	0.109
3300.0	3835.0	0.110
3330.0	3875.0	0.110
3825.0	4420.0	0.111
3870.0	4460.0	0.111
4135.0	4780.0	0.110
4185.0	4835.0	0.110
4480.0	5185.0	0.110
4535.0	5230.0	0.110
5000.0	5770.0	0.110
5080.0	5840.0	0.111
5500.0	6305.0	0.111
5650.0	6480.0	0.111
	AVERAGE:	0.110

* SEE TEXT FOR METHOD OF CALCULATION

TABLE AII-20. DETERMINATION OF AVERAGE CORRECTION AREA FROM $\tau = A + B\sigma$ FIT OF CONTROLLED-AREA FRICTION EXPERIMENTS*

LOAD (LB)	CONFINING P. (PSI)	CALCULATED AREA (SQ. IN.)
MESA VERDE SS. #100 GRIT ROUGHNESS; ALPHA=45		
500.0	560.0	0.130
590.0	625.0	0.135
815.0	1000.0	0.110
850.0	1000.0	0.115
1020.0	1025.0	0.134
1290.0	1550.0	0.109
1300.0	1530.0	0.112
1375.0	1580.0	0.114
1455.0	1720.0	0.110
1685.0	1995.0	0.110
1700.0	1990.0	0.111
1750.0	2000.0	0.113
1925.0	2255.0	0.110
2180.0	2570.0	0.109
2250.0	2530.0	0.114
2320.0	2575.0	0.116
2510.0	2900.0	0.111
2600.0	2985.0	0.111
2630.0	2960.0	0.114
2655.0	2975.0	0.114
2735.0	3185.0	0.110
2810.0	3210.0	0.112
2830.0	3205.0	0.113
2930.0	3275.0	0.114
2970.0	3365.0	0.113
3235.0	3680.0	0.112
3270.0	3675.0	0.113
3320.0	3720.0	0.114
3465.0	3910.0	0.113
3700.0	4126.0	0.114
	AVERAGE:	0.114

* SEE TEXT FOR METHOD OF CALCULATION

TABLE AII-21. DETERMINATION OF AVERAGE CORRECTION AREA FROM $\tau = A + B\sigma$ FIT OF CONTROLLED-AREA FRICTION EXPERIMENTS*

LOAD (LB)	CONFINING P. (PSI)	CALCULATED AREA (SQ. IN.)
KELLY LS. #80 DRY GOUGE; 1.0-MM THICK; ALPHA=45		
765.0	975.0	0.106
1485.0	1765.0	0.110
1530.0	1810.0	0.111
1760.0	2085.0	0.110
1820.0	2125.0	0.111
2075.0	2435.0	0.110
2135.0	2505.0	0.110
2450.0	2935.0	0.108
2535.0	2990.0	0.109
3000.0	3445.0	0.112
3035.0	3490.0	0.112
3400.0	3900.0	0.112
3440.0	3970.0	0.111
3720.0	4255.0	0.112
3755.0	4320.0	0.111
4065.0	4635.0	0.112
4140.0	4710.0	0.112
4375.0	5005.0	0.111
4450.0	5080.0	0.112
4830.0	5420.0	0.114
4850.0	5480.0	0.113
5300.0	5990.0	0.113
5320.0	6070.0	0.111
5755.0	6505.0	0.112
5825.0	6560.0	0.113
6290.0	7070.0	0.113
6335.0	7120.0	0.113
6720.0	7500.0	0.114
	AVERAGE:	0.111

* SEE TEXT FOR METHOD OF CALCULATION

TABLE AII-22. DETERMINATION OF AVERAGE CORRECTION AREA FROM $\tau = A + B\sigma$ FIT OF CONTROLLED-AREA FRICTION EXPERIMENTS*

LOAD (LB)	CONFINING P. (PSI)	CALCULATED AREA (SQ. IN.)
MESA VERDE SS. #80 DRY GOUGE; 1.0-MM THICK; ALPHA=45		
600.0	730.0	0.103
650.0	715.0	0.114
710.0	735.0	0.121
1030.0	1280.0	0.101
1325.0	1600.0	0.104
1340.0	1605.0	0.105
1425.0	1625.0	0.110
1625.0	1935.0	0.105
1850.0	2190.0	0.106
1870.0	2200.0	0.106
1875.0	2205.0	0.107
1940.0	2320.0	0.105
2200.0	2600.0	0.106
2210.0	2605.0	0.106
2275.0	2620.0	0.109
2550.0	2960.0	0.108
2725.0	3175.0	0.107
2730.0	3175.0	0.108
2785.0	3200.0	0.109
2875.0	3310.0	0.109
3310.0	3795.0	0.109
3325.0	3820.0	0.109
3525.0	4060.0	0.109
3780.0	4305.0	0.110
3825.0	4360.0	0.110
3910.0	4510.0	0.109
4275.0	4930.0	0.109
4380.0	5000.0	0.110
4575.0	5230.0	0.109
4630.0	5280.0	0.110
4900.0	5570.0	0.110
4935.0	5630.0	0.110
5280.0	6025.0	0.110
5350.0	6110.0	0.110
5480.0	6230.0	0.110
5800.0	6570.0	0.110
5835.0	6620.0	0.110
6150.0	6910.0	0.111
6175.0	6980.0	0.111
6430.0	7260.0	0.111
6475.0	7280.0	0.111
6770.0	7625.0	0.111
	AVERAGE:	0.109

* SEE TEXT FOR METHOD OF CALCULATION

TABLE AII-23. RECORDED VALUES OF AXIAL LOAD L AND CONFINING PRESSURE σ_c AND CALCULATED VALUES OF SHEAR STRESS τ AND NORMAL STRESS σ FOR UNCORRECTED AREA AND CORRECTED AREA

RECORDED DATA		CALCULATED DATA							
		UNCORRECTED AREA (AO)				CORRECTED AREA (AO')			
L	σ_c	τ		σ		τ		σ	
(LB)	(PSI)	(PSI)	(BARS)	(PSI)	(BARS)	(PSI)	(BARS)	(PSI)	(BARS)
LS. #100 GRIT ROUGHNESS; ALPHA=45 (AO=0.736; AO'=0.110 SQ. IN.)									
860	1140	14	0	1154	79	3339	230	4479	308
1200	1430	100	6	1530	105	4739	326	6169	425
1250	1480	109	7	1589	109	4941	340	6421	442
1600	1930	121	8	2051	141	6307	434	8237	567
1675	1970	152	10	2122	146	6628	457	8598	592
2020	2400	172	11	2572	177	7981	550	10381	715
2075	2450	184	12	2634	181	8206	565	10656	734
2320	2790	181	12	2971	204	9150	630	11940	823
2370	2835	192	13	3027	208	9355	645	12190	840
2825	3340	249	17	3589	247	11170	770	14510	1000
2880	3390	261	18	3651	251	11395	785	14785	1019
3300	3835	324	22	4159	286	13082	902	16917	1166
3330	3875	324	22	4199	289	13198	910	17073	1177
3825	4420	388	26	4808	331	15176	1046	19596	1351
3870	4460	399	27	4859	335	15360	1059	19820	1366
4135	4780	419	28	5199	358	16405	1131	21185	1460
4185	4835	425	29	5260	362	16605	1144	21440	1478
4480	5185	450	31	5635	388	17771	1225	22956	1582
4535	5230	465	32	5695	392	17998	1240	23228	1601
5000	5770	511	35	6281	433	19842	1368	25612	1765
5080	5840	531	36	6371	439	20170	1390	26010	1793
5500	6305	583	40	6888	474	21847	1506	28152	1941
5650	6480	598	41	7078	488	22441	1547	28921	1994

TABLE AII-24. RECORDED VALUES OF AXIAL LOAD L AND CONFINING PRESSURE σ_c AND CALCULATED VALUES OF SHEAR STRESS τ AND NORMAL STRESS σ FOR UNCORRECTED AREA AND CORRECTED AREA

RECORDED DATA		CALCULATED DATA							
		UNCORRECTED AREA (AO)				CORRECTED AREA (AO')			
L	σ_c	τ		σ		τ		σ	
(LB)	(PSI)	(PSI)	(BARS)	(PSI)	(BARS)	(PSI)	(BARS)	(PSI)	(BARS)
LS. #100 GRIT ROUGHNESS; DUPLICATE; ALPHA=45 (AO=0.736; AO'=0.110 SQ. IN.)									
700	900	25	1	925	63	2731	188	3631	250
720	935	21	1	956	65	2805	193	3740	257
1100	1320	87	6	1407	97	4339	299	5659	390
1130	1360	87	6	1447	99	4456	307	5816	401
1420	1740	94	6	1834	126	5584	385	7324	505
1485	1775	121	8	1896	130	5862	404	7637	526
1825	2200	139	9	2339	161	7195	496	9395	647
1885	2235	163	11	2398	165	7450	513	9685	667
2315	2790	177	12	2967	204	9127	629	11917	821
2355	2815	192	13	3007	207	9297	641	12112	835
2570	3050	220	15	3270	225	10156	700	13206	910
2650	3140	230	15	3370	232	10475	722	13615	938
3020	3490	306	21	3796	261	11982	826	15472	1066
3065	3530	317	21	3847	265	12166	838	15696	1082
3470	3965	374	25	4339	299	13790	950	17755	1224
3540	4075	367	25	4442	306	14053	968	18128	1249
3980	4550	428	29	4978	343	15815	1090	20365	1404
4025	4620	424	29	5044	347	15985	1102	20605	1420
4420	5025	490	33	5515	380	17578	1211	22603	1558
4450	5080	483	33	5563	383	17687	1219	22767	1569
4880	5590	520	35	6110	421	19386	1336	24976	1722
5025	5780	523	36	6303	434	19950	1375	25730	1774
5490	6270	594	40	6864	473	21819	1504	28089	1936

TABLE AII-24. (CONTINUED)

RECORDED DATA		CALCULATED DATA							
		UNCORRECTED AREA (AO)				CORRECTED AREA (AO')			
L	σ_c	τ		σ		τ		σ	
(LB)	(PSI)	(PSI)	(BARS)	(PSI)	(BARS)	(PSI)	(BARS)	(PSI)	(BARS)
5550	6310	615	42	6925	477	22072	1521	28382	1956
5910	6695	667	46	7362	507	23516	1621	30211	2082
5980	6780	672	46	7452	513	23791	1640	30571	2107

TABLE AII-25. RECORDED VALUES OF AXIAL LOAD L AND CONFINING PRESSURE σ_c AND CALCULATED VALUES OF SHEAR STRESS τ AND NORMAL STRESS σ FOR UNCORRECTED AREA AND CORRECTED AREA

RECORDED DATA		CALCULATED DATA							
		UNCORRECTED AREA (AO)				CORRECTED AREA (AO')			
L	σ_c	τ		σ		τ		σ	
(LB)	(PSI)	(PSI)	(BARS)	(PSI)	(BARS)	(PSI)	(BARS)	(PSI)	(BARS)
LS. #600 GRIT ROUGHNESS; ALPHA=45 (AO=0.736; AO'=0.110 SQ. IN.)									
680	770	76	5	846	58	2705	186	3475	239
1030	1200	99	6	1299	89	4081	281	5281	364
1125	1250	139	9	1389	95	4488	309	5738	395
1375	1675	96	6	1771	122	5412	373	7087	488
1480	1820	95	6	1915	132	5817	401	7637	526
1670	2000	134	9	2134	147	6590	454	8590	592
1720	2050	143	9	2193	151	6793	468	8843	609
2005	2410	157	10	2567	176	7908	545	10318	711
2050	2480	152	10	2632	181	8078	556	10558	727
2380	2860	186	12	3046	210	9388	647	12248	844
2440	2925	195	13	3120	215	9628	663	12553	865
2715	3190	249	17	3439	237	10745	740	13935	960
2755	3220	261	18	3481	240	10912	752	14132	974
3115	3630	301	20	3931	271	12344	851	15974	1101
3160	3700	296	20	3996	275	12513	862	16213	1117
3480	4060	334	23	4394	302	13788	950	17848	1230
3540	4120	344	23	4464	307	14030	967	18150	1251
3825	4425	386	26	4811	331	15173	1046	19598	1351
3850	4485	372	25	4857	334	15257	1051	19742	1361
4130	4730	440	30	5170	356	16407	1131	21137	1457
4160	4800	426	29	5226	360	16509	1138	21309	1469
4635	5320	488	33	5808	400	18408	1269	23728	1635
4690	5420	476	32	5896	406	18608	1282	24028	1656

TABLE AII-25. (CONTINUED)

RECORDED DATA		CALCULATED DATA							
		UNCORRECTED AREA (AO)				CORRECTED AREA (AO')			
L	σ_c	τ		σ		τ		σ	
(LB)	(PSI)	(PSI)	(BARS)	(PSI)	(BARS)	(PSI)	(BARS)	(PSI)	(BARS)
5100	5840	544	37	6384	440	20261	1397	26101	1799

TABLE AII-26. RECORDED VALUES OF AXIAL LOAD L AND CONFINING PRESSURE σ_c AND CALCULATED VALUES OF SHEAR STRESS τ AND NORMAL STRESS σ FOR UNCORRECTED AREA AND CORRECTED AREA

RECORDED DATA		CALCULATED DATA							
		UNCORRECTED AREA (AO)				CORRECTED AREA (AO')			
L	σ_c	τ		σ		τ		σ	
(LB)	(PSI)	(PSI)	(BARS)	(PSI)	(BARS)	(PSI)	(BARS)	(PSI)	(BARS)
SS. #100 GRIT ROUGHNESS; ALPHA=45 (AO=0.739; AO'=0.114 SQ. IN.)									
500	560	58	4	618	42	1912	131	2472	170
590	625	86	5	711	49	2275	156	2900	199
815	1000	51	3	1051	72	3074	211	4074	280
850	1000	75	5	1075	74	3228	222	4228	291
1020	1025	177	12	1202	82	3961	273	4986	343
1290	1550	97	6	1647	113	4882	336	6432	443
1300	1530	114	7	1644	113	4936	340	6466	445
1375	1580	140	9	1720	118	5240	361	6820	470
1455	1720	124	8	1844	127	5521	380	7241	499
1685	1995	142	9	2137	147	6392	440	8387	578
1700	1990	155	10	2145	147	6461	445	8451	582
1750	2000	184	12	2184	150	6675	460	8675	598
1925	2255	174	12	2429	167	7315	504	9570	659
2180	2570	189	13	2759	190	8276	570	10846	747
2250	2530	257	17	2787	192	8603	593	11133	767
2320	2575	282	19	2857	196	8887	612	11462	790
2510	2900	248	17	3148	217	9558	659	12458	859
2600	2985	266	18	3251	224	9911	683	12896	889
2630	2960	299	20	3259	224	10055	693	13015	897
2655	2975	308	21	3283	226	10157	700	13132	905
2735	3185	257	17	3442	237	10403	717	13588	936
2810	3210	296	20	3506	241	10719	739	13929	960
2830	3205	312	21	3517	242	10809	745	14014	966

TABLE AII-26. (CONTINUED)

RECORDED DATA		CALCULATED DATA							
		UNCORRECTED AREA (AO)				CORRECTED AREA (AO')			
L	σ_c	τ		σ		τ		σ	
(LB)	(PSI)	(PSI)	(BARS)	(PSI)	(BARS)	(PSI)	(BARS)	(PSI)	(BARS)
2930	3275	344	23	3619	249	11213	773	14488	998
2970	3365	326	22	3691	254	11343	782	14708	1014
3235	3680	348	24	4028	277	12348	851	16028	1105
3270	3675	374	25	4049	279	12504	862	16179	1115
3320	3720	386	26	4106	283	12701	875	16421	1132
3465	3910	389	26	4299	296	13242	913	17152	1182
3700	4126	440	30	4566	314	14165	976	18291	1261

TABLE AII-27. RECORDED VALUES OF AXIAL LOAD L AND CONFINING PRESSURE σ_c AND CALCULATED VALUES OF SHEAR STRESS τ AND NORMAL STRESS σ FOR UNCORRECTED AREA AND CORRECTED AREA

RECORDED DATA		CALCULATED DATA							
		UNCORRECTED AREA (AO)				CORRECTED AREA (AO')			
L	σ_c	τ		σ		τ		σ	
(LB)	(PSI)	(PSI)	(BARS)	(PSI)	(BARS)	(PSI)	(BARS)	(PSI)	(BARS)
SS. #100 GRIT ROUGHNESS; DUPLICATE; ALPHA=45 (AO=0.739; AO'=0.114 SQ. IN.)									
925	1100	75	5	1175	81	3507	241	4607	317
975	1125	97	6	1222	84	3713	256	4838	333
1225	1435	111	7	1546	106	4655	320	6090	419
1470	1780	104	7	1884	129	5557	383	7337	505
1500	1785	122	8	1907	131	5686	392	7471	515
1525	1800	131	9	1931	133	5788	399	7588	523
1750	2100	134	9	2234	154	6625	456	8725	601
1800	2130	152	10	2282	157	6829	470	8959	617
2230	2660	178	12	2838	195	8450	582	11110	766
2275	2675	201	13	2876	198	8640	595	11315	780
2570	3020	228	15	3248	223	9761	673	12781	881
2630	3060	249	17	3309	228	10005	689	13065	900
3040	3490	311	21	3801	262	11588	798	15078	1039
3075	3525	318	21	3843	264	11724	808	15249	1051
3575	4120	358	24	4478	308	13619	939	17739	1223
3650	4170	384	26	4554	314	13923	960	18093	1247
3950	4515	415	28	4930	339	15067	1038	19582	1350
3980	4580	402	27	4982	343	15166	1045	19746	1361
4400	5065	444	3.0	5509	379	16765	1155	21830	1505
4480	5125	468	32	5593	385	17086	1178	22211	1531

TABLE AII-28. RECORDED VALUES OF AXIAL LOAD L AND CONFINING PRESSURE σ_c AND CALCULATED VALUES OF SHEAR STRESS τ AND NORMAL STRESS σ FOR UNCORRECTED AREA AND CORRECTED AREA

RECORDED DATA		CALCULATED DATA							
		UNCORRECTED AREA (AO)				CORRECTED AREA (AO')			
L	σ_c	τ		σ		τ		σ	
(LB)	(PSI)	(PSI)	(BARS)	(PSI)	(BARS)	(PSI)	(BARS)	(PSI)	(BARS)
SS. #600 GRIT ROUGHNESS; ALPHA=45 (AO=0.739; AO'=0.114 SQ. IN.)									
780	990	32	2	1022	70	2926	201	3916	270
805	1000	44	3	1044	72	3030	208	4030	277
900	1150	33	2	1183	81	3372	232	4522	311
1250	1510	90	6	1600	110	4727	325	6237	430
1270	1500	109	7	1609	110	4820	332	6320	435
1280	1530	101	6	1631	112	4849	334	6379	439
1380	1690	88	6	1778	122	5207	359	6897	475
1550	1875	111	7	1986	136	5860	404	7735	533
1575	1875	128	8	2003	138	5970	411	7845	540
1610	1915	131	9	2046	141	6103	420	8018	552
1700	2010	145	10	2155	148	6451	444	8461	583
1995	2325	187	12	2512	173	7587	523	9912	683
2025	2320	210	14	2530	174	7721	532	10041	692
2040	2335	212	14	2547	175	7779	536	10114	697
2325	2685	230	15	2915	201	8854	610	11539	795
2460	2870	229	15	3099	213	9354	644	12224	842
2475	2875	237	16	3112	214	9417	649	12292	847
2530	2900	261	18	3161	217	9646	665	12546	865
2650	3010	287	19	3297	227	10117	697	13127	905
2900	3280	322	22	3602	248	11079	763	14359	990
2925	3290	334	23	3624	249	11183	771	14473	997
2940	3325	326	22	3651	251	11232	774	14557	1003
3060	3450	345	23	3795	261	11696	806	15146	1044

TABLE AII-28. (CONTINUED)

RECORDED DATA		CALCULATED DATA							
		UNCORRECTED AREA (AO)				CORRECTED AREA (AO')			
L	σ_c	τ		σ		τ		σ	
(LB)	(PSI)	(PSI)	(BARS)	(PSI)	(BARS)	(PSI)	(BARS)	(PSI)	(BARS)
3225	3575	394	27	3969	273	12357	851	15932	1098
3250	3590	403	27	3993	275	12459	859	16049	1106
3265	3650	384	26	4034	278	12495	861	16145	1113
3425	3835	399	27	4234	291	13104	903	16939	1167

TABLE AII-29. RECORDED VALUES OF AXIAL LOAD L AND CONFINING PRESSURE σ_c AND CALCULATED VALUES OF SHEAR STRESS τ AND NORMAL STRESS σ FOR UNCORRECTED AREA AND CORRECTED AREA

RECORDED DATA		CALCULATED DATA							
		UNCORRECTED AREA (AO)				CORRECTED AREA (AO')			
L	σ_c	τ		σ		τ		σ	
(LB)	(PSI)	(PSI)	(BARS)	(PSI)	(BARS)	(PSI)	(BARS)	(PSI)	(BARS)
#80 DRY LS. GOUGE; 1-MM THICK; ALPHA=45 (AO=0.736; AO'=0.111 SQ. IN.)									
765	975	32	2	1007	69	2958	203	3933	271
1485	1765	126	8	1891	130	5806	400	7571	522
1530	1810	134	9	1944	134	5986	412	7796	537
1760	2085	153	10	2238	154	6885	474	8970	618
1820	2125	173	11	2298	158	7135	491	9260	638
2075	2435	192	13	2627	181	8129	560	10564	728
2135	2505	197	13	2702	186	8364	576	10869	749
2450	2935	196	13	3131	215	9568	659	12503	862
2535	2990	227	15	3217	221	9923	684	12913	890
3000	3445	315	21	3760	259	11791	812	15236	1050
3035	3490	316	21	3806	262	11926	822	15416	1062
3400	3900	359	24	4259	293	13365	921	17265	1190
3440	3970	351	24	4321	297	13510	931	17480	1205
3720	4255	399	27	4654	320	14629	1008	18884	1302
3755	4320	390	26	4710	324	14754	1017	19074	1315
4065	4635	444	30	5079	350	15993	1102	20628	1422
4140	4710	457	31	5167	356	16293	1123	21003	1448
4375	5005	469	32	5474	377	17204	1186	22209	1531
4450	5080	483	33	5563	383	17505	1206	22585	1557
4830	5420	571	39	5991	413	19046	1313	24466	1686
4850	5480	554	38	6034	416	19106	1317	24586	1695
5300	5990	605	41	6595	454	20878	1439	26868	1852
5320	6070	579	39	6649	458	20928	1442	26998	1861

TABLE AII-29. (CONTINUED)

RECORDED DATA		CALCULATED DATA							
		UNCORRECTED AREA (AO)				CORRECTED AREA (AO')			
L	σ_c	τ		σ		τ		σ	
(LB)	(PSI)	(PSI)	(BARS)	(PSI)	(BARS)	(PSI)	(BARS)	(PSI)	(BARS)
5755	6505	657	45	7162	493	22670	1563	29175	2011
5825	6560	677	46	7237	498	22958	1582	29518	2035
6290	7070	738	50	7808	538	24798	1709	31868	2197
6335	7120	743	51	7863	542	24976	1722	32096	2212
6720	7500	815	56	8315	573	26520	1828	34020	2345

TABLE AII-30. RECORDED VALUES OF AXIAL LOAD L AND CONFINING PRESSURE σ_c AND CALCULATED VALUES OF SHEAR STRESS τ AND NORMAL STRESS σ FOR UNCORRECTED AREA AND CORRECTED AREA

RECORDED DATA		CALCULATED DATA							
		UNCORRECTED AREA (AO)				CORRECTED AREA (AO')			
L	σ_c	τ		σ		τ		σ	
(LB)	(PSI)	(PSI)	(BARS)	(PSI)	(BARS)	(PSI)	(BARS)	(PSI)	(BARS)
>#230 DRY LS. GOUGE; 1-MM THICK; ALPHA=45 (AO=0.736; AO'=0.111 SQ. IN.)									
570	700	37	2	737	50	2217	152	2917	201
635	740	61	4	801	55	2490	171	3230	222
1000	1200	79	5	1279	88	3904	269	5104	351
1065	1230	108	7	1338	92	4182	288	5412	373
1350	1640	97	6	1737	119	5261	362	6901	475
1405	1700	104	7	1804	124	5478	377	7178	494
1920	2280	164	11	2444	168	7508	517	9788	674
1950	2320	164	11	2484	171	7623	525	9943	685
2480	2920	224	15	3144	216	9711	669	12631	870
2530	2950	243	16	3193	220	9921	684	12871	887
2925	3420	277	19	3697	254	11465	790	14885	1026
2975	3450	296	20	3746	258	11675	805	15125	1042
3345	3925	309	21	4234	291	13105	903	17030	1174
3385	3995	302	20	4297	296	13250	913	17245	1189
3650	4300	329	22	4629	319	14291	985	18591	1281
3705	4370	331	22	4701	324	14504	1000	18874	1301
4130	4820	395	27	5215	359	16193	1116	21013	1448
4200	4880	413	28	5293	364	16478	1136	21358	1472
4525	5270	439	30	5709	393	17747	1223	23017	1587
4600	5325	462	31	5787	399	18058	1245	23383	1612
5100	5850	539	37	6389	440	20047	1382	25897	1785
5130	5890	540	37	6430	443	20163	1390	26053	1796
5505	6400	539	37	6939	478	21597	1489	27997	1930

TABLE AII-30. (CONTINUED)

RECORDED DATA		CALCULATED DATA							
		UNCORRECTED AREA (AO)				CORRECTED AREA (AO')			
L	σ_c	τ		σ		τ		σ	
(LB)	(PSI)	(PSI)	(BARS)	(PSI)	(BARS)	(PSI)	(BARS)	(PSI)	(BARS)
5590	6480	557	38	7037	485	21940	1512	28420	1959
6120	7005	655	45	7660	528	24065	1659	31070	2142
6230	7160	652	44	7812	538	24483	1688	31643	2181
6750	7695	738	50	8433	581	26557	1831	34252	2361

TABLE AII-31. RECORDED VALUES OF AXIAL LOAD L AND CONFINING PRESSURE σ_c AND CALCULATED VALUES OF SHEAR STRESS τ AND NORMAL STRESS σ FOR UNCORRECTED AREA AND CORRECTED AREA

RECORDED DATA		CALCULATED DATA							
		UNCORRECTED AREA (AO)				CORRECTED AREA (AO')			
L	σ_c	τ		σ		τ		σ	
(LB)	(PSI)	(PSI)	(BARS)	(PSI)	(BARS)	(PSI)	(BARS)	(PSI)	(BARS)
#80 WET LS. GOUGE; 1-MM THICK; ALPHA=45 (AO=0.736; AO'=0.111 SQ. IN.)									
710	800	82	5	882	60	2798	192	3598	248
765	870	84	5	954	65	3010	207	3880	267
1145	1380	87	6	1467	101	4467	308	5847	403
1165	1420	81	5	1501	103	4537	312	5957	410
1665	2025	118	8	2143	147	6487	447	8512	586
1730	2060	145	10	2205	152	6762	466	8822	608
2060	2445	176	12	2621	180	8056	555	10501	724
2105	2490	185	12	2675	184	8236	567	10726	739
2500	2955	220	15	3175	218	9783	674	12738	878
2540	2970	240	16	3210	221	9956	686	12926	891
2790	3290	250	17	3540	244	10922	753	14212	979
2845	3310	277	19	3587	247	11160	769	14470	997
3140	3630	318	21	3948	272	12329	850	15959	1100
3175	3655	329	22	3984	274	12474	860	16129	1112
3585	4125	372	25	4497	310	14086	971	18211	1255
3630	4160	386	26	4546	313	14271	983	18431	1270
3950	4535	415	28	4950	341	15525	1070	20060	1383
4025	4600	434	29	5034	347	15830	1091	20430	1408
4450	5100	473	32	5573	384	17495	1206	22595	1557
4500	5150	482	33	5632	388	17695	1220	22845	1575
4925	5630	530	36	6160	424	19369	1335	24999	1723
4995	5705	540	37	6245	430	19647	1354	25352	1747
5475	6250	594	40	6844	471	21537	1484	27787	1915

TABLE AII-31. (CONTINUED)

RECORDED CATA		CALCULATED DATA							
		UNCORRECTED AREA (AO)				CORRECTED AREA (AO')			
L	σ_c	τ		σ		τ		σ	
(LB)	(PSI)	(PSI)	(BARS)	(PSI)	(BARS)	(PSI)	(BARS)	(PSI)	(BARS)
5575	6365	604	41	6969	480	21930	1512	28295	1950
6015	6815	678	46	7493	516	23687	1633	30502	2103
6090	6885	694	47	7579	522	23989	1654	30874	2128
6455	7330	720	49	8050	555	25411	1752	32741	2257
6525	7410	727	50	8137	561	25686	1771	33096	2281
7050	8000	789	54	8789	606	27756	1913	35756	2465

TABLE AII-32. RECORDED VALUES OF AXIAL LOAD L AND CONFINING PRESSURE σ_c AND CALCULATED VALUES OF SHEAR STRESS τ AND NORMAL STRESS σ FOR UNCORRECTED AREA AND CORRECTED AREA

RECORDED DATA		CALCULATED DATA							
		UNCORRECTED AREA (AO)				CORRECTED AREA (AO')			
L	σ_c	τ		σ		τ		σ	
(LB)	(PSI)	(PSI)	(BARS)	(PSI)	(BARS)	(PSI)	(BARS)	(PSI)	(BARS)
>#230 WET LS. GOUGE; 1-MM THICK; ALPHA=45 (AO=0.736; AO'=0.111 SQ. IN.)									
730	880	55	3	935	64	2848	196	3728	257
775	905	73	5	978	67	3038	209	3943	271
1080	1270	98	6	1368	94	4229	291	5499	379
1165	1310	136	9	1446	99	4592	316	5902	406
1420	1725	102	7	1827	125	5533	381	7258	500
1510	1780	135	9	1915	132	5911	407	7691	530
2015	2390	173	11	2563	176	7881	543	10271	708
2060	2450	174	12	2624	180	8054	555	10504	724
2375	2850	188	12	3038	209	9273	639	12123	835
2460	2910	216	14	3126	215	9626	663	12536	864
2875	3400	253	17	3653	251	11250	775	14650	1010
2960	3450	285	19	3735	257	11608	800	15058	1038
3280	3825	315	21	4140	285	12862	886	16687	1150
3315	3875	314	21	4189	288	12994	895	16869	1163
3720	4370	342	23	4712	324	14571	1004	18941	1305
3785	4425	358	24	4783	329	14837	1022	19262	1328
4165	4875	391	27	5266	363	16323	1125	21198	1461
4220	4885	424	29	5309	366	16566	1142	21451	1479
4825	5605	475	32	6080	419	18931	1305	24536	1691
4960	5760	489	33	6249	430	19462	1341	25222	1739
5620	6485	575	39	7060	486	22072	1521	28557	1968
5675	6550	580	40	7130	491	22288	1536	28838	1988
6320	7260	663	45	7923	546	24838	1712	32098	2213

TABLE AII-32. (CONTINUED)

RECORDED DATA		CALCULATED DATA							
		UNCORRECTED AREA (AO)				CORRECTED AREA (AO')			
L	σ_c	τ		σ		τ		σ	
(LB)	(PSI)	(PSI)	(BARS)	(PSI)	(BARS)	(PSI)	(BARS)	(PSI)	(BARS)
6395	7325	681	47	8006	552	25143	1733	32468	2238
7030	8020	765	52	8785	605	27656	1906	35676	2459

TABLE AII-33. RECORDED VALUES OF AXIAL LOAD L AND CONFINING PRESSURE σ_c AND CALCULATED VALUES OF SHEAR STRESS τ AND NORMAL STRESS σ FOR UNCORRECTED AREA AND CORRECTED AREA

RECORDED DATA		CALCULATED DATA							
		UNCORRECTED AREA (AO)				CORRECTED AREA (AO')			
L	σ_c	τ		σ		τ		σ	
(LB)	(PSI)	(PSI)	(BARS)	(PSI)	(BARS)	(PSI)	(BARS)	(PSI)	(BARS)
#80 DRY SS. GOUGE; 1-MM THICK; ALPHA=45 (AO=0.737; AO'=0.109 SQ. IN.)									
600	730	42	2	772	53	2387	164	3117	214
650	715	83	5	798	55	2624	180	3339	230
710	735	114	7	849	58	2889	199	3624	249
1030	1280	58	4	1338	92	4084	281	5364	369
1325	1600	98	6	1698	117	5277	363	6877	474
1340	1605	106	7	1711	118	5344	368	6949	479
1425	1625	154	10	1779	122	5724	394	7349	506
1625	1935	134	9	2069	142	6486	447	8421	580
1850	2190	160	11	2350	162	7391	509	9581	660
1870	2200	168	11	2368	163	7477	515	9677	667
1875	2205	169	11	2374	163	7498	516	9703	669
1940	2320	156	10	2476	170	7739	533	10059	693
2200	2600	192	13	2792	192	8791	606	11391	785
2210	2605	196	13	2801	193	8835	609	11440	788
2275	2620	233	16	2853	196	9125	629	11745	809
2550	2960	249	17	3209	221	10217	704	13177	908
2725	3175	261	18	3436	236	10912	752	14087	971
2730	3175	264	18	3439	237	10935	753	14110	972
2785	3200	289	19	3489	240	11175	770	14375	991
2875	3310	295	20	3605	248	11533	795	14843	1023
3310	3795	348	23	4143	285	13285	916	17080	1177
3325	3820	345	23	4165	287	13342	919	17162	1183
3525	4060	361	24	4421	304	14139	974	18199	1254

TABLE AII-33. (CONTINUED)

RECORDED DATA		CALCULATED DATA							
		UNCORRECTED AREA (AO)				CORRECTED AREA (AO')			
L	σ_c	τ		σ		τ		σ	
(LB)	(PSI)	(PSI)	(BARS)	(PSI)	(BARS)	(PSI)	(BARS)	(PSI)	(BARS)
3780	4305	411	28	4716	325	15186	1047	19491	1343
3825	4360	414	28	4774	329	15365	1059	19725	1360
3910	4510	397	27	4907	338	15680	1081	20190	1392
4275	4930	435	30	5365	369	17145	1182	22075	1522
4380	5000	471	32	5471	377	17591	1212	22591	1557
4575	5230	488	33	5718	394	18371	1266	23601	1627
4630	5280	501	34	5781	398	18598	1282	23878	1646
4900	5570	539	37	6109	421	19692	1357	25262	1741
4935	5630	533	36	6163	424	19822	1366	25452	1754
5280	6025	569	39	6594	454	21207	1462	27232	1877
5350	6110	574	39	6684	460	21486	1481	27596	1902
5480	6230	602	41	6832	471	22022	1518	28252	1947
5800	6570	649	44	7219	497	23320	1607	29890	2060
5835	6620	648	44	7268	501	23456	1617	30076	2073
6150	6910	717	49	7627	525	24756	1706	31665	2183
6175	6980	699	48	7679	529	24835	1712	31815	2193
6430	7260	732	50	7992	551	25865	1783	33125	2283
6475	7280	752	51	8032	553	26061	1796	33341	2298
6770	7625	780	53	8405	579	27242	1878	34867	2404

TABLE AII-34. RECORDED VALUES OF AXIAL LOAD L AND CONFINING PRESSURE σ_c AND CALCULATED VALUES OF SHEAR STRESS τ AND NORMAL STRESS σ FOR UNCORRECTED AREA AND CORRECTED AREA

RECORDED DATA		CALCULATED DATA							
		UNCORRECTED AREA (AO)				CORRECTED AREA (AO')			
L	σ_c	τ		σ		τ		σ	
(LB)	(PSI)	(PSI)	(BARS)	(PSI)	(BARS)	(PSI)	(BARS)	(PSI)	(BARS)
>#230 DRY SS. GOUGE; 1-MM THICK; ALPHA=45 (AO=0.739; AO'=0.109 SQ. IN.)									
665	740	79	5	819	56	2680	184	3420	235
670	745	80	5	825	56	2700	186	3445	237
710	800	80	5	880	60	2856	196	3656	252
980	1170	78	5	1248	86	3910	269	5080	350
1125	1340	91	6	1431	98	4490	309	5830	402
1180	1380	108	7	1488	102	4722	325	6102	420
1590	1865	143	9	2008	138	6361	438	8226	567
1625	1900	149	10	2049	141	6504	448	8404	579
1875	2200	168	11	2368	163	7500	517	9700	668
1890	2225	166	11	2391	164	7557	521	9782	674
2120	2480	194	13	2674	184	8484	585	10964	755
2140	2500	197	13	2697	186	8566	590	11066	763
2350	2785	197	13	2982	205	9387	647	12172	839
2380	2810	205	14	3015	207	9512	655	12322	849
2670	3060	276	19	3336	230	10717	738	13777	949
2700	3110	271	18	3381	233	10830	746	13940	961
2980	3440	296	20	3736	257	11949	823	15389	1061
3030	3490	305	21	3795	261	12154	837	15644	1078
3275	3730	350	24	4080	281	13157	907	16887	1164
3335	3775	368	25	4143	285	13410	924	17185	1184
3675	4220	376	25	4596	316	14747	1016	18967	1307
3730	4260	393	27	4653	320	14980	1032	19240	1326
4100	4620	464	31	5084	350	16497	1137	21117	1455

TABLE AII-34. (CONTINUED)

RECORDED DATA		CALCULATED DATA							
		UNCORRECTED AREA (AO)				CORRECTED AREA (AO')			
L	σ_c	τ		σ		τ		σ	
(LB)	(PSI)	(PSI)	(BARS)	(PSI)	(BARS)	(PSI)	(BARS)	(PSI)	(BARS)
4125	4660	460	31	5120	353	16592	1143	21252	1465
4370	4960	476	32	5436	374	17565	1211	22525	1553
4425	4990	498	34	5488	378	17803	1227	22793	1571
4930	5660	505	34	6165	425	19784	1364	25444	1754
5040	5790	515	35	6305	434	20224	1394	26014	1793
5400	6135	586	40	6721	463	21703	1496	27838	1919
5435	6190	582	40	6772	466	21836	1505	28026	1932
5985	6770	664	45	7434	512	24069	1659	30839	2126
6030	6890	634	43	7524	518	24215	1669	31105	2144
6425	7190	752	51	7942	547	25877	1784	33067	2279
6450	7280	724	49	8004	551	25947	1788	33227	2290
6800	7635	783	54	8418	580	27375	1887	35010	2413
6835	7675	786	54	8461	583	27515	1897	35190	2426
7065	7920	820	56	8740	602	28448	1961	36368	2507

TABLE AII-35. RECORDED VALUES OF AXIAL LOAD L AND CONFINING PRESSURE σ_c AND CALCULATED VALUES OF SHEAR STRESS τ AND NORMAL STRESS σ FOR UNCORRECTED AREA AND CORRECTED AREA

RECORDED DATA		CALCULATED DATA							
		UNCORRECTED AREA (AO)				CORRECTED AREA (AO')			
L	σ_c	τ		σ		τ		σ	
(LB)	(PSI)	(PSI)	(BARS)	(PSI)	(BARS)	(PSI)	(BARS)	(PSI)	(BARS)
#80 WET SS. GOUGE; 1-MM THICK; ALPHA=45 (AO=0.739; AO'=0.109 SQ. IN.)									
725	850	65	4	915	63	2900	199	3750	258
770	860	90	6	950	65	3102	213	3962	273
875	1025	79	5	1104	76	3501	241	4526	312
1025	1185	101	6	1286	88	4109	283	5294	365
1040	1180	113	7	1293	89	4180	288	5360	369
1080	1195	133	9	1328	91	4356	300	5551	382
1330	1545	127	8	1672	115	5328	367	6873	473
1355	1560	136	9	1696	116	5435	374	6995	482
1600	1890	137	9	2027	139	6394	440	8284	571
1645	1900	162	11	2062	142	6595	454	8495	585
1990	2325	183	12	2508	172	7965	549	10290	709
2020	2330	201	13	2531	174	8101	558	10431	719
2325	2680	233	16	2913	200	9325	642	12005	827
2350	2685	247	17	2932	202	9437	650	12122	835
2660	3000	299	20	3299	227	10701	737	13701	944
2685	3005	314	21	3319	228	10814	745	13819	952
2965	3350	331	22	3681	253	11925	822	15275	1053
3000	3350	354	24	3704	255	12086	833	15436	1064
3335	3785	363	25	4148	286	13405	924	17190	1185
3355	3800	369	25	4169	287	13489	930	17289	1192
3865	4400	415	28	4815	331	15529	1070	19929	1374
3900	4425	426	29	4851	334	15677	1080	20102	1386
4200	4790	446	30	5236	361	16871	1163	21661	1493

TABLE AII-35. (CONTINUED)

RECORDED DATA		CALCULATED DATA							
		UNCORRECTED AREA (AO)				CORRECTED AREA (AO')			
L	σ_c	τ		σ		τ		σ	
(LB)	(PSI)	(PSI)	(BARS)	(PSI)	(BARS)	(PSI)	(BARS)	(PSI)	(BARS)
4280	4840	475	32	5315	366	17213	1186	22053	1520
4615	5180	532	36	5712	393	18579	1281	23759	1638
4645	5245	520	35	5765	397	18684	1288	23929	1649
4920	5560	548	37	6108	421	19788	1364	25348	1747
4970	5610	557	38	6167	425	19993	1378	25603	1765
5255	5900	605	41	6505	448	21155	1458	27055	1865
5280	5925	609	42	6534	450	21257	1465	27182	1874
5755	6520	633	43	7153	493	23139	1595	29659	2044
5825	6625	628	43	7253	500	23407	1613	30032	2070
6435	7140	783	54	7923	546	25948	1789	33088	2281
6490	7245	768	52	8013	552	26148	1802	33393	2302
6810	7600	807	55	8407	579	27438	1891	35038	2415
6835	7595	826	57	8421	580	27555	1899	35150	2423

TABLE AII-36. RECORDED VALUES OF AXIAL LOAD L AND CONFINING PRESSURE σ_c AND CALCULATED VALUES OF SHEAR STRESS τ AND NORMAL STRESS σ FOR UNCORRECTED AREA AND CORRECTED AREA

RECORDED DATA		CALCULATED DATA							
		UNCORRECTED AREA (AO)				CORRECTED AREA (AO')			
L	σ_c	τ		σ		τ		σ	
(LB)	(PSI)	(PSI)	(BARS)	(PSI)	(BARS)	(PSI)	(BARS)	(PSI)	(BARS)
>#230 WET SS. GOUGE; 1-MM THICK; ALPHA=45 (AO=0.739; AO'=0.109 SQ. IN.)									
640	700	83	5	783	53	2585	178	3285	226
670	720	93	6	813	56	2713	187	3433	236
725	860	60	4	920	63	2895	199	3755	258
960	1125	87	6	1212	83	3841	264	4966	342
980	1130	98	6	1228	84	3930	270	5060	348
1025	1210	88	6	1298	89	4096	282	5306	365
1240	1450	113	7	1563	107	4963	342	6413	442
1450	1710	126	8	1836	126	5796	399	7506	517
1800	2090	172	11	2262	156	7211	497	9301	641
1830	2130	173	11	2303	158	7329	505	9459	652
2250	2600	222	15	2822	194	9021	621	11621	801
2300	2660	226	15	2886	198	9220	635	11880	819
2730	3140	277	19	3417	235	10952	755	14092	971
2770	3190	279	19	3469	239	11111	766	14301	986
3140	3570	339	23	3909	269	12618	870	16188	1116
3180	3600	351	24	3951	272	12787	881	16387	1129
3450	3975	346	23	4321	297	13838	954	17813	1228
3490	4010	356	24	4366	301	14004	965	18014	1242
4000	4500	456	31	4956	341	16098	1109	20598	1420
4050	4570	455	31	5025	346	16292	1123	20862	1438
4445	5050	482	33	5532	381	17864	1231	22914	1579
4500	5130	479	33	5609	386	18077	1246	23207	1600
5050	5740	546	37	6286	433	20295	1399	26035	1795

TABLE AII-36. (CONTINUED)

RECORDED DATA		CALCULATED DATA							
		UNCORRECTED AREA (AO)				CORRECTED AREA (AO')			
L	σ_c	τ		σ		τ		σ	
(LB)	(PSI)	(PSI)	(BARS)	(PSI)	(BARS)	(PSI)	(BARS)	(PSI)	(BARS)
5090	5820	533	36	6353	438	20438	1409	26258	1810
5550	6260	625	43	6885	474	22328	1539	28588	1971
5580	6310	620	42	6930	477	22441	1547	28751	1982
6200	6910	739	51	7649	527	24985	1722	31895	2199
6215	6930	740	51	7670	528	25044	1726	31974	2204
6600	7410	760	52	8170	563	26570	1831	33980	2342
6660	7480	766	52	8246	568	26810	1848	34290	2364
6950	7730	837	57	8567	590	28015	1931	35745	2464
7000	7810	831	57	8641	595	28205	1944	36015	2483
7350	8200	872	60	9072	625	29615	2041	37815	2607

TABLE AII-37. RECORDED VALUES OF AXIAL LOAD L AND CONFINING PRESSURE σ_c AND CALCULATED VALUES OF SHEAR STRESS τ AND NORMAL STRESS σ FOR UNCORRECTED AREA AND CORRECTED AREA

RECORDED DATA		CALCULATED DATA							
		UNCORRECTED AREA (AO)				CORRECTED AREA (AO')			
L	σ_c	τ		σ		τ		σ	
(LB)	(PSI)	(PSI)	(BARS)	(PSI)	(BARS)	(PSI)	(BARS)	(PSI)	(BARS)
#80 DRY LS. AND SS. GOUGE; 1-MM THICK; ALPHA=45 (AO=0.736; AO'=0.109 SQ. IN.)									
575	690	45	3	735	50	2292	158	2982	205
1000	1190	84	5	1274	87	3992	275	5182	357
1025	1205	93	6	1298	89	4099	282	5304	365
1675	2010	132	9	2142	147	6678	460	8688	599
1675	2015	130	8	2145	147	6675	460	8690	599
2310	2770	184	12	2954	203	9211	635	11981	826
2310	2775	181	12	2956	203	9208	634	11983	826
2770	3250	256	17	3506	241	11081	764	14331	988
2775	3260	255	17	3515	242	11099	765	14359	990
3170	3740	283	19	4023	277	12671	873	16411	1131
3200	3780	283	19	4063	280	12788	881	16568	1142
3720	4330	362	24	4692	323	14899	1027	19229	1325
3730	4350	358	24	4708	324	14935	1029	19285	1329
4060	4800	358	24	5158	355	16223	1118	21023	1449
4080	4820	361	24	5181	357	16305	1124	21125	1456
4580	5375	423	29	5798	399	18321	1263	23696	1633
4605	5400	428	29	5828	401	18423	1270	23823	1642
5300	6180	510	35	6690	461	21221	1463	27401	1889
5345	6225	518	35	6743	464	21405	1475	27630	1905
5920	6820	611	42	7431	512	23745	1637	30565	2107
5950	6850	617	42	7467	514	23868	1645	30718	2117
6625	7635	683	47	8318	573	26572	1832	34207	2358
6660	7670	689	47	8359	576	26715	1841	34385	2370

TABLE AII-37. (CONTINUED)

RECORDED DATA		CALCULATED DATA							
		UNCORRECTED AREA (AO)				CORRECTED AREA (AO')			
L	σ_c	τ		σ		τ		σ	
(LB)	(PSI)	(PSI)	(BARS)	(PSI)	(BARS)	(PSI)	(BARS)	(PSI)	(BARS)
7220	8275	767	52	9042	623	28981	1998	37256	2568

TABLE AII-38. RECORDED VALUES OF AXIAL LOAD L AND CONFINING PRESSURE σ_c AND CALCULATED VALUES OF SHEAR STRESS τ AND NORMAL STRESS σ FOR UNCORRECTED AREA AND CORRECTED AREA

RECORDED DATA		CALCULATED DATA							
		UNCORRECTED AREA (AO)				CORRECTED AREA (AO')			
L	σ_c	τ		σ		τ		σ	
(LB)	(PSI)	(PSI)	(BARS)	(PSI)	(BARS)	(PSI)	(BARS)	(PSI)	(BARS)
#80 DRY LS. GOUGE; 1-DIA. THICK; ALPHA=45 (AO=0.736; AO'=0.111 SQ. IN.)									
565	675	46	3	721	49	2207	152	2882	198
600	710	52	3	762	52	2347	161	3057	210
1070	1175	139	9	1314	90	4232	291	5407	372
1120	1225	148	10	1373	94	4432	305	5657	390
1430	1680	131	9	1811	124	5601	386	7281	502
1480	1750	130	8	1880	129	5791	399	7541	519
1875	2200	173	11	2373	163	7345	506	9545	658
1965	2230	219	15	2449	168	7736	533	9966	687
2350	2720	236	16	2956	203	9225	636	11945	823
2400	2785	237	16	3022	208	9418	649	12203	841
2760	3160	294	20	3454	238	10852	748	14012	966
2805	3200	305	21	3505	241	11035	760	14235	981
3185	3690	318	21	4008	276	12501	861	16191	1116
3240	3720	341	23	4061	280	12734	878	16454	1134
3600	4190	350	24	4540	313	14121	973	18311	1262
3640	4235	355	24	4590	316	14278	984	18513	1276
4030	4660	407	28	5067	349	15823	1090	20483	1412
4090	4710	423	29	5133	353	16068	1107	20778	1432
4490	5190	455	31	5645	389	17630	1215	22820	1573
4535	5250	455	31	5705	393	17802	1227	23052	1589
5170	5900	562	38	6462	445	20338	1402	26238	1809
5220	5980	556	38	6536	450	20523	1415	26503	1827
5805	6620	633	43	7253	500	22838	1574	29458	2031

TABLE AII-38. (CONTINUED)

RECORDED DATA		CALCULATED DATA							
		UNCORRECTED AREA (AO)				CORRECTED AREA (AO')			
L	σ_c	τ		σ		τ		σ	
(LB)	(PSI)	(PSI)	(BARS)	(PSI)	(BARS)	(PSI)	(BARS)	(PSI)	(BARS)
5875	6700	641	44	7341	506	23113	1593	29813	2055
6420	7310	706	48	8016	552	25263	1741	32573	2245
6550	7500	699	48	8199	565	25754	1775	33254	2292
7030	7965	793	54	8758	603	27684	1908	35649	2457

TABLE AII-39. RECORDED VALUES OF AXIAL LOAD L AND CONFINING PRESSURE σ_c AND CALCULATED VALUES OF SHEAR STRESS τ AND NORMAL STRESS σ FOR UNCORRECTED AREA AND CORRECTED AREA

RECORDED DATA		CALCULATED DATA							
		UNCORRECTED AREA (AO)				CORRECTED AREA (AO')			
L	σ_c	τ		σ		τ		σ	
(LB)	(PSI)	(PSI)	(BARS)	(PSI)	(BARS)	(PSI)	(BARS)	(PSI)	(BARS)
#80 DRY LS. GOUGE; 1.5-MM THICK; ALPHA=45 (AO=0.736; AO'=0.111 SQ. IN.)									
795	980	50	3	1030	71	3091	213	4071	280
870	1070	56	3	1126	77	3383	233	4453	307
1360	1650	98	6	1748	120	5301	365	6951	479
1410	1685	115	7	1800	124	5508	379	7193	495
1725	2105	119	8	2224	153	6717	463	8822	608
1860	2160	183	12	2343	161	7298	503	9458	652
2300	2780	172	11	2952	203	8970	618	11750	810
2330	2800	182	12	2982	205	9095	627	11895	820
2700	3205	231	15	3436	236	10559	728	13764	949
2760	3260	244	16	3504	241	10802	744	14062	969
3230	3780	304	20	4084	281	12659	872	16439	1133
3260	3810	309	21	4119	284	12779	881	16589	1143
3535	4140	331	22	4471	308	13853	955	17993	1240
3705	4310	361	24	4671	322	14534	1002	18844	1299
4325	5070	403	27	5473	377	16946	1168	22016	1518
4400	5110	434	29	5544	382	17264	1190	22374	1542
4900	5680	488	33	6168	425	19232	1326	24912	1717
5000	5780	506	34	6286	433	19632	1353	25412	1752
5365	6210	539	37	6749	465	21061	1452	27271	1880
5440	6360	515	35	6875	474	21324	1470	27684	1908
6185	7100	651	44	7751	534	24310	1676	31410	2165
6240	7210	634	43	7844	540	24503	1689	31713	2186
6850	7800	753	51	8553	589	26955	1858	34755	2396

TABLE AII-39. (CONTINUED)

RECORDED DATA		CALCULATED DATA							
		UNCORRECTED AREA (AO)				CORRECTED AREA (AO')			
L	σ_c	τ		σ		τ		σ	
(LB)	(PSI)	(PSI)	(BARS)	(PSI)	(BARS)	(PSI)	(BARS)	(PSI)	(BARS)
6900	7900	737	50	8637	595	27131	1870	35031	2415
7195	8215	780	53	8995	620	28302	1951	36517	2517

TABLE AII-40. RECORDED VALUES OF AXIAL LOAD L AND CONFINING PRESSURE σ_c AND CALCULATED VALUES OF SHEAR STRESS τ AND NORMAL STRESS σ FOR UNCORRECTED AREA AND CORRECTED AREA

RECORDED DATA		CALCULATED DATA							
		UNCORRECTED AREA (AO)				CORRECTED AREA (AO')			
L	σ_c	τ		σ		τ		σ	
(LB)	(PSI)	(PSI)	(BARS)	(PSI)	(BARS)	(PSI)	(BARS)	(PSI)	(BARS)
#80 DRY SS. GOUGE; 1-DIA. THICK; ALPHA=45 (AO=0.739; AO'=0.109 SQ. IN.)									
640	780	43	2	823	56	2545	175	3325	229
850	810	170	11	980	67	3494	240	4304	296
1080	1290	85	5	1375	94	4309	297	5599	386
1305	1320	222	15	1542	106	5326	367	6646	458
1520	1850	103	7	1953	134	6047	416	7897	544
1700	1910	195	13	2105	145	6843	471	8753	603
1980	2400	139	9	2539	175	7882	543	10282	708
2120	2420	224	15	2644	182	8514	587	10934	753
2650	3110	237	16	3347	230	10600	730	13710	945
2725	3150	268	18	3418	235	10924	753	14074	970
3100	3620	287	19	3907	269	12410	855	16030	1105
3215	3675	337	23	4012	276	12910	890	16585	1143
3450	4100	284	19	4384	302	13775	949	17875	1232
3530	4125	325	22	4450	306	14130	974	18255	1258
3965	4600	382	26	4982	343	15888	1095	20488	1412
4020	4640	399	27	5039	347	16120	1111	20760	1431
4580	5360	418	28	5778	398	18329	1263	23689	1633
4670	5470	424	29	5894	406	18687	1288	24157	1665
5145	5960	501	34	6461	445	20620	1421	26580	1832
5280	6115	514	35	6629	457	21162	1459	27277	1880
5725	6615	565	39	7180	495	22953	1582	29568	2038
5790	6680	577	39	7257	500	23219	1600	29899	2061
6270	7215	634	43	7849	541	25153	1734	32368	2231

TABLE AII-40. (CONTINUED)

RECORDED DATA		CALCULATED DATA							
		UNCORRECTED AREA (AO)				CORRECTED AREA (AO')			
L	σ_c	τ		σ		τ		σ	
(LB)	(PSI)	(PSI)	(BARS)	(PSI)	(BARS)	(PSI)	(BARS)	(PSI)	(BARS)
6350	7340	626	43	7966	549	25458	1755	32798	2261
6860	7885	698	48	8583	591	27525	1897	35410	2441
6975	7980	729	50	8709	600	28005	1930	35985	2481
7250	8275	767	52	9042	623	29119	2007	37394	2578

TABLE AII-41. RECORDED VALUES OF AXIAL LOAD L AND CONFINING PRESSURE σ_c AND CALCULATED VALUES OF SHEAR STRESS τ AND NORMAL STRESS σ FOR UNCORRECTED AREA AND CORRECTED AREA

RECORDED DATA		CALCULATED DATA							
		UNCORRECTED AREA (AO)				CORRECTED AREA (AO')			
L	σ_c	τ		σ		τ		σ	
(LB)	(PSI)	(PSI)	(BARS)	(PSI)	(BARS)	(PSI)	(BARS)	(PSI)	(BARS)
#80 DRY SS. GOUGE; 1.5-MM THICK; ALPHA=45 (AO=0.739; AO'=0.109 SQ. IN.)									
685	790	68	4	858	59	2747	189	3537	243
720	825	74	5	899	62	2890	199	3715	256
1050	1265	77	5	1342	92	4184	288	5449	375
1105	1300	97	6	1397	96	4418	304	5718	394
1760	2170	105	7	2275	156	6988	481	9158	631
1825	2190	139	9	2329	160	7276	501	9466	652
2230	2705	156	10	2861	197	8876	612	11581	798
2275	2750	164	11	2914	200	9060	624	11810	814
2715	3240	216	14	3456	238	10834	746	14074	970
2755	3290	219	15	3509	241	10992	757	14282	984
3085	3625	274	18	3899	268	12338	850	15963	1100
3120	3680	270	18	3950	272	12471	859	16151	1113
3600	4205	333	22	4538	312	14411	993	18616	1283
3665	4265	347	23	4612	317	14679	1012	18944	1306
4090	4800	367	25	5167	356	16361	1128	21161	1459
4170	4870	386	26	5256	362	16693	1150	21563	1486
4570	5330	427	29	5757	396	18298	1261	23628	1629
4660	5400	452	31	5852	403	18676	1287	24076	1659
5150	6030	469	32	6499	448	20608	1420	26638	1836
5220	6120	471	32	6591	454	20884	1439	27004	1861
6025	6920	616	42	7536	519	24177	1666	31097	2144
6060	6980	610	42	7590	523	24308	1675	31288	2157
6400	7400	630	43	8030	553	25657	1769	33057	2279

TABLE AII-41. (CONTINUED)

RECORDED DATA		CALCULATED DATA							
		UNCORRECTED AREA (AO)				CORRECTED AREA (AO')			
L	σ_c	τ		σ		τ		σ	
(LB)	(PSI)	(PSI)	(BARS)	(PSI)	(BARS)	(PSI)	(BARS)	(PSI)	(BARS)
6475	7480	640	44	8120	559	25961	1790	33441	2305
7090	8130	732	50	8862	611	28457	1962	36587	2522

TABLE AII-42. RECORDED VALUES OF AXIAL LOAD L AND CONFINING PRESSURE σ_c AND CALCULATED VALUES OF SHEAR STRESS τ AND NORMAL STRESS σ FOR UNCORRECTED AREA AND CORRECTED AREA

RECORDED DATA		CALCULATED DATA							
		UNCORRECTED AREA (AO)				CORRECTED AREA (AO')			
L	σ_c	τ		σ		τ		σ	
(LB)	(PSI)	(PSI)	(BARS)	(PSI)	(BARS)	(PSI)	(BARS)	(PSI)	(BARS)
#80 DRY LS. GOUGE; 1-MM THICK; ALPHA=30 (AO=0.736; AO'=0.326 SQ. IN.)									
450	575	15	1	584	40	348	24	776	53
580	630	68	4	669	46	497	34	917	63
920	1200	21	1	1212	83	702	48	1605	110
960	1260	19	1	1271	87	729	50	1681	115
1505	1990	23	1	2003	138	1137	78	2646	182
1550	2030	32	2	2048	141	1179	81	2711	186
2090	2690	64	4	2727	188	1611	111	3620	249
2150	2735	80	5	2781	191	1671	115	3700	255
2585	3230	122	8	3300	227	2034	140	4404	303
2650	3275	140	9	3356	231	2101	144	4488	309
3150	3920	155	10	4009	276	2486	171	5355	369
3180	3980	147	10	4065	280	2500	172	5423	373
3660	4575	172	11	4674	322	2880	198	6237	430
3750	4660	188	12	4768	328	2963	204	6370	439
4075	5065	204	14	5182	357	3219	221	6923	477
4165	5175	209	14	5295	365	3291	226	7075	487
4830	5905	284	19	6069	418	3858	266	8132	560
4920	6020	287	19	6186	426	3928	270	8288	571
5495	6650	353	24	6854	472	4419	304	9201	634
5640	6810	369	25	7023	484	4542	313	9432	650
6275	7585	407	28	7820	539	5050	348	10500	724
6460	7720	457	31	7984	550	5237	361	10743	740
6770	8050	497	34	8337	574	5506	379	11229	774

TABLE AII-43. RECORDED VALUES OF AXIAL LOAD L AND CONFINING PRESSURE σ_c AND CALCULATED VALUES OF SHEAR STRESS τ AND NORMAL STRESS σ FOR UNCORRECTED AREA AND CORRECTED AREA

RECORDED DATA		CALCULATED DATA							
		UNCORRECTED AREA (AO)				CORRECTED AREA (AO')			
L	σ_c	τ		σ		τ		σ	
(LB)	(PSI)	(PSI)	(BARS)	(PSI)	(BARS)	(PSI)	(BARS)	(PSI)	(BARS)
#80 DRY LS. GOUGE; 1-MM THICK; ALPHA=37.5 (AO=0.747; AO'=0.219 SQ. IN.)									
460	560	26	1	580	40	743	51	1130	77
495	595	32	2	620	42	804	55	1212	83
860	1110	19	1	1125	77	1360	93	2153	148
905	1150	29	2	1172	80	1440	99	2255	155
1300	1670	33	2	1696	116	2060	142	3250	224
1385	1715	67	4	1766	121	2226	153	3423	236
1755	2210	67	4	2261	155	2802	193	4360	300
1810	2240	88	6	2307	159	2909	200	4472	308
2290	2855	101	7	2933	202	3671	253	5672	391
2320	2910	94	6	2982	205	3710	255	5757	396
2680	3330	124	8	3425	236	4301	296	6631	457
2735	3400	126	8	3496	241	4389	302	6768	466
3300	4130	138	9	4236	292	5282	364	8183	564
3370	4170	164	11	4296	296	5417	373	8327	574
3935	4840	206	14	4998	344	6340	437	9705	669
3980	4900	206	14	5058	348	6410	441	9819	676
4535	5520	266	18	5724	394	7335	505	11148	768
4600	5580	279	19	5794	399	7449	513	11296	778
5095	6185	306	21	6420	442	8248	568	12514	862
5175	6250	327	22	6501	448	8393	578	12690	875
5700	6850	376	25	7139	492	9261	638	13956	962
5775	6915	394	27	7217	497	9395	647	14124	973
6380	7590	459	31	7942	547	10404	717	15573	1073

TABLE AII-43. (CONTINUED)

RECORDED DATA		CALCULATED DATA							
		UNCORRECTED AREA (AO)				CORRECTED AREA (AO')			
L	σ_c	τ		σ		τ		σ	
(LB)	(PSI)	(PSI)	(BARS)	(PSI)	(BARS)	(PSI)	(BARS)	(PSI)	(BARS)
6475	7690	472	32	8052	555	10565	728	15797	1089
6925	8240	497	34	8621	594	11292	778	16904	1165

TABLE AII-44. RECORDED VALUES OF AXIAL LOAD L AND CONFINING PRESSURE σ_c AND CALCULATED VALUES OF SHEAR STRESS τ AND NORMAL STRESS σ FOR UNCORRECTED AREA AND CORRECTED AREA

RECORDED DATA		CALCULATED DATA							
		UNCORRECTED AREA (AO)				CORRECTED AREA (AO')			
L	σ_c	τ		σ		τ		σ	
(LB)	(PSI)	(PSI)	(BARS)	(PSI)	(BARS)	(PSI)	(BARS)	(PSI)	(BARS)
#80 DRY LS. GOUGE; 1-MM THICK; ALPHA=60 (AO=0.745; AO'=0.079 SQ. IN.)									
580	720	25	1	763	52	2867	197	5686	392
675	810	41	2	882	60	3349	230	6610	455
1060	1360	27	1	1407	97	5221	359	10403	717
1100	1400	33	2	1457	100	5423	373	10793	744
1415	1810	38	2	1876	129	6972	480	13886	957
1480	1870	50	3	1957	134	7302	503	14518	1000
1880	2300	96	6	2467	170	9308	641	18423	1270
1930	2350	104	7	2530	174	9561	659	18910	1303
2390	2900	133	9	3131	215	11844	816	23414	1614
2420	2950	129	8	3173	218	11987	826	23712	1634
2760	3320	166	11	3608	248	13690	943	27032	1863
2835	3380	184	12	3699	255	14075	970	27759	1913
3175	3760	217	14	4136	285	15774	1087	31082	2143
3215	3800	223	15	4186	288	15976	1101	31472	2169
3640	4340	236	16	4749	327	18072	1246	35641	2457
3710	4410	246	17	4837	333	18425	1270	36324	2504
4100	4910	256	17	5355	369	20346	1402	40151	2768
4170	4985	265	18	5444	375	20697	1427	40834	2815
4785	5610	351	24	6219	428	23798	1640	46829	3228
4850	5670	363	25	6300	434	24128	1663	47461	3272
5530	6490	403	27	7189	495	27500	1896	54122	3731
5665	6620	426	29	7358	507	28184	1943	55436	3822
6300	7325	489	33	8173	563	31359	2162	61641	4250

TABLE AII-44. (CONTINUED)

RECORDED DATA		CALCULATED DATA							
		UNCORRECTED AREA (AO)				CORRECTED AREA (AO')			
L	σ_c	τ		σ		τ		σ	
(LB)	(PSI)	(PSI)	(BARS)	(PSI)	(BARS)	(PSI)	(BARS)	(PSI)	(BARS)
6360	7420	483	33	8257	569	31647	2182	62234	4290
6875	7980	540	37	8916	614	34227	2359	67263	4637

TABLE AII-45. RECORDED VALUES OF AXIAL LOAD L AND CONFINING PRESSURE σ_c AND CALCULATED VALUES OF SHEAR STRESS τ AND NORMAL STRESS σ FOR UNCORRECTED AREA AND CORRECTED AREA

RECORDED DATA		CALCULATED DATA							
		UNCORRECTED AREA (AO)				CORRECTED AREA (AO')			
L	σ_c	τ		σ		τ		σ	
(LB)	(PSI)	(PSI)	(BARS)	(PSI)	(BARS)	(PSI)	(BARS)	(PSI)	(BARS)
#80 DRY SS. GOUGE; 1-MM THICK; ALPHA=30 (AO=0.739; AO'=0.320 SQ. IN.)									
950	1190	41	2	1213	83	770	53	1634	112
985	1200	57	3	1233	85	813	56	1669	115
1305	1620	63	4	1656	114	1064	73	2234	154
1370	1670	79	5	1715	118	1130	77	2322	160
1720	2100	98	6	2156	148	1418	97	2918	201
1730	2130	91	6	2182	150	1418	97	2949	203
1990	2490	87	6	2540	175	1614	111	3422	235
2040	2510	108	7	2572	177	1673	115	3476	239
2415	2965	131	9	3040	209	1984	136	4110	283
2465	2980	153	10	3068	211	2045	141	4160	286
2715	3260	179	12	3363	231	2262	155	4566	314
2740	3290	180	12	3394	234	2283	157	4608	317
3210	3830	222	15	3958	272	2685	185	5380	370
3245	3880	221	15	4007	276	2710	186	5445	375
3730	4480	245	16	4621	318	3107	214	6274	432
3785	4520	260	17	4670	322	3164	218	6347	437
4145	4980	272	18	5137	354	3452	238	6973	480
4205	5020	290	20	5187	357	3516	242	7050	486
4825	5680	367	25	5892	406	4069	280	8029	553
4880	5775	358	24	5982	412	4102	282	8143	561
5525	6515	416	28	6755	465	4655	320	9202	634
5585	6580	423	29	6824	470	4708	324	9298	641
6250	7300	501	34	7589	523	5296	365	10357	714

TABLE AII-45. (CONTINUED)

RECORDED DATA		CALCULATED DATA							
		UNCORRECTED AREA (AO)				CORRECTED AREA (AO')			
L	σ_c	τ		σ		τ		σ	
(LB)	(PSI)	(PSI)	(BARS)	(PSI)	(BARS)	(PSI)	(BARS)	(PSI)	(BARS)
6320	7400	498	34	7688	530	5347	368	10487	723
7145	8230	622	42	8589	592	6104	420	11754	810

TABLE AII-46. RECORDED VALUES OF AXIAL LOAD L AND CONFINING PRESSURE σ_c AND CALCULATED VALUES OF SHEAR STRESS τ AND NORMAL STRESS σ FOR UNCORRECTED AREA AND CORRECTED AREA

RECORDED DATA		CALCULATED DATA							
		UNCORRECTED AREA (AO)				CORRECTED AREA (AO')			
L	σ_c	τ		σ		τ		σ	
(LB)	(PSI)	(PSI)	(BARS)	(PSI)	(BARS)	(PSI)	(BARS)	(PSI)	(BARS)
#80 DRY SS. GOUGE; 1-MM THICK; ALPHA=37.5 (AO=0.736; AO'=0.215 SQ. IN.)									
530	680	19	1	694	47	862	59	1341	92
570	725	23	1	743	51	930	64	1438	99
825	1070	24	1	1088	75	1336	92	2095	144
860	1105	30	2	1128	77	1398	96	2177	150
1080	1400	32	2	1424	98	1749	120	2742	189
1170	1480	52	3	1520	104	1913	131	2948	203
1600	2040	64	4	2089	144	2608	179	4041	278
1625	2080	61	4	2127	146	2645	182	4110	283
1950	2500	72	4	2555	176	3172	218	4934	340
2000	2550	80	5	2612	180	3261	224	5052	348
2370	2995	108	7	3078	212	3877	267	5970	411
2425	3025	130	8	3124	215	3986	274	6083	419
2825	3450	187	12	3593	247	4679	322	7040	485
2880	3500	199	13	3653	251	4779	329	7167	494
3490	4275	225	15	4448	306	5775	398	8706	600
3590	4360	250	17	4551	313	5958	410	8932	615
4215	5080	312	21	5319	366	7014	483	10462	721
4300	5160	329	22	5412	373	7167	494	10659	734
4870	5820	384	26	6115	421	8128	560	12057	831
5000	5950	407	28	6262	431	8358	576	12363	852
5525	6580	447	30	6923	477	9233	636	13664	942
5620	6660	471	32	7021	484	9407	648	13878	956
6145	7270	521	35	7669	528	10292	709	15167	1045

TABLE AII-46. (CONTINUED)

RECORDED CATA		CALCULATED DATA							
		UNCORRECTED AREA (AO)				CORRECTED AREA (AO')			
L	σ_c	τ		σ		τ		σ	
(LB)	(PSI)	(PSI)	(BARS)	(PSI)	(BARS)	(PSI)	(BARS)	(PSI)	(BARS)
6250	7350	551	38	7773	535	10489	723	15399	1061
6890	8110	604	41	8573	591	11560	797	16980	1170

TABLE AII-47. RECORDED VALUES OF AXIAL LOAD L AND CONFINING PRESSURE σ_c AND CALCULATED VALUES OF SHEAR STRESS τ AND NORMAL STRESS σ FOR UNCORRECTED AREA AND CORRECTED AREA

RECORDED DATA		CALCULATED DATA							
		UNCORRECTED AREA (AO)				CORRECTED AREA (AO')			
L	σ_c	τ		σ		τ		σ	
(LB)	(PSI)	(PSI)	(BARS)	(PSI)	(BARS)	(PSI)	(BARS)	(PSI)	(BARS)
#80 DRY SS. GOUGE; 1-MM THICK; ALPHA=60 (AO=0.733; AO'=0.078 SQ. IN.)									
510	625	30	2	678	46	2560	176	5060	348
580	695	41	2	767	52	2918	201	5750	396
925	1080	78	5	1216	83	4667	321	9164	631
980	1130	89	6	1285	88	4951	341	9705	669
1325	1640	72	5	1765	121	6645	458	13150	906
1400	1700	90	6	1857	128	7035	485	13886	957
1785	2180	110	7	2371	163	8965	618	17708	1220
1875	2200	155	10	2468	170	9456	651	18578	1280
2260	2720	157	10	2992	206	11368	783	22410	1545
2310	2750	173	11	3051	210	11633	802	22899	1578
2640	3180	182	12	3496	241	13278	915	26179	1805
2665	3195	190	13	3525	243	13411	924	26423	1821
3090	3680	231	15	4081	281	15560	1072	30631	2111
3120	3700	240	16	4117	283	15718	1083	30924	2132
3450	4140	245	16	4565	314	17359	1196	34208	2358
3480	4170	250	17	4603	317	17513	1207	34504	2378
4005	4720	322	22	5277	363	20189	1392	39689	2736
4050	4750	335	23	5331	367	20426	1408	40129	2766
4480	5275	362	24	5902	406	22586	1557	44395	3060
4520	5320	366	25	5954	410	22788	1571	44791	3088
5040	5880	431	29	6626	456	25433	1753	49931	3442
5095	5970	424	29	6705	462	25699	1771	50482	3480
5500	6480	443	30	7247	499	27727	1911	54504	3757

TABLE AII-47. (CONTINUED)

RECORDED DATA		CALCULATED DATA							
		UNCORRECTED AREA (AO)				CORRECTED AREA (AO')			
L	σ_c	τ		σ		τ		σ	
(LB)	(PSI)	(PSI)	(BARS)	(PSI)	(BARS)	(PSI)	(BARS)	(PSI)	(BARS)
5565	6540	455	31	7329	505	28061	1934	55144	3802
6100	7090	533	36	8013	552	30793	2123	60426	4166
6200	7200	544	37	8143	561	31301	2158	61415	4234
6775	7820	616	42	8887	612	34224	2359	67099	4626
6955	8080	609	42	9136	629	35111	2420	68894	4750
7300	8425	664	45	9575	660	36877	2542	72298	4984

TABLE AII-48. RECORDED VALUES OF AXIAL LOAD L AND CONFINING PRESSURE σ_c AND CALCULATED VALUES OF SHEAR STRESS τ AND NORMAL STRESS σ FOR UNCORRECTED AREA AND CORRECTED AREA

RECORDED DATA		CALCULATED DATA							
		UNCORRECTED AREA (AO)				CORRECTED AREA (AO')			
L	σ_c	τ		σ		τ		σ	
(LB)	(PSI)	(PSI)	(BARS)	(PSI)	(BARS)	(PSI)	(BARS)	(PSI)	(BARS)
#80 WET LS. GOUGE; P=37.9 BARS; ALPHA=45 (AO=0.736; AO'=0.111 SQ. IN.)									
850	1100	27	1	1127	77	3278	226	4378	301
885	1180	11	0	1191	82	3396	234	4576	315
1095	1380	53	3	1433	98	4242	292	5622	387
1127	1460	35	2	1495	103	4346	299	5806	400
1420	1830	49	3	1879	129	5481	377	7311	504
1480	1900	55	3	1955	134	5716	394	7616	525
1860	2325	101	6	2426	167	7215	497	9540	657
1905	2375	106	7	2481	171	7393	509	9768	673
2345	2850	168	11	3018	208	9138	630	11988	826
2370	2900	160	11	3060	210	9225	636	12125	836
2805	3355	228	15	3583	247	10957	755	14312	986
2865	3405	243	16	3648	251	11202	772	14607	1007
3240	3900	251	17	4151	286	12644	871	16544	1140
3300	3950	266	18	4216	290	12889	888	16839	1161
3625	4340	292	20	4632	319	14158	976	18498	1275
3665	4410	284	19	4694	323	14304	986	18714	1290
4160	4930	361	24	5291	364	16273	1122	21203	1461
4210	4980	370	25	5350	368	16473	1135	21453	1479
4855	5705	445	30	6150	424	19016	1311	24721	1704
5030	5870	482	33	6352	437	19722	1359	25592	1764
5500	6490	491	33	6981	481	21529	1484	28019	1931
5610	6600	511	35	7111	490	21970	1514	28570	1969
6305	7370	598	41	7968	549	24715	1704	32085	2212

TABLE AII-48. (CONTINUED)

RECORDED DATA		CALCULATED DATA							
		UNCORRECTED AREA (AO)				CORRECTED AREA (AO')			
L	σ_c	τ		σ		τ		σ	
(LB)	(PSI)	(PSI)	(BARS)	(PSI)	(BARS)	(PSI)	(BARS)	(PSI)	(BARS)
6395	7470	609	42	8079	557	25071	1728	32541	2243
6900	7990	692	47	8682	598	27086	1867	35076	2418

TABLE AII-49. RECORDED VALUES OF AXIAL LOAD L AND CONFINING PRESSURE σ_c AND CALCULATED VALUES OF SHEAR STRESS τ AND NORMAL STRESS σ FOR UNCORRECTED AREA AND CORRECTED AREA

RECORDED DATA		CALCULATED DATA							
		UNCORRECTED AREA (AO)				CORRECTED AREA (AO')			
L	σ_c	τ		σ		τ		σ	
(LB)	(PSI)	(PSI)	(BARS)	(PSI)	(BARS)	(PSI)	(BARS)	(PSI)	(BARS)
#80 WET LS. GOUGE; P=86.9 BARS; ALPHA=45 (AO=0.736; AO'=0.111 SQ. IN.)									
1800	2200	122	8	2322	160	7008	483	9208	634
1850	2250	131	9	2381	164	7208	496	9458	652
2230	2720	154	10	2874	198	8685	598	11405	786
2270	2790	147	10	2937	202	8830	608	11620	801
2700	3240	214	14	3454	238	10542	726	13782	950
2740	3290	216	14	3506	241	10697	737	13987	964
3140	3800	233	16	4033	278	12244	844	16044	1106
3205	3830	262	18	4092	282	12521	863	16351	1127
3555	4250	290	20	4540	313	13888	957	18138	1250
3600	4305	293	20	4598	317	14063	969	18368	1266
4170	4940	362	25	5302	365	16313	1124	21253	1465
4200	5000	353	24	5353	369	16418	1132	21418	1476
4780	5670	412	28	6082	419	18696	1289	24366	1680
4875	5770	426	29	6196	427	19074	1315	24844	1712
5330	6300	470	32	6770	466	20859	1438	27159	1872
5460	6425	496	34	6921	477	21382	1474	27807	1917
6195	7210	603	41	7813	538	24300	1675	31510	2172
6290	7300	623	42	7923	546	24683	1701	31983	2205
6920	8010	696	47	8706	600	27166	1873	35176	2425

TABLE AII-50. RECORDED VALUES OF AXIAL LOAD L AND CONFINING PRESSURE σ_c AND CALCULATED VALUES OF SHEAR STRESS τ AND NORMAL STRESS σ FOR UNCORRECTED AREA AND CORRECTED AREA

RECORDED DATA		CALCULATED DATA							
		UNCORRECTED AREA (AO)				CORRECTED AREA (AO')			
L	σ_c	τ		σ		τ		σ	
(LB)	(PSI)	(PSI)	(BARS)	(PSI)	(BARS)	(PSI)	(BARS)	(PSI)	(BARS)
#80 WET SS. GOUGE; P=34.5 BARS; ALPHA=45 (AO=0.739; AO'=0.109 SQ. IN.)									
950	1100	92	6	1192	82	3807	262	4907	338
1120	1150	182	12	1332	91	4562	314	5712	393
1350	1650	88	6	1738	119	5367	370	7017	483
1585	1700	222	15	1922	132	6420	442	8120	559
1910	2280	152	10	2432	167	7621	525	9901	682
2120	2330	269	18	2599	179	8559	590	10889	750
2350	2815	182	12	2997	206	9372	646	12187	840
2530	2860	281	19	3141	216	10175	701	13035	898
2845	3325	262	18	3587	247	11387	785	14712	1014
3010	3380	346	23	3726	256	12117	835	15497	1068
3315	3900	292	20	4192	289	13256	913	17156	1182
3420	3960	333	23	4293	296	13708	945	17668	1218
3715	4380	323	22	4703	324	14851	1023	19231	1325
3850	4420	394	27	4814	331	15450	1065	19870	1370
4125	4870	355	24	5225	360	16487	1136	21357	1472
4190	4920	374	25	5294	365	16760	1155	21680	1494
4495	5300	391	26	5691	392	17969	1238	23269	1604
4565	5350	413	28	5763	397	18265	1259	23615	1628
5050	5890	471	32	6361	438	20220	1394	26110	1800
5145	5950	506	34	6456	445	20625	1422	26575	1832
5585	6500	528	36	7028	484	22369	1542	28869	1990
5625	6550	530	36	7080	488	22527	1553	29077	2004
6170	7080	634	43	7714	531	24762	1707	31842	2195

TABLE AII-50. (CONTINUED)

RECORDED DATA		CALCULATED DATA							
		UNCORRECTED AREA (AO)				CORRECTED AREA (AO')			
L	σ_c	τ		σ		τ		σ	
(LB)	(PSI)	(PSI)	(BARS)	(PSI)	(BARS)	(PSI)	(BARS)	(PSI)	(BARS)
6270	7180	652	44	7832	540	25171	1735	32351	2230
7000	8010	731	50	8741	602	28105	1937	36115	2490

TABLE AII-51. RECORDED VALUES OF AXIAL LOAD L AND CONFINING PRESSURE σ_c AND CALCULATED VALUES OF SHEAR STRESS τ AND NORMAL STRESS σ FOR UNCORRECTED AREA AND CORRECTED AREA

RECORDED DATA		CALCULATED DATA							
		UNCORRECTED AREA (AO)				CORRECTED AREA (AO')			
L	σ_c	τ		σ		τ		σ	
(LB)	(PSI)	(PSI)	(BARS)	(PSI)	(BARS)	(PSI)	(BARS)	(PSI)	(BARS)
#80 WET SS. GOUGE; P=79.3 BARS; ALPHA=45 (AO=0.739; AO'=0.109 SQ. IN.)									
1370	1610	121	8	1731	119	5479	377	7089	488
1590	1710	220	15	1930	133	6438	443	8148	561
1780	2130	139	9	2269	156	7100	489	9230	636
1985	2200	243	16	2443	168	8005	551	10205	703
2370	2930	138	9	3068	211	9406	648	12336	850
2725	3000	343	23	3343	230	10999	758	13999	965
3100	3720	237	16	3957	272	12360	852	16080	1108
3400	3780	410	28	4190	288	13706	945	17486	1205
3700	4425	290	20	4715	325	14759	1017	19184	1322
3915	4460	418	28	4878	336	15728	1084	20188	1391
4280	5220	285	19	5505	379	17023	1173	22243	1533
4520	5300	408	28	5708	393	18083	1246	23383	1612
5050	6025	404	27	6429	443	20152	1389	26177	1804
5240	6115	487	33	6602	455	20979	1446	27094	1868
5545	6700	469	32	7169	494	22544	1554	29244	2016
5825	6800	541	37	7341	506	23320	1607	30120	2076
6350	7430	581	40	8011	552	25413	1752	32843	2264
6470	7510	622	42	8132	560	25923	1787	33433	2305
7150	8350	662	45	9012	621	28623	1973	36973	2549

TABLE AII-52. RECORDED VALUES OF AXIAL LOAD L AND CONFINING PRESSURE σ_c AND CALCULATED VALUES OF SHEAR STRESS τ AND NORMAL STRESS σ FOR UNCORRECTED AREA AND CORRECTED AREA

RECORDED DATA		CALCULATED DATA							
		UNCORRECTED AREA (AO)				CORRECTED AREA (AO')			
L	σ_c	τ		σ		τ		σ	
(LB)	(PSI)	(PSI)	(BARS)	(PSI)	(BARS)	(PSI)	(BARS)	(PSI)	(BARS)
#80 WET SS. GOUGE; P=34.5 BARS; KINETIC DATA (AO=0.739; AO'=0.109 SQ. IN.)									
1120	1150	182	12	1332	91	4562	314	5712	393
1585	1700	222	15	1922	132	6420	442	8120	559
2120	2330	269	18	2599	179	8559	590	10889	750
2530	2860	281	19	3141	216	10175	701	13035	898
3010	3380	346	23	3726	256	12117	835	15497	1068
3420	3960	333	23	4293	296	13708	945	17668	1218
3850	4420	394	27	4814	331	15450	1065	19870	1370
4190	4920	374	25	5294	365	16760	1155	21680	1494
4565	5350	413	28	5763	397	18265	1259	23615	1628
5145	5950	506	34	6456	445	20625	1422	26575	1832
5625	6550	530	36	7080	488	22527	1553	29077	2004
6270	7180	652	44	7832	540	25171	1735	32351	2230

TABLE AII-53. RECORDED VALUES OF AXIAL LOAD L AND CONFINING PRESSURE σ_c AND CALCULATED VALUES OF SHEAR STRESS τ AND NORMAL STRESS σ FOR UNCORRECTED AREA AND CORRECTED AREA

RECORDED DATA		CALCULATED DATA							
		UNCORRECTED AREA (AO)				CORRECTED AREA (AO')			
L	σ_c	τ		σ		τ		σ	
(LB)	(PSI)	(PSI)	(BARS)	(PSI)	(BARS)	(PSI)	(BARS)	(PSI)	(BARS)
#80 WET SS. GOUGE; P=34.5 BARS; STATIC DATA (AO=0.739; AO'=0.109 SQ. IN.)									
950	1100	92	6	1192	82	3807	262	4907	338
1350	1650	88	6	1738	119	5367	370	7017	483
1910	2280	152	10	2432	167	7621	525	9901	682
2350	2815	182	12	2997	206	9372	646	12187	840
2845	3325	262	18	3587	247	11387	785	14712	1014
3315	3900	292	20	4192	289	13256	913	17156	1182
3715	4380	323	22	4703	324	14851	1023	19231	1325
4125	4870	355	24	5225	360	16487	1136	21357	1472
4495	5300	391	26	5691	392	17969	1238	23269	1604
5050	5890	471	32	6361	438	20220	1394	26110	1800
5585	6500	528	36	7028	484	22369	1542	28869	1990
6170	7080	634	43	7714	531	24762	1707	31842	2195
7000	8010	731	50	8741	602	28105	1937	36115	2490

TABLE AII-54. RECORDED VALUES OF AXIAL LOAD L AND CONFINING PRESSURE σ_c AND CALCULATED VALUES OF SHEAR STRESS τ AND NORMAL STRESS σ FOR UNCORRECTED AREA AND CORRECTED AREA

RECORDED DATA		CALCULATED DATA							
		UNCORRECTED AREA (AO)				CORRECTED AREA (AO')			
L	σ_c	τ		σ		τ		σ	
(LB)	(PSI)	(PSI)	(BARS)	(PSI)	(BARS)	(PSI)	(BARS)	(PSI)	(BARS)
#80 WET SS. GOUGE; P=79.3 BARS; KINETIC DATA (AO=0.739; AO'=0.109 SQ. IN.)									
1590	1710	220	15	1930	133	6438	443	8148	561
1985	2200	243	16	2443	168	8005	551	10205	703
2725	3000	343	23	3343	230	10999	758	13999	965
3400	3780	410	28	4190	288	13706	945	17486	1205
3915	4460	418	28	4878	336	15728	1084	20188	1391
4520	5300	408	28	5708	393	18083	1246	23383	1612
5240	6115	487	33	6602	455	20979	1446	27094	1868
5825	6800	541	37	7341	506	23320	1607	30120	2076
6470	7510	622	42	8132	560	25923	1787	33433	2305

TABLE AII-55. RECORDED VALUES OF AXIAL LOAD L AND CONFINING PRESSURE σ_c AND CALCULATED VALUES OF SHEAR STRESS τ AND NORMAL STRESS σ FOR UNCORRECTED AREA AND CORRECTED AREA

RECORDED DATA		CALCULATED DATA							
		UNCORRECTED AREA (AO)				CORRECTED AREA (AO')			
L	σ_c	τ		σ		τ		σ	
(LB)	(PSI)	(PSI)	(BARS)	(PSI)	(BARS)	(PSI)	(BARS)	(PSI)	(BARS)
#80 WET SS. GOUGE; P=79.3 BARS; STATIC DATA (AO=0.739; AO'=0.109 SQ. IN.)									
1370	1610	121	8	1731	119	5479	377	7089	488
1780	2130	139	9	2269	156	7100	489	9230	636
2370	2930	138	9	3068	211	9406	648	12336	850
3100	3720	237	16	3957	272	12360	852	16080	1108
3700	4425	290	20	4715	325	14759	1017	19184	1322
4280	5220	285	19	5505	379	17023	1173	22243	1533
5050	6025	404	27	6429	443	20152	1389	26177	1804
5645	6700	469	32	7169	494	22544	1554	29244	2016
6350	7430	581	40	8011	552	25413	1752	32843	2264
7150	8350	662	45	9012	621	28623	1973	36973	2549

APPENDIX III

Computer Programs

J. S. DURTSCHE

7-4-73

COMPUTER PROGRAM FOR PLOTTING:

(1) STRESS-STRAIN CURVES

```
      REAL*8 EE,FF,BB,AA,CC,AB,B1,SX,SY,SXY,SX2
      DIMENSION AL(99), D(99), AS(99), ASB(99),SC(99),DC(99),ANS(10),
      SS(10),ASN(99),X(9),SIG(5),S(5),R(5),AMS(5,9),EE(9),FF(9),Y(9),
      ASCP(99),ASCPB(99)
      READ 10,M
   10 FORMAT (I2)
      CALL PLOT(5.0,1.5,-3)
      CALL PLOT(20.0,0.0, 3)
      PRINT 61
   61 FORMAT(1H1)
      DO 100 J=1,M
```

```
      K=J
      READ 11,CL,A,CP,N
   11 FORMAT (F5.3/F5.3/F6.1/I2)
      IF(J-7)81,81,82
   81 PRINT 32,K
   32 FORMAT(//////9X,'TABLE AII-',I2,'.  RECORDED VALUES AXIAL LOAD AND
       DISPLACEMENT WITH CALCULATED DATA FOR STRESS-'/30X,'STRAIN FRACTU
      RE TEST ON A KELLY LIMESTONE CORE*')
      GC TO 84
   82 PRINT 83,K
   83 FCRMAT(//////9X,'TABLE AII-',I2,'.  RECORDED VALUES AXIAL LOAD AND
       DISPLACEMENT WITH CALCULATED DATA FOR STRESS-'/24X,'STRAIN FRACTU
      RE TEST ON A MESA VERDE SANDSTONE TEST CORE*')
   84 PRINT 30
   30 FORMAT(9X,'-------------------------------------------------------
      -----------------------------------')
      PRINT 33
   33 FORMAT(9X,'AXIAL LOAD',3X,'AXIAL DISPL.',3X,'AXIAL STRESS',12X,'-'
      ,8X,'EQUIP. STRAIN',3X,'AXIAL STRAIN')
      PRINT 34
   34 FORMAT (13X,4H(LB),7X, 4H(IN)        ,8X,14H(PSI)    (BARS),5X,14H(
      PSI)    (BARS),3X,9H(PERCENT), 6X,9H(PERCENT)  )
      PRINT 51
   51 FORMAT(9X,'-------------------------------------------------------
      -----------------------------------')
      DO 50 I=1,N
      READ 21, AL(I),D(I)
   21 FORMAT (F7.1,F6.4)
      AS(I) = AL(I)/A
      ASB(I) = AS(I)/14.5038
      ASCP(I) = AS(I)-CP
      ASCPB(I) = ASCP(I)/14.5038

           CALCULATION OF EQUIPMENT STRAIN CORRECTION (SC)
```

```
      A1 = -250.
      B1 = 185000.
      A2 = -1694.
      B2 = 283300.
      IF(ASCP(I)-2470.)13,15,15
   13 SC(I)=(ASCP(I)-A1)/B1
      GO TO 14
   15 SC(I)=(ASCP(I)-A2)/B2

   14 ASN(I) = (D(I)/CL)*100.-SC(I)
      DC(I) = D(I)*2.54

          ORIGIN CORRECTION (STRAIN)


      IF(J-2)38,36,40
   38 ASN(I) = ASN(I) + 2.2
      GO TO 39
   36 ASN(I) = ASN(I) + 1.3
      GO TO 39
   40 IF(J-4)41,42,43
   41 ASN(I) = ASN(I) + 0.5
      GO TO 39
   42 ASN(I) = ASN(I) + 1.5
      GO TO 39
   43 IF(J-6)44,46,39
   44 ASN(I)= ASN(I) +0.3
      GO TO 39
   46 ASN(I) = ASN(I) +0.6
```

```
39 PRINT 35,AL(I),D(I),        AS(I),ASB(I),ASCP(I),ASCPB(I),SC(I),ASN(
   I)
35 FORMAT(12X,F7.1,5X,F6.4,         5X,F7.1,2X,F6.1,5X,F7.1,2X,F6.1,
   3X,F5.2,10X,F5.2)
   IF (I-N)52,56,56
52 IF(I-27)50,55,50
55 PRINT 57,K
57 FORMAT(1H1//////41X,'TABLE AII-',I2,'.  (CONTINUED)')
   PRINT 59
59 FORMAT(9X,'---------------------------------------------------------
   ------------------------------------')
   GO TO 50
56 PRINT 58
58 FORMAT(9X,'---------------------------------------------------------
   ------------------------------------')
   PRINT 60,CP,A
60 FORMAT(9X,'* CONFINING P:    = ',F6.1,' PSI; AREA OF CORE:  AO = '
   ,F5.3,' SQ. IN.')
50 CONTINUE
   PRINT 37
37 FORMAT (1H1)
   ASN(N+1)= 0.0
   ASN(N+2)= 1.0
   ASCP(N+1) = 0.0
   ASCP(N+2) = 10000.0
   IF(J-3)17,18,18
17 CALL AXIS(0.0,0.0,'AXIAL STRAIN ( ), %',-19,5.0,0.0,ASN(N+1),ASN(N
   +2),10.0)
   CALL AXIS(0.0,0.0,'   -    , PSI',         12,7.0,90.0,ASCP(N+1),
   ASCP(N+2),10.0)
   CALL SYMBOL(1.00,6.30,0.25,15HKELLY LS.      ,0.0,15)
   CALL SYMBOL(1.00,6.30,0.25,15HKELLY LS.      ,0.0,15)
   CALL SYMBOL(1.00,6.05,0.100,1,0.0,-1)
   CALL SYMBOL(1.20,6.00,0.1,5H  = 0 ,0.0,5)
```

```
      CALL SYMBOL(1.00,5.85,0.100,2,0.0,-1)
      CALL SYMBOL(1.20,5.80,0.100,13H  = 40.7 BARS ,0.0,13)
      CALL SYMBOL(1.00,5.65,0.100,3,0.0,-1)
      CALL SYMBOL(1.20,5.60,0.100,13H  = 55.2 BARS ,0.0,13)
      CALL SYMBOL(1.00,5.45,0.100,4,0.0,-1)
      CALL SYMBOL(1.20,5.40,0.100,14H  = 137.9 BARS ,0.0,14)
      CALL SYMBOL(1.00,5.25,0.100,5,0.0,-1)
      CALL SYMBOL(1.20,5.20,0.100,14H  = 344.7 BARS ,0.0,14)
      CALL SYMBOL(1.00,5.05,0.100,6,0.0,-1)
      CALL SYMBOL(1.20,5.00,0.100,14H  = 535.1 BARS ,0.0,14)
      CALL SYMBOL(1.00,4.85,0.1,7,0.0,-1)
      CALL SYMBOL(1.20,4.80,0.100,14H  = 668.8 BARS ,0.0,14)
      CALL AXIS(5.0,0.0,'   -   , BARS',          -13,7.0,90.0,0.0,689.4
      744,13.78949)
      CALL AXIS(0.0,7.0,'  ', 2,5.0,0.0,    ASN(N+1),ASN(N+2),10.0)
   18 CALL LINE(ASN,ASCP,N,1,1,J)
      CALL LINE(ASN,ASCP,N,1,1,J)
  100 CONTINUE



      CALL PLOT(15.0,0.0,-3)
      CALL PLOT(0.0,0.0,999)
      STOP
      END
```

LINEAR LEAST-SQUARE BEST FIT

STRESS-STRAIN

YOUNG'S MODULUS

J. S. DURTSCHE

7-8-73

```
      REAL*8 SX,SY,SXY,SX2,A1,B1,SY2
      READ 10,M
   10 FORMAT(I2)
      DO 100 J=1,M
      SX=0.
      SY=0.
      SXY=0.
      SX2=0.
      SY2=0.
      PRINT 15,J
   15 FORMAT(1H1////10X,4HJ = ,I2/////22X,37HAXIAL STRESS (PSI)   AXIAL
      STRAIN (%)/)
      READ 12,N
   12 FORMAT(I2)
      DO 150 I=1,N
```

```
      READ 11,AS,ASNP
   11 FORMAT (F7.1,F4.2)
      PRINT 16,AS,ASNP
   16 FORMAT(/30X,F7.1,10X,F4.2)
      ASC=AS/1000.
      SX=SX+ASNP
      SY=SY+ASC
      SXY=SXY+ASNP*ASC
      SX2=SX2+ASNP**2
      SY2 = SY2+ASC**2
  150 CONTINUE
      B1 = ((N*SXY-SX*SY)/(N*SX2-SX**2))*100000.
      BB1 = B1/14503800.
      A1 = ((SY/N)*1000.-B1*((SX/100.)/N))
      X0 = -A1/B1
      X42K = (42000.-A1)/(B1)
      R = (N*SXY-SX*SY)/((N*SX2-SX**2)*(N*SY2-SY**2))**0.5
      RR = R**2
      PRINT 20,B1,BB1,X0,X42K,R,RR
   20 FORMAT( 1H1///15X,5HB1 = ,F15.5,7H PSI = ,F7.3,5H MBAR/15X,5HX0 =
     ,F15.5/13X,7HX42K = ,F15.5//16X,4HR = ,F11.5/15X,2H 2/15X,5HR  = ,
     F11.5/1H1)
  100 CONTINUE
      STOP
      END
```

```
          PROGRAM FOR DETERMINING LEAST-SQUARE FITS 1)
                                 E
      Y = A + BX AND 2) Y = A1 + B1X  FOR 1) LS. AND 2) SS.
          NORMAL STRESS VS. SHEAR STRESS (AT FRACTURE)


                          J. S. DURTSCHE
                             7-1-73


      REAL*8 SX,SY,SX2,SY2,SXY,AVEX,AVEY,B,A,SS2,SYY2,SYY22,SXYY2,AVEYY2
     ,B2,A2,RR,RR2
      DIMENSION ANS(99),SS(99),AO(99),ALFA(99),CP(99),AL(99),AP(99),SS2(
     99)
      CALL PLOT( 5.0,1.5,-3)
      READ 11,M
   11 FORMAT(I2)
      DO 30 J=1,M
      SXYY2 = 0
      SYY22 = 0
      SYY2 = 0
      SX = 0
      SX2 = 0
      SY = 0
      SY2 = 0
      SXY = 0
      READ 10, N,E
```

```
10 FORMAT(I2/F5.3)
   PRINT 13
13 FORMAT(1H3)
   DO 15 I=1,N
   READ 17, CP(I),AL(I),AO(I),ALFA(I)
17 FORMAT(2F7.1,F5.3,F5.1)
   AP(I) = AL(I)/AO(I)
   ALPHA = ALFA(I)
   ALFA(I) = ALFA(I)/57.29578
   SS(I) = ((AP(I)-CP(I)) /2.)*SIN(2.*ALFA(I))
   SS2(I) = SS(I)**E
   ANS(I) = (AP(I)+CP(I))/2.-((AP(I)-CP(I))/2.)*COS(2.*ALFA(I))
   PRINT 18, AO(I),ALPHA,  CP(I),AL(I),ANS(I),SS(I),SS2(I)
18 FORMAT(// 5X,5HAO = ,F5.3, 5X,7HALFA = ,F5.1, 5X,5HCP = ,F7.1, 5X,
   5HAL = ,F7.1, 5X,6HANS = ,F7.1,5X,5HSS = ,F7.1,5X,6HSS2 = ,F14.1)
   PRINT 45,E
45 FORMAT(/20X,4HE = ,F5.3)
   SX = SX+ANS(I)
   SY = SY+SS(I)
   SYY2 = SYY2+SS2(I)
   SX2 = SX2+ANS(I)**2
   SY2 = SY2+SS(I)**2
   SYY22 = SYY22+SS2(I)**2
   SXY = SXY+ANS(I)*SS(I)
   SXYY2 = SXYY2+ANS(I)*SS2(I)
15 CONTINUE
   DO 20 K=1,2
   ANS(N+1) = 0.
   ANS(N+2) = 5000.
   SS(N+1) = 0.0
   SS(N+2) = 7000.0
   CALL AXIS(0.0,0.0,'NORMAL STRESS ( ), PSI',-22,7.0,0.0,ANS(N+1)
   ,ANS(N+2),10.0)
   CALL AXIS(0.0,0.0,'SHEAR STRESS ( ), PSI',21,5.0,90.0,SS(N+1),
```

```
      SS(N+2),10.0)
      IF(J-2)25,26,26
   26 CALL SYMBOL(1.00,4.30,0.250,15HMESA VERDE SS. ,0.0,15)
      GO TO 27
   25 CALL SYMBOL(1.00,4.30,0.250, 9HKELLY LS. ,0.0,9)
   27 CALL SYMBOL(1.00,3.90,0.200,17HFRACTURE STRENGTH ,0.0,17)
      CALL LINE(ANS,SS,N,1,-1,1)
      CALL AXIS(0.0,5.0,'NORMAL STRESS ( ), BARS',23,7.0,0.0,0.0,344.737
     2, 9.84963)
      CALL AXIS(7.0,0.0,'SHEAR STRESS ( ), BARS',-22,5.0,90.0,0.0,482.63
     21,10.72516)
   20 CONTINUE
      AVEX = SX/N
      AVEY = SY/N
      AVEYY2 = SYY2/N
      B = ((N*SXY)-(SX*SY))/((N*SX2)-(SX**2))
      A = AVEY-(B*AVEX)
      B2 = ((N*SXYY2)-(SX*SYY2))/((N*SX2)-(SX**2))
      A2 = AVEYY2 -(B2*AVEX)
      RR = (((N*SXY)-(SX*SY))/((N*SX2-(SX**2))*(N*SY2-(SY**2)))**0.5)**2
      RR2=(((N*SXYY2)-(SX* SYY2))/((N*SX2-(SX**2))*(N*SYY22-(SYY2**2)))*
     *0.5)**2
      PRINT 35, A,B,A2,B2,RR,RR2
   35 FORMAT(1H1,5X////20X,4HA = ,F8.2,4H PSI  /20X,4HB = ,F7.4//20X,
     5HA1 = ,F20.2,12H PSI SQUARED /20X,5HB1 = ,F15.5///30X,F6.4/30X,F6
     .4, 24H LINEARITY, RESPECTIVELY )
      PRINT 36
   36 FORMAT(1H1)


      CALL PLOT(12.0,0.0,-3)
   30 CONTINUE
```

```
CALL PLOT(0.0,0.0,99)
STOP
END
```

```
            PROGRAM FOR DETERMINING E IN LEAST-SQUARE FIT

                                                   E
                                    Y = A + BX
                                        OR

                                     E
                                    Y   = A + BX


                                   J. S. DURTSCHE

                                   7-10-73


      REAL*8 SX,SY,SXY,SX2,SY2,B,A,RR
      DIMENSION ANS(99),SS(99),SSS(99)
      READ 10, M
   10 FORMAT(I2)
      DO 100 J=1,M
      PRINT 28
   28 FORMAT(1H1///10X,28HNORMAL STRESS   SHEAR STRESS  //)

          CHOICE OF STARTING E (MINUS E-INCREMENT)
```

```
   IF(J-2)32,33,31
32 E=0.900
   GO TO 31
33 E=0.900


31 READ 20, N
20 FORMAT(I2)
   DO 30 I=1,N
   READ 25, ANS(I),SS(I)
25 FORMAT(2F7.1)
   PRINT 29,ANS(I),SS(I)
29 FORMAT(/14X,F7.1,9X,F7.1)
30 CONTINUE
   PRINT 35
35 FORMAT(1H1///10X,34H     E          A          B          R*R     //)
   DO 50 IJ=1,11

           CHOICE OF E INCREMENT

   E = E + 0.100

   SX = 0
   SY=0
   SXY=0
   SX2=0
   SY2=0
   DO 40 I=1,N
   SSS(I)=SS(I)**E
```

```
      SX=SX+ANS(I)
      SY=SY+SSS(I)
      SXY=SXY+ANS(I)*SSS(I)
      SX2 = SX2+ANS(I)**2
      SY2 = SY2 + SSS(I)**2
   40 CONTINUE
      B=((N*SXY)-(SX*SY))/((N*SX2)-(SX**2))
      A = SY/N-(B*(SX/N))
      RR = (((N*SXY)-(SX*SY))/((N*SX2-(SX**2))*(N*SY2-(SY**2)))**0.5)**2
      PRINT 45, E,A,B,RR
   45 FORMAT(14X,F5.3,2X,F13.2,2X,F9.2,2X,F9.8)
   50 CONTINUE
  100 CONTINUE
      STOP
      END
```

PROGRAM FOR PLOTTING THE RATIO Y TO X VS. X:

$$Y/X = (A+BX)^{1/E}/X$$

WHERE Y = SHEAR STRESS, X = NORMAL STRESS,
AND A, B, AND E ARE LEAST-SQUARE PARAMETERS

J. S. DURTSCHE

7-1-73

```
   READ 10, M
10 FORMAT (I2)
   PRINT 12
12 FORMAT (1H1)
   CALL PLOT(5.0,1.5,-3)
   CALL PLOT(20.0,0.0,3)
   DO 100 J=1,M
   READ 15, A,B,E
15 FORMAT (F11.1,F10.3,F5.3)
   DO 50 I=1,2
   CALL AXIS(0.0,0.0,'NORMAL STRESS ( ), PSI',-22,7.0,0.0,0.0,5000.0,
   10.0)
```

```
      CALL AXIS(0.0,0.0,30H       INTERNAL FRICTION (    ) ,30,5.0,90.0,
      0.0,0.4,10.0)
      IF(J-2)20,21,22
   20 CALL SYMBOL(2.8,4.10,0.25,9HKELLY LS. ,0.0,9)
      GO TO 22
   21 CALL SYMBOL(2.8,4.10,0.25,14HMESA VERDE SS. ,0.0,14)
   22 CALL SYMBOL(2.8,3.70,0.15,17HFRACTURE            ,0.0,17)
      CALL AXIS(0.0,5.0,'NORMAL STRESS ( ), BARS',23,7.0,0.0,0.0,344.737
      2, 9.84963)
      CALL AXIS(7.0,0.0,'  ',-2,5.0,90.0,0.0,0.40,10.0)
   50 CONTINUE
```

GENERATION OF CURVE Y/X

```
   31 ANS=0.40
   33 DO 75 IJ=1,59
      ANS = ANS + 0.10
      SLOPE =(((A+B*ANS*5000.)**(1./E))/(ANS*5000.))/0.4
      IF(SLOPE)75,75,208
  208 IF(SLOPE-4.5)209,75,75
  209 CALL SYMBOL(ANS,SLOPE,0.1,1,0.0,-1)
      CALL SYMBOL(ANS,SLOPE,0.1,1,0.0,-1)
      IF(ANS-6.4)75,51,51
   51 IJ=59
   75 CONTINUE
      IF(J-2)60,100,100
   60 CALL PLOT(12.0,0.0,-3)
  100 CONTINUE
      CALL PLOT(16.0,0.0,-3)
```

```
CALL PLOT(C.0,0.0,999)
STOP
END
```

```
                    PROGRAM FOR CALCULATION OF
                      CORRECTED AREA


                      J. S. DURTSCHE

                        9-10-73


   DIMENSION CP(99),AL(99),ACRCT(99),ACRCTT(99),NAME(20)

          L.-S. FIT CONSTANTS FOR CONTROLLED AREA TEST



          TABLE #


   READ (5,10) ALFA,N
10 FORMAT(F5.1/I2)
   READ (5,12) (NAME(J),J=1,15)
12 FORMAT(15A4)
```

```
      ALFA = ALFA/57.29578
      ATOT = 0.
      DO 100 I=1,N
      READ (5,20) CP(I),AL(I)
   20 FORMAT(2F6.1)
      ACRCT(I) =(AL(I)*(B*(COS(2.*ALFA)-1.)+SIN(2.*ALFA)))/(CP(I)*B*(1.+
       COS(2.*ALFA)) + CP(I)*SIN(2.*ALFA) + 2.*A)
      ATOT = ATOT+ACRCT(I)
  100 CONTINUE
      AAVE = ATOT/N
      WRITE (6,30)
   30 FORMAT(1H1)
      WRITE(6,32) K
   32 FORMAT(    //17X,'TABLE AII-',I2,'.  DETERMINATION OF AVERAGE CORR
      ECTION AREA'/15X,'FROM   = A + B  FIT OF CONTROLLED-AREA FRICTION
      EXPERIMENTS*')
      WRITE (6,34)
   34 FORMAT(15X,60('-'))
      WRITE (6,36)
   36 FORMAT(15X,'LOAD (LB)    CONFINING P. (PSI)    CALCULATED AREA (SQ
      . IN.)')
      WRITE (6,34)
   56 FORMAT(/)
      WRITE (6,35) (NAME(J),J=1,15)
   35 FORMAT(/15X,15A4/)
      DO 55 IJ=1,N
      WRITE (6,38) AL(IJ),CP(IJ),ACRCT(IJ)
   38 FORMAT(16X,F6.1,12X,F6.1,18X,F5.3)
   55 CONTINUE
      WRITE (6,40) AAVE
   40 FORMAT(/48X,'AVERAGE:  ',F5.3 )
      WRITE(6,34)
      WRITE(6,43)
   43 FORMAT(15X,'* SEE TEXT FOR METHOD OF CALCULATION')
```

```
WRITE (6,30)
STOP
END
```

```
                 PROGRAM FOR DETERMINING LEAST-SQUARE FIT

                                  E
                       Y = A + BX


                       J. S. DURTSCHE

                          7-1-73


      REAL*8 SX,SY,SX2,SY2,SXY,B,A,RR
      DIMENSION CP(99),AL(99),AO(99),AP(99),ALFA(20),SS(99),ANS(99),
      AC1(20),AOO(99)
      CALL PLOT(5.0,1.5,-3)
      CALL PLOT( 20.0,0.0,3)
      READ 11, M
   11 FORMAT(I2)
      DO 30 J=1,M
      IF(J-3)102,101,101
  102 CALL AXIS(0.0,0.0,'NORMAL STRESS ( ), PSI',-22,5.0,0.0,0.0,7500.,1
      0.0)
      CALL AXIS(0.0,0.0,'SHEAR STRESS ( ), PSI',21,7.0,90.0,0.0,5000.,10
      .0)
      CALL AXIS(0.0,7.0,'NORMAL STRESS ( ), BARS', 23,5.0,0.0,0.0,517.10
      58,10.34212)
```

```
      CALL AXIS(5.0,0.0,'SHEAR STRESS ( ), BARS',-22,7.0,90.,0.0,344.738
     ,13.78949)
```

LABELS FOR GRAPHS

```
  101 PRINT 31
   31 FORMAT( 1H1,     10X,4HAREA,10X,1HA,13X,1HB,12X,1HE,12X,2HRR//)
      READ 10, ALFA(J),AO1(J),N,E
   10 FORMAT( F5.1,F5.3/I2/F5.3)
      ALFA(J)=ALFA(J)/57.29578
      AO(1) = AC1(J)


      DC 25 I=1,N
      READ 17, CP(I),AL(I)
   17 FCRMAT (2F6.1)
   25 CONTINUE
  100 CCNTINUE
      DO 50 K=1,1
   36 DO 50 L=1,1


   86 CONTINUE
   81 SX=0
      SY=0
```

```
      SX2=0
      SY2=0
      SXY=0
      DO 15  I=1,N
      AP(I)  =  AL(I)/AO(K)
      SS(I)  =  ((AP(I)-CP(I))/2.)*SIN(2.*ALFA(J))
      ANS(I)=((AP(I)+CP(I))/2.)-(((AP(I)-CP(I))/2.)*COS(2.*ALFA(J)))
      PRINT 82,  AL(I),CP(I),ANS(I),SS(I)
   82 FORMAT(10X,4F20.3)
      ANS(I)  =  ANS(I)**E
      SX=SX+ANS(I)
      SY=SY+SS(I)
      SX2=SX2+ANS(I)**2
      SY2=SY2+SS(I)**2
      SXY  =  SXY+ANS(I)*SS(I)
      ANS(I)  =  ANS(I)**(1./E)
   53 ANS(I)  =  ANS(I)/7500.
      SS(I)  =  SS(I)/5000.
      IF(ANS(I)-5.)1C8,109,109
  1C8 CALL  SYMBOL(ANS(I),SS(I),0.100,J,0.0,-1)
      CALL  SYMBOL(ANS(I),SS(I),0.100,J,0.0,-1)
  109 ANS(I)  =  ANS(I)*7500.
      SS(I)  =  SS(I)*5000.
   52 CONTINUE
   15 CONTINUE
      AVEX  =  SX/N
      AVEY  =  SY/N
      B=  ((N*SXY)-(SX*SY))/((N*SX2)-(SX**2))
      A  =  AVEY  -(B*AVEX)
      RR  =  (((N*SXY)-(SX*SY))/((N*SX2-(SX**2))*(N*SY2-(SY**2)))**0.5)**2
```

PLOT ROUTINE FOR PLOTTING

$$Y = A + BX^{E}$$

```
      IF(K-2)56,72,72
   56 A1 = A/5000.
      DO 72 LM=1,2
      X1P=0
      CALL PLOT(0.0,A1,3)
      DO 72 JI=1,50
      X1P=X1P+0.1
      Y1P=(A+B*((X1P*7500.)**E))/5000.
      IF(X1P-5.0)99,72,72
   99 CALL PLOT(X1P,Y1P,2)
   72 CONTINUE


   77 PRINT 35, AO(K),A,B,E,RR
   35 FORMAT(10X,F5.3,F12.7,6X,F11.7,F9.3,F20.10/ )
      COEF5K = A/5000. + B*(5000.**(E-1.))
      ABAR = A/14.5038
      PRINT 92, ABAR
   92 FORMAT(///30X, 4HA = ,F7.3, 5H BARS)
   50 CONTINUE
      PRINT 22, J
   22 FORMAT( ///30X,14HEND DATA SET # ,I2)
   30 CONTINUE
      CALL PLOT(9.0,0.0,-3)
      CALL PLOT(5.0,0.0,-3)
      CALL PLOT(0.0,0.0,999)
      STOP
      END
```

PROGRAM FOR PLOTTING COEF. OF FRICTION:
RATIO OF SHEAR STRESS TO NORMAL
STRESS AS A FUNCTION OF NORMAL
STRESS:

$$\text{COEF.} = Y/X = A/X + BX^{E-1}$$

WHERE Y = SHEAR STRESS, X = NORMAL STRESS,
AND A, B, AND E ARE LEAST-SQUARE PARAMETERS

J. S. DURTSCHE

7-1-73

```
      READ 10, M
   10 FORMAT (I2)
      PRINT 12
   12 FORMAT(1H1)
      CALL PLOT(5.0,1.5,-3)
      CALL PLOT(20.0,0.0,3)
      DO 100 J=1,M
   80 READ 15, A,B,E
```

```
15 FORMAT(F7.2,F6.4,F6.4)
   BE = B*E
   IF(J-3)34,34,35
34 AY = 7.0
   AY1 = 0.2
   GO TO 33
35 AY = 7.0
   AY1 = 0.2
33 IF(J-3)43,44,45
45 IF(J-6)43,44,46
46 IF(J-8)44,43,47
47 IF(J-10)43,44,48
48 IF(J-13)43,44,44
43 CALL AXIS(0.0,0.0,'NORMAL STRESS ( ), PSI',-22,5.12,0.,0.0,7500.,
   10.0)
   CALL AXIS(0.0,0.0,'COEF. OF FRICTION',17,AY,90.0,0.0,AY1,10.0)
   CALL AXIS(0.0,AY,'NORMAL STRESS ( ), BARS',23,5.12,0.,0.0,517.1058
   ,10.34212)
   CALL AXIS(5.12,0.,'  ',-2,AY,90.0,0.0,AY1,10.0)
44 IF(J-3)20,21,26
26 IF(J-6)22,21,27
27 IF(J-8)21,23,28
28 IF(J-10)23,21,29
29 IF(J-12)24,24,21
```

LABELS FOR GRAPHS

```
20 CALL SYMBOL(1.0,6.1,0.25,14HKELLY LS.        ,0.0,14)
   CALL SYMBOL(1.0,6.1,0.25,14HKELLY LS.        ,0.0,14)
```

```
      CALL SYMBOL(1.0,5.75,0.1,1,0.0,-1)
      CALL SYMBOL(1.2,5.7,0.1,21H#80 LS. GOUGE:  P = 0 ,0.0,21)
      CALL SYMBOL(1.0,5.55,0.1,2,0.0,-1)
      CALL SYMBOL(1.2,5.50,0.1,13HP = 37.9 BARS ,0.0,13)
      CALL SYMBOL(1.0,5.35,0.1,3,0.0,-1)
      CALL SYMBOL(1.2,5.30,0.1,13HP = 86.9 BARS ,0.0,13)
      GO TO 21
   22 CALL SYMBOL(1.0,6.1,0.25,14HMESA VERDE SS. ,0.0,14)
      CALL SYMBOL(1.0,5.8,0.12,'P = 34.5 BARS',0.0,13)
      CALL SYMBOL(1.0,5.65,0.1,1,0.0,-1)
      CALL SYMBOL(1.2,5.6,0.1,'KINETIC DATA',0.0,12)
      CALL SYMBOL(1.0,5.45,0.1,2,0.0,-1)
      CALL SYMBOL(1.2,5.4,0.1,'STATIC DATA',0.0,11)
      CALL SYMBOL(2.8,5.8,0.12,'P = 79.3 BARS',0.0,13)
      CALL SYMBOL(2.8,5.65,0.1,3,0.0,-1)
      CALL SYMBOL(3.0,5.6,0.1,'KINETIC DATA',0.0,12)
      CALL SYMBOL(2.8,5.45,0.1,4,0.0,-1)
      CALL SYMBOL(3.0,5.4,0.1,'STATIC DATA',0.0,11)
      GO TO 21
   23 CALL SYMBOL(1.0,6.1,0.25,14HMESA VERDE SS. ,0.0,14)
      CALL SYMBOL(1.0,6.1,0.25,14HMESA VERDE SS. ,0.0,14)
      CALL SYMBOL(1.0,5.75,0.1,1,0.0,-1)
      CALL SYMBOL(1.2,5.7,0.1,21H#80 SS. GOUGE:  P = 0 ,0.0,21)
      CALL SYMBOL(1.0,5.55,0.1,2,0.0,-1)
      CALL SYMBOL(1.2,5.50,0.1,13HP = 34.5 BARS ,0.0,13)
      CALL SYMBOL(1.0,5.35,0.1,3,0.0,-1)
      CALL SYMBOL(1.2,5.30,0.1,13HP = 79.3 BARS ,0.0,13)
      GO TO 21
   24 CALL SYMBOL(1.0,6.1,0.25,14HKELLY LS.      ,0.0,14)
      CALL SYMBOL(1.0,6.1,0.25,14HKELLY LS.      ,0.0,14)
      CALL SYMBOL(1.0,5.6,0.25,14HMESA VERDE SS. ,0.0,14)
      CALL SYMBOL(1.0,5.6,0.25,14HMESA VERDE SS. ,0.0,14)
      CALL SYMBOL(1.0,5.25,0.1,1,0.0,-1)
      CALL SYMBOL(1.2,5.2,0.1,'#80 LS. GOUGE',0.0,13)
```

```
      CALL SYMBOL(1.0,5.05,0.1,2,0.0,-1)
      CALL SYMBOL(1.2,5.0,0.1,'#80 SS. GOUGE',0.0,13)
      CALL SYMBOL(1.0,4.85,0.1,3,0.0,-1)
      CALL SYMBOL(1.2,4.8,0.1,'#80 LS. AND SS. GOUGE',0.0,21)
```

EQUATION OF COEF. OF FRICTION IS $Y/X = A/X + BX^{E-1}$

```
   21 AYY = AY-1.7
      ANS = 0.0
      DO 50 I=1,49
      ANS = ANS+0.1
      SLOPE = (A/(ANS*7500.) + (B*((ANS*7500.)**(E-1))))/AY1
      IF (J-4)61,62,62
   61 K= J
   71 IF(SLOPE-AYY)72,72,50
   73 I=48
      GO TO 50
   72 IF(SLOPE-0.1)50,50,74
   74 CCNTINUE
      CALL SYMBOL(ANS,SLOPE,0.100,K,  0.0,-1)
      CALL SYMBOL(ANS,SLOPE,0.100,K,  0.0,-1)
      GO TO 50
   62 IF(J-8)63,64,64
   63 K=J-3
      GO TO 71
   64 IF(J-11)65,66,66
   65 K=J-7
      GO TO 71
   66 K=J-10
```

```
      GO TO 71
   50 CONTINUE
      SLOPE1 = SLOPE*AY1
      ANS1 = ANS*7500.
      PRINT 25, A,B,E,SLOPE1
   25 FORMAT(///10X,10HA (PSI) = ,F8.2,10X,4HB = ,F9.7,10X,4HE = ,F6.4,1
     0X,'FINAL COEF. = ',F6.4)
      PRINT 222, ANS1
  222 FORMAT(10X,'FINAL COEF. COMPUTED AT X = ',F7.1,' PSI')
      IF (J-3)100,55,56
   55 CALL PLOT(10.0,0.0,-3)
      GO TO 100
   56 IF(J-7)100,55,58
   58 IF(J-10)100,55,100
  100 CONTINUE
      CALL PLOT (14.0,0.0,-3)
      CALL PLOT(0.0,0.0,999)
      STOP
      END
```

PROGRAM FOR PLOTTING COEF. VS. ALPHA

J. S. DURTSCHE

8-15-73

```
      CALL PLOT(5.0,3.0,-3)
      CALL PLOT(20.0,0.0,3)
      READ 10,M
   10 FORMAT(I2)
      DO 100 J=1,M
      READ 20, COEF,ALPHA
   20 FORMAT(F5.3,F4.1)
   30 IF(J-3)35,40,32
   32 IF(J-5)40,35,33
   33 IF(J-7)35,40,40
   35 AX = 20.
      AY = 0.2
      CALL AXIS(0.0,0.0,'      SAWCUT ANGLE ( ), DEG.',-28,4.0,0.0,0.0,
      AX,10.0)
      CALL AXIS(0.0,0.0,'      COEF. OF FRICTION',23,3.98,90.0,.4,AY,10.
      0)
      CALL AXIS(0.0,4.0,'  ',2,4.0,0.0,0.0,AX,10.0)
      CALL AXIS(4.0,0.0,'  ',-2,3.98,90.,0.4,AY,10.0)
      CALL SYMBOL(1.0,3.55,.18,'  = 2.53 KB.',0.0,12)
      CALL SYMBOL(1.0,3.31,0.12,1,0.0,-1)
```

```
      CALL SYMBOL(1.22,3.25,0.12,'#80 LS. GOUGE',0.0,13)
      CALL SYMBOL(1.0,3.11,0.12,3,0.0,-1)
      CALL SYMBOL(1.22,3.05,0.12,'#80 SS. GOUGE',0.0,13)
   40 IF(J-4)42,42,43
   42 K = 1
      GO TO 50
   43 K = 3
   50 ALFA = ALPHA/AX
      COEFF = (COEF-0.4)/AY
      CALL SYMBOL(ALFA,COEFF,0.1,K,0.0,-1)
      CALL SYMBOL(ALFA,COEFF,0.1,K,0.0,-1)
  100 CONTINUE
      CALL PLOT (12.0,0.0,-3)
      CALL PLOT(0.0,0.0,999)
      STOP
      END
```

```
            PROGRAM FOR PLOTTING SHEARING STRESS TO CAUSE
            FRACTURE MINUS SHEARING STRESS TO CAUSE SLIDING
            VS. NORMAL STRESS FOR BOTH LS. AND SS. (FRAC-
            TURE AND CONTROLLED AREA FRICTION TESTS WITH
            GOUGE)


                      J. S. DURTSCHE

                       9-10-73


      DIMENSION AI(5),BI(5),A(5),B(5)


            PLOT AXES AND LABELS


      AY = 2000.
      AY1 = 137.895
      AY2 = 9.193
      CALL PLOT(5.0,3.0,-3)
      CALL PLOT(20.0,0.0, 3)
      DO 31 L=1,2
      CALL AXIS(0.0,0.0,'NORMAL STRESS ( ), PSI',-22,5.12,0.,0.0,7500.,
```

```
      10.0)
      CALL AXIS(0.0,0.0,'(   - ), PSI',11,5.0,90.0,0.0,AY,10.0)
      CALL AXIS(0.0,5.00,'NORMAL STRESS ( ), BARS',23,5.12,0.,0.0,517.10
     58,10.34212)
      CALL AXIS(5.12,0.0,'(   - ), BARS',-12,5.0,90.0,0.0,AY1,AY2)
      CALL SYMBOL(1.0,4.56,0.12,1,0.0,-1)
      CALL SYMBOL(1.21,4.5,0.12,'KELLY LS.',0.0,9)
      CALL SYMBOL(1.0,4.21,0.12,2,0.0,-1)
      CALL SYMBOL(1.21,4.15,0.12,'MESA VERDE SS.',0.0,14)
   31 CCNTINUE


      READ 5,M
    5 FORMAT(I2)
      DO 100 J=1,M
      PRINT 80
   80 FORMAT(1H1)
      READ 10,AI(J),BI(J),E,A(J),B(J)
   10 FORMAT(F11.1,F9.3,F5.3/F6.2,F6.4)


                 GENERATION OF FUNCTION AS X VARIES


      X = 0.1
      DO 50 I=1,47
      X = X+0.1
      YI = (AI(J)+BI(J)*7500.*X)**(1./E)
      Y = (A(J)+B(J)*7500.*X)
      XPRINT = X*7500.
      YDEL = YI-Y
      PRINT 25, XPRINT,YDEL,J
   25 FORMAT(10X,'X = ',F7.1,10X,'Y = ',F8.1,' PSI',10X,'FOR J = ',I1)
      YDELP = YDEL/AY
```

```
      CALL SYMBOL(X,YDELP,0.1,J,0.0,-1)
      CALL SYMBOL(X,YDELP,0.1,J,0.0,-1)
   50 CONTINUE
  100 CONTINUE
      PRINT 75
   75 FORMAT(1H1)
      CALL PLOT(14.0,0.0,-3)
      CALL PLOT(0.0,0.0,999)
      STOP
      END
```

REFERENCES

Berry, L. G., and B. Mason, Mineralogy, pp. 200-203, Freeman, San Francisco, 1959.

Blackwell, M. L., The influence of pore fluids on the frictional properties of quartzose sandstone, M.S. thesis, Texas A&M Univ., College Station, 1973.

Bolt, B. A., C. Lomnitz, and T. V. McEvilly, Seismological evidence on the tectonics of central and northern California and the Mendocino escarpment, _Bull. Seismol. Soc. Am._, _58_, 1725-1767, 1968.

Bombolakis, E. G., Study of the brittle fracture process under uniaxial compression, _Tectonophysics_, _18_, 231-248, 1973.

Borg, I. Y., Microscopic examination of undeformed and laboratory deformed Wagon Wheel rocks, _Rep. UCRL-51014_, 17 pp., Lawrence Livermore Lab., Livermore, Calif., 1971.

Bowden, F. P., and D. Tabor, _The Friction and Lubrication of Solids_, vol. I, Clarendon Press, Oxford, 1950.

Brace, W. F., An extension of the Griffith theory of fracture to rocks, _J. Geophys. Res._, _65_, 3477-3480, 1960.

Brace, W. F., Brittle fracture of rocks, in _State of Stress in the Earth's Crust_, edited by W. R. Judd, pp. 111-174, Elsevier, New York, 1964.

Brace, W. F., Micromechanics in rock systems, Int. Conf. Struct. Solid Mech. Eng. Des. (Univ. Southampton, 1969), Proc., pp. 187-204, Wiley, New York, 1971.

Brace, W. F., Laboratory studies of stick-slip and their application to earthquakes, in Forerunners of Strong Earthquakes, Tectonophysics, 14, edited by E. F. Savarensky and T. Rikitake, pp. 189-200, 1972.

Brace, W. F., and J. D. Byerlee, Stick-slip as a mechanism for earthquakes, Science, 153, 990-992, 1966.

Brace, W. F., and J. D. Byerlee, California earthquakes: why only shallow focus? Science, 168, 1573-1574, 1970.

Brace, W. F., and R. J. Martin, A test of the law of effective stress for crystalline rocks of low porosity, Int. J. Rock Mech. Mining Sci., 5, 415-426, 1968.

Brace, W. F., B. W. Paulding, and C. H. Scholz, Dilatancy in the fracture of crystalline rocks, J. Geophys. Res., 71, 3939-3953, 1966.

Brace, W. F., E. Silver, K. Hadley, and C. Goetze, Cracks and pores: a closer look, Science, 178, 162-164, 1972.

Brown, J. W., An investigation of microseismic activity in rock under tension, M. S. thesis, 84 pp., Penn. State Univ., State College, 1965.

Brown, J. W., and M. M. Singh, An investigation of microseismic activity in rock under tension, Trans. Am. Soc. Mech. Eng., 238, 255-267, 1967.

Brune, J. N., T. L. Henyey, and R. F. Roy, Heat flow, stress, and rate of slip along the San Andreas fault, California, J. Geophys. Res., 74, 3821-3827, 1969.

Byerlee, J. D., The frictional characteristics of Westerly Granite, Ph.D. thesis, Mass. Inst. Technol., Cambridge, 1966.

Byerlee, J. D., Frictional characte istics of granite under high confining pressure, J. Geophys. Res., 62, 3639-3648, 1967a.

Byerlee, J. D., Theory of friction based on brittle fracture, J. Appl. Phys., 38, 2928-2934, 1967b.

Byerlee, J. D., Brittle-ductile transitions in rocks, J. Geophys. Res., 73, 4741-4750, 1968.

Byerlee, J. D., Reply to K. J. Hsü, 'Comments on the paper by J. D. Byerlee,' J. Geophys. Res., 74, 5349-5350, 1969.

Byerlee, J. D., The mechanics of stick-slip, Tectonophysics, 9, 475-486, 1970a.

Byerlee, J. D., Static and kinetic friction of granite at high normal stress, Int. J. Rock Mech. Mining Sci., 7, 577-582, 1970b.

Byerlee, J. D., and W. F. Brace, Stick-slip, stable sliding, and earthquakes: effect of rock type, pressure, strain rate and stiffness, J. Geophys. Res., 73, 6031-6039, 1968.

Byerlee, J. D., and W. F. Brace, High-pressure mechanical instability in rocks, Science, 164, 713-715, 1969.

Byerlee, J. D., and W. F. Brace, Modification of sliding characteristics by fluid injection and its significance for earthquake prediction (abstract), Eos Trans. AGU, 51, 423, 1970.

Byerlee, J. D., M. G. Wilson, and L Peselnick, Elastic shock activity and fluid injection (abstract), Geol. Soc. Am., Abstr. with Programs, 4, 135, 1972.

Chayes, F., Petrographic Modal Analysis, pp. 39-40, Wiley, New York, 1956.

Chugh, Y. P., J. R. Hardy, Jr., and R. Stefanko, An investigation of the frequency spectra of microseismic activity in rock under tension, in Proc. Tenth Symp. Rock Mech., Univ. Texas (Austin), AIME, New York, 1968.

Christie, J. M., H. C. Heard, and P. N. LaMori, Experimental deformation of quartz single crystals at 27 to 30 kilobars confining pressure and 24°C, Am. J. Sci., 262, 26-55, 1964.

Colback, P. S. B., and B. L. Wiid, The influence of moisture content on the compressive strength of rock, Third Canadian Symp. Rock Mech., Toronto, pp. 65-83, 1965.

Cottrell, A. H., Dislocations and Plastic Flow in Crystals, p. 32, Clarendon Press, Oxford, 1953.

Coulson, J. H., The effects of surface roughness on the shear strength of joints in rock, technical report MRD-2-70, 283 pp., Missouri River Div., Corps of Engineers, Omaha, Neb., 1965.

Dally, J. W., and W. F. Riley, Experimental Stress Analysis, pp. 143-279, McGraw-Hill, New York, 1965.

Dieterich, J. H., Time-dependent friction in rocks, J. Geophys. Res., 77, 3690-3697, 1972.

Donath, F. A., and L. S. Fruth, Dependence of strain-rate effects on deformation mechanism and rock type, J. Geology, 79, 347-371, 1971.

Drennon, C. B., and R. L. Handy, Stick-slip of lightly loaded limestone, Int. J. Rock Mech. Mining Sci., 9, 603-615, 1972.

Durelli, A. J., and W. F. Riley, Introduction to Photomechanics, Prentice-Hall, Englewood Cliffs, N.J., 1965.

Eaton, J. P., W. H. K. Lee, and L. C. Pakiser, Use of microearthquakes in the study of the mechanics of earthquake generation along the San Andreas fault in central California, Tectonophysics, 9, 259-282, 1970.

Edmond, O., and S. A. F. Murrell, Experimental observations on rock fracture at pressures up to 7 kbar and the implications for earthquake faulting, Tectonophysics, 16, 71-87, 1973.

Edmond, J. M., and M. S. Paterson, Volume changes during the deformation of rocks at high pressures, Int. J. Rock Mech. Mining Sci., 9, 161-182, 1972.

Elders, W. A., R. W. Rex, T. Meidav, P. T. Robinson, and S. Biehler, Crustal spreading in southern California, Science, 178, 15-24, 1972.

Friedman, G. M., Identification of carbonate minerals by staining methods, J. Sed. Petrol., 29, 87-97, 1959.

Garg, S. K., and A. Nur, Effective stress laws for fluid-saturated porous rocks, J. Geophys. Res., 78, 5911-5921, 1973.

Griffith, A. A., The phenomena of rupture and flow in solids, Phil. Trans. Roy. Soc., London, A221, 163-198, 1921.

Hammond, A. L., Earthquake prediction (II): prototype instrumental networks, Science, 180, 940-941, 1973.

Handin, J., Strength and ductility, in Handbook of Physical Constants, Geol. Soc. Am. Memoir 97, edited by S. P. Clark, Jr., pp. 223-289, 1966.

Handin, J., On the Coulomb-Mohr failure criterion, J. Geophys. Res., 74, 5343-5348, 1969.

Handin, J., and J. T. Engelder, The mechanical properties and fabric of quartz fault-gouge, semi-annual progress report no. 2 (part II), contract 14-08-0001-12723, 44 pp., Center for Tectonophysics, Texas A&M Univ., College Station, 1973.

Handin, J., R. V. Hager, M. Friedman, and J. N. Feather, Experimental deformation of sedimentary rocks under confining pressure: pore pressure tests, Bull. Am. Assoc. Petrol. Geologists, 47, 717-755, 1963.

Handin, J., and D. W. Stearns, Sliding friction of rock (abstract), Eos Trans. AGU, 45, 103, 1964.

Hardy, H. R., Jr., Recent studies of the mechanical behavior of geologic materials using ultrasonic and microseismic techniques, Earthquake Notes, 40, 29-50, 1969.

Heard, H. C., Transition from brittle to ductile flow in Solenhofen Limestone as a function of temperature, confining pressure and interstitial fluid pressure, Geol. Soc. Am. Mem. 79, 193-226, 1960.

Hobbs, D. W., The behavior of broken rock under triaxial compression, Int. J. Rock Mech. Mining Sci., 7, 125-148, 1970.

Hoek, E., Brittle failure of rock, in Rock Mechanics in Engineering Practice, edited by K. G. Stagg and O. C. Zienkiewicz, pp. 99-124, Wiley, London, 1968.

Hubbert, M. K., and W. W. Rubey, Role of fluid pressure in mechanics of overthrust faulting, Bull. Geol. Soc. Am., 70, 115-166, 1959.

Humston, J. A., Experimental study of stick-slip in Tennessee Sandstone, M.S. thesis, Texas A&M Univ., College

Station, Texas, 1972.

Hsü, K. J., Role of cohesive strength in the mechanics of overthrust faulting and of landsliding, Geol. Soc. Am. Bull., 80, 927-952, 1969.

Jaeger, J. C., Friction of rocks and stability of rock slopes, Geotechnique, 21, 97-134, 1971.

Jaeger, J. C., and N. G. W. Cook, Fundamentals of Rock Mechanics, pp. 53-73, 310-334, 384-390, Chapman and Hall, London, 1971a.

Jaeger, J. C., and N. G. W. Cook, Friction in granular materials, Int. Conf. Struct. Solid Mech. Eng. Des. Civ. Eng. Mater., Southampton Univ. (1969), Pap. 22, 10 pp., 1971b.

Johnson, T., F. Wu, and C. Scholz, Source parameters for stick-slip and for earthquakes, Science, 179, 278-280, 1973.

Lajtai, E. Z., Shear strength of weakness planes in rocks, Int. J. Rock Mech. Mining Sci., 6, 499-515, 1969.

Lane, K. S., and W. J. Heck, Triaxial testing for strength of rock joints, Proc. Sixth Symp. Rock Mech., Rolla, Mo., pp. 98-108, 1964.

Logan, J. M., T. Iwasaki, M. Friedman, and S. A. Kling, Experimental investigation of sliding friction in multilithologic specimens, in Engineering Case Studies, Geol. Soc. Am., edited by Pincus, 1973, in press.

Logan, J. M., The influence of surface roughness and gouge on frictional sliding (abstract), Eos Trans. AGU, 53, 512-513, 1972.

Logan, J. M., I. Takeshi, and M. Friedman, Experimental investigation of sliding friction in multilithogic specimens, Geol. Soc. Am., 2, 608-609, 1970.

Maurer, W. C., Shear failure of rock under compression, Soc. Petrol. Eng. J., 5, 167-175, 1965.

McKenzie, D. P., The relation between fault plane solutions for earthquakes and the directions of the principal stresses, Bull. Seismol. Soc. Am., 59, 591-601, 1969.

McGarr, A., Stable deformation of rock near deep-level tabular excavations, J. Geophys. Res., 76, 7088-7106, 1971.

Mogi, K., Effect of the intermediate principal stress on rock failure, J. Geophys. Res., 72, 5117-5131, 1967.

Mogi, K., Fracture and flow of rocks under high triaxial compression, J. Geophys. Res., 76, 1255-1269, 1971.

Morland, L. W., Finite deformation plasticity theory with application to geologic materials, J. Geophys. Res., 76, 7062-7078, 1971.

Müller, G., and M. Gastner, The "karbonat-bombe:" a simple device for the determination of the carbonate content in sediments, soils, and other minerals, N. Jb. Miner. Mh., 10, 466-469, 1971.

Murrell, S. A. F., A criterion for brittle fracture of rocks and concrete under triaxial stress, and the effect of pore pressure on the criterion, in Rock Mechanics, edited by C. Fairhurst, pp. 563-577, Pergamon, New York, 1963.

Murrell, S. A. F., The effect of triaxial stress systems on the strength of rocks at atmospheric temperatures, Geophys. J., 10, 231-281, 1965.

Nabarro, F. R. N., Z. S. Basinski, and D. B. Holt, The plasticity of pure single crystals, Adv. Phys., 13, 193-323, 1964.

Nur, A., and J. R. Booker, Aftershocks caused by pore fluid flow? Science, 175, 885 - 887, 1972.

Nur, A., and J. D. Byerlee, An exact effective stress law for elastic deformation of rock with fluids, J. Geophys. Res., 76, 6414-6419, 1971.

Obert, L., and W. Duvall, Use of subaudible noise for prediction of rockbursts, U.S. Bur. Mines Rep. Invest., 3634, 13 pp., 1942.

Orowan, E., Mechanism of seismic faulting, Geol. Soc. Am. Mem., 79, 323-345, 1960.

Post, D., Photoelasticity, in Manual on Experimental Stress

Analysis, edited by W. H. Tuppeny, Jr., and A. S. Kobayashi, pp. 29-48, Soc. for Exper. Stress. Anal., Westport, Conn., 1965.

Pratt, H. R., A. D. Black, and F. J. Bonney, Frictional properties of Cedar City Quartz Diorite, Air Force Weap. Lab. Tech. Rep. AFWL-TR-71-56, 91 pp., 1972.

Press, F., and W. F. Brace, Earthquake prediction, Science, 152, 1575-1584, 1966.

Rabinowicz, E., Friction and Wear of Materials, pp. 52-64, 97-98, Wiley, New York, 1965.

Ramsay, J. G., Folding and Fracturing of Rocks, pp. 255-297, McGraw-Hill, New York, 1967.

Richter, C. F., Elementary Seismology, p. 196, Freeman, San Francisco, 1958.

Robinson, L. H., Jr., The effect of pore and confining pressure on the failure process in sedimentary rock, Colo. Sch. Mines Quart., 54, 177-199, 1959.

Rodgers, J., Distinction between calcite and dolomite on polished surfaces, Am. J. Sci., 238, 788-798, 1940.

Ryabinin, Yu. N., B. I. Beresnev, and E. D. Martinov, Mechanical properties and processes in solids under high pressure, J. Geophys. Res., 76, 1370-1375, 1971.

Schock, R. N., H. C. Heard, and D. R. Stephens, Stress-strain behavior of granodiorite and two graywackes on compression to 20 kilobars, J. Geophys. Res., 78, 5922-5941, 1973.

Scholz, C. H., Microfracturing of rock in compression, Ph.D. thesis, 160 pp., Massachusetts Inst. of Technol., Cambridge, 1967.

Scholz, C. H., Microfracturing and the inelastic deformation of rock, J. Geophys. Res., 73, 1417-1432, 1968a.

Scholz, C. H., The frequency-magnitude relation of microfracturing in rock and its relation to earthquakes, Bull. Seismol. Soc. Am., 58, 399-415, 1968b.

Scholz, C. H., Mechanism of creep in brittle rock, J. Geophys. Res., 73, 3295-3302, 1968c.

Scholz, C. H., Microfractures, aftershocks, and seismicity, Bull. Seismol. Soc. Am., 58, 1117-1130, 1968d.

Scholz, C. H., An experimental study of the fracturing process in brittle rock, J. Geophys. Res., 73, 1447-1454, 1968e.

Scholz, C. H., The roll of microfracturing in rock deformation, in Proc. Second Int. Congr. Rock. Mech., Belgrade, Yugoslavia, pp. 2-8, 1970.

Scholz, C. H., P. Molnar, T. Johnson, Detailed studies of frictional sliding of granite and implications for the earthquake mechanism, J. Geophys. Res., 77, 6392-6406, 1972.

Scholz, C. H., L. R. Sykes, and Y. P. Aggarwal, Earthquake prediction: a physical basis, Science, 181, 803-

810, 1973.

Scholz, C. H., M. Wyss, and S. W. Smith, Seismic and aseismic slip on the San Andreas fault, J. Geophys. Res., 74, 2049-2069, 1969.

Seifert, K. E., Strength of the Adirondack anorthosite at elevated temperatures and pressures, Geol. Soc. Am. Bull., 80, 2053-2060, 1969.

Sibson, R. H., Interactions between temperature and pore-fluid pressure during earthquake faulting and a mechanism for partial or total stress relief, Nature, 243, 66-68, 1973.

Swanson, R. S., Development of constitutive equations for rocks, Ph.D. thesis, Univ. of Utah, Salt Lake City, 1969.

Swolfs, H. S., Influence of pore fluid chemistry and temperature on fracture of sandstone under confining pressure, Ph.D. thesis, Texas A&M Univ., College Station, 1971.

Walpole, R. E., Introduction to Statistics, pp. 271, 281-286, MacMillan, London, 1968.

Walsh, J. B., The effect of cracks on the uniaxial elastic compression of rocks, J. Geophys. Res., 70, 399-411, 1965.

Walsh, J. D., and W. F. Brace, Cracks and pores in rocks, Proc. First Congr. Int. Soc. Rock Mech., Lisbon, 1, 643-646, 1966.

Wawersik, W. R., and C. Fairhurst, A study of brittle rock fracture in laboratory compression experiments, _Int. J. Rock Mech. Mining Sci._, _7_, 561-575, 1970.

Weertman, J., Theory of fatigue crack growth based on a BCS crack theory with work hardening, _Int. J. Fracture_, _9_, 125-231, 1973.

Whitcomb, J. H., J. D. Garmany, and D. L. Anderson, Earthquake prediction: variation of seismic velocities before the San Francisco earthquake, _Science_, _180_, 632-635, 1973.

Wolters, R., Frictional resistance on shearing joints, _Proc. Geomech. Colloq. (18th), Austrian Soc. Geomech. Rock Mech._, _Suppl._, _1_, 3-19, 1970.

Wood, M. D., and S. S. Allen, Recurrence of seismic migrations along the central California segment of the San Andreas fault system, Nature, 244, 213-215, 1973.

This dissertation is accepted on behalf of the faculty of the Institute by the following committee:

A. J. Bradding
Adviser

William R. Sanford

James D. Kent

Marshall Deiter

Dec. 3, 1973
Date